HAL
open science

# Inférence et modélisation de la dépendance spatiale des extrêmes neigeux dans les Alpes françaises par processus max-stables

Gilles Nicolet

▶ **To cite this version:**

Gilles Nicolet. Inférence et modélisation de la dépendance spatiale des extrêmes neigeux dans les Alpes françaises par processus max-stables. Climatologie. Université Grenoble Alpes, 2017. Français. NNT : 2017GREAU017 . tel-01618950v2

**HAL Id: tel-01618950**

**https://theses.hal.science/tel-01618950v2**

Submitted on 15 Jan 2018

**HAL** is a multi-disciplinary open access archive for the deposit and dissemination of scientific research documents, whether they are published or not. The documents may come from teaching and research institutions in France or abroad, or from public or private research centers.

L'archive ouverte pluridisciplinaire **HAL**, est destinée au dépôt et à la diffusion de documents scientifiques de niveau recherche, publiés ou non, émanant des établissements d'enseignement et de recherche français ou étrangers, des laboratoires publics ou privés.

Communauté UNIVERSITÉ Grenoble Alpes

# THÈSE

Pour obtenir le grade de

**DOCTEUR DE LA COMMUNAUTÉ UNIVERSITÉ GRENOBLE ALPES**

Spécialité : **Sciences de la Terre et Univers, Environnement**

Arrêté ministériel : 25 mai 2016

Présentée par


## Gilles NICOLET


Thèse dirigée par **Nicolas ECKERT** et
codirigée par **Samuel MORIN**

préparée au sein d'**Irstea Grenoble – Equipe ETNA**
et du **CNRM/CEN (Météo-France – CNRS)**
dans l'École Doctorale **Terre Univers Environnement**

# Inférence et modélisation de la dépendance spatiale des extrêmes neigeux dans les Alpes françaises par processus max-stables

Thèse soutenue publiquement le **16 juin 2017**,
devant le jury composé de :

**Prof. Anne-Catherine FAVRE**
Professeure, Grenoble INP – Ense$^3$, Présidente
**Prof. Liliane BEL**
Professeure, AgroParisTech, Rapportrice
**Dr. Juan Ignacio LOPEZ-MORENO**
Tenured Scientist, Instituto Pirenaico de Ecología, Rapporteur
**Dr. Juliette BLANCHET**
CR CNRS, Institut des Géosciences de l'Environnement, Examinatrice
**Prof. Anthony C. DAVISON**
Professeur, Ecole Polytechnique Fédérale de Lausanne, Examinateur
**Dr. Philippe NAVEAU**
DR CNRS, Laboratoire des Sciences du Climat et de l'Environnement, Examinateur
**Dr. Nicolas ECKERT**
ICPEF, Irstea Grenoble, Directeur de thèse
**Dr. Samuel MORIN**
ICPEF, Météo-France – CNRS, CNRM/CEN, Co-Directeur de thèse

*A mon père*

# Remerciements

Mes premiers remerciements vont à mes encadrants. En plus de ses compétences scientifiques, je remercie Nicolas Eckert pour sa gentillesse et sa décontraction qui ont rendu l'atmosphère de travail d'autant plus agréable. Je le remercie aussi beaucoup pour sa compréhension lors des moments difficiles. Je remercie Samuel Morin, et en particulier pour la grande patience dont il a fait preuve lors de ses explications. Je ne le remercierai jamais assez pour avoir si longuement insisté sur l'importance du travail de pédagogie pour les non-spécialistes. Je remercie Juliette Blanchet pour sa sympathie et sa disponibilité, ainsi que pour son coup d'œil pour repérer les erreurs qui m'a été très utile.

Je remercie mon jury de thèse : Anne-Catherine pour l'avoir présidé, Liliane Bel et Nachó Lopez-Moreno pour avoir rapporté mon manuscrit, ainsi que Anthony Davison et Philippe Naveau. Je remercie les personnes qui ont participé à mon comité de suivi de thèse : Anne-Laure Fougères, Emmanuel Paquet et Benjamin Renard, pour leurs lectures attentives, leurs conseils et leurs remarques. Je remercie Guillaume Evin et David Penot pour leur aide. Je suis très reconnaissant envers mes encadrantes de stage de master, Cécile Mercadier et Anne-Laure Fougères pour m'avoir initié aux statistiques extrêmes. Je salue Quentin avec qui j'ai fait mon stage.

Je suis très reconnaissant à Météo France et au CEN, et particulièrement à toutes les personnes impliquées dans la constitution des jeux de données utilisés dans cette thèse. Je remercie Déborah pour les réanalyses SAFRAN - Crocus. Je remercie le LabEx OSUG@2020 pour avoir participé au financement de ma thèse et mon Ecole Doctorale Terre Univers Environnement. Un grand merci à Christine pour son excellent travail à l'ED. Je remercie le personnel du restaurant Sodexo du CTP pour leur sympathie et leur bonne humeur.

Je salue mes collègues (anciens et actuels) d'Irstea Grenoble que j'ai côtoyé durant ma thèse : Simon, Perrine, Hugo, Coraline, Guillaume P., Guillaume D., Félix, Elodie, Firmin, Antoine, Alexandra, Ségolène, Clément, Manon, Loïc, Pauline, Jiaying, Hao, Pascal H., Pascal S., Hoan, Gaëtan, Raphaël, Eva, Adel, Didier, Mohamed, Thierry, Fred, Hervé, Gwenola, Bertrand, Thomas, Christian, Valérie, Anne-Sophie, Geneviève, ainsi que tous ceux que j'ai oublié. Une mention spéciale pour les personnes qui ont partagé mon bureau, François, Mélanie, Costanza et Yoichi pour tous les bons moments passés ensemble.

Je salue Nicolas, Xiaoxiu, Yann, Mao, Hélène, Wentao, Meina, Cédric, Zhu, Ying, Chao, Patrick, Yanning, Dan, Donatien, Rudy, Shanshan, Alexandra, Cyril, Mamoun et tous ceux que tous ceux que j'ai oublié.

Je remercie ma famille, particulièrement Julia, Franck, Lisa et Yann. Je remercie ma Maman. Je remercie Lingran pour sa patience et sa gentillesse.

# Abstract

Extreme snowfall and extreme snow depths are among the most dangerous hazards in the mountainous regions. Max-stable processes, which connect extreme value statistics and geostatistics by modeling the spatial dependence of extremes, offer a suitable framework to deal with. Two challenging issues concerning spatial dependence of extremes are broached in this thesis through the examples of snowfall and snow depths in the French Alps: model selection and temporal nonstationarity. We process two winter maxima data sets of 3-day snowfall (90 stations from 1958 to 2013) and snow depths (82 stations from 1970 to 2013). First, we introduce a leave-two-out cross-validation procedure appropriate for evaluating the predictive ability of max-stable processes to model the dependence structure of spatial extremes. We compare five of the most commonly used max-stable processes, using as a case study the snowfall maxima data set. This approach allows us to show that the extremal-t, geometric Gaussian and Brown-Resnick processes are able to represent as well the structure of dependence of the data, regardless of the number of stations or years. Then, we show, using a data-based approach allowing to make minimal modeling assumptions, that snowfall extremes tended to become less spatially dependent over time, with the dependence range reduced roughly by half during the study period. We demonstrate that this is attributable at first to the increase in temperature and its major control on the snow/rain partitioning. A magnitude effect, with less dependent extremes due to a decrease in winter cumulated snowfall, also exists. Finally, we tackle the first-ever use of max-stable processes with temporal trends in the spatial dependence structure. This approach is applied to snow depth winter maxima modeled by a Brown-Resnick process. We show that the spatial dependence of extreme snow depths is impacted by climate change in a similar way to that has been observed for extreme snowfall.

**Keywords**: snowfall, snow depths, spatial extremes, max-stable processes, climate change, French Alps

# Résumé étendu

Ce résumé étendu a été préparé sous la forme d'un article de synthèse pour La Houille Blanche.

# INFERENCE ET MODELISATION DE LA DEPENDANCE SPATIALE DES EXTREMES NEIGEUX DANS LES ALPES FRANÇAISES PAR PROCESSUS MAX-STABLES

Gilles NICOLET[1,2], Nicolas ECKERT [1], Samuel MORIN[2], Juliette BLANCHET[3]

[1]Université Grenoble Alpes, Irstea, UR ETGR, 2 rue de la Papeterie-BP 76, F-38402 St-Martin-d'Hères, France - e-mail: gilles.nicolet@irstea.fr

[2]Météo France – CNRS, CNRM UMR 3589, CEN, Grenoble, France

[3]Univ. Grenoble Alpes, CNRS, IGE, F-38000 Grenoble, France

La gestion des risques dans les régions montagneuses nécessite une caractérisation des extrêmes neigeux. Nous utilisons le cadre des processus max-stables, qui relient statistique des valeurs extrêmes et géostatistique, pour étudier la dépendance spatiale des maxima hivernaux de cumuls de chutes de neige sur 3 jours et de hauteurs de neige dans les Alpes françaises. Deux questions sont abordées : la sélection de modèle et la non-stationnarité temporelle. Nous commençons par introduire une procédure de validation-croisée que nous utilisons pour évaluer les capacités de plusieurs processus max-stables à capturer la structure de dépendance spatiale des maxima de chutes de neige. Ensuite, nous mettons en évidence une baisse de la dépendance spatiale des chutes de neige extrêmes durant ces dernières décennies. Enfin, nous montrons comment modéliser des tendances temporelles dans une structure de dépendance spatiale des extrêmes à travers l'exemple des maxima de hauteurs de neige. Pour les extrêmes de chutes comme de hauteurs de neige, la dépendance spatiale est fortement impactée par le changement climatique, premièrement par l'effet de la hausse de la température sur la phase (neige ou pluie) de la précipitation, et ensuite par la baisse du cumul hivernal des chutes de neige.

**MOTS CLEFS :** extrêmes neigeux, dépendance spatiale, processus max-stables, changement climatique, Alpes françaises.

## *Inferring and modeling spatial dependence of snow extremes in the French Alps using max-stable processes*

Risk management in mountainous regions requires a precise assessment of snow extremes. We adopt the framework of max-stable processes, which connect extreme value statistics and geostatistics, to investigate the spatial dependence of winter maxima of 3-day snowfall and snow depths in the French Alps. Two important issues are broached: model selection and temporal non-stationarity. First, we introduce a cross-validation procedure which is used to assess the predictive ability of several max-stable processes to capture the spatial dependence structure of snowfall maxima. Then, we highlight a decrease in spatial dependence of extreme snowfall during the last decades. Lastly, we show a way to model temporal trends in a spatial dependence of extremes through the example of snow depth maxima. For both extreme snowfall and extreme snow depths, we find that the spatial dependence is strongly impacted by climate change, at first by the effect of the increase in temperature on the snow rain partitioning, also by the decrease in winter cumulated snowfall.

**KEY WORDS :** snow extremes, spatial dependence, max-stable processes, climate change, French Alps.

## I INTRODUCTION

Les chutes de neige extrêmes et les hauteurs de neige extrêmes sont importantes pour la gestion des risques dans les régions montagneuses, à cause des forts dégâts humains et économiques qu'elles sont susceptibles d'occasionner. Elles peuvent provoquer la surcharge et l'effondrement de bâtiments, l'interruption du trafic routier, ferroviaire, ou aérien, occasionner des avalanches et

contribuer aux inondations. Elles ont également un fort impact sur le cycle de l'eau, l'industrie touristique et les écosystèmes montagnards.

La théorie des valeurs extrêmes [Coles, 2001], qui permet d'interpoler au-delà des plus fortes observations mesurées, offre un cadre approprié pour étudier les extrêmes neigeux. Par exemple, l'approche dite des « maxima par blocs » [Gumbel, 1958] consiste à modéliser les maxima de blocs d'une certaine longueur (par exemple annuels) par la loi GEV (*Generalized Extreme Value*). Cependant, les extrêmes de chutes de neige et de hauteurs de neige apparaissent non pas isolés, mais regroupés spatialement. En effet, plus les positions considérées sont proches et plus les extrêmes ont tendance à apparaitre simultanément. En généralisant la théorie des valeurs extrêmes au cas spatial, les processus max-stables [de Haan, 1984] offrent un cadre approprié pour la modélisation spatiale des hauteurs de neige extrêmes [Blanchet et Davison, 2011] et des chutes de neige extrêmes [Gaume *et al.*, 2013]. Les maxima hivernaux sont modélisés par la loi GEV tandis que leur structure de dépendance spatiale est modélisée par le processus max-stable.

Dans cette contribution, nous abordons deux aspects de la modélisation statistique de la dépendance spatiale des extrêmes neigeux à travers le cadre des processus max-stables. Premièrement, la sélection de modèles qui est une question importante du fait de nombreux modèles de processus max-stables disponibles dans la littérature. Ensuite, la non-stationnarité temporelle de la dépendance spatiale qui, malgré le contexte actuel désormais bien établi de changement climatique, n'a jamais été étudiée jusqu'ici. Nous commençons par introduire les processus max-stables. Puis nous présentons les deux jeux de données utilisés. Ensuite, nous proposons une procédure de validation croisée adaptée à l'évaluation de la capacité des processus max-stables à prédire la structure de dépendance spatiale des extrêmes. Nous continuons en exposant une approche pour mettre en évidence les tendances temporelles dans la dépendance spatiale des maxima de chutes de neige. Enfin, nous montrons comment modéliser les tendances temporelles dans une structure de dépendance spatiale avec une application aux maxima de hauteurs de neige.

# II THEORIE DES VALEURS EXTREMES DANS LE CAS SPATIAL

## II.1 Loi GEV

On s'intéresse à la variable $Y(x)$ du maximum hivernal de neige (chutes ou hauteurs) en une localisation $x$ des Alpes françaises. Grâce à la théorie des valeurs extrêmes [Coles, 2001] nous savons que nous pouvons modéliser $Y(x)$ par une loi GEV( $\mu(x), \sigma(x), \xi(x)$ ), dont la fonction de répartition est

$$P(Y(x) \le y) = F_{\mu(x),\sigma(x),\xi(x)}(y) = \exp\left\{-\left[1+\xi(x)\left(\frac{y-\mu(x)}{\sigma(x)}\right)\right]^{-1/\xi(x)}\right\}, \qquad (1)$$

où $\mu(x)$, $\sigma(x)$ et $\xi(x)$ sont respectivement les paramètres de position, d'échelle et de forme et telle que $1+\xi(x)\left(\frac{z-\mu(x)}{\sigma(x)}\right) > 0$ . La fonction $F_{\mu(x),\sigma(x),\xi(x)}$ est nulle lorsque $\xi(x) > 0$ et $y \le \mu(x) - \frac{\sigma(x)}{\xi(x)}$ et égale à 1 si $\xi(x) < 0$ et $y \ge \mu(x) - \frac{\sigma(x)}{\xi(x)}$ .

Pour plus de commodité, il est possible de standardiser $Y(x)$ en distribution Fréchet unitaire (c'est-à-dire GEV(1,1,1)) en utilisant la transformation

$$Z(x) = \frac{-1}{\log\left\{F_{\mu(x),\sigma(x),\xi(x)}(Y(x))\right\}} \tag{2}$$

ce que nous ferons systématiquement dans cet article.

### II.2 Processus max-stables

Le processus $\{Z(x)\}_{x\in\chi}$ des maxima standardisés en Fréchet unitaire peut être modélisé par un processus max-stable [de Haan, 1984]. Les processus max-stables généralisent la théorie des valeurs extrêmes au cas spatial en modélisant la structure de dépendance entre les maxima $Z(x)$. Il existe plusieurs modèles de processus max-stables, chaque modèle représentant une manière spécifique de modéliser la dépendance spatiale. Par exemple, pour le processus de Brown-Resnick [Kabluchlo *et al.*, 2009], l'expression de la loi bivariée pour $Z(x_1)$ et $Z(x_2)$ (où $x_1$ et $x_2$ sont deux positions) est donnée par

$$P(Z(x_1) < z_1, Z(x_2) < z_2) = \exp\left\{-\frac{1}{z_1}\Phi\left(\frac{a}{2}+\frac{1}{a}\log\frac{z_2}{z_1}\right)-\frac{1}{z_2}\Phi\left(\frac{a}{2}+\frac{1}{a}\log\frac{z_1}{z_2}\right)\right\} \tag{3}$$

où $\phi$ désigne la fonction de répartition de la loi normale standard et $a=\sqrt{2\gamma(h)}$ avec $\gamma$ le semi-variogramme du processus. Le semi-variogramme puissance $\gamma(h)=(h/\lambda)^{\kappa}$ avec $\lambda$ et $\kappa$ ses paramètres d'amplitude et de forme, est souvent utilisé. Nous nous intéressons aussi dans cet article aux processus de Smith [Smith, 1990], de Schlather [Schlather, 2002], gaussien géométrique [Davison *et al.*, 2012] et extrémal-t [Opitz, 2013] pour lesquels nous avons des expressions analogues à celle indiquée en (3) pour les lois bivariées.

L'anisotropie est prise en compte à travers une transformation spatiale. Par exemple, en dimension 3, nous remplaçons les coordonnées de $x$ par $x'=Vx$ avec

$$V = \begin{pmatrix} \cos\psi & -\sin\psi & 0 \\ w_1^{-1}\sin\psi & w_1^{-1}\cos\psi & 0 \\ 0 & 0 & w_2 \end{pmatrix} \tag{4}$$

avec $\psi \in [0,\pi)$ l'angle d'anisotropie (qui correspond à l'angle de plus forte dépendance), $w_1 > 1$ le ratio d'anisotropie et $w_2 > 0$ le poids pour l'altitude. La distance euclidienne calculée après une telle transformation est appelée distance 2-D modifiée ou distance 3-D modifiée, selon que la dimension verticale soit considérée ou non.

### II.3 Coefficient extrémal, fonction extrémale et portée de la dépendance extrémale

La dépendance extrémale entre les deux variables aléatoires $Z(x_1)$ et $Z(x_2)$ de loi Fréchet unitaire peut être mesurée avec le coefficient extrémal $\theta$ [Schlather et Tawn, 2003 ; Naveau *et al.*, 2009] défini par

$$P(Z(x_1) < z, Z(x_2) < z) = \exp\left\{\frac{-\theta}{z}\right\} = P\{Z(x_1) < z\}^{\theta}, \quad z > 0. \tag{5}$$

Le coefficient extrémal est compris entre 1 (dépendance complète) et 2 (indépendance). Ainsi, plus le coefficient extrémal est proche de 1, plus la dépendance extrémale en $x_1$ et $x_2$ est importante, c'est-à-dire que les maxima les plus forts ont tendance à avoir lieu durant le même hiver en $x_1$ et $x_2$.

Pour chacun des processus max-stables indiqués précédemment, nous avons une expression du coefficient extrémal $\theta(h)$ en fonction de la distance $h$ entre $x_1$ et $x_2$. $\theta(h)$ représente ainsi la force de la dépendance extrémale en fonction de la distance et est appelée fonction extrémale. Nous avons par exemple pour le processus de Brown-Resnick $\theta(h) = 2\phi(a/2)$.

Nous définissons la portée de la dépendance extrémale comme la distance $h_0$ telle que $\theta(h_0) = 1.9$. La portée désigne la distance à partir de laquelle les extrêmes sont quasi indépendants.

# III JEUX DE DONNEES

## III.1 Maxima hivernaux de chutes et de hauteurs de neige dans les Alpes françaises

Le premier jeu de données que nous utilisons est composé de cumuls de chutes de neige sur 3 jours (durée la plus usuelle des tempêtes hivernales dans les Alpes françaises [Bocchiola *et al.*, 2006 ; Eckert *et al.*, 2010, 2011 ; Gaume *et al.*, 2012]) mesurés sur 90 stations de 1958 à 2013 (Figure 1 (a)). Le second est un jeu de données de hauteurs de neige mesurées sur 82 stations de 1970 à 2013 (Figure 1 (b)). On considère les maxima hivernaux avec une période hivernale définie du 15 novembre au 15 mai. Afin de ne considérer que la structure de dépendance spatiale, la loi GEV est ajustée ponctuellement à ces maxima par maximum de vraisemblance. Chaque distribution locale est ensuite transformée en Fréchet unité via la transformation (2).

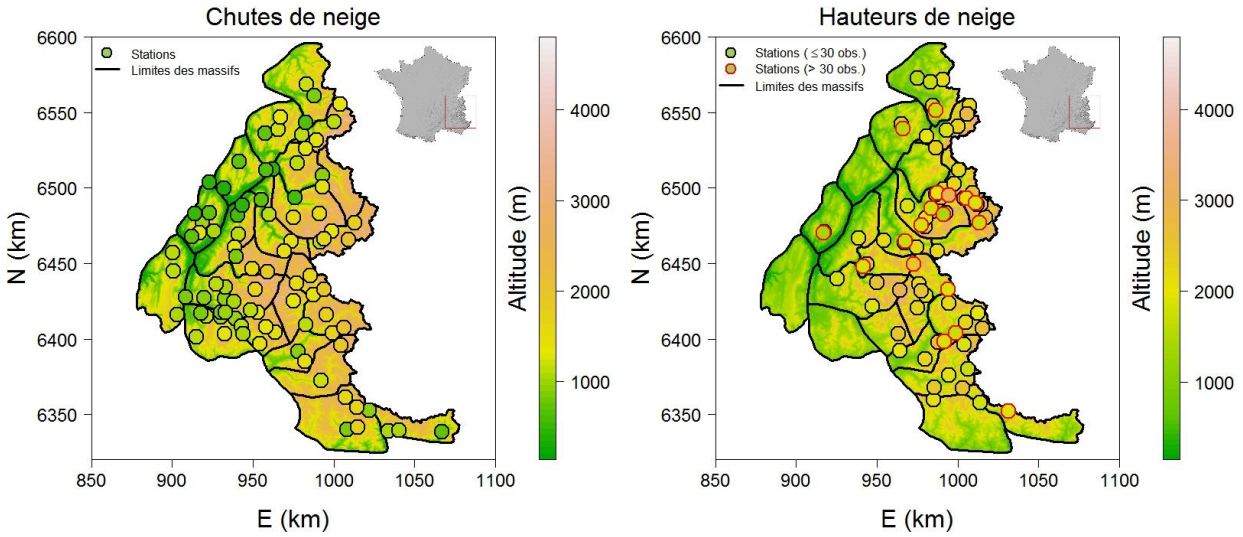


**Figure 1 :** Zone d'étude dans le sud-est de la France avec les 23 massifs des Alpes françaises et les stations concernant les chutes de neige (à gauche) et les hauteurs de neige (à droite). Les lignes délimitent les massifs et les points indiquent les stations. Dans le jeu de données concernant les hauteurs de neige, les stations avec au moins 30 maxima sont indiquées en rouge.

## III.2 Variables locales et synoptiques

Afin d'étudier l'influence du climat sur la dépendance spatiale des extrêmes de neige, nous considérons plusieurs variables représentant plusieurs aspects du climat hivernal des Alpes françaises. Les variables locales considérées sont le cumul hivernal de chutes de neige, la moyenne de l'équivalent en eau de neige (masse totale de neige par unité de surface), le ratio neige/précipitation (cumul de précipitation neigeuse divisé par le cumul de précipitation totale) et la température (minimum, moyenne et maximum quotidiens). Ces variables sont disponibles à travers des réanalyses nivo-météorologiques SAFRAN - Crocus [Durand *et al.*, 2009a, 2009b] pour chacun des massifs. Afin d'avoir une valeur globale pour les Alpes et nonobstant leur

variabilité inter-massifs, nous considérons leurs moyennes sur les massifs à 2 altitudes : 1800 m et 2400 m.

Puisque le climat hivernal des Alpes françaises est surtout influencé par des flux venant de l'Atlantique nord, nous considérons aussi les indices NAO (Oscillation Nord Atlantique [Jones *et al.*, 1997 ; Osborn, 2006]) et AMO (Oscillation Atlantique Multidécennale [Kaplan *et al.*, 1998 ; Enfield *et al.*, 2001]). Nous utilisons la version non stationnarisée de l'AMO qui inclut le récent réchauffement climatique [Kaplan *et al.*, 1998].

Nous considérons les moyennes hivernales de chacune de ces variables locales et synoptiques.

## IV SELECTION DE PROCESSUS MAX-STABLES POUR CHUTES DE NEIGE PAR VALIDATION-CROISEE

Comme il existe plusieurs modèles paramétriques max-stables, la question se pose de savoir lequel a la meilleure capacité d'ajustement aux données, ce qui veut dire dans notre cas lequel permet de mieux modéliser la dépendance extrémale d'un jeu de données. Nous proposons un cadre pratique pour discriminer les processus max-stables en évaluant leur capacité à prédire la structure de dépendance spatiale des extrêmes [Nicolet *et al.*, 2017a]. Les processus de Smith, de Schlather, de Brown-Resnick, gaussien géométrique et extrémal-t ont été ainsi mis en compétition dans le but de déterminer le meilleur pour prédire la dépendance spatiale des maxima de chutes de neige précédemment introduits. L'ajustement de ces processus max-stables se fait par maximisation de la vraisemblance composite [Padoan *et al.*, 2010]. Les paramétrisations de chacun de ces modèles (par exemple le choix du semi-variogramme dans le processus de Brown-Resnick) ont été préalablement sélectionnées par CLIC (*Composite Likelihood Information Criterion* [Padoan *et al.*, 2010]), qui est un critère de vraisemblance pénalisée analogue à l'AIC dans le cas des vraisemblances composites. La Figure 2 montre les fonctions extrémales issues des modèles considérés. Nous pouvons observer que les fonctions extrémales des modèles extrémal-t, gaussien géométrique et de Brown-Resnick sont proches des moyennes par classes de distances des estimations empiriques du coefficient extrémal, montrant ainsi la qualité de leurs ajustements. En revanche, les fonctions extrémales de Smith et de Schlather sont loin des moyennes par classes de distances.

La sélection de modèle proposée se base sur une procédure de validation-croisée dite *leave-two-out* : pour chaque paire de stations $(x_i, x_j)$, on mesure la qualité de l'estimation de la distribution bivariée de $(Z(x_i), Z(x_j))$ estimée sur les 88 stations restantes. Pour cela, un large panel de critères est introduit. Certains critères se basent sur l'estimation de la probabilité d'excès joints

$$\lambda(x_i, x_j, z_T) = P(Z(x_i) > z_T, Z(x_j) > z_T) \tag{6}$$

où $(x_i, x_j)$ est une paire de stations et $z_T$ le niveau de retour sur $T$ années. L'écart entre les estimations issues des modèles $\lambda_{\text{mod}}(x_i, x_j, z_T)$ et les estimations empiriques $\lambda_{emp}(x_i, x_j, z_T)$ est mesuré à travers la racine carrée de l'erreur quadratique moyenne (critère RMSE), l'erreur absolue moyenne (MAE), la racine carrée de l'erreur normalisée quadratique moyenne (RMSNE), l'erreur normalisée absolue moyenne (MANE) et le coefficient de détermination ($R^2$). D'autres critères sont utilisés : les critères *FF* et $N_T$, utilisés par Garavaglia *et al.* [2011], Renard *et al.* [2013] et Blanchet *et al.* [2015] pour mesurer la fiabilité de l'estimation des distributions univariées, ont été adaptés au cas bivarié en les appliquant au minimum en deux stations $M(i, j) = \min(Z(x_i), Z(x_j))$. Le critère *FF* mesure la qualité de l'estimation de la distribution du maximum de $M(i, j)$ sur l'ensemble des hivers. Le critère $N_T$ se focalise sur le nombre de dépassements du niveau de retour sur $T$ années qui doit suivre une distribution binomiale.

Excepté pour le $R^2$ (plus on est proche de 1, meilleur est le modèle), pour tous ces critères le meilleur modèle est celui qui prend la plus petite valeur.

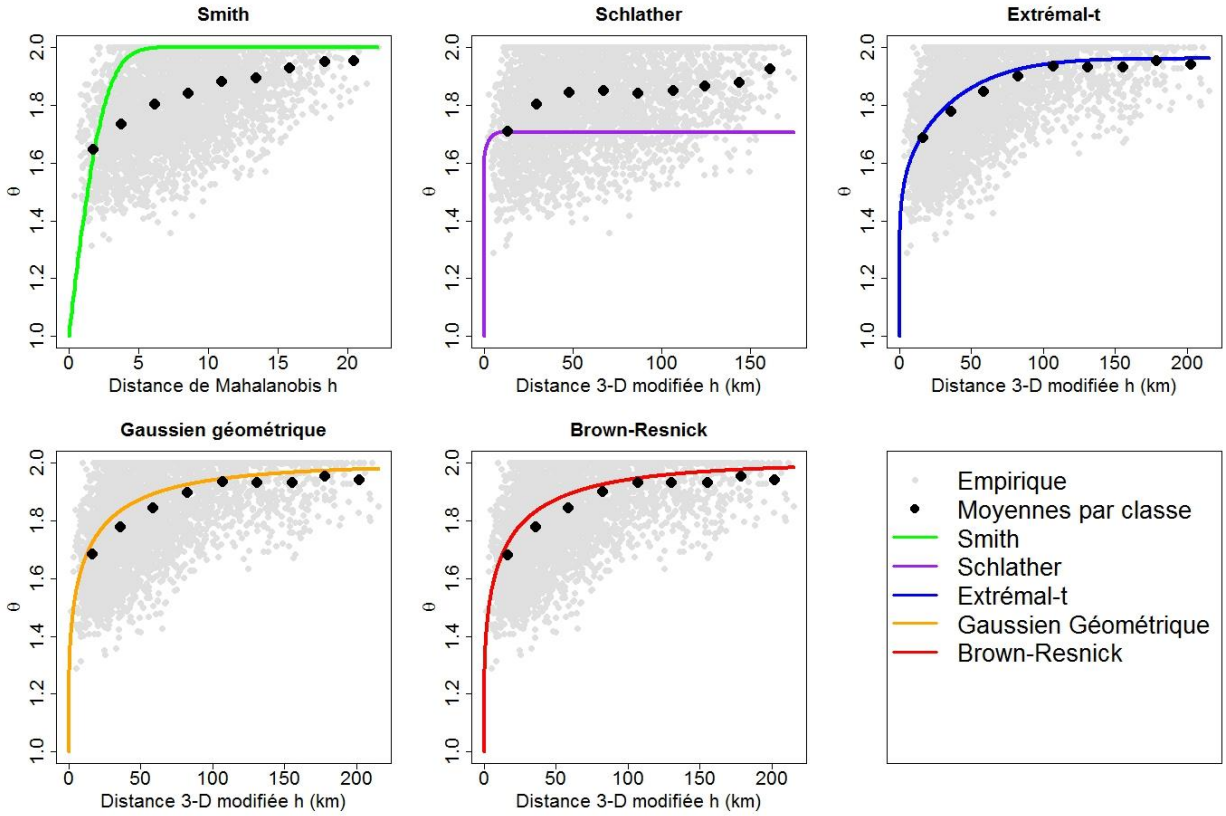


**Figure 2 :** Chutes de neige. Fonctions extrémales issues des processus de Smith, de Schlather, extrémal-t, gaussien géométrique et de Brown-Resnick estimés. Les points gris représentent les estimations empiriques du coefficient extrémal pour toutes les paires de stations. Les points noirs indiquent les moyennes des estimations empiriques par classes de distances.

| Famille | RMSE | MAE | RMSNE | MANE | $R^2$ | $N_{10}$ | $N_{20}$ | FF |
|---|---|---|---|---|---|---|---|---|
| E-t | **0.0242** | 0.0159 | 0.559 | **0.403** | **0.918** | **0.200** | 0.195 | **0.193** |
| GG | 0.0243 | **0.0158** | 0.551 | 0.404 | 0.918 | 0.202 | 0.195 | 0.199 |
| BR | 0.0243 | 0.0158 | **0.550** | 0.404 | 0.918 | 0.201 | **0.195** | 0.199 |
| Sm | 0.0283 | 0.0172 | 0.600 | 0.484 | 0.889 | 0.269 | 0.279 | 0.281 |
| Sc | 0.0308 | 0.0212 | 0.797 | 0.511 | 0.868 | 0.293 | 0.290 | 0.285 |

**Tableau 1 :** Chutes de neige. Validation croisée : critères RMSE, MAE, RMSNE, MANE, $R^2$, $N_T$ avec $T$=10 et $T$=20 et *FF* pour les processus de Schlather (Sc), gaussien géométrique (GG) et extrémal-t (E-t) avec la fonction de corrélation de Gneiting-Matérn pour le processus sous-jacent *W*, le processus de Brown-Resnick (BR) avec le semi-variogramme puissance et le processus de Smith (Sm). Les valeurs en gras indiquent le meilleur modèle pour chaque critère (parfois seulement distinguable au 4ème ou 5ème chiffre significatif).

Les processus de Smith et de Schlather sont surpassés par les autres processus max-stables selon tous les critères (Tableau 1), dû à leur manque de flexibilité. Le processus de Schlather est le moins performant selon tous les critères. Selon les critères RMSE, MANE, $R^2$, $N_{10}$ et *FF* le processus extrémal-t est légèrement meilleur que les processus Brown-Resnick et gaussien géométrique. Cependant, le processus gaussien géométrique a le meilleur MAE et le processus de Brown-Resnick les meilleurs RMSNE et $N_{20}$. Néanmoins, dans tous les cas, les processus extrémal-t, gaussien géométrique et Brown-Resnick fournissent des résultats extrêmement proches. Les performances de ces trois processus max-stables sont similaires quel que soit le nombre de stations et quel que soit le nombre d'années d'observations [Nicolet *et al.*, 2017a].

Les bonnes performances des processus extrémal-t, gaussien géométrique et Brown-Resnick montrent qu'ils sont tous les trois appropriés pour modéliser la dépendance spatiale de nos maxima de chutes de neige. On peut toutefois préférer utiliser le processus de Brown-Resnick qui nécessite l'estimation de moins de paramètres que les deux autres processus.

## V BAISSE DE LA DEPENDENCE SPATIALE DES CHUTES DE NEIGE EXTREMES SUR LES DERNIERES DECENNIES

L'évolution temporelle de la dépendance spatiale des maxima de chutes de neige est quantifiée à travers une approche dite *data-based*, c'est-à-dire en se basant autant que possible sur les données tout en faisant très peu d'hypothèses de modélisation [Nicolet *et al*, 2016]. Ceci a l'avantage de s'assurer que les éventuelles tendances temporelles mises en évidence ne sont pas des conséquences des hypothèses de modélisation. Les seuls choix de modélisation nécessaires sont le modèle de la fonction extrémale, la manière de calculer la distance entre les stations et la stationnarité temporelle des distributions marginales. Nous évoquons ici uniquement les résultats obtenus avec la fonction extrémale de Brown-Resnick, la distance 2-D modifiée et la stationnarité temporelle des distributions marginales, mais d'autres hypothèses ne modifient pas les conclusions.

L'évolution temporelle de la structure de dépendance est mesurée à travers des fenêtres glissantes sur 20 ans (la Figure 3(a) illustre cette approche pour la première fenêtre d'estimation). Pour chacune des fenêtres, le coefficient extrémal est estimé pour chaque paire de stations (en gris sur la Figure 3(a)). La fonction extrémale de Brown-Resnick est ensuite ajustée à ces estimations par moindres carrés (courbe rouge sur la figure). La proximité entre la courbe de la fonction extrémale et les points noirs des moyennes par classes de distance des estimations du coefficient extrémal montre la justesse de l'estimation. On en déduit la portée de la dépendance extrémale qui peut ainsi être calculée pour chaque fenêtre. Par exemple, pour la première fenêtre, nous avons $h_0 = 200\,\text{km}$.

L'anisotropie est préalablement estimée en utilisant toute les données, puis fixée pour chaque fenêtre d'estimation. L'anisotropie estimée ( $\hat{\psi} = 35.84°$ et $\hat{w}_1 = 2.78$ ) montre un angle d'anisotropie qui correspond à l'orientation des principaux massifs et des principales vallées dans les Alpes françaises. Ce phénomène s'explique par l'effet de l'orographie sur les flux atmosphériques générant les précipitations extrêmes.

Nous observons une tendance positive du coefficient extrémal pour les larges distances (au-delà de 100 km) et, par conséquent, une tendance temporelle négative dans la dépendance extrémale (Figure 3(b)). La portée de la dépendance extrémale présente une forte tendance négative avec une division par 2 durant la période (Figure 3(c)). La significativité de cette tendance est montrée par les intervalles de confiance à 95% estimés par la méthode delta (propagation de la variance d'estimation). Cependant, la majeure partie de cette baisse est concentrée durant la période 1978-1997 suivie par une relative stabilisation dans les dernières années.

Les corrélations entre la portée de la dépendance extrémale et les moyennes glissantes sur 20 ans (par souci de consistance avec la fenêtre glissante sur 20 ans) des variables locales et synoptiques précédemment introduites permettent d'établir le lien entre l'évolution de la dépendance extrémale des chutes de neige et l'évolution du climat. Une forte corrélation positive existe avec le cumul hivernal de chutes de neige (0.86 à 1800 m et 0.78 à 2400 m), la moyenne en équivalant en eau (0.90 et 0.84) et le ratio neige/précipitation (0.91 et 0.76). La portée de la dépendance extrémale est corrélée négativement avec la température moyenne (-0.90 à 1800 m et -0.92 à 2400 m), l'AMO (-0.86), la NAO (-0.68) et le temps (-0.84). Même si l'importance de

ces corrélations doit être relativisée par le fait que de considérer des moyennes glissantes les augmente, leur forte amplitude reste notable.

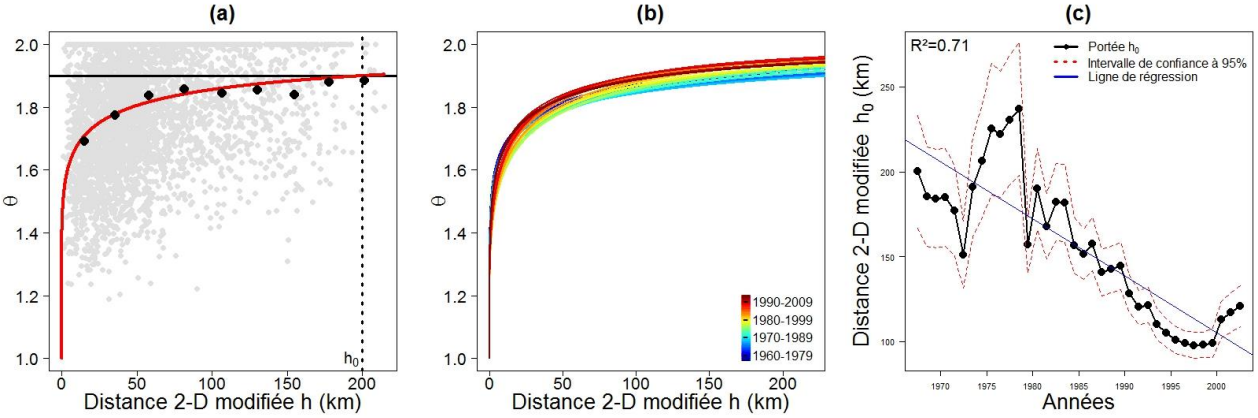


**Figure 3 :** Chutes de neige. (a) Fonction extrémale pour la première fenêtre d'estimation (1958-1977) : estimations du coefficient extrémal pour chaque paires de stations (points gris), moyennes par classes de distance (points noirs) et fonction extrémale de Brown-Resnick ajustée sur les estimations par paires (courbe rouge). La portée de la dépendance extrémale $h_0$ est égale à 200 km. (b) Evolution temporelle de la fonction extrémale de Brown-Resnick, des fenêtres d'estimation les plus anciennes (en bleu) jusqu'aux plus récentes (en rouge). (c) Evolution temporelle de la portée de la dépendance extrémale. L'axe des abscisses indique le centre de la fenêtre d'estimation. L'intervalle de confiance à 95% est calculé par la méthode delta.

Les corrélations négatives entre la portée de la dépendance extrémale et les variables liées à la température (température moyenne à l'échelle des Alpes françaises et AMO qui se réfère à la température de la surface de la mer dans le nord de l'Océan Atlantique) montrent que la dépendance des extrêmes de chutes de neige est plus faible lorsque les températures hivernales sont plus hautes. De plus, la période de plus forte baisse de la portée de la dépendance extrémale est concomitante non seulement avec celle de plus forte croissante de température moyenne, mais aussi avec celle de plus forte décroissance du ratio neige/précipitation [Nicolet *et al.*, 2016]. Ceci nous indique que la baisse de la dépendance spatiale des maxima de chutes de neige serait due en premier lieu à la baisse du ratio neige/pluie provoquée par l'augmentation de la température, en particulier dans le contexte de changement de régime climatique des années 1980 [Reid *et al.*, 2015]. Cette baisse du ratio neige/pluie rend les chutes de neige extrêmes plus isolées spatialement avec l'augmentation d'événements avec des chutes de neige pour les stations les plus hautes et de la pluie pour les stations de basse altitude.

Il semble également y avoir un effet d'intensité avec une dépendance extrémale plus forte durant les hivers les plus neigeux. En effet, la portée de la dépendance extrémale reste très corrélée avec les variables de neige (cumul de chutes de neige et neige en équivalent en eau) à 2400 m, alors que le ratio neige/précipitation est proche de 1 durant toute la période d'étude. Cela est cohérent avec la corrélation négative avec la NAO car une NAO négative dans les Alpes de l'ouest est associée avec des hivers plus froids mais aussi avec des chutes de neige plus intenses.

## VI MODELISATION DE TENDANCES TEMPORELLES DANS LA DEPENDANCE SPATIALE DES HAUTEURS DE NEIGE EXTREMES

Nous montrons dans cette partie comment modéliser d'éventuelles tendances temporelles dans une dépendance spatiale avec une application aux hauteurs de neige [Nicolet *et al*, 2017b]. Le principe de cette méthode consiste à modéliser des tendances dans la structure de dépendance d'un processus de Brown-Resnick avec des covariables appropriées. Les covariables utilisées

sont le temps, l'AMO, la NAO, la température (minimum, moyenne et maximum quotidiens), le cumul hivernal de chutes de neige et le ratio neige précipitation, toutes considérées à travers leurs moyennes mobiles sur 17 ans. Les tendances sont linéaires pour les deux paramètres $\lambda$ et $\kappa$ du semi-variogramme. Nous considérons tous les modèles possibles avec une ou deux covariables, excepté ceux associant des paires de covariables montrant une corrélation supérieure à 0.8.

Le processus de Brown-Resnick est préalablement ajusté avec une hypothèse stationnaire afin d'estimer les paramètres d'anisotropie. Comme dans le cas des chutes de neige, l'angle d'anisotropie estimé $\hat{\psi} = 51.52°$ correspond à l'orientation des principaux massifs et des principales vallées dans les Alpes françaises. La dépendance spatiale de ces deux variables est donc impactée de manière assez similaire par l'orographie. Par contre, l'anisotropie est un peu moins marquée dans le cas des hauteurs de neige ($\hat{w}_1 = 1.79$) et l'effet de l'altitude est plus faible ($\hat{w}_2 = 36.66$). On constate aussi que la dépendance spatiale des hauteurs de neige est plus forte (Figure 4(a)). Cela est dû aux effets cumulatifs impliqués dans la formation du manteau neigeux qui rendent plus lisse l'évolution spatiale des hauteurs de neige.

Les modèles non-stationnaires sont ajustés par vraisemblance composite et sélectionnés par CLIC. Le meilleur modèle avec une covariable est celui utilisant le cumul de chutes de neige à 1800 m (Figure 4(b)). La deuxième covariable la plus efficace est le ratio neige précipitation à 1800 m et la troisème est le cumul de chutes de neige à 2400 m. Les quatre autres modèles qui surpassent le modèle stationnaire sont ceux utilisant les températures moyenne et maximum (à 1800 m et à 2400 m). L'inefficacité du ratio neige précipitation à 2400 m peut être expliquée par le fait qu'à cette altitude, le ratio est proche de 1 durant toute la période d'étude. Aucun modèle avec deux covariables ne surpasse le modèle utilisant le cumul de chutes de neige à 1800 m comme seule covariable et qui est donc le meilleur modèle [Nicolet *et al.*, 2017b].

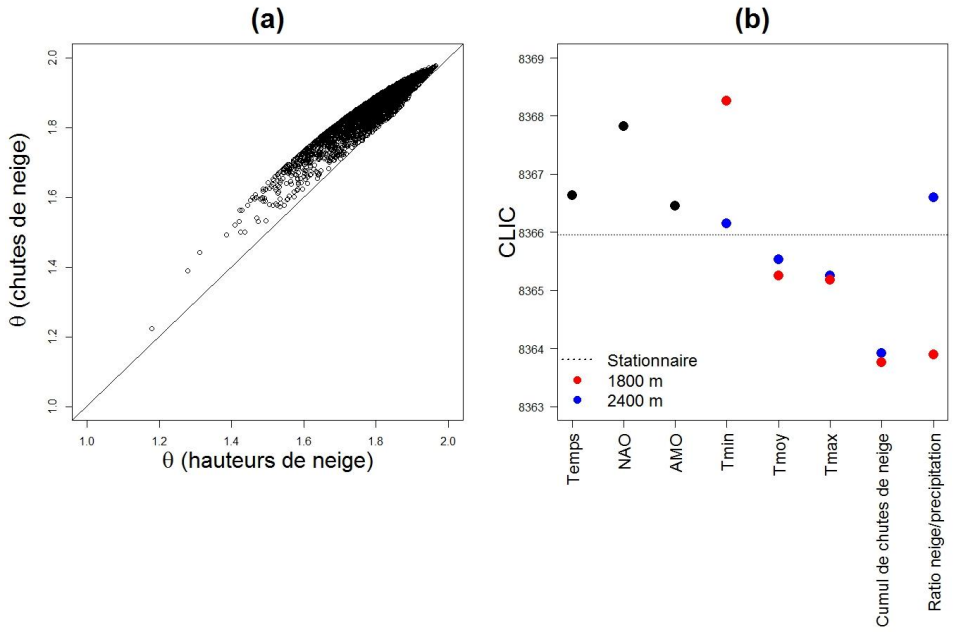


**Figure 4 :** Hauteurs de neige. (a) Comparaison entre les estimations du coefficient extrémal pour les hauteurs de neige et pour les chutes de neige. Ces estimations sont calculées pour toutes les paires de stations du jeu de données sur les hauteurs de neige. (b) CLIC pour les modèles non-stationnaires avec une covariable. Les covariables sont le temps, la NAO, l'AMO, les températures minimale, moyenne et maximale quotidiennes (Tmin, Tmoy et Tmax, respectivement), le cumul hivernal de chutes de neige et le ratio neige/précipitation. Les températures, le cumul de chutes de neige et le ratio neige/ précipitation sont considérées à deux altitudes : à 1800 m (en rouge) et à 2400 m (en bleu).

La fonction extrémale issue du meilleur modèle montre une tendance temporelle positive du coefficient extrémal pour les distances supérieures à 50 km (Figure 5(a)), et donc une baisse de la dépendance extrémale. L'évolution temporelle de la portée de la dépendance extrémale montre une très forte baisse dans les années 1980, puis une stabilisation après 1990 (Figure 5(b)). Les estimations très larges de la portée de la dépendance extrémale au début de la période d'étude doivent être interprétées avec précaution du fait du manque d'observation avant 1983. Néanmoins l'évolution temporelle de la portée de la dépendance extrémale des maxima de hauteurs de neige apparait donc extrêmement similaire à celle concernant les maxima de chutes de neige. Les meilleures covariables (cumuls de chutes de neige, ratio neige précipitation à 1800 m, températures moyenne et maximum) suggèrent des causes identiques. La baisse de la dépendance des hauteurs de neige extrêmes est due tout d'abord à l'effet de l'augmentation de la température sur la phase (neige ou pluie) de la précipitation. Il y a ensuite un effet d'intensité, avec moins de dépendance spatiale lorsque le cumul de chutes de neige décroit, que l'on peut observer quand la fonction extrémale est représentée en fonction du cumul de neige à 1800 m (Figure 5(c)).

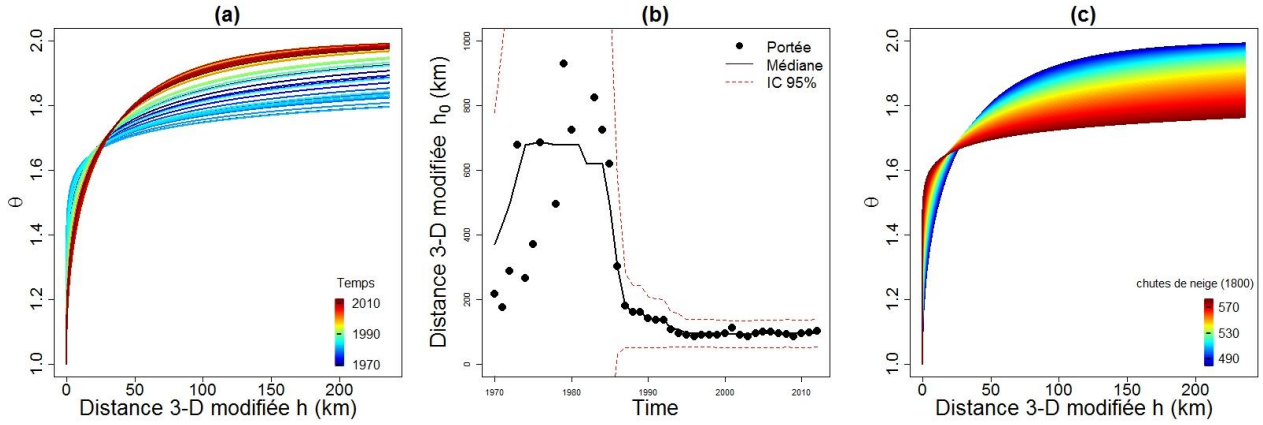


**Figure 5 :** Hauteurs de neige. Modèle sélectionné par CLIC avec le cumul de chutes de neige à 1800 m comme covariable. (a) Evolution temporelle de la fonction extrémale issue du modèle. (b) Evolution temporelle de la portée de la dépendance extrémale calculée sur des fenêtres glissantes de 17 ans. La ligne pleine représente la médiane glissante sur 17 ans de la portée. (c) Evolution de la fonction extrémale en fonction du cumul hivernal de chutes de neige à 1800 m.

## VII CONCLUSION

Cet article a abordé deux problématiques concernant la modélisation statistique de la dépendance spatiale des extrêmes de neige dans les Alpes françaises à travers le cadre des processus max-stables : la sélection de modèles et la non-stationnarité temporelle. Nous avons présenté une vue d'ensemble des méthodes et des conclusions issues des articles Nicolet *et al.* [2016, 2017a, 2017b] produits dans le cadre d'une thèse de doctorat. Cet article porte ainsi à la connaissance de la communauté hydrologique d'une manière unifiée et synthétique des résultats et un formalisme présentant un fort intérêt pour elle.

Nous avons introduit une procédure de validation croisée qui a permis de montrer que les processus gaussien géométrique, de Brown-Resnick et extrémal-t sont tous trois capables de prédire la dépendance spatiale des chutes de neige extrêmes. En revanche, les processus de Smith et de Schlather montrent de moins bons résultats à cause de leur manque de flexibilité.

A travers une approche dite *data-based*, nous avons mis en évidence une baisse de la dépendance spatiale des chutes de neige extrêmes dans les années 1980. Puis, nous avons montré comment des tendances temporelles dans une dépendance spatiale peuvent être modélisées en appliquant cette approche aux hauteurs de neige extrêmes. Cela a montré une baisse de la

dépendance spatiale similaire à celle concernant les chutes de neige extrêmes. Ces deux baisses sont causées par l'impact de la hausse de la température sur la phase (pluie ou neige) de la précipitation ainsi que par la baisse du cumul hivernal de neige.

Nous avons montré en outre que la dépendance spatiale de ces deux variables est fortement influencée par l'orographie avec une plus forte dépendance dans la direction des principaux massifs et vallées. Par contre, la dépendance spatiale est plus forte pour les hauteurs de neige extrêmes que pour les chutes de neige extrêmes à cause des effets cumulatifs impliqués dans la formation du manteau neigeux.

L'approche adoptée dans cette étude est nouvelle, et notamment concernant la mise en évidence et la modélisation de tendances temporelles dans la dépendance spatiale des extrêmes neigeux. Cette problématique peut concerner les extrêmes de toutes les variables potentiellement impactées par le changement climatique. Des approches similaires appliquées dans d'autres contextes pourraient être intéressantes pour anticiper l'évolution de certains risques naturels sous l'effet du changement climatique. Elles permettront peut-être de généraliser les conclusions obtenues, tant du point de vue de la capacité prédictive respective des modèles max-stables considérés que de l'évolution temporelle de la dépendance spatiale des extrêmes climatiques.

## VIII REMERCIEMENTS

Nous remercions le LabEx OSUG@2020 (Investissements d'avenir – ANR10 LABX56) pour sa participation au financement de la thèse du premier auteur. Nous remercions les centaines d'observateurs de la neige et le personnel de Météo France impliqué dans la collecte et la constitution des jeux de données utilisés.

## IX REFERENCES

Blanchet, J., Davison, A. C. (2011). Spatial modeling of extreme snow depth. *The Annals of Applied Statistics*, pages 1699–1725.

Blanchet, J., Touati, J., Lawrence, D., Garavaglia, F., Paquet, E. (2015). Evaluation of a compound distribution based on weather pattern subsampling for extreme rainfall in Norway. *Natural Hazards, Earth System Sciences*, 15(12):2653–2667.

Bocchiola, D., Medagliani, M., Rosso, R. (2006). Regional snow depth frequency curves for avalanche hazard mapping in central Italian Alps. *Cold Regions Science and Technology*, 46(3):204–221.

Coles, S. (2001). *An Introduction to Statistical Modeling of Extreme Values*. Springer, London.

Davison, A. C., Padoan, S. A., Ribatet, M. (2012). Statistical modeling of spatial extremes. *Statistical science*, 27(2):161–186.

de Haan, L. (1984). A spectral representation for max-stable processes. *The annals of probability*, 12(4):1194–1204.

Durand, Y., Giraud, G., Laternser, M., Etchevers, P., Mérindol, L., Lesaffre, B. (2009a). Reanalysis of 47 years of climate in the French Alps (1958-2005): Climatology, trends for snow cover. *Journal of applied meteorology, climatology*, 48(12):2487–2512.

Durand, Y., Laternser, M., Giraud, G., Etchevers, P., Lesaffre, B., Mérindol, L. (2009b). Reanalysis of 44 yr of climate in the French Alps (1958-2002): Methodology, model validation, climatology, trends for air temperature, precipitation. *Journal of Applied Meteorology, Climatology*, 48(3):429–449.

Eckert, N., Coleou, C., Castebrunet, H., Deschatres, M., Giraud, G., Gaume, J. (2010). Cross-comparison of meteorological, avalanche data for characterising avalanche cycles: the example of December 2008 in the eastern part of the French Alps. *Cold Regions Science, Technology*, 64(2):119–136.

Enfield, D., Mestas-Nunez, A., Trimble, P. (2001). The Atlantic multidecadal oscillation, its relation to rainfall, river flows in the continental U.S. *Geophysical Research Letters*, 28(10):2077–2080.

Garavaglia, F., Lang, M., Paquet, E., Gailhard, J., Garçon, R., Renard, B. (2011). Reliability, robustness of rainfall compound distribution model based on weather pattern sub-sampling. *Hydrology, Earth System Sciences Discussions*, 15:519–532.

Gaume, J., Chambon, G., Eckert, N., Naaim, M. (2012). Relative influence of mechanical and meteorological factors on avalanche release depth distributions: An application to French Alps. *Geophysical Research Letters*, 39(12).

Gaume, J., Eckert, N., Chambon, G., Naaim, M., Bel, L. (2013). Mapping extreme snowfalls in the French Alps using max-stable processes. *Water Resources Research*, 49(2):1079–1098.

[Gumbel, E. (1958). *Statistics of extremes*. Columbia University Press, New York.

Jones, P. D., Jonsson, T., Wheeler, D. (1997). Extension to the North Atlantic Oscillation using early instrumental pressure observations from Gibraltar, South-West Iceland. *International Journal of climatology*, 17(13):1433–1450.

Kabluchko, Z., Schlather, M., de Haan, L. (2009). Stationary max-stable fields associated to negative definite functions. *The Annals of Probability*, 37(5):2042–2065.

Kaplan, A., Cane, M., Kushnir, Y., Clement, A., Blumenthal, M., Rajagopalan, B. (1998). Analyses of global sea surface temperature 1856-1991. *Journal of Geophysical Research: Oceans*, 103(18):567–18.

Naveau, P., Guillou, A., Cooley, D., Diebolt, J. (2009). Modelling pairwise dependence of maxima in space. *Biometrika*, 96(1):1–17.

Nicolet, G., Eckert, N., Morin, S., Blanchet, J. (2016). Decreasing spatial dependence in extreme snowfall in the French Alps since 1958 under climate change. *Journal of Geophysical Research: Atmospheres*, 121(14):8297–8310.

Nicolet, G., Eckert, N., Morin, S., Blanchet, J. (2017a). A multi-criteria leave-two-out cross-validation procedure for max-stable process selection. Soumis pour publication.

Nicolet, G., Eckert, N., Morin, S., Blanchet, J. (2017b). Modeling the trend in the spatial dependence of extremes: application to climate change impacts on snow depth maxima in the French Alps. Soumis pour publication.

Opitz, T. (2013). Extremal t processes: Elliptical domain of attraction, a spectral representation. *Journal of Multivariate Analysis*, 122:409–413.

Osborn, T. J. (2006). Recent variations in the winter North Atlantic Oscillation. *Weather*, 61(12):353–355.

Padoan, S. A., Ribatet, M., Sisson, S. A. (2010). Likelihood-based inference for max-stable processes. *Journal of the American Statistical Association*, 105(489)(489):263–277.

Reid, P. C., Hari, R. E., Beaugrand, G., Livingstone, D. M., Marty, C., Straile, D., Barichivich, J., Goberville, E., Adrian, R., Aono, Y., et al. (2015). Global impacts of the 1980s regime shift. *Global change biology*.

Renard, B., Kochanek, K., Lang, M., Garavaglia, F., Paquet, E., Neppel, L., Najib, K., Carreau, J., Arnaud, P., Aubert, Y., et al. (2013). Data-based comparison of frequency analysis methods: A general framework. *Water Resources Research*, 49(2):825–843.

Schlather, M. (2002). Models for stationary max-stable random fields. *Extremes*, 5(1):33–44.

Schlather, M., Tawn, J. A. (2003). A dependence measure for multivariate, spatial extreme values: Properties, inference. *Biometrika*, 90(1):139–156.

Smith, R. L. (1990). Max-stable processes, spatial extremes. [Disponible à http://www.stat.unc.edu/postscript/rs/spatex.pdf].

# Contents

**Remerciements** **v**

**Abstract** **vii**

**Résumé étendu** **ix**

**List of figures** **xxxi**

**List of tables** **xxxiii**

**Introduction** **1**

Motivation . . . . . 3

Extreme value theory . . . . . 3

Snow extremes . . . . . 3

Max-stable processes . . . . . 4

Models of max-stable processes . . . . . 7

Temporal nonstationarity in max-stable processes . . . . . 8

Outline of this thesis . . . . . 12

Main objectives . . . . . 12

Detailed overview . . . . . 13

**1 State of the art of the mathematical tools used in this thesis** **17**

1.1 Introduction . . . . . 19

1.2 Extreme value theory . . . . . 19

1.2.1 Univariate case . . . . . 19

1.2.2 Bivariate case . . . . . 21

1.3 Geostatistics . . . . . 24

1.3.1 Gaussian process . . . . . 24

1.3.2 Correlation function . . . . . 24
1.3.3 Semivariogram . . . . . 28
1.4 Max-stable processes . . . . . 28
1.4.1 Definition . . . . . 28
1.4.2 De Haan's spectral representation . . . . . 30
1.4.3 Extremal function . . . . . 30
1.4.4 Max-stable models . . . . . 31
1.4.5 Anisotropy . . . . . 39
1.4.6 Max-stable models inference and selection . . . . . 40

**2 A multi-criteria leave-two-out cross-validation procedure for max-stable process selection 43**
Abstract . . . . . 45
2.1 Introduction . . . . . 46
2.2 Data . . . . . 49
2.3 Method . . . . . 49
2.3.1 Max-stable processes . . . . . 49
2.3.2 Model comparison criteria . . . . . 53
2.3.3 Workflow . . . . . 56
2.4 Results . . . . . 58
2.4.1 Model preselection with CLIC . . . . . 58
2.4.2 Cross-validation . . . . . 58
2.4.3 Sensitivity to the number of stations and to the number of years . . 59
2.5 Discussion and conclusion . . . . . 61
Appendix A $N_T$ and *FF* criteria . . . . . 67
A.1 $N_T$ and *FF* criteria in the univariate case . . . . . 67
A.2 $N_T$ criterion in the bivariate case . . . . . 67
A.3 *FF* criterion in the bivariate case . . . . . 68
Appendix B Semivariograms and correlation functions used in this work . . . 69
Appendix C Model preselection with CLIC . . . . . 70
Appendix D The parameters of the five retained models for cross-validation . 73
Appendix E Comparison of the models for specific return periods . . . . . 73

**3 Decreasing spatial dependence in extreme snowfall in the French Alps since 1958 under climate change 77**
Abstract . . . . . 79

3.1 Introduction . . . . . 80
3.2 Data . . . . . 82
3.2.1 Winter maximum snowfall in the French Alps . . . . . 82
3.2.2 Local and synoptic variables . . . . . 82
3.3 Methods . . . . . 85
3.3.1 Extreme value statistics in the univariate case and standardization of snowfall maxima . . . . . 85
3.3.2 Extreme value statistics in the spatial case . . . . . 86
3.3.3 Extremal coefficient and extremal function . . . . . 87
3.3.4 Anisotropy and distances . . . . . 88
3.3.5 Estimation of the extremal dependence over moving time windows 90
3.3.6 Range of extremal dependence . . . . . 91
3.4 Results and discussion . . . . . 93
3.4.1 Local and synoptic variables . . . . . 93
3.4.2 Results using the entire study period . . . . . 95
3.4.3 Results using moving time windows . . . . . 96
3.5 Conclusion and outlook . . . . . 101

**4 Modeling the trend in the spatial dependence of extremes: application to the assessment of climate change impact on snow depth maxima in the French Alps 103**
Abstract . . . . . 105
4.1 Introduction . . . . . 106
4.2 Data set . . . . . 108
4.2.1 Snow Depths . . . . . 108
4.2.2 Covariates . . . . . 110
4.3 Method . . . . . 113
4.3.1 Brown-Resnick Max-Stable Process . . . . . 113
4.3.2 Inference and Model Selection . . . . . 116
4.4 Workflow . . . . . 118
4.4.1 Standardization into Unit Fréchet . . . . . 118
4.4.2 Stationary Case . . . . . 118
4.4.3 Moving Time Window . . . . . 119
4.4.4 Nonstationary Case . . . . . 120
4.4.5 Alternative Composite Likelihood . . . . . 120
4.5 Results . . . . . 120

4.5.1 Stationary Case . . . . . 120
4.5.2 Time Moving Window . . . . . 120
4.5.3 Nonstationary Brown-Resnick Model . . . . . 122
4.5.4 Alternative Composite Likelihood . . . . . 127
4.6 Discussion . . . . . 127
4.6.1 Anisotropy in the Spatial Dependence and Comparison with Extreme Snowfall . . . . . 127
4.6.2 Temporal Changes . . . . . 131
4.6.3 Climate Control . . . . . 131
4.6.4 Pros and Cons of the Proposed Modeling Approach . . . . . 132
4.7 Conclusion and Outlooks . . . . . 133

**Conclusions and perspectives** **135**
Procedure of model selection for max-stable processes . . . . . 137
A leave-two-out cross-validation and a panel of criteria for max-stable processes . . . . . 137
Comparison between five max-stable processes using leave-two-out cross-validation on a case study of snowfall maxima in the French Alps . 138
Temporal evolution of the spatial dependence of extreme snowfall and extreme snow depth . . . . . 139
Data-based approach to investigate temporal evolution of the spatial dependence of geophysical extremes . . . . . 139
Modeling temporal trends in the spatial dependence structure of max-stable processes . . . . . 140
Decreasing spatial dependence in extreme snowfall and extreme snow depths in the French Alps under climate change . . . . . 141
Perspectives . . . . . 142
Cross-validation procedure with other data sets and/or other models of max-stable processes . . . . . 142
Use of threshold-based models . . . . . 143
Temporal evolution of the extremal dependence of other spatial phenomena 143
Marginal distributions and non stationary spatial dependence structure . 144

**Bibliography** **157**

**Appendix I. List of the stations of the snowfall data set** **159**

**Appendix II. List of the stations of the snow depth data set 163**

# List of Figures


1 (Left) 3-day cumulated snowfall during the heavy snow episode from 24 to 26 March 2017 in France. (Right) Snow water equivalent (on the ground) on 29 March 2017 in France. . . . . 5
2 Realizations of (a) a Gaussian process and (b) a max-stable process . . . . 6
3 Realizations of the (a) Smith, (b) Schlather, (c) geometric Gaussian, (d) Brown-Resnick, and (e) extremal-t processes . . . . . 9
4 Five year moving averages of winter maximum snow depth for each massif of French Alps from 1960 to 2010 . . . . . 11
5 Study area in the southeast of France, where the 23 massifs of the French Alps are located. . . . . 14

1.1 Plot of the GEV density function . . . . . 20
1.2 Plot of the correlation functions of Table 1.3.2 . . . . . 26
1.3 Realization of a stationary isotropic Gaussian process . . . . . 27
1.4 Plot of the semivariograms defined in Table 1.2 . . . . . 29
1.5 (a) Extremal function for the Smith process. (b) One realization of the Smith process. . . . . 32
1.6 (a) Extremal function for the Schlather process. (b) One realization of the Schlather process. . . . . 33
1.7 (a) Extremal function for the geometric Gaussian process.(b) One realisation of the geometric Gaussian process. . . . . 35
1.8 (a) Extremal function of Brown-Resnick process. (b) One realization of the Brown-Resnick process. . . . . 36
1.9 (a) Extremal function for the extremal-t process. (b) One realization of the extremal-t process. . . . . 38

2.1 (a) Study area in the southeast of France, where the 23 massifs of the French Alps are located. (b) Data availability for each station. . . . . 50

2.2 Cross-validation. Joint exceedance probability as function of return period for four pair of stations. . . . . 60
2.3 RMSE, MAE, $R^2$, RMSNE, MANE, $N_{10}$, $N_{20}$ and $FF$ criteria according to the number of stations. . . . . 62
2.4 RMSE, MAE, $R^2$, RMSNE, MANE, $N_{10}$, $N_{20}$ and $FF$ criteria according to the number of years. . . . . 63
2.5 Rescaled CLIC for max-stable processes fitted by composite likelihood. . . 71
2.6 Cross-validation. Boxplots of estimates of the probability of exceeding jointly the $T$-year return level ($T = 5, 10, 20, 33$ years) for all pairs of stations. 75
2.7 Cross-validation. RMSE, MAE, RMSNE and MANE as function of return period. . . . . 76

3.1 Study area in the southeast of France, where the 23 massifs of the French Alps are located. . . . . 83
3.2 (a) Data availability for each station. (b) Histogram of station elevation. . 84
3.3 Example of the calculation of the crossing distance . . . . . 90
3.4 Extremal coefficient function for the first (1958-1977) and the last (1993-2012) estimation windows using the modified 2-D distance . . . . . 92
3.5 20-year moving averages of the considered variables: cumulated snowfall, mean snow water equivalent, snow precipitation ratio, and mean temperature . . . . . 94
3.6 Estimated Brown-Resnick, geometric Gaussian and extremal-t extremal functions in the case of the 2-D modified distance . . . . . 95
3.7 (a) Temporal evolution of the fitted Brown-Resnick extremal functions under the 2-D modified distance. (b) Temporal evolution of the range of extremal dependence. . . . . 97
3.8 Same as Figure 3.7(b) with (a) geometric Gaussian extremal function and (b) extremal-t extremal function. . . . . 100
3.9 Same as Figure 3.7(b) when the marginal distributions are estimated and transformed into unit Fréchet on each estimation window. . . . . 100
3.10 Same as Figure 3.7(b) with (a) modified 3-D distance and (b) crossing distance. . . . . 101

4.1 Snow depth data set. (a) Study area in the southeast of France, where the 23 massifs of the French Alps are located. (b) Data availability for each station. (c) Histogram of station elevation. . . . . 109

4.2 The 17-year moving averages of the considered covariates. . . . . 112
4.3 Stationary case. Estimated extremal function in the hypothesis of temporal stationarity. . . . . 121
4.4 Time moving window. (a) Temporal evolution of the fitted extremal functions. (b) Temporal evolution of the range of extremal dependence. (c–d) Temporal evolution of the estimates of $\lambda$ and $\kappa$ . . . . . 123
4.5 Nonstationary Brown-Resnick model: rescaled CLIC for the models using one covariate. . . . . 124
4.6 Nonstationary Brown-Resnick model: rescaled CLIC for the models using two covariates. . . . . 126
4.7 Nonstationary Brown-Resnick model. Model selected by CLIC with cumulated snowfall at 1800 m as covariate. (a) Temporal evolution of the extremal function stemming from the model. (b) Temporal evolution of range of extremal dependence. (c) Evolution of the extremal function as function of cumulated snowfall at 1800. . . . . 128
4.8 Alternative composite likelihood. Model with cumulated snowfall at 1800 m as covariate but maximizing the alternative composite likelihood $\tilde{l}$. (a) Temporal evolution of the extremal function stemming from the model. (b) Temporal evolution of the range of extremal dependence. (c) Evolution of the extremal function as function of cumulated snowfall at 1800 m. . . . 129
4.9 Comparison between snow depth and snowfall model-based estimates of extremal coefficient. . . . . 130

# List of Tables


1.1 Usual correlation functions . . . . . 25
1.2 Usual semivariograms . . . . . 28

2.1 Cross-validation. RMSE, MAE, RMSNE, MANE, $R^2$, $N_{10}$, $N_{20}$ and $FF$ criteria. . . . . 59
2.2 Correlation functions. . . . . 69
2.3 Semivariograms. . . . . 70
2.4 Rescaled CLIC, RMSE, MAE, RMSNE, MANE, $R^2$, $N_{10}$, $N_{20}$ and $FF$ using the full data set for the extremal-t, geometric Gaussian and Schlather processes with the Gneiting-Matérn correlation function, the Brown-Resnick process with the power semivariogram and the Smith process. . . . . 72
2.5 Parameterization of the five studied models. . . . . 73

3.1 Correlation table between the range of dependance and the considered winter climate variables . . . . . 98

4.1 Covariates (Section 4.2.2). Correlation table for the 17-year moving averages of covariates[a] . . . . . 111
4.2 Nonstationary Brown-Resnick model (Section 4.5.3): models with one covariate. Estimated parameters and sign of the contribution to the extremal coefficient $\theta(100)$[a] . . . . . 125

3 List of the stations of the snowfall data set (part 1) . . . . . 160
4 List of the stations of the snowfall data set (part 2) . . . . . 161

5 List of the stations of the snow depth data set (part 1) . . . . . 164
6 List of the stations of the snow depth data set (part 2) . . . . . 165

# Introduction

# Motivation

## Extreme value theory

Extreme events have been attracting a growing interest during these last years, especially as far as financial crashes, floods, heat waves or storms are concerned. Although these events are very rare, their catastrophic consequences make it necessary to have tools which are able to properly measure their probability of occurrence. The main difficulty of this task is the length of the observation records associated to the risk that we want to measure. Indeed, we classically need to assess some events which have never been explicitly measured, typically a 100 year return level with less than 50 years of data. This issue can be addressed by using extreme value theory (Coles, 2001; Beirlant et al., 2004; de Haan and Ferreira, 2006) which offers a suitable framework to extrapolate beyond the highest recorded observations. The two main approaches of extreme value theory are the so-called "block maxima" (Gumbel, 1958) and "peak over threshold" (Pickands, 1975; Davison and Smith, 1990). The first one suggests to model maxima (for instance annual maxima) through the generalized extreme value (GEV) distribution. The second one models the excesses beyond a high threshold by a generalized Pareto distribution (GPD), with the advantage to potentially use more observations than in the "block maxima" approach, but with the drawback of having to deal with temporal effects like seasonality or temporal dependence. Extreme value theory is widely used in hydrology, finance/insurance and climatology to assess the probability of occurrence of extreme events (Finkenstadt and Rootzén, 2003; Reiss and Thomas, 2007; Embrechts et al., 2013).

## Snow extremes

One of the most dangerous hazards in mountainous regions is extreme snow events. Specifically, heavy snowfall and heavy snow depths are crucial for risk management because of their potential economic and human damages. They can cause overloading and collapse of buildings. They can produce subsequent flooding because of snowmelt. When they are combined to unstable snowpack, extreme snow cover and extreme snow precipitation contribute to avalanches, and are thus very relevant for avalanche prevention (Schneebeli and Laternser, 2004; Gaume et al., 2012). Extreme snowfall is often associated to snow storms which can stop road, railway and air traffic. Snow cover is very important for water storage and for the tourism industry, and has a strong impact

on mountain ecosystems (Keller et al., 2005; Wipf et al., 2009). Extreme value statistics have been applied to extreme snow events, for instance to 3-day snowfall in Italian and Swiss Alps (Bocchiola et al., 2006, 2008), to extreme snowfall and extreme snow depth in Switzerland (Blanchet et al., 2009; Blanchet and Lehning, 2010), and to extreme snowfall and avalanche slab depths in the French Alps (Gaume et al., 2012, 2013b).

Figure 1 represents 3-day snowfall during the heavy snow episode from 24 to 26 March 2017 and snow water equivalent (on the ground) on 29 March 2017 in France. There is a strong spatial dependence for the extreme values of snowfall (in green in Figure 1(left)) which do not appear isolated but in cluster. We can observe the same phenomenon for the extreme values of snow winter equivalent (in pink in Figure 1(right)) with a smoother spatial evolution. Extreme snow events do not occur in a unique location only, but in an area where all the locations are impacted. Thus, if an extreme value is observed in a location, it is likely to observe extreme values in neighboring locations. This spatial dependence for extreme values does not concern only snow variables but more generally almost all climate variables, for instance rainfall, temperature or wind. The dependence in extremes (or extremal dependence) is different from the statistical dependence which can be addressed through correlation or semivariogram analyses. The extremal dependence means the tendency of two variables or more to experience extreme values simultaneously. There exist random variables which are dependent strictly speaking but not dependent in extremes and it is even always the case with Gaussian variables. A suitable modeling of climate extremes should take into account this spatial dependence in extremes which can represent a useful part of the information for the evaluation of the risk.

## Max-stable processes

Geostatistics (Cressie, 1993; Diggle and Ribeiro Jr., 2007) is the field of statistics which focuses on spatial data. However, classic geostatistics, usually based on the Gaussian distribution (e.g., Gaussian processes) under which extremes are independent, is not able to model suitably the spatial dependence of extremes.

Max-stable processes (de Haan and Ferreira, 2006) are the generalization of multivariate extreme value theory to the infinite dimension and are mostly used to model spatial extremes. All the margins of max-stable processes (i.e., the random vectors defined by the values taken by the process at a finite number of specific locations) hold the

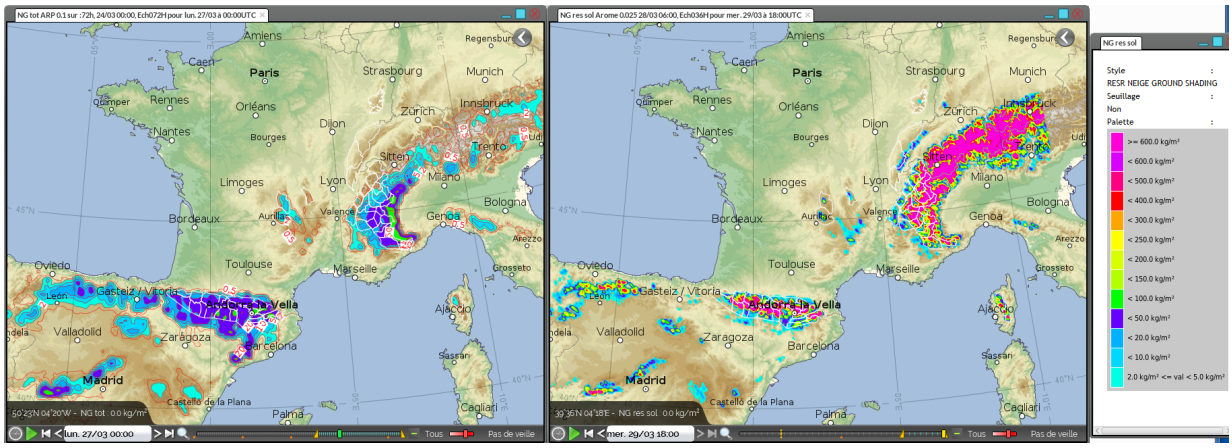


***Figure 1:*** *(Left) 3-day cumulated snowfall during the heavy snow episode from 24 to 26 March 2017 in France calculated by the ARPEGE numerical weather prediction model from Météo-France. (Right) Snow water equivalent (on the ground) on 29 March 2017 in France calculated by the AROME numerical weather prediction model from Météo-France.*

max-stability property. A random vector is called "max-stable" when any maximum of independent copies can be rescaled so as to follow the same distribution of this vector. In the univariate random variable case, to be max-stable and non degenerate is equivalent to follow the GEV distribution.

Figure 2 shows a realization of a Gaussian process and a realization of a max-stable process. In comparison with Gaussian processes, max-stable processes provide realizations which are less smooth and with values far beyond the mean of the spatial field. In a way, max-stable processes connect extreme value statistics and geostatistics by providing models which are able to deal with heavy tailed spatial phenomena.

There exist many advantages of using max-stable processes for a better comprehension of the spatial evolution of the studied variable at extreme level and for a finer assessment of the related risk. Max-stable processes allow to make estimates of joint exceedance probabilities, that is to say the probability of exceeding given very large values in several locations simultaneously. They also allow to estimate conditional exceedance probabilities, for instance the probability of exceeding a large value in a certain location knowing that a large value was exceeded in a second location. These estimations can be

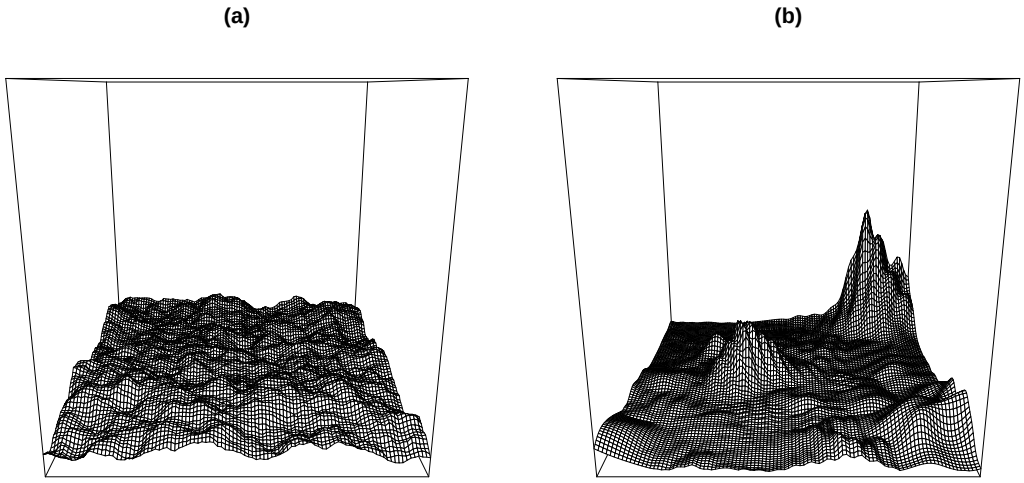


***Figure 2:*** *Realizations of (a) a Gaussian process and (b) a max-stable process on the square* $[0, 10]^2$. *The Gaussian process is a isotropic Gaussian process with zero mean and Whittle-Matérn correlation function with* $\lambda = 1$ *and* $\kappa = 1$. *The max-stable process is a isotropic geometric Gaussian process with Whittle-Matérn correlation function with* $\sigma^2 = 5$, $\lambda = 4$ *and* $\kappa = 1$.

done in the locations where there is no observation and can lead to the construction of return levels maps. Conditional simulations of max-stable processes can be used to make predictions throughout the study area. In addition, there exist a suitable framework for drawing inference using max-stable processes (Padoan et al., 2010).

Max-stable processes have been applied within the fields of geophysical and climate science by Blanchet and Davison (2011) to extreme snow depths in Switzerland, and by Gaume et al. (2012, 2013b) to extreme snowfall and to avalanche slab thicknesses in the French Alps. Furthermore, they were used for extreme temperatures in Korea (Lee et al., 2013), for extreme wind gusts in the Netherlands (Ribatet, 2013), for extreme wave heights in the North Atlantic Ocean (Raillard et al., 2014) and in the Gulf of Lions (Chailan et al., 2014), for extreme precipitation in the South of France (Bechler et al., 2015) and for extreme river discharges in the upper Danube basin (Asadi et al., 2015).

## Models of max-stable processes

Max-stable processes model two features of the studied spatial phenomenon. First, the marginal distributions of extremes, which belongs to the GEV family following the univariate extreme value theory. Second, the structure of spatial dependence which models the behavior of extremes toward each other, and particularly the tendency to occur simultaneously. Marginal distributions and dependence structure can be estimated simultaneously (Gaume et al., 2013b) or in two steps (Blanchet and Davison, 2011).

There is no unique way to model the spatial dependence structure. There exist several models of max-stable process, each one being a specific manner to model this dependence structure. The first two max-stable processes which were introduced are the Smith (Smith, 1990) and Schlather (Schlather, 2002) processes. However, these two models have some major drawbacks. The Smith process provides realizations which are too smooth and as a consequence, usually not realistic for climate variables (Reich and Shaby, 2012; Wadsworth and Tawn, 2012). The Schlather process assumes dependence in extremes at two locations regardless of the distance between them, which is questionable in many cases (Blanchet and Davison, 2011; Davison et al., 2012).

Several new max-stable models were introduced recently to solve these drawbacks. The geometric Gaussian process (Davison et al., 2012) has a similar expression of the bivariate marginal distribution (that is to say the bivariate distribution at two specific locations) than the Smith process, but providing more realistic realizations. The Brown-Resnick process (Kabluchko et al., 2009) is a generalization of the geometric Gaussian process with the possibility to impose extremal dependence between locations which are far apart, which could be a very appealing assumption for the modeling of climate extremes. The extremal-t process (Opitz, 2013) is a generalization of the Schlather process with an additional parameter which controls the strength of the extremal dependence between the most distant locations.

Figure 3 shows realizations of the Smith, Schlather, geometric Gaussian, Brown-Resnick and extremal-t processes. The realization of the Smith process (Figure 3(a)) does not seem realistic for climate variables with the largest values forming perfect ellipses (in yellow and orange). The realization of the Schlather process (Figure 3(b)) is potentially more realistic, but the yellow and orange areas of the largest values extend much, which does not correspond to to highly variable data such as rainfall and snow. The realizations of the geometric Gaussian (Figure 3(c)), Brown-Resnick (Figure 3(d))

and extremal-t (Figure 3(e)) processes avoid these two drawbacks, potentially coping for climate variable data better than in the Smith process case, and allowing areas for the largest values which are more concentrated and less extended than in the Schlather process case.

Padoan et al. (2010) showed how max-stable processes could be fitted using pairwise composite likelihood maximization techniques with an illustration on extreme rainfall in the United States. Castruccio et al. (2016) investigated composite likelihood inference of higher order. The selection between models of max-stable process is usually done through the Composite Likelihood Information Criterion (CLIC) (Padoan et al., 2010) which is the analogous to Akaike Information Criterion (AIC) (Akaike, 1974) in the case of composite likelihood. This way, the Schlather process was found to be more suitable than the Smith process for extreme snow depths in Switzerland (Blanchet and Davison, 2011), the geometric Gaussian and Brown-Resnick processes outperformed the Smith and Schlather processes for extreme rainfall in Switzerland (Davison et al., 2012) and the Brown-Resnick process outperformed the Smith and Schlather processes for extreme snowfall in the French Alps (Gaume et al., 2013b). But even if the CLIC is able to classify several models of max-stable processes, it does not evaluate the predictive ability of a max-stable process. Still, the predictive quality of models of max-stable processes is crucial because their main applications are for risk assessment.

## Temporal nonstationarity in max-stable processes

One of the most crucial issues for snow variables modeling is temporal nonstationarity, especially in the current context of climate change (Stocker et al., 2013). In the Swiss Alps, decreasing trends have been found for snow depth, duration of continuous snow cover and number of snowfall days (Laternser and Schneebeli, 2003). Mean snow depth and snow cover duration have also negative trends in the French Alps (Durand et al., 2009a). Negative trends of snow duration and snowfall were also observed in the Italian Alps (Valt and Cianfarra, 2010). These trends may have strong consequences, for instance for the Alpine ecosystem (Keller et al., 2005; Wipf et al., 2009).

The variables which are strongly impacted by climate change like temperature and, to a lesser extent, precipitation can be impacted non only in their averages, but also in their extreme values (Easterling et al., 2000; Klein Tank and Können, 2003). Temporal nonstationary is thus an challenging issue for the study of climate extremes (Cooley, 2009; Katz, 2010). Figure 4 shows the temporal evolution of the winter maximum snow depth for the 23 massifs of the French Alps (five year moving averages computed from

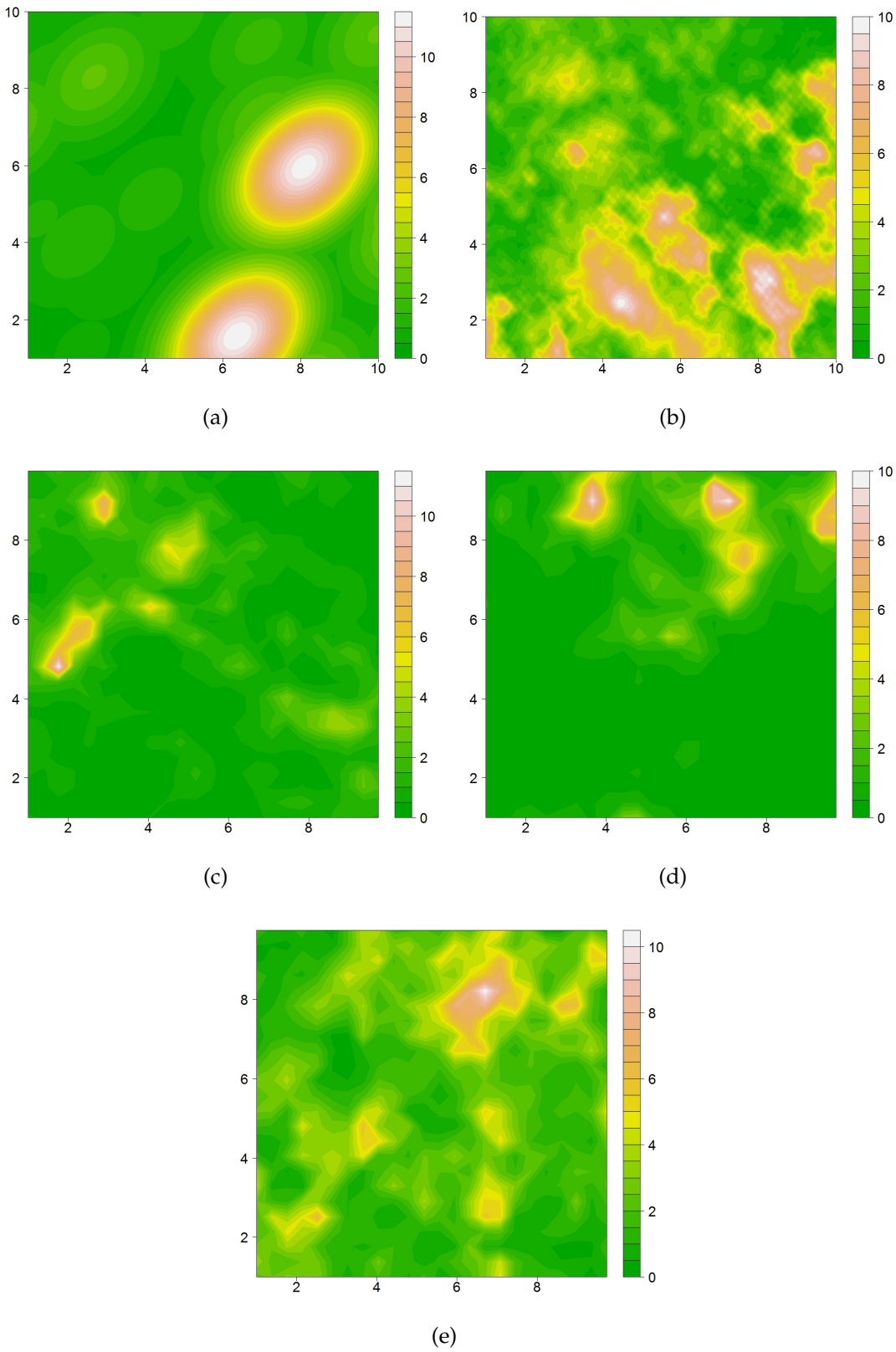


***Figure 3:*** *Realizations of the (a) Smith, (b) Schlather, (c) geometric Gaussian, (d) Brown-Resnick, and (e) extremal-t processes on the square* $[0,1]^2$*. The covariance matrix of the Smith process is* $0.5\mathbb{1} + Id$*. The Schlather, geometric Gaussian and extremal-t processes use the Whittle-Matérn correlation function with* $\lambda = 1$ *and* $\kappa = 1$*. We have* $\nu = 2$ *and* $\sigma^2 = 2$ *for the extremal-t and geometric Gaussian processes, respectively. The Brown-Resnick process uses the power semivariogram with* $\lambda = 1$ *and* $\kappa = 1.5$*.*

SAFRAN-Crocus reanalyses (Durand et al., 2009a) at 1800 m). These maxima show a strong temporal nonstationarity. Specifically, they exhibit a strong decrease from 1979 to 1990 more or less visible in all massifs. This decrease is related to the 1980s regime shift (Reid et al., 2015) and particularly to the recent strong warming now almost surely attributed to human activities (Stocker et al., 2013). A possibility to take into account nonstationarity in extreme value statistics is to use time as a covariate (and/or time-dependent covariates) for the parameters of the extreme value distribution to be estimated. This way, Marty and Blanchet (2012) found negative temporal trends in extreme snow depths and extreme snowfall in Switzerland. However, they did not model the spatial dependence of extremes.

Most of the studies using max-stable processes assume temporal stationarity, both in the marginal GEV distributions and in the spatial dependence structure of extremes. The ones in which nonstationarity is modeled use time-dependent covariates for the GEV parameters of the marginal distributions. This way, Westra and Sisson (2011) highlighted the influence of global sea surface temperature and South Oscillation Index on extreme precipitations in Australia, whereas Shang et al. (2011) and Zhang et al. (2014) showed a relation between El Ninõ Southern Oscillation and extreme precipitation in California and in China. However, they all assumed temporal stationarity in the spatial dependence structure.

Few studies model temporal aspects in the spatial dependence structure of max-stable processes. Raillard (2011) applied a space-time Smith process to extreme wave heights. Using space-time correlation functions, Steinkohl (2013) extended the Brown-Resnick process to the space-time case and used it for extreme rainfall in Florida. Huser and Davison (2014) introduced a space-time troncated Schlather process which explicitly represents the movement of a heavy rainfall event through time and applied it to extreme precipitation in Switzerland. The aim of these three works is to model the temporal dependence in extremes using observations recorded at short time lag. They do not consider a possible temporal nonstationarity in the spatial dependence structure of extremes over longer, climatic, time scales.

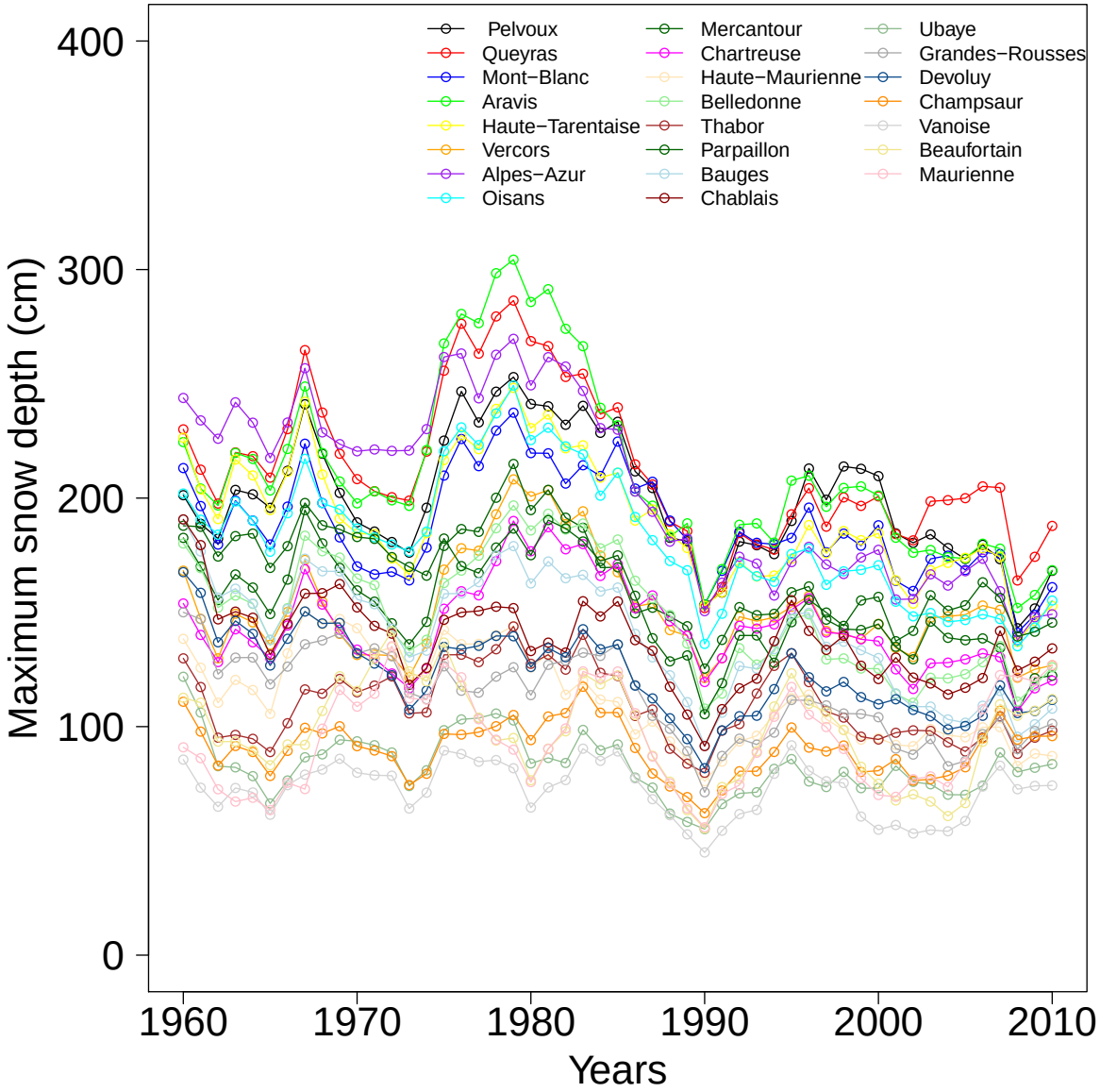


***Figure 4:*** *Five year moving averages of winter maximum snow depth for each massif of French Alps from 1960 to 2010 (SAFRAN-Crocus reanalyses at 1800 m on a flat aspect from Durand et al. (2009a)).*

# Outline of this thesis

## Main objectives

Two challenging issues concerning spatial extreme value analysis were chosen for investigation in this thesis. The first one concerns procedures of model selection able to evaluate the predictive ability of max-stable processes. The second one relates to possible temporal nonstationarity in the spatial dependence structure of climate extremes. These two questions are broached through the example of snowfall and snow depth in the French Alps. However, the interest of the approaches developed to broached these two questions goes beyond snow variables only.

The issue of model selection procedure well-suited for max-stable processes is relevant for all the variables which can be modeled by these processes, even if the results may be different according to the variable of interest. Indeed, the best choice to model extreme snowfall may not be the same as the one concerning extreme temperatures or extreme wave heights (for example). However, a selection procedure for max-stable processes applied to a specific variable does not need to be modified to be usable for other variables.

In the current context of climate change, temporal nonstationarity in the spatial dependence structure concerns potentially almost all climate extremes: extreme precipitations, extreme temperatures, extreme winds, etc. Snowfall and snow depths, severely impacted by climate change and linked with two major climate variables –namely precipitation and temperature– are very relevant choices to investigate this issue.

The comparison between snowfall and snow depths is interesting because these two snow-related variables differ from the fact that the first one is instantaneous while the other one is cumulative. The studies of Blanchet and Davison (2011) concerning extreme snow depths in Switzerland and of Gaume et al. (2013b) regarding extreme snowfall in the French Alps show that the extremes of these variables have the common point of being both anisotropic with more spatial dependence in the direction of the main massifs and valleys. This is due to the influence of orography on the atmospheric fluxes generating extreme precipitation. However, these studies also suggest that extreme snow depths would be more spatially dependent than extreme snowfall, because of the cumulative effects involved in the formation of snow cover. However, these phenomena have never been addressed by comparing extreme snowfall and extreme snow depths in the same area, what is done in the thesis.

Two very suitable data sets from Météo-France were used for these investigations:

- a large data set of 3-day cumulated snowfall with a very good spatial and temporal coverage (90 stations from 1958 to 2012) (used in Chapters 2 and 3);
- a snow depth data set less extended spatially and temporally (81 stations from 1970 to 2012), but showing an excellent altitude coverage with many stations above 2000 m (Chapter 4).

Figure 5 shows the study area with the station locations for the two data sets. The lists of the stations with their coordinates are given in Appendixes I and II.

This thesis focuses on the spatial dependence structure of extremes and does not consider the issue of estimating the marginal distributions. This is why the marginal distributions are standardized into unit Fréchet at each station. This work combines empirical (Chapter 3) and model-based (Chapters 2 and 4) approaches. Chapter 2 is dedicated to a procedure of model selection for max-stable processes by focusing on their spatial dependence structure. The issue of temporal nonstationarity is broached in Chapters 3 and 4.

The body of the thesis is made of one state-of-the-art chapter, three chapters in the form of journal articles and a final chapter for the general conclusions and the outlooks. The first article was submitted to *Spatial Statistics*, the second one was published in *Journal of Geophysical Research: Atmospheres*, and the third one was submitted to *Water Resources Research*.

## Detailed overview

Chapter 1 is a state of the art of the mathematical tools used in this thesis. Max-stable processes rely on two fields of statistics, extreme value theory and geostatistics, which are approached in the first two sections. Then, max-stable processes are defined in the last section. The models of max-stable processes considered in this thesis are introduced and the issues of inference and model selection are broached. This chapter does not deal with the applications of max-stable processes. The state of the art of their applications in several fields (snow studies, climatology, hydrology, risk managements, etc.) is done in the next chapters.

Chapter 2 deals with the issue of model selection in the case of max-stable processes. We introduce a leave-two-out cross-validation procedure appropriate to evaluate their predictive ability concerning the spatial dependence structure. This procedure is applied to five of the most famous max-stable processes: Smith, Schlather, Brown-Resnick, geometric Gaussian and extremal-t processes. To this aim, a large panel of statistical

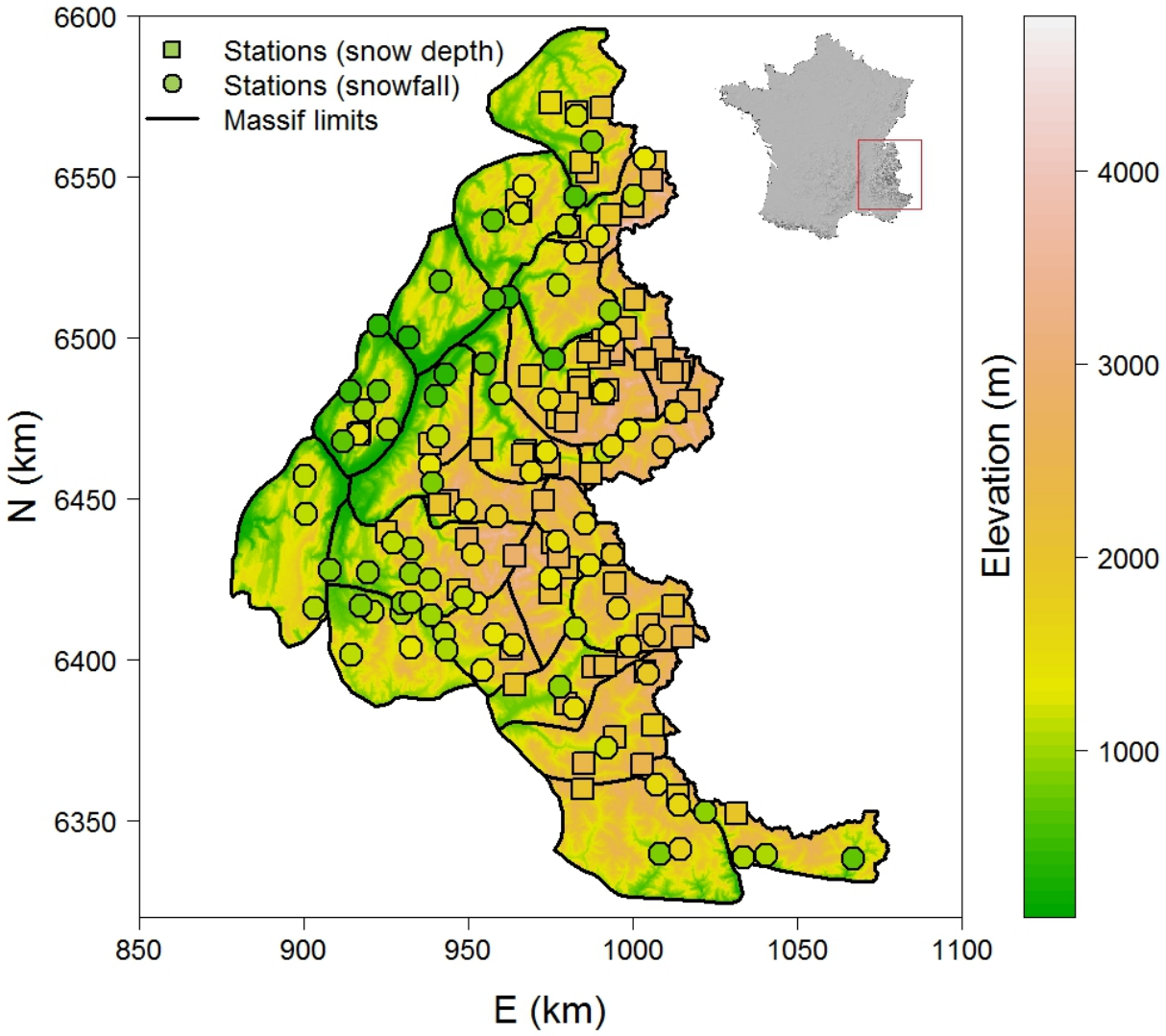


***Figure 5:*** *Study area in the southeast of France, where the 23 massifs of the French Alps are located. Lines denote massif limits. Squares and circles represent snow depth stations and snowfall stations, respectively.*

criteria is presented and applied. The snowfall data set is used as a case study. The Smith and Schlather processes are found less suitable than the others. Thanks to this procedure, we show that Brown-Resnick, geometric Gaussian and extremal-t processes are able to capture the spatial dependence structure of snowfall maxima almost as well as each other. Finally, these criteria are used to assess the sensibility of these processes to the number of stations and to the number of years of observations.

Chapter 3 investigates the temporal changes in the spatial dependence structure in extreme snowfall in the French Alps. To this end, the data set of 3 day snowfall maxima is used. The temporal evolution of the extremal dependence is estimated over a 20 year moving estimation window. The range of extremal dependence which represents the distance above which extremes are almost independent, is derived for each window. We find that this range has reduced roughly by half during the study period, showing that snowfall extremes have exhibited a tendency of being less spatially dependent over time. We show that this decreasing trend is attributable at first to the increase in temperature and its control over the snow/rain discrimination. A magnitude effect, with less dependent extremes due to a decrease in intensity of precipitation, also exists.

Chapter 4 addresses the temporal nonstationarity in the spatial dependence structure of spatial extremes by using a Brown-Resnick process with temporal trends in its spatial dependence structure. This approach is applied to the snow depth winter maxima data set in order to study the temporal evolution of the spatial dependence in extreme snow depths. Several climatic covariates are used to model climate control on the spatial dependence of extreme snow depths and to investigate the variables which impact this spatial dependence. We find a marked negative temporal trend in the spatial dependence of extreme snow depths with a strong decrease in the range of extremal dependence during the 1980s. We show that, as for extreme snowfall in Chapter 3, this decrease in extremal dependence is mainly due to the effect of the increase of temperature on the snow precipitation ratio and to a decrease in intensity of precipitation.

Finally, the last chapter is dedicated to the conclusions and perspectives of this thesis.

# Chapter 1

# State of the art of the mathematical tools used in this thesis

## 1.1 Introduction

This chapter introduces the mathematical tools used in this thesis. Max-stable processes link two fields of statistics, extreme value theory and geostatistics, so that both shall be introduced.

Extreme value theory (Coles, 2001; Beirlant et al., 2004; de Haan and Ferreira, 2006) is a suitable framework for estimating high quantiles, mostly for risk management purpose. In particular, section 1.2 deals with the block maxima approach which consists in modeling block maxima of the variable of interest with the aim to extrapolate beyond the highest recorded observations. Only univariate and bivariate cases are broached but the approach can be extended to higher dimensions.

Geostatistics (Cressie, 1993; Diggle and Ribeiro Jr., 2007) is the field of statistics which focuses on the modeling of spatial phenomena, especially for interpolation purpose. Geostatistics widely uses Gaussian processes, correlation functions and semivariograms which are introduced in section 1.3. However, Gaussian processes are too smooth to be able to capture the behavior of extreme values of spatial phenomena.

Max-stable processes (Davison et al., 2012; Cooley et al., 2012; Ribatet and Sedki, 2012; Ribatet, 2013; Davison and Huser, 2015) generalize univariate extreme value theory to the infinite dimension. This framework can be seen as a "geostatistics of extremes" capable of modeling extremes in space. Section 1.4 introduces max-stable processes and broaches some practical difficulties such as inference and model selection.

## 1.2 Extreme value theory

### 1.2.1 Univariate case

Extreme value theory can be addressed by different approaches. The one used here is the so-called block maxima approach.

Let $M_n = \max\{X_1, \ldots, X_n\}$, with $\{X_n\}$ a sequence of independent identically distributed random variables. The Fisher-Tippett-Gnedenko theorem (Fisher and Tippett, 1928; Gnedenko, 1943) shows that if there are sequences $\{a_n\} > 0$ and $\{b_n\}$ such as $\dfrac{M_n - b_n}{a_n}$ converge in distribution to a non degenerate distribution $G$, then $G$ is the GEV (Generalized Extreme Value) distribution (Coles, 2001) whose cumulative distribution function is

$$G(x) = \exp\left\{-\left[1 + \xi\left(\frac{x-\mu}{\sigma}\right)\right]^{-1/\xi}\right\} \tag{1.1}$$

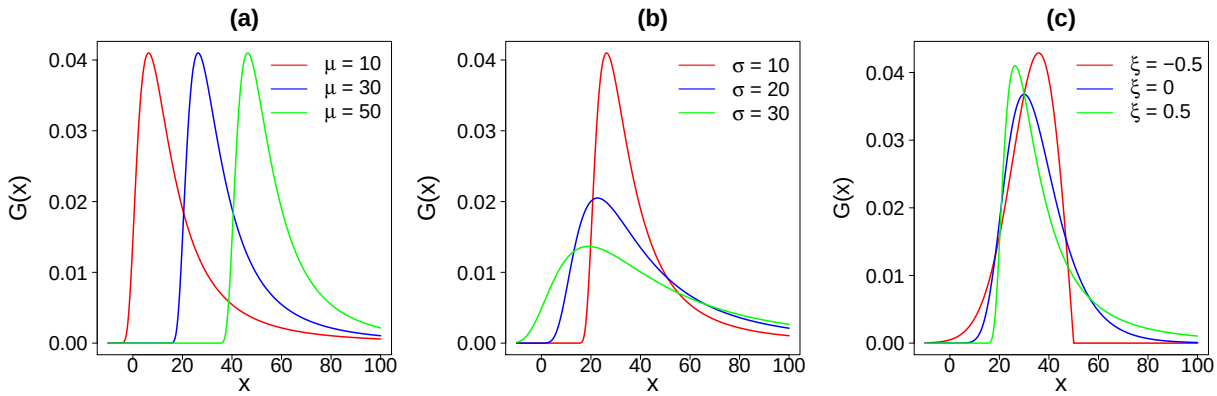


***Figure 1.1:*** *Plot of the GEV density function with (a)* $\mu \in \{10, 30, 50\}$, $\sigma = 10$, $\xi = 0.5$, *(b)* $\mu = 30$, $\sigma \in \{10, 30, 50\}$, $\xi = 0.5$ *and (c)* $\mu = 30$, $\sigma = 10$, $\xi \in \{-0.5, 0, 0.5\}$.

with $x$ such that $1 + \xi \left( \dfrac{x - \mu}{\sigma} \right) > 0$. The function $G$ is equal to 0 when $\xi > 0$ and $x \leq \mu - \frac{\sigma}{\xi}$, and equal to 1 when $\xi < 0$ and $x \geq \mu - \frac{\sigma}{\xi}$.

This result means that for a large enough $n$, one can approximate the distribution of $M_n$ by the GEV distribution. The block maxima method consists in grouping a sample into blocks of equal length in order to determine the maxima for each block (e.g., annual maxima), and then a GEV distribution is fitted to the sample of maxima.

The conclusion of Fisher-Tippett-Gnedenko theorem holds with dependent random variables $\{X_n\}$ without long-range temporal dependence at extreme levels (this condition is called $D(u_n)$ condition in Leadbetter (1983)) which is not a restricting condition in practice.

The GEV distribution has three parameters (Figure 1.1). The location parameter $\mu$ indicates the center of the distribution. The scale parameter $\sigma$ specifies the size of deviation around $\mu$. The shape parameter $\xi$ is the most important in extreme value theory: it determines the tail behaviour of the distribution. There are three cases:

- $\xi > 0$ : Fréchet distribution (heavy tailed),
- $\xi < 0$ : reversed Weibull (or simply Weibull) distribution (bounded),
- $\xi \to 0$ : Gumbel distribution (not bounded, light tailed).

Regardless of value of GEV parameters, the GEV distribution is a max-stable distribution. This means that any maximum of independent random variables following the same GEV distribution can be rescaled so as to follow this distribution. Precisely, if $\{Z_i\}$ are independent copies of a GEV distributed random variable $Z$, there exist two sequences $\{c_n\} > 0$ and $\{d_n\}$ such as

$$\frac{\max_{i=1}^{n} Z_i - d_n}{c_n} \stackrel{d}{=} Z(x) \quad \forall n \in \mathbb{N}. \tag{1.2}$$

The GEV distribution is the unique non-degenerate univariate max-stable distribution.

The transformation

$$x \to \frac{-1}{\log(G(x))} \tag{1.3}$$

can be used to transform a GEV distribution into a unit Fréchet distribution, whose cumulative distribution function is $G(x) = e^{-1/x}$ (that is to say the specific case of a GEV distribution with parameters $\mu = 1$, $\sigma = 1$ and $\xi = 1$).

### 1.2.2 Bivariate case

Let $\{X_{n,1}\}$ and $\{X_{n,2}\}$ be two sequences of independent identically distributed random variables. If, in an analogous way than in section 1.2.1, there exist normalizing sequences $\{a_{n,i}\}$ and $\{b_{n,i}\}$ ($i \in \{1, 2\}$) such as the vector

$$\left\{ \frac{\max_{i=1}^{n} X_{i,1} - b_{n,1}}{a_{n,1}}, \frac{\max_{i=1}^{n} X_{i,2} - b_{n,2}}{a_{n,2}} \right\}$$

converges in distribution to a non degenerate bivariate distribution $G$, then $G$ is a bivariate extreme value distribution. As in the univariate case, the distribution $G$ is max-stable and the temporal independance hypothesis can be relaxed ($D(u_n)$ condition in Leadbetter (1983)). In the bivariate case, max-stability means that if $\{Z_1, Z_2\}$ follows the max-stable distribution $G$, thus for all series $\{Z_{n,1}, Z_{n,2}\}$ of independent copies of $\{Z_1, Z_2\}$ there exists sequences $\{c_{1,n}, c_{2,n}\} > 0$ and $\{d_{1,n}, d_{2,n}\}$ such as

$$\left\{ \frac{\max_{i=1}^{n} Z_{1,i} - d_{1,n}}{c_{1,n}}, \frac{\max_{i=1}^{n} Z_{2,i} - d_{2,n}}{c_{2,n}} \right\} \stackrel{d}{=} \{Z_1, Z_2\} \quad \forall n \in \mathbb{N}. \tag{1.4}$$

The marginal distributions of the limiting vector $(Z_1, Z_2)$ (i.e., the random variables $Z_1$ and $Z_2$ defined by its components) follow a GEV distribution. Using the transformation (1.3), one can assume without restriction that the distributions of $Z_1$ and $Z_2$ are unit Fréchet.

#### 1.2.2.1 Exponent measure

Assume that $Z_1$ and $Z_2$ follow a unit Fréchet distribution. Then, there exists a function $V$, called exponent measure (Coles, 2001, Chap. 8), such that the bivariate distribution can be written

$$\mathbb{P}\left(Z_1 < z_1, Z_2 < z_2\right) = \exp\left\{-V(z_1, z_2)\right\} \qquad z_1, z_2 > 0. \tag{1.5}$$

The function $V$ holds the properties

$$V(z_1, \infty) = \frac{1}{z_1} \text{ and } V(\infty, z_2) = \frac{1}{z_2} \qquad z_1, z_2 > 0 \tag{1.6}$$

and

$$V(tz_1, tz_2) = t^{-1} V(z_1, z_2) \qquad z_1, z_2, t > 0 \tag{1.7}$$

due to the max-stability property.

The variables $Z_1$ and $Z_2$ are independent when

$$V(z_1, z_2) = \frac{1}{z_1} + \frac{1}{z_2} \qquad z_1, z_2 > 0, \tag{1.8}$$

and completely dependent when

$$V(z_1, z_2) = \frac{1}{\min(z_1, z_2)} \qquad z_1, z_2 > 0. \tag{1.9}$$

The exponent measure has the spectral representation

$$V(z_1, z_2) = \int_{\mathcal{S}_2} \max\left\{\frac{w_1}{z_1}, \frac{w_2}{z_2}\right\} \mathrm{d}M(w_1, w_2) \tag{1.10}$$

with $M$ a measure on the 2-dimensional simplex $\mathcal{S}_2$.

#### 1.2.2.2 Extremal coefficient

To assess the extremal dependence between two unit Fréchet random variables $Z_1$ and $Z_2$, one can use the extremal coefficient $\theta$ (Schlather and Tawn, 2003) defined by

$$\mathbb{P}\left(Z_1 < z, Z_2 < z\right) = \exp\left\{\frac{-V(1,1)}{z}\right\} = \exp\left\{\frac{-\theta}{z}\right\} = \mathbb{P}\left\{Z_1 < z\right\}^{\theta}, \qquad z > 0. \tag{1.11}$$

Extremal coefficient ranges between 1 (complete dependence) and 2 (independence). The property

$$\lim_{z\to\infty} \mathbb{P}\left(Z_2 > z | Z_1 > z\right) = 2 - \theta \tag{1.12}$$

holds and means that if $\theta$ is near 1, $Z_1$ and $Z_2$ have a tendency to take their extreme values together. Conversely, $\theta$ near 2 means that the probability of seeing $Z_1$ and $Z_2$ having extremes simultaneously is close to zero.

#### 1.2.2.3 Madogram

Another tool to assess dependence between $Z_1$ and $Z_2$ is the F-madogram (Cooley et al., 2006; Naveau et al., 2009) defined by

$$\mu_F = \frac{1}{2}\mathbb{E}\left[|F_1(Z_1) - F_2(Z_2)\ |\right] \tag{1.13}$$

where $F_i$ is the cumulative distribution function of the random variable $Z_i$. When $Z_1$ and $Z_2$ are unit Fréchet, $F_i(z) = \exp(-1/z)$ , the F-madogram is linked to the extremal coefficient through the formula:

$$\theta = \frac{1 + 2\mu_F}{1 - 2\mu_F} \tag{1.14}$$

which provides a convenient way to evaluate $\theta$ by estimating $\mu_F$ through

$$\hat{\mu}_F = \frac{1}{2N}\sum_{i=1}^{N} |\hat{F}(z_{1,i}) - \hat{F}(z_{2,i})| \tag{1.15}$$

with $\{z_{1,i}, z_{2,i}\}$ $N$ observations of $\{Z_1, Z_2\}$.

## 1.3 Geostatistics

### 1.3.1 Gaussian process

A process $\{W(x)\}_{x\in\chi}$ defined on a spatial domain $\chi$ (for instance a subset of $\mathbb{R}^2$) is called Gaussian process if for all $x_1, \dots x_n$, the distribution of $(W(x_1), \dots, W(x_n))$ is multivariate Gaussian. This process is completely defined by its mean function $\mu(x) = \mathbb{E}[W(x)]$ and its covariance function $\mathrm{C}(x_1, x_2) = \mathrm{Cov}(W(x_1), W(x_2))$ (Diggle and Ribeiro Jr., 2007, Chap. 3).

The Gaussian process is stationary if the function $\mu$ is constant and $\mathrm{C}(x_1, x_2)$ depends on the vector difference $x_2 - x_1$ only, that is to say $\mu(x) = \mu$ and $\mathrm{C}(x_1, x_2) = \mathrm{C}(x_2 - x_1)$. The variance $\mathrm{C}(0) = \sigma^2$ of a stationary Gaussian process is constant.

If $\mathrm{C}(x_1, x_2)$ depends on the distance $h = \|x_2 - x_1\|$ only and not on the orientation of the vector $x_2 - x_1$, the Gaussian process is isotropic.

### 1.3.2 Correlation function

The correlation function of a stationary Gaussian process is defined by

$$\rho(x_2 - x_1) = \frac{\mathrm{C}(x_2 - x_1)}{\sigma^2} \tag{1.16}$$

A stationary Gaussian process is isotropic when $\rho$ depends on the distance $h = \|x_2 - x_1\|$ only. For isotropic stationary Gaussian processes, several usual families of correlation function constitute suitable models (see Table 1.1 and Figure 1.2).

One can modify the correlation function $\rho$ with a nugget effect:

$$\rho_*(h) = \begin{cases} 1 & h = 0 \\ \dfrac{\sigma^2}{\sigma^2 + \tau^2}\rho(h) & h > 0 \end{cases}$$

with the aim of representing, with the $\tau$ parameter, measurement errors and/or microscale variation.

Figure 1.3 shows an example of a realization of a stationary isotropic Gaussian process with exponential correlation function and $\lambda = 1$.

| Family | Correlation function |
|---|---|
| Circular | $\rho(h) = 1 - \frac{2}{\pi}\left[\frac{h}{\lambda}\sqrt{1-\left(\frac{h}{\lambda}\right)^2} + \arcsin\left(\frac{h}{\lambda}\right)\right]$ |
| Cubic | $\rho(h) = 1 - 7\left(\frac{h}{\lambda}\right)^2 + \frac{35}{4}\left(\frac{h}{\lambda}\right)^3 - \frac{7}{2}\left(\frac{h}{\lambda}\right)^5 + \frac{3}{4}\left(\frac{h}{\lambda}\right)^7$ |
| Exponential | $\rho(h) = \exp\left\{-\left(\frac{h}{\lambda}\right)\right\}$ |
| Gaussian | $\rho(h) = \exp\left\{-\left(\frac{h}{\lambda}\right)^2\right\}$ |
| Gneiting | $\rho(h) = \left[1 + 8\left(\frac{sh}{\lambda}\right) + 25\left(\frac{sh}{\lambda}\right)^2 + 32\left(\frac{sh}{\lambda}\right)^3\right]\left(1 - \frac{sh}{\lambda}\right)^8$ |
| Spherical | $\rho(h) = 1 - \frac{3}{2}\left(\frac{h}{\lambda}\right) + \frac{1}{2}\left(\frac{h}{\lambda}\right)^3$ |
| Wave | $\rho(h) = \frac{\sin(h/\lambda)}{h/\lambda}$ |
| Bessel | $\rho(h) = \left(\frac{2\lambda}{h}\right)^{\kappa}\Gamma(\kappa+1)\, J_\kappa\left(\frac{h}{\lambda}\right)$ |
| Cauchy | $\rho(h) = \left[1 + \left(\frac{h}{\lambda}\right)^2\right]^{-\kappa}$ |
| Gamma | $\rho(h) = \frac{1}{(1+h/\lambda)^{\kappa}}$ |
| Powered exponential | $\rho(h) = \exp\left\{-\left(\frac{h}{\lambda}\right)^{\kappa}\right\}$ |
| Whittle-Matérn | $\rho(h) = \frac{2^{1-\kappa}}{\Gamma(\kappa))}\left(\frac{h}{\lambda}\right)^{\kappa} K_\kappa\left(\frac{h}{\lambda}\right)$ |
| Generalized Cauchy | $\rho(h) = \left[1 + \left(\frac{h}{\lambda}\right)^{\kappa_2}\right]^{-\kappa/\kappa_2}$ |
| Gneiting-Matérn | $\rho(h) = \rho_\lambda^{gneiting}(h/\kappa_2)\,\rho_{\lambda,\kappa}^{matern}(h)$ |

***Table 1.1:*** *Usual correlation functions. The parameter $\lambda > 0$ is the range parameter. The parameter $\kappa > 0$ is the smoothness parameter (for the Bessel family $\kappa \geq \frac{d-2}{2}$ with $d$ the dimension of the space and for the powered exponential family $0 < \kappa \leq 2$). In the expression of the Gneiting correlation function, $s = 0.301187465825$. For the circular, cubic, Gneiting and spherical families $h < \lambda$, and $\rho(h) = 0$ when $h \geq \lambda$. The functions $\Gamma$, $J_\kappa$ and $K_\kappa$ are respectively the Gamma function, the Bessel function of the first kind of order $\kappa$ and the modified Bessel function of order $\kappa$. The correlation functions of the generalized Cauchy and Gneiting-Matérn families own a second smoothness parameter $\kappa_2 > 0$ (for the Generalized Cauchy correlation function $0 < \kappa_2 \leq 2$). In the expression of the Gneiting-Matérn correlation function, $\rho_\lambda^{gneiting}$ and $\rho_{\lambda,\kappa}^{matern}$ denote Gneiting and Whittle-Matérn correlation functions respectively.*

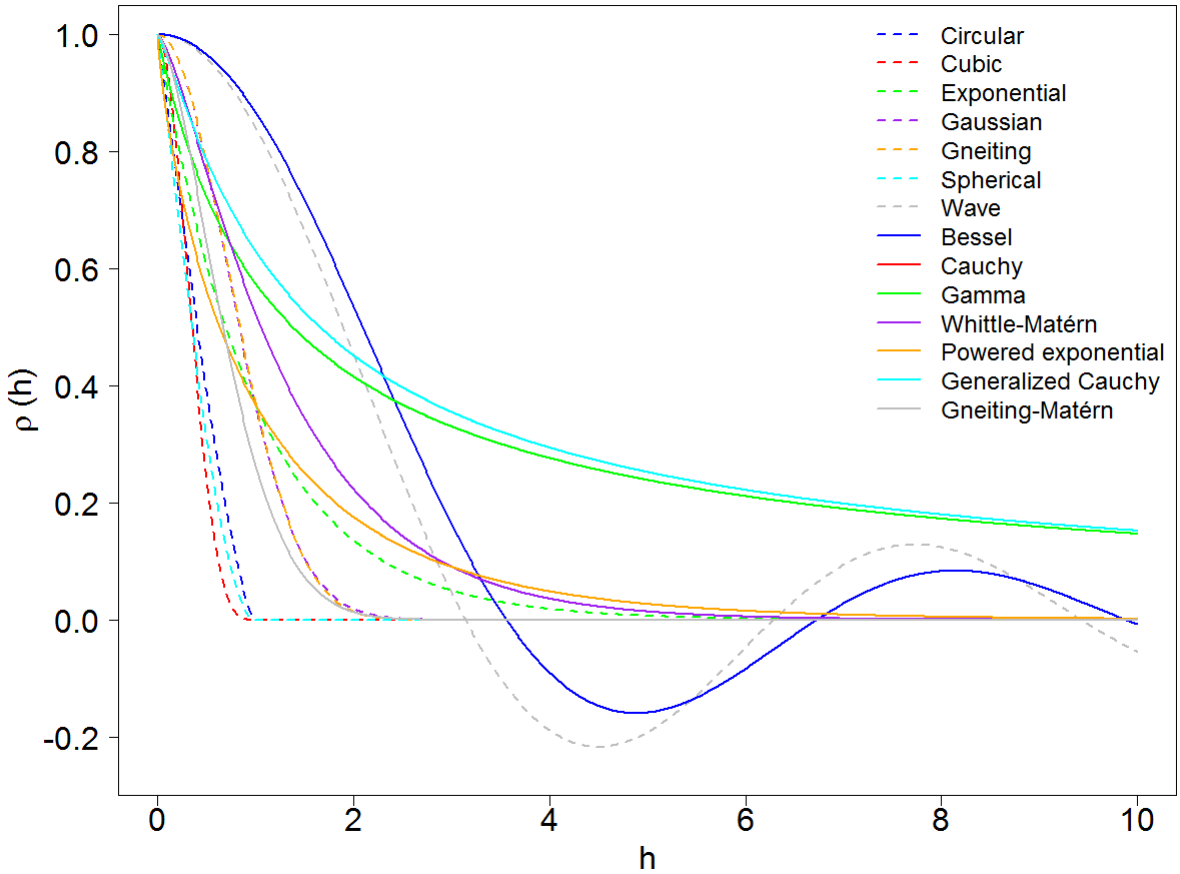


***Figure 1.2:*** *Plot of the correlation functions of Table 1.3.2 with* $\lambda = 1$, $\kappa = 0.8$ *and* $\kappa_2 = 1.2$.

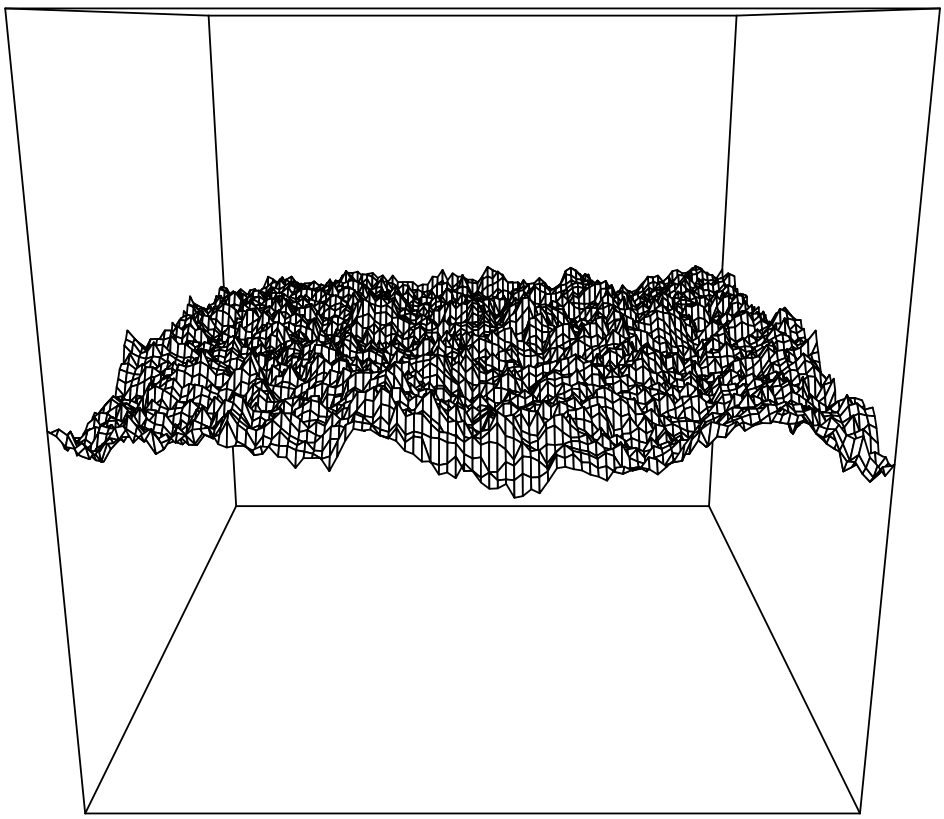

***Figure 1.3:*** *Realization of a stationary isotropic Gaussian process on the square* $[0, 10]^2$ *with zero mean and exponential correlation function with* $\lambda = 1$

| Family | Semivariogram |
|---|---|
| Linear | $\gamma(h) = \dfrac{h}{\lambda}$ |
| Power | $\gamma(h) = \left(\dfrac{h}{\lambda}\right)^{\kappa}$ |
| Correlation function-based | $\gamma(h) = \sigma^2 (1 - \rho(h))$ |

***Table 1.2:*** *Usual semivariograms. For linear and Power families, $\lambda > 0$ is the scale parapeter and $\kappa > 0$ is the shape parameter. It is possible to define a semivariogram with every correlation functions $\rho$ and a variance parameter $\sigma^2$ which defines the sill of the semivariogram.*

### 1.3.3 Semivariogram

The semivariogram $\gamma$ of a stationary Gaussian process is defined by

$$\gamma(x_2 - x_1) = \frac{1}{2}\mathrm{Var}\left(W(x_2) - W(x_1)\right) = \frac{1}{2}\mathbb{E}\left[|W(x_2) - W(x_1)|^2\right]. \tag{1.17}$$

If $\gamma$ depends on the length $h = \|x_2 - x_1\|$ only, then the process is isotropic. In this case, usual semivariograms are linear and power semivariograms, or semivariograms based on an usual correlation function (Table 1.2 and Figure 1.4). Instead of correlation function-based semivariograms, linear and power semivariograms are not bounded.

## 1.4 Max-stable processes

### 1.4.1 Definition

Max-stable processes generalize extreme value theory to infinite dimension and are mostly used in a spatial framework. Let $\chi$ be a space (generally a subset of $\mathbb{R}^2$ or $\mathbb{R}^3$). Let $\{X(x)\}_{x\in\chi}$ be a process on $\chi$ and $\{X_i(x)\}_{x\in\chi}$ be independent copies of this process. If there exist two sequences of continuous functions $\{a_n(x)\}$ and $\{b_n(x)\}$ such as

$$\left\{\frac{\max_{i=1}^{n} X_i(x) - b_n(x)}{a_n(x)}\right\}_{x\in\chi} \xrightarrow{d} \{Z(x)\}_{x\in\chi} \tag{1.18}$$

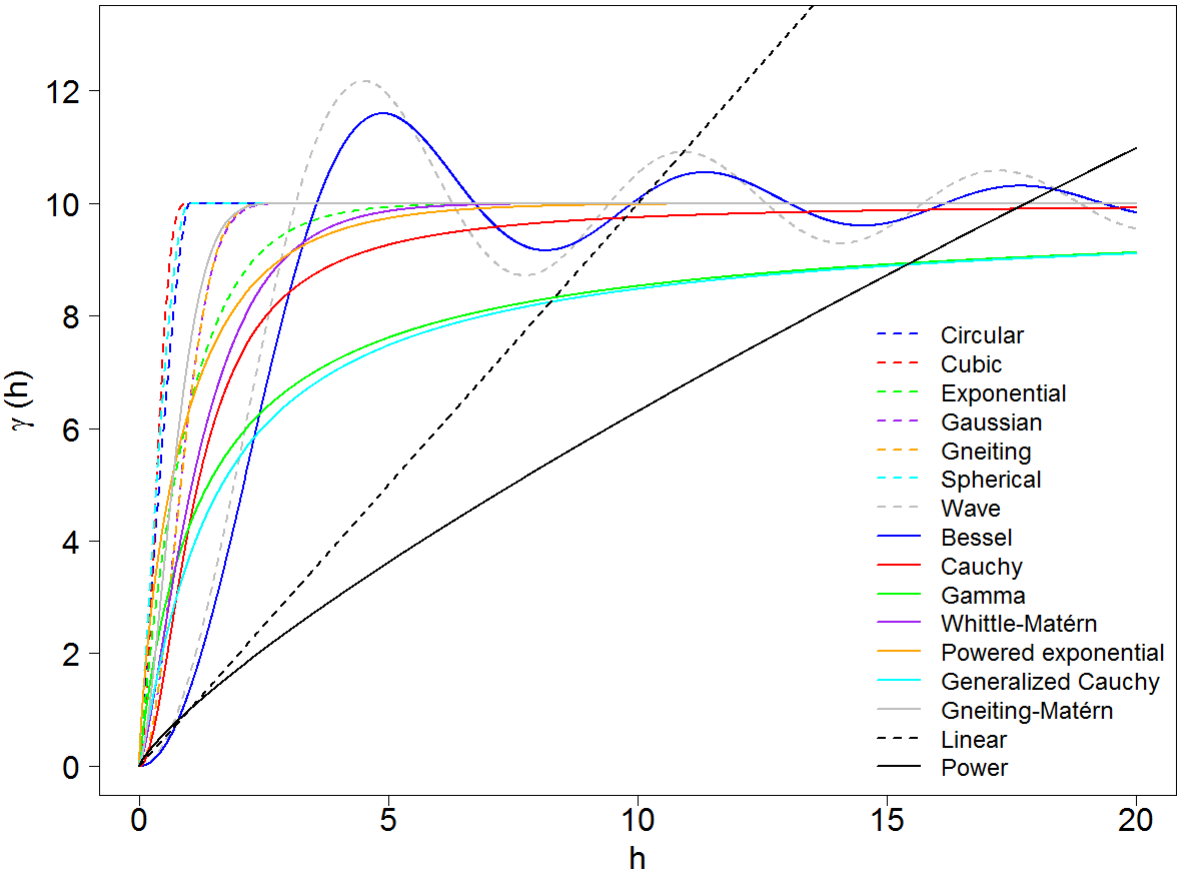


***Figure 1.4:*** *Plot of the semivariograms defined in Table 1.2 with* $\sigma^2 = 10$, $\lambda = 1$, $\kappa = 0.8$ *and* $\kappa_2 = 1.2$.

then the limiting process $\{Z(x)\}_{x\in\chi}$ is a max-stable process in the sense that all the marginal distributions (i.e., the random vectors $\{Z(x_i)\}_{i=1,\dots,n}$ defined by the values of $Z$ at several specific locations $x_1,\dots,x_n \in \chi$) are max-stable. That is to say there exist two sequences of continuous functions $\{c_n(x)\}$ and $\{d_n(x)\}$ such as

$$\left\{\frac{\max_{i=1}^n Z_i(x) - d_n(x)}{c_n(x)}\right\}_{x\in\chi} \stackrel{d}{=} \{Z(x)\}_{x\in\chi} \tag{1.19}$$

with $Z_i$ independent copies of $Z$.

In particular, every univariate margins $Z(x)$ are GEV distributions. Through the transformation (1.3), we can suppose that every univariate distribution is unit Fréchet. The process $\{Z(x)\}_{x\in\chi}$ is a max-stable process with unit Fréchet margins if and only if (1.19) holds with $c_n(x) = n$ and $d_n(x) = 0$. In the following, we will consider max-stable processes with unit Fréchet margins only.

### 1.4.2 De Haan's spectral representation

Every max-stable process with unit Fréchet margins holds the spectral representation

$$Z(x) = \sup_{i\geq 1} \eta_i W_i(x). \tag{1.20}$$

with $\{\eta_i\}_{i\geq 1}$ the points of a Poisson process on $\mathbb{R}_+$ with intensity $\eta^{-2}\mathrm{d}\eta$ and $\{W_i\}_{i\geq 1}$ independent copies of a positive process $W(x)$ with mean 1 (de Haan, 1984). Different choices for $W$ lead to different models of max-stable processes (Davison et al., 2012; Ribatet, 2013).

Every multivariate margin is given for any positions $\{x_1,\dots,x_k\}$ by the formula

$$\mathbb{P}\left(Z(x_1) < z_1,\dots,Z(x_k) < z_k\right) = \exp\left[-\mathbf{E}\left\{\max_{j=1,\dots,k} \frac{W(x_j)}{z_j}\right\}\right] \qquad z_j > 0 \quad \forall j. \tag{1.21}$$

### 1.4.3 Extremal function

For each pair of locations $x_1$ and $x_2$, we can consider the extremal coefficient $\theta(x_1, x_2)$ of the two unit Fréchet variables $Z(x_1)$ and $Z(x_2)$. We have from equations (1.21) and (1.11):

$$\theta(x_1, x_2) = \mathbf{E}\left[\max\left\{W(x_1), W(x_2)\right\}\right]. \tag{1.22}$$

$\theta(x_1, x_2)$ is usually modeled as a function $\theta(h)$ of the distance $h = \|x_2 - x_1\|$ between $x_1$ and $x_2$. $\theta(h)$ represents the strength of extremal dependence as a function of distance and is therefore termed the extremal function.

### 1.4.4 Max-stable models

Here, we introduce the five models of max-stable processes considered in this thesis.

#### 1.4.4.1 Smith process

The easiest way to use de Haan's spectral representation is to take $W_i(x) = f(x - X_i)$ in (1.20) with $f$ a density function and $\{X_i\}$ a homogeneous Poisson process on $\chi$.

Smith (1990) proposes to take $f$ as the density function of a multivariate normal distribution. The Smith process (also called Gaussian extreme value process) is defined by

$$Z(x) = \max_{i \geq 1} \eta_i f(x - X_i). \tag{1.23}$$

Here, $f$ is the density function of a multivariate normal distribution with mean 0 and covariance matrix $\Sigma$, $\{\eta_i, X_i\}_{i \geq 1}$ is the points of a Poisson process on $(0, \infty) \times \chi$ with intensity $\eta^{-2} \mathrm{d}\eta \times \mathrm{d}\mu$ ($\mu$ is the Lebesgue measure on $\chi$).

Smith gave a rainfall-storm interpretation: $X_i$ is the center of a storm, $f$ the shape of the storm and $\eta_i$ its magnitude. In this way, the process is a rainfall-storm which is the maximum of several independent rainfall events.

The exponent measure for $Z(x_1)$ and $Z(x_2)$ (with $x_1$ and $x_2$ two locations) is given by

$$V(z_1, z_2) = \frac{1}{z_1} \Phi\left(\frac{a}{2} + \frac{1}{a} \log \frac{z_2}{z_1}\right) + \frac{1}{z_2} \Phi\left(\frac{a}{2} + \frac{1}{a} \log \frac{z_1}{z_2}\right), \tag{1.24}$$

with $\Phi$ the distribution function of the standard normal distribution and $a$ the Mahalanobis distance which is defined as $a = \sqrt{(x_2 - x_1)^T \Sigma^{-1} (x_2 - x_1)}$.

The extremal function is

$$\theta(x_1, x_2) = 2\Phi\left(\frac{a}{2}\right). \tag{1.25}$$

When the distance between $x_1$ and $x_2$ increases infinitely, then $\theta(x_1, x_2)$ converges to 2, that is to say extremal independence (Figure 1.5(a)).

The major drawback of the Smith process is its lack of flexibility owing to the fact that the shape $f$ of the storms is deterministic (Blanchet and Davison, 2011). This leads to models unrealistic for natural phenomena (Figure 1.5(b)).

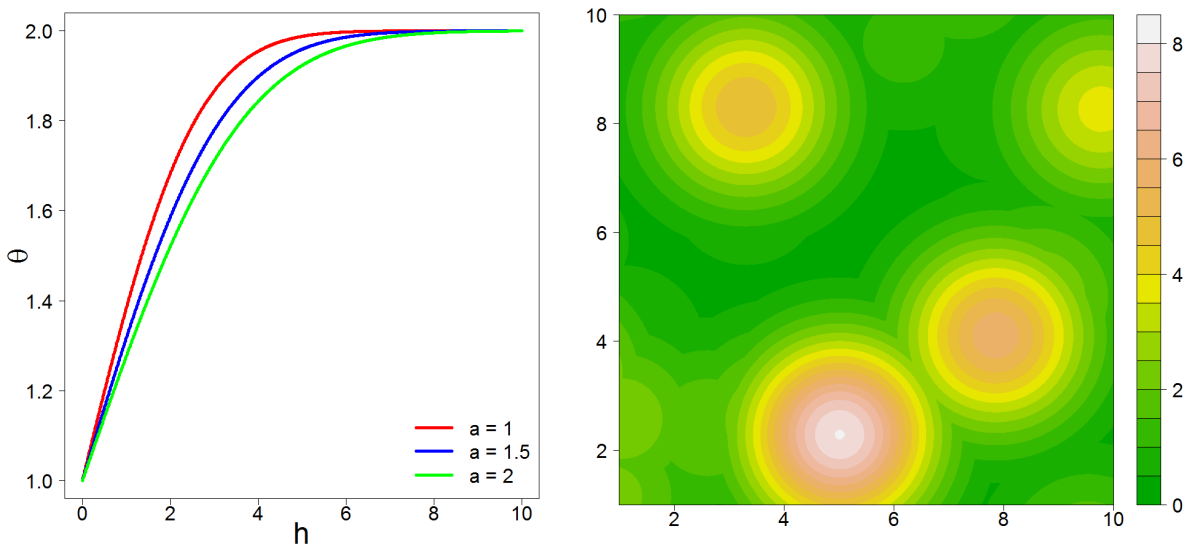


(a) (b)

***Figure 1.5:*** *(a) Extremal function for the Smith process with a covariance matrix a Id with* $a = 1$ *(red),* $a = 1.5$ *(blue) and* $a = 2$ *(green).(b) One realization of the Smith process on the square* $[0, 10]^2$ *with covariance matrix* $1.5\,Id$ *(in blue in (a)).*

#### 1.4.4.2 Schlather process

A more flexible max-stable model is introduced in Schlather (2002) by considering the shape of the storm as random (compare Figures 1.5(b) and 1.6(b)).

Schlather process (or extremal Gaussian process) is defined by

$$Z(x) = \max_{i \geq 1} \eta_i \max\{0, Y_i(x)\}, \tag{1.26}$$

with $\{\eta_i\}_{i\geq 1}$ the points of a Poisson process on $\mathbb{R}_+$ with intensity $\sqrt{2\pi}\eta^{-2}\mathrm{d}\eta$ and $\{Y_i(x)\}$ is independent copies of a stationary Gaussian process with correlation function $\rho$.

The exponent measure is given by

$$V(z_1, z_2) = \frac{1}{2}\left(\frac{1}{z_1} + \frac{1}{z_2}\right)\left(1 + \sqrt{1 - 2(\rho(h) + 1)\frac{z_1 z_2}{(z_1 + z_2)^2}}\right) \tag{1.27}$$

with $h = \|x_2 - x_1\|$ the Euclidean distance between the two locations.

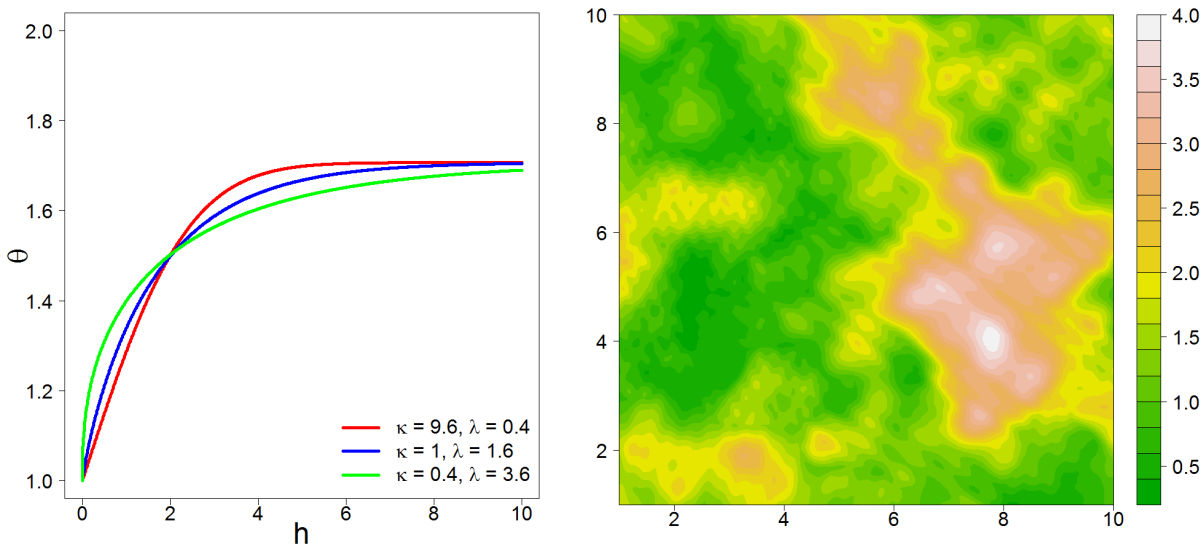


(a) (b)

***Figure 1.6:*** *(a) Extremal function for the Schlather process with the Whittle-Matérn covariance function for* $\{\kappa = 9.6, \lambda = 0.4\}$ *(red),* $\{\kappa = 1, \lambda = 1.6\}$ *(blue) and* $\{\kappa = 0.4, \lambda = 3.6\}$ *(green). (b) One realization of the Schlather process on the square* $[0, 10]^2$ *with the Whittle-Matérn correlation function with* $\kappa = 1$ *and* $\lambda = 1.6$ *(in blue in (a)).*

The flaw of the Schlather process is that the extremal function given by

$$\theta(x_1, x_2) = 1 + \sqrt{\frac{1 - \rho(h)}{2}} \tag{1.28}$$

is such as $\theta(x_1, x_2) \leq 1.838$ in $\mathbb{R}^2$ and $\theta(x_1, x_2) \leq 1.780$ in $\mathbb{R}^3$ (Blanchet and Davison, 2011), that is to say, extremes between two locations are never independent, regardless of the distance between the locations. In particular, there is always dependence when the distance between two locations increases infinitely which is often not realistic. For $h = \|x_2 - x_1\| \to \infty$, we have $\theta(x_1, x_2) \to 1 + 1/\sqrt{2} \simeq 1.707$ (Figure 1.6(a)). Even if this drawback is less visible graphically than the one of the Smith process, we can observe on the right of the Figure 1.6(b) a large cluster of very large values in yellow, orange and white.

#### 1.4.4.3 Geometric Gaussian process

The geometric Gaussian process (Davison et al., 2012) is the process defined by

$$Z(x) = \max_{i \geq 1} \eta_i \exp\left(\sigma Y_i(x) - \frac{\sigma^2}{2}\right). \tag{1.29}$$

Note $\{\eta_i\}_{i\geq 1}$ points of a Poisson process on $\mathbb{R}_+$ with intensity $\eta^{-2}\mathrm{d}\eta$ and $\{Y_i(x)\}$ independent copies of a Gaussian process with mean 0, variance $\sigma^2$ and correlation function $\rho$.

The exponent measure is by (1.24) as in Smith process but with $a = \sqrt{2\sigma^2(1-\rho(h))}$. The use of a correlation function instead of Mahalanobis distance produces more realistic realisations than with the Smith process (Figure 1.7(b)).

In the same way that with the Schlather process, the extremal function

$$\theta(x_1, x_2) = 2\Phi\left(\frac{a}{2}\right) \tag{1.30}$$

does not converge to 2 (extremal independence) when $h \to \infty$ (Figure 1.7(a)):

$$\theta(x_1, x_2) \underset{h\to\infty}{\longrightarrow} 2\Phi\left(\sqrt{\frac{\sigma^2}{2}}\right). \tag{1.31}$$

But unlike the Schlather process that imposes a limit of 1.707, the limit is not fixed and is controlled by the variance parameter $\sigma^2$. The extremal function converges to extremal independence (that is to say converges to 2) when $\sigma^2 \longrightarrow \infty$.

#### 1.4.4.4 Brown-Resnick process

A process previously defined in Brown and Resnick (1977) was generalized in Kabluchko et al. (2009). Brown-Resnick process is defined by

$$Z(x) = \max_{i \geq 1} \eta_i \exp\left\{W_i(x) - \gamma(x)\right\}. \tag{1.32}$$

Note $\{\eta_i\}_{i\geq 1}$ points of a Poisson process on $\mathbb{R}_+$ with intensity $\eta^{-2}\mathrm{d}\eta$ and $\{Y_i(x)\}$ independent copies of a Gaussian process with stationary increment and such that $Y_i(0) = 0$ almost surely and note $\gamma$ its semivariogram.

The expression of exponent measure is again given by (1.24) as in Smith and geometric Gaussian models but with $a = \sqrt{2\gamma(h)}$.

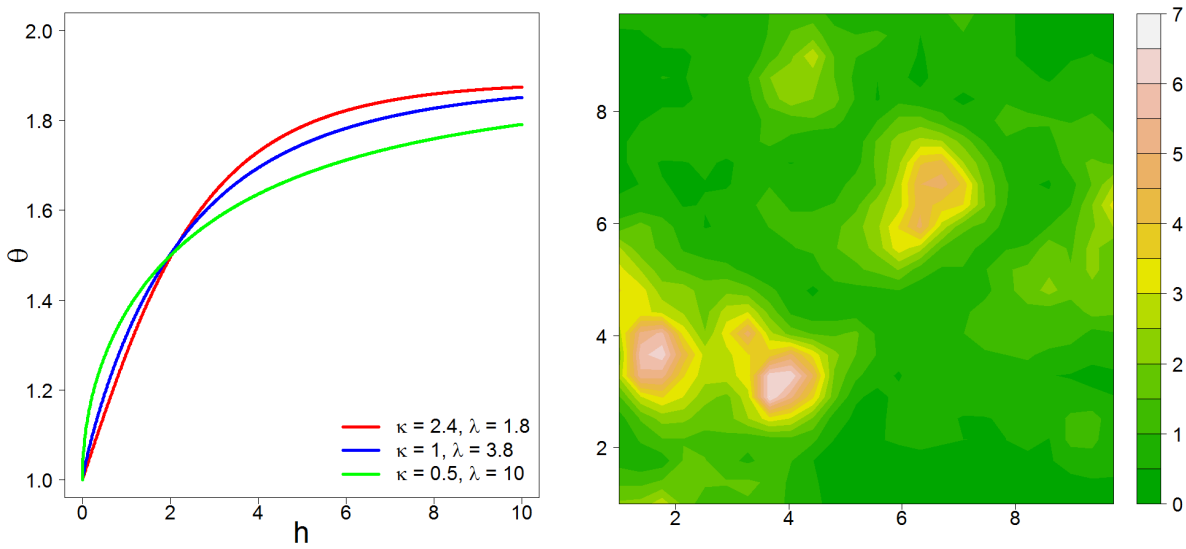


(a) (b)

***Figure 1.7:*** *(a) Extremal function for the geometric Gaussian process with* $\sigma^2 = 5$ *the Whittle-Matérn covariance function for* $\{\kappa = 2.4, \lambda = 1.8\}$ *(red),* $\{\kappa = 1, \lambda = 3.8\}$ *(blue) and* $\{\kappa = 0.5, \lambda = 10\}$ *(green).(b) One realisation of the geometric Gaussian process on the square* $[0, 10]^2$ *with* $\sigma^2 = 5$ *and the Whittle-Matérn correlation function with* $\kappa = 1$, $\lambda = 3.8$ *(in blue in (a)).*

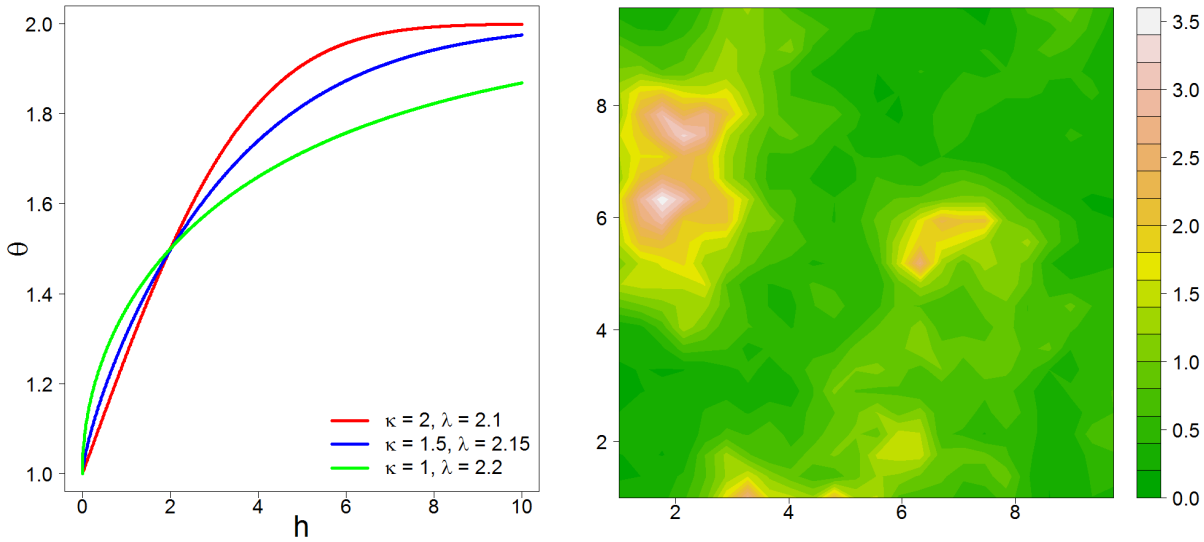


(a) (b)

***Figure 1.8:*** *(a) Extremal function of Brown-Resnick process with the semivariogram* $\gamma(h) = (h/\lambda)^{\kappa}$ *for* $\{\kappa = 2, \lambda = 2.1\}$ *(red),* $\{\kappa = 1.5, \lambda = 2.15\}$ *(blue) and* $\{\kappa = 1, \lambda = 2.2\}$ *(green). (b) One realization of the Brown-Resnick process on the square* $[0, 10]^2$ *with the semivariogram* $\gamma(h) = (h/2.15)^{1.5}$ *(in blue in (a)).*

If the semivariogram $\gamma$ is based on a correlation function $\rho$ as described in subsection 1.3.3, that is to say $\gamma(h) = \sigma^2(1 - \rho(h))$, then the Brown-Resnick process with semivariogram $\gamma$ is equivalent to the Geometric Gaussian process with correlation function $\rho$. Thus, the Brown-Resnick process is a generalization of the Geometric Gaussian process.

The main interest of using the Brown-Resnick process instead of the geometric Gaussian one is if the semivariogram $\gamma$ is not bounded, for instance a linear or a power semivariogram (Table 1.2). In this case, the extremal coefficient

$$\theta(x_1, x_2) = 2\Phi\left(\frac{a}{2}\right) \tag{1.33}$$

converges to 2 when the distance $h$ between $x_1$ and $x_2$ increases infinitly (Figure 1.8(a)). In this way, Brown-Resnick process provides realistic realization (Figure 1.8(b)) imposing extremal independence for large distances.

#### 1.4.4.5 Extremal-t process

The extremal-t process generalizes the Schlather process. The spectral representation of the extremal-t process is given in Opitz (2013) :

$$Z(x) = \max_{i \geq 1} \eta_i \max \{0, Y_i(x)\}^{\nu} . \tag{1.34}$$

Here $\{\eta_i\}_{i\geq 1}$ are the points of a Poisson process on $\mathbb{R}_+$ with intensity $c_\nu \eta^{-2} \mathrm{d}\eta$, with a coefficient $c_\nu$ equals to $\sqrt{\pi} 2^{-\frac{\nu-2}{2}} \Gamma\left(\frac{\nu+1}{2}\right)^{-1}$ $(\nu \geq 1)$, $\Gamma$ is the Gamma function and $\{Y_i(x)\}$ are independent copies of a stationary Gaussian process. If $\nu = 1$ the process is the Schlather model.

The exponent measure is given by

$$V(z_1, z_2) = \frac{1}{z_1} T_{\nu+1}\left(-\frac{\rho(h)}{b} + \frac{1}{b}\left(\frac{z_2}{z_1}\right)^{1/\nu}\right) + \frac{1}{z_2} T_{\nu+1}\left(-\frac{\rho(h)}{b} + \frac{1}{b}\left(\frac{z_1}{z_2}\right)^{1/\nu}\right) \tag{1.35}$$

with $b = \sqrt{\frac{1-\rho^2(h)}{\nu+1}}$ and $T_\nu$ is the the Student distribution with $\nu$ degrees of freedom.

As for the Schlather process, the extremal function

$$\theta(x_1, x_2) = 2T_{\nu+1}\left(\sqrt{\frac{\nu+1}{1-\rho^2(h)}} - \sqrt{\frac{\nu+1}{1-\rho^2(h)}}\rho(h)\right) \tag{1.36}$$

does not converge to 2 (extremal independence) when $h$ increases infinitely (Figure 1.9(a)):

$$\theta(x_1, x_2) \underset{h\to\infty}{\longrightarrow} 2T_{\nu+1}(\sqrt{\nu+1}). \tag{1.37}$$

But contrary to the Schlather process that imposes 1.707 as limit, the limit of the extremal-t extremal function $2T_{\nu+1}(\sqrt{\nu+1})$ is controlled by the sill parameter $\nu$. The two extreme cases are the Schlather process ($\nu = 1$) and extremal independence ($\nu \to \infty$). In the same way as the geometric Gaussian process, the extremal-t process produces realistic realizations (Figure 1.9(b)) by being able to be model extremal independence for large distances contrary to the Schlather process.

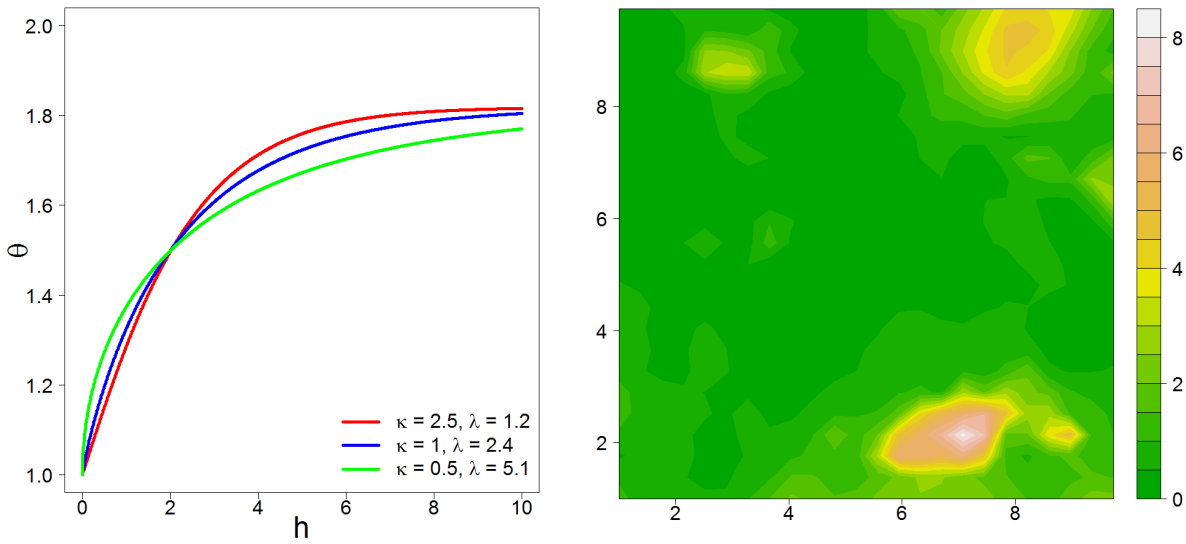


(a) (b)

***Figure 1.9:*** *(a) Extremal function for the extremal-t process on the square* $[0, 10]^2$ *with* $\nu = 2$ *and the Whittle-Matérn covariance function for* $\{\kappa = 2.5, \lambda = 1.2\}$ *(red),* $\{\kappa = 1, \lambda = 2.4\}$ *(blue) and* $\{\kappa = 0.5, \lambda = 5.1\}$ *(green). (b) One realization of the extremal-t process with* $\nu = 2$ *and the Whittle-Matérn correlation function with* $\kappa = 1$ *and* $\lambda = 2.4$ *(in blue in (a)).*

#### 1.4.4.6 Other max-stable process models

Other max-stable process models can be found in the literature. For instance, Smith and Stephenson (2009) and Reich and Shaby (2012) introduced two max-stable processes connected to the Smith process but more flexible. Wadsworth and Tawn (2012) introduced the Gaussian-Gaussian process which is a superposition of the Smith and Schlather processes. Davison and Gholamrezaee (2012) suggested to use a troncated Schlather process. Recently, Xu and Genton (2016) and Beranger et al. (2016) extended respectively the geometric Gaussian and extremal-t processes to the more flexible Tukey and extremal-skew-t processes. However, these max-stable process models are not considered in this work.

### 1.4.5 Anisotropy

Anisotropy can be directly modeled by Smith process with a non spherical covariance matrix $\Sigma$. To account for anisotropy in the others processes, it is possible to use a spatial transformation (Diggle and Ribeiro Jr., 2007, p. 58): for instance in 2-dimensions, coordinates of $x$ in $\mathbb{R}^2$ are replaced with $x' = Vx$ with

$$V = \begin{pmatrix} \cos\alpha & -\sin\alpha \\ r^{-1}\sin\alpha & r^{-1}\cos\alpha \end{pmatrix}. \tag{1.38}$$

The parameter $r > 1$ is called anisotropy ratio and the parameter $\alpha \in [0, \pi)$ is the anisotropy angle.

In 3-dimensions we take

$$V = \begin{pmatrix} \cos\alpha & -\sin\alpha & 0 \\ r^{-1}\sin\alpha & r^{-1}\cos\alpha & 0 \\ 0 & 0 & w \end{pmatrix} \tag{1.39}$$

with $r > 1$ the anisotropy ratio, $\alpha \in [0, \pi)$ the anisotropy angle, and $w > 0$ the weight parameter for altitude. Spatial transformations of this kind are used in Blanchet and Davison (2011) and in Gaume et al. (2013b).

### 1.4.6 Max-stable models inference and selection

Due to computational issues, the full log-likelihood of max-stable processes is usually intractable. To estimate parameters of a max-stable process, we can maximize the pairwise composite log-likelihood (Padoan et al., 2010)

$$l(\beta) = \sum_{n=1}^{N} \sum_{i=1}^{K-1} \sum_{j=i+1}^{K} \log f(z_{n,i}, z_{n,j}; \beta) \tag{1.40}$$

with $K$ the number of stations, $N$ the number of maxima for each location, $z_{n,i}$ the maxima at location $i$ for year $n$, $f$ the bivariate distribution of the max-stable process and $\beta$ the vector of parameters of the bivariate distribution.

The use of alternatives to pairwise composite log-likelihood have been investigated through triplewise composite log-likelihood (Genton et al., 2011; Huser and Davison, 2013), partition-composite log-likelihood (Bienvenüe and Robert, 2014) or composite log-likelihood of higher order (Castruccio et al., 2016). Bayesian inference is also possible (Thibaud et al., 2017).

The maximum pairwise composite likelihood estimator $\hat{\beta}$ is consistent and satisfies (Padoan et al., 2010; Ribatet, 2013)

$$\sqrt{n}\left(\hat{\beta} - \beta_0\right) \longrightarrow \mathcal{N}(0, H^{-1}(\beta_0)J(\beta_0)H^{-1}(\beta_0)) \qquad n \to \infty \tag{1.41}$$

with $\beta_0$ the true vector of parameters, and $H(\beta)$ and $J(\beta)$ the Hessian and Jacobian information matrices defined by

$$H(\beta) = -\sum_{n=1}^{N} \sum_{i=1}^{K-1} \sum_{j=i+1}^{K} \frac{\partial^2 \log f(z_{n,i}, z_{n,j}; \beta)}{\partial\beta\partial\beta^t} \tag{1.42}$$

and

$$J(\beta) = \sum_{n=1}^{N} \left\{ \sum_{i=1}^{K-1} \sum_{j=i+1}^{K} \frac{\partial \log f(z_{n,i}, z_{n,j}; \beta)}{\partial\beta} \right\} \left\{ \sum_{i=1}^{K-1} \sum_{j=i+1}^{K} \frac{\partial \log f(z_{n,i}, z_{n,j}; \beta)}{\partial\beta} \right\}'. \tag{1.43}$$

The related classical inference criterion to discriminate max-stable models is the CLIC (Composite Likelihood Information Criterion) (Padoan et al., 2010)

$$\text{CLIC} = -2\left\{ l(\hat{\beta}) - tr(\hat{J}(\hat{\beta})\hat{H}^{-1}(\hat{\beta})) \right\} \tag{1.44}$$

The lower the CLIC, the better the model. An alternative to CLIC, less usual and not considered in this thesis, is the CLBIC (Composite Bayesian Likelihood Information Criterion) (Gao and Song, 2010).

# Chapter 2

# A multi-criteria leave-two-out cross-validation procedure for max-stable process selection

The content of this chapter is submitted to Spatial Statistics. The authors are Gilles Nicolet, Nicolas Eckert, Samuel Morin and Juliette Blanchet.

# Abstract

Max-stable processes are the extension of the univariate extreme value theory to the spatial case. Contrary to the univariate case, there is no unique parametric form for the limiting distribution in the spatial case, and several max-stable processes can be found in the literature. Selecting the best of them for the data under study is still an open question. This paper proposes a procedure for discriminating max-stable processes by focusing on their spatial dependence structure. Specifically, it combines a leave-two-out cross-validation scheme and a large panel of adapted criteria. We compare five of the most commonly used max-stable processes, using as a case study a large data set of winter maxima of 3-day precipitation amounts in the French Alps (90 stations from 1958 to 2012). All the introduced criteria show that the extremal-t, geometric Gaussian and Brown-Resnick processes are equally able to represent the structure of dependence of the data, regardless of the number of stations or years. Although these results have to be confirmed by replicating the study in other contexts, they may be valid for a wide range of environmental applications.

## 2.1 Introduction

Model selection is a classical issue in statistics, whether to make a choice between several families of parametric models or to make a selection between several explanatory variables. A proper model selection should be done through the use of statistical criteria, which should be able to measure the ability of a model to predict or explain data, or to compare and rank models. The well-known coefficient of determination $R^2$ (Barrett, 1974) and the adjusted coefficient of determination $\hat{R}^2$ (Srivastava et al., 1995) consider the proportion of total variability explained by the model. Likelihood-ratio tests (Vuong, 1989) can be used to compare nested models. Non-nested models can be compared using Bayes factor (Kass and Raftery, 1995) or likelihood based criteria such as the Akaike Information Criterion (AIC, Akaike (1974)) or the Bayesian Information Criterion (BIC, Schwarz et al. (1978)). However, although these criteria are able to compare models, they do not measure the suitability of a given model for prediction. A classical method for assessing the predictive efficiency of a model is cross-validation (Arlot et al., 2010) which consists in splitting data, once or several times, into two parts: the first one is used to fit the model and the second one for validation (Pujol et al., 2007; Blanchet and Lehning, 2010; Westra et al., 2013).

In extreme value statistics (Coles, 2001), one generally extrapolates far beyond the highest recorded observation, mostly for risk mitigation purpose. That is why the predictive ability of the models is particularly crucial. A proper model selection in extreme value statistics should therefore particularly consider the predictive qualities of the models in competition. In the "block maxima" approach of univariate extreme value theory, the Fisher-Tippett-Gnedenko theorem (Fisher and Tippett, 1928; Gnedenko, 1943) ensures that the limiting distribution for maxima of random variables is the GEV (Generalized Extreme Value) distribution. Therefore, in this case, model selection does not rely on the choice of the distribution, but rather on the choice of covariates for GEV parameters or, ultimately, on the sign of the shape parameter which determines the type of distribution (Fréchet, Gumbel or reversed Weibull). However, in the multivariate case, there is no unique parametric form for the limiting distribution and it is necessary to find a parametric extreme value copula flexible enough to capture the structure of dependence (Ribatet and Sedki, 2012; Davison et al., 2012), or to work in a nonparametric framework (Capéraà et al., 1997; Zhang et al., 2008). Max-stable processes (de Haan, 1984) are the extension of the multivariate GEV distribution to the infinite dimension and are mostly used in a spatial context (Davison et al., 2012; Ribatet, 2013). Max-stable processes are usually considered with unit Fréchet margins, and in this case they all may

be expressed through the de Haan's spectral representation (de Haan, 1984). However, several parametric distributions resulting from this representation exist, each proposal of the literature representing a specific way of modeling the spatial dependence structure of extreme values. Model selection is thus an important issue.

The first two max-stable processes to be introduced are the Smith (Smith, 1990) and Schlather (Schlather, 2002) processes. However, they have some major drawbacks. The Smith process provides too smooth realizations which are usually not realistic (Reich and Shaby, 2012; Wadsworth and Tawn, 2012). The Schlather process assumes rather strong dependence in extremes (extremal dependence) at two locations regardless of the distance apart, which is questionable for many data (Blanchet and Davison, 2011; Davison et al., 2012). One way to solve this difficulty is to divide the studied area into several sub-regions in which the non-independence assumption of the Schlather process may hold (Blanchet and Davison, 2011; Lee et al., 2013). However, the choice of these sub-regions may be an issue in itself. Several new max-stable processes were introduced recently to solve these drawbacks. Smith and Stephenson (2009) suggested an extended Smith process. The Brown-Resnick (Kabluchko et al., 2009) and geometric Gaussian (Davison et al., 2012) processes have similar expression of the joint distribution as the Smith process but with more realistic realizations. Reich and Shaby (2012) proposed a max-stable process connected to the Smith process but including a nugget term and thus producing also more realistic realizations. Wadsworth and Tawn (2012) introduced the Gaussian-Gaussian process which is a superposition of the Smith and Schlather processes in order to keep the advantages of both families without their drawbacks. Davison and Gholamrezaee (2012) suggested to use a truncated Schlather process instead of the classical Schlather process with the aim of reaching independence in extremes far apart. The extremal-t process (Opitz, 2013) is a generalization of the Schlather process with an additional parameter controlling the extremal dependence between locations far apart. Recently, the geometric Gaussian process was extended to the even more flexible Tukey process (Xu and Genton, 2016).

Several applications of max-stable processes (Shang et al., 2011; Westra and Sisson, 2011; Lee et al., 2013; Raillard et al., 2014; Zhang et al., 2014) make the choice of considering only one max-stable process to model the data. Others studies use the Composite Likelihood Information Criterion (CLIC (Padoan et al., 2010)) to compare different families of max-stable processes or to compare different choices in the parametrization of a given max-stable process (e.g., the choice of the correlation function in Schlather process (Blanchet and Davison, 2011)). On this basis, the Schlather process was found to be more suitable than the Smith process for extreme snow depth in Switzerland (Blanchet and

Davison, 2011). The geometric Gaussian and Brown-Resnick processes outperformed the Smith and Schlather processes for extreme rainfall in Switzerland (Davison et al., 2012). The Brown-Resnick process outperformed the Smith and Schlather processes for extreme snowfall in the French Alps (Gaume et al., 2013b). Yet, none of these studies considered selection criteria able to compare the predictive ability of the different processes. Indeed, in the same way as AIC criteria for example, CLIC is based on the value of the composite likelihood with a penalization on the complexity of the model. Also, most of these papers consider together the question of model selection regarding marginal distributions in term of covariates for the GEV parameters and regarding the spatial dependence structure.

This paper proposes a practical framework for discriminating between max-stable processes by evaluating their predictive ability. We introduce a panel of statistical criteria well suited to compare several max-stable processes by considering their spatial dependence in extremes. We evaluate this in a systematic leave-two-out cross-validation scheme. The proposed framework is not data-specific and may be used in many applications. For sake of illustration, we consider in this paper a case study consisting in a large data set of 3 days cumulated snowfall maxima in the French Alps (90 stations from 1958 to 2012), which have already been investigated in Nicolet et al. (2016). We consider the Brown-Resnick, geometric Gaussian and extremal-t processes, which have previously been found to be suitable for hydrological applications (Davison et al., 2012; Gaume et al., 2013b; Bechler et al., 2015), as well as the first two max-stable processes to be introduced, the Smith and Schlather processes. We also consider a large set of correlation functions for the Schlather, geometric Gaussian and extremal-t processes. The models are estimated by maximum composite likelihood (Padoan et al., 2010), and for each process, one paramerization (corresponding to the choice of a family of correlation functions or semivariograms) is selected by CLIC. The five resulting models are compared by assessing, for each pair of stations, goodness-of-fit of the bivariate distribution derived from the model fitted on the remaining 88 other stations. We use the root mean square error (RMSE), mean average error (MAE), root mean square normalized error (RMSNE), mean average normalized error (MANE) and coefficient of determination ($R^2$) to measure the deviation between empirical and max-stable-based estimations of the probability of jointly exceeding a given quantile at two locations. We also consider the *FF* and $N_T$ criteria which are usually used to assess the reliability of univariate distribution estimation (Garavaglia et al., 2011; Renard et al., 2013; Blanchet et al., 2015). The *FF* criterion is based on the maxima over all the study period whereas the $N_T$ criterion

focuses on the distribution of the number of exceedances of the T-year return level. Here, these criteria are tailored to the bivariate case by being applied to the minima at two locations. Last but not least, the sensitivity of the models to the number of stations and to the number of years of observations is investigated.

## 2.2 Data

Our data set is composed of winter maxima of 3 days cumulated snowfalls with a winter period defined from 15 November to 15 May. We choose a period of 3 days because this is the most usual time scale of winter storms and hence is often considered in avalanche forecasting (Bocchiola et al., 2006; Eckert et al., 2010, 2011; Gaume et al., 2012). Daily data are available from 15 November 1958 to 15 May 2013 in the French Alps through observations of precipitation done mostly manually (climatological and dedicated snow observing networks). We use all the observations whose type of precipitation (rain or snow) was registered as snow. If the indication about the phase of precipitation is missing, we retain precipitations measured when minimal daily temperature is lower than 2°C. Since several locations of measurement were slightly modified during the study period, we pooled together the stations with less than 100 m difference in elevation and less than 2 km in distance in the 2-D plane. Finally, we retain the 90 stations which have at least 40 winter maximum values (computed from a moving window of 3 days) during the study period (Figure 2.1). Their elevation ranges from 291 m to 2012 m. Hence, the station set is a good compromise between spatial and altitudinal coverage and length of records.

## 2.3 Method

### 2.3.1 Max-stable processes

#### 2.3.1.1 Definition and spectral representation

Let $\chi$ be a space and $\{X_i(x)\}_{x\in\chi}$ a process with $i$ denoting the number of the day in the block ($1 \leq i \leq n_0$ with $n_0$ the length of the block). Spatial extreme value theory (Davison et al., 2012; Cooley et al., 2012) ensures that the process of block maxima

$$\{Z(x)\}_{x\in\chi} = \left\{ \max_{1\leq i\leq n_0} X_i(x) \right\}_{x\in\chi}, \tag{2.1}$$

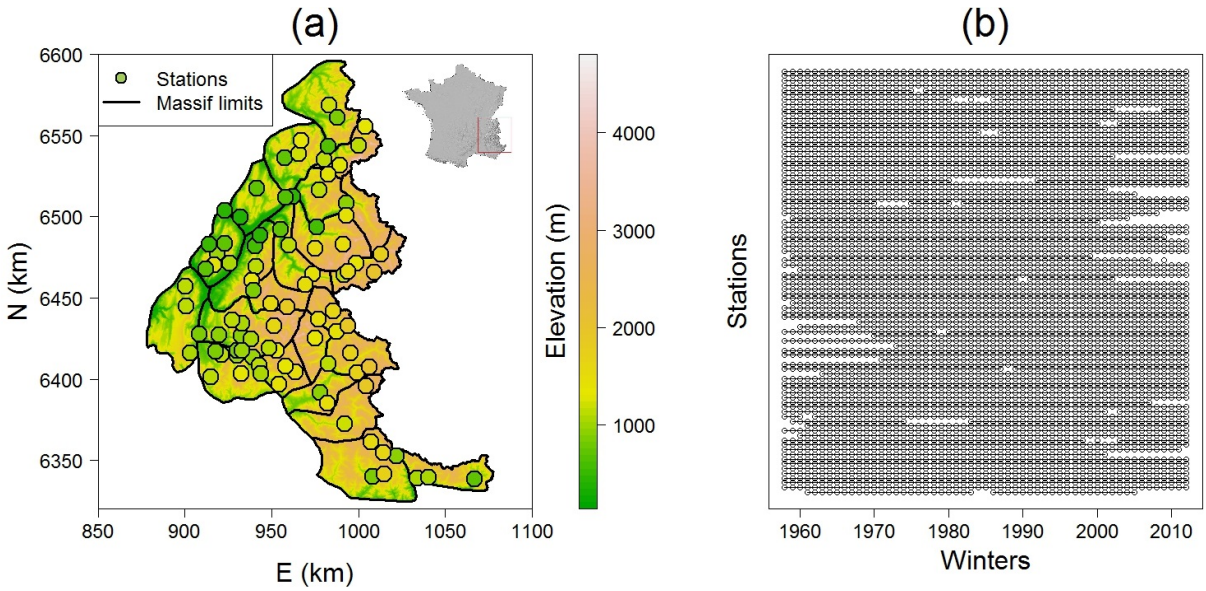


***Figure 2.1:*** *(a) Study area in the southeast of France, where the 23 massifs of the French Alps are located. Lines denote massif limits, and dots denote the positions of the stations. The color code represents elevation. (b) Data availability for each station. Each line represents one station, and each point means that the winter maximum is available for that station.*

with $n_0$ sufficiently large, should be modeled as a max-stable process (de Haan, 1984). Every univariate margins $Z(x)$ of a max-stable process $Z$ are GEV($\mu(x)$,$\sigma(x)$,$\xi(x)$) distributed, i.e., with cumulative distribution function

$$F_{\mu(x),\sigma(x),\xi(x)}(z) = \exp\left\{-\left[1+\xi(x)\left(\frac{z-\mu(x)}{\sigma(x)}\right)\right]^{-1/\xi(x)}\right\} \tag{2.2}$$

with $\mu(x)$, $\sigma(x)$ and $\xi(x)$ denoting respectively the location, scale and shape parameters at position $x$, and $z$ is such that $1+\xi(x)\left(\frac{z-\mu(x)}{\sigma(x)}\right) > 0$. The function $F$ is equal to 0 in the case of $\xi(x) > 0$ and $z \leq \mu(x) - \frac{\sigma(x)}{\xi(x)}$, and equal to 1 if $\xi(x) < 0$ and $z \geq \mu(x) - \frac{\sigma(x)}{\xi(x)}$.

Since here only the dependence of $\{Z(x)\}_{x\in\chi}$ is of interest we normalize, without loss of generality, the margins into unit Fréchet (i.e., GEV(1,1,1)) by using the transformation

$$Z(x) \to \frac{-1}{\log\left\{F_{\mu(x),\sigma(x),\xi(x)}(Z(x))\right\}}. \tag{2.3}$$

In this case, de Haan (1984) ensures that the process $\{Z(x)\}_{x\in\chi}$ can be written as

$$Z(x) = \sup_{i\geq 1} \eta_i W_i(x), \qquad x \in \chi \tag{2.4}$$

with $\{\eta_i\}_{i\geq 1}$ the points of a Poisson process on $\mathbb{R}_+$ with intensity $\eta^{-2}d\eta$ and $\{W_i(x)\}_{i\geq 1}$ independent copies of a nonnegative process $\{W(x)\}$ with mean 1. Different choices for $\{W_i(x)\}$ in (2.4) lead to different families of max-stable processes.

#### 2.3.1.2 Parametric max-stable families

Here we describe the five parametric families considered in this study for modeling spatial dependence in extremes.

The Smith process (Smith, 1990) is obtained by taking $W_i(x) = g(x - X_i)$ in (2.4) with $g$ the density function of a multivariate Gaussian distribution with mean 0 and covariance matrix $\Sigma$ and $\{\eta_i, X_i\}$ the points of a Poisson process on $\mathbb{R}_+ \times \chi$ with intensity $\eta^{-2}d\eta\, dx$. The bivariate distribution of this process for $Z(x_1)$ and $Z(x_2)$ (with $x_1$ and $x_2$ two locations) is

$$\mathbb{P}\left(Z(x_1) < z_1, Z(x_2) < z_2\right) = \exp\left\{-\frac{1}{z_1}\Phi\left(\frac{a}{2} + \frac{1}{a}\log\frac{z_2}{z_1}\right) - \frac{1}{z_2}\Phi\left(\frac{a}{2} + \frac{1}{a}\log\frac{z_1}{z_2}\right)\right\} \tag{2.5}$$

with $\Phi$ the distribution function of the standard normal distribution and $a$ the Mahalanobis distance which is defined as $a = \sqrt{(x_2 - x_1)^T\Sigma^{-1}(x_2 - x_1)}$.

The Schlather process (Schlather, 2002) uses $W_i(x) = \sqrt{2\pi}\max\{0, Y_i(x)\}$ with $\{Y_i(x)\}$ independent copies of a stationary Gaussian process with correlation function $\rho$. The bivariate distribution is given by

$$\mathbb{P}\left(Z(x_1) < z_1, Z(x_2) < z_2\right) = \exp\left\{-\frac{1}{2}\left(\frac{1}{z_1} + \frac{1}{z_2}\right)\left(1 + \sqrt{1 - 2(\rho(h)+1)\frac{z_1 z_2}{(z_1+z_2)^2}}\right)\right\} \tag{2.6}$$

with $h$ the Euclidean distance between the two locations $x_1$ and $x_2$.

The geometric Gaussian process (Davison et al., 2012)) takes $W_i(x) = \exp\left(\sigma Y_i(x) - \frac{\sigma^2}{2}\right)$ with $\{Y_i(x)\}$ independent copies of a stationary Gaussian process with mean 0, variance $\sigma^2$ and correlation function $\rho$. The bivariate distribution function is the same as for the Smith process with $a = \sqrt{2\sigma^2(1 - \rho(h))}$ in (2.5).

The Brown-Resnick process (Kabluchko et al., 2009) generalizes the geometric Gaussian process with $W_i(x) = \exp\{Y_i(x) - \gamma(x)\}$, where $\{Y_i(x)\}$ are independent copies of a Gaussian process with stationary increments and such that $W_i(0) = 0$ almost surely. The process uses a semivariogram $\gamma$. Expression for the bivariate distribution is the same as for the Smith process with $a = \sqrt{2\gamma(h)}$ in (2.5).

The extremal-t process (Opitz, 2013) uses $W_i(x) = c_\nu \max\{0, Y_i(x)\}^\nu$ with $c_\nu$ equals to $\sqrt{\pi}2^{-\frac{\nu-2}{2}}\Gamma\left(\frac{\nu+1}{2}\right)^{-1}$ $(\nu \geq 1)$, $\Gamma$ the Gamma function and $\{Y_i(x)\}$ independent copies of a stationary Gaussian process. If $\nu = 1$ we recover the Schlather process. The bivariate distribution is given by

$$\mathbb{P}\left(Z(x_1) < z_1, Z(x_2) < z_2\right) = \exp\left\{-\frac{1}{z_1}T_{\nu+1}\left(\frac{1}{b}\left(\frac{z_2}{z_1}\right)^{1/\nu} - \frac{\rho(h)}{b}\right) - \frac{1}{z_2}T_{\nu+1}\left(\frac{1}{b}\left(\frac{z_1}{z_2}\right)^{1/\nu} - \frac{\rho(h)}{b}\right)\right\} \quad (2.7)$$

with $b = \sqrt{\frac{1-\rho^2(h)}{\nu+1}}$ and $T_\nu$ is the distribution function of the Student distribution with $\nu$ degrees of freedom.

#### 2.3.1.3 Inference

Due to computational issues, the full log-likelihood of max-stable processes is usually intractable. Parameter estimation is often performed by maximizing the pairwise composite log-likelihood (Padoan et al., 2010)

$$l(\beta) = \sum_{n=1}^{N}\sum_{i=1}^{K-1}\sum_{j=i+1}^{K} \log f(z_{n,i}, z_{n,j}; \beta) \quad (2.8)$$

with $K$ the number of stations, $N$ the number of years, $z_{n,i}$ the maxima at location $i$ for year $n$, $f$ the max-stable bivariate density associated to equations (2.5)–(2.7) and $\beta$ the vector of parameters.

### 2.3.2 Model comparison criteria

#### 2.3.2.1 Composite Likelihood Information Criterion

The classical inference criterion to discriminate max-stable models is the CLIC (Composite Likelihood Information Criterion) (Padoan et al., 2010)

$$\text{CLIC} = -2\left\{l(\hat{\beta}) - tr(\hat{J}\hat{H}^{-1})\right\} \tag{2.9}$$

with $\hat{\beta}$ the vector which maximizes the composite likelihood $l$ in (2.8), $\hat{H}$ and $\hat{J}$ the Hessian and Jacobian information matrices defined by

$$H = -\sum_{n=1}^{N}\sum_{i=1}^{K-1}\sum_{j=i+1}^{K}\frac{\partial^2 \log f(z_{n,i}, z_{n,j}; \hat{\beta})}{\partial\beta\partial\beta^t} \tag{2.10}$$

and

$$J = \sum_{n=1}^{N}\left\{\sum_{i=1}^{K-1}\sum_{j=i+1}^{K}\frac{\partial \log f(z_{n,i}, z_{n,j}; \hat{\beta})}{\partial\beta}\right\}\left\{\sum_{i=1}^{K-1}\sum_{j=i+1}^{K}\frac{\partial \log f(z_{n,i}, z_{n,j}; \hat{\beta})}{\partial\beta}\right\}'. \tag{2.11}$$

It is considered that the lower the CLIC, the better the model. As in Blanchet and Davison (2011), we rescaled the CLIC by dividing by K-1.

#### 2.3.2.2 RMSE, MAE, RMSNE, MANE and $R^2$ criteria

In extreme value statistics, one deals with very low exceedance probabilities which are usually defined through return periods or large quantiles. For each pair of stations $(x_i, x_j)$ and each return period $T$, we define the probability of joint exceedance by

$$\lambda(x_i, x_j, z_T) = \mathbb{P}\left\{Z(x_i) > z_T, Z(x_j) > z_T\right\} \tag{2.12}$$

with $z_T = \frac{-1}{\log(1-1/T)}$ the T-year return level of unit Fréchet variables, and $\lambda(x_i, x_j, z_T)$ denotes the probability of exceeding $z_T$ at the two locations $x_i$ and $x_j$ during the same block period. The probability of joint exceedance is assessed using the decomposition:

$$\begin{aligned}\lambda(x_i, x_j, z_T) &= 1 - \mathbb{P}\left\{Z(x_i) < z_T\right\} - \mathbb{P}\left\{Z(x_j) < z_T\right\} \\ &\quad + \mathbb{P}\left\{Z(x_i) < z_T, Z(x_j) < z_T\right\} \\ &= 1 - 2\left(1 - \frac{1}{T}\right) + \mathbb{P}\left\{Z(x_i) < z_T, Z(x_j) < z_T\right\}\end{aligned} \tag{2.13}$$

In (2.13), $\mathbb{P}\left\{Z(x_i) < z_T, Z(x_j) < z_T\right\}$ is given by the bivariate distribution in (2.5), (2.6) or (2.7), depending on the family of max-stable processes.

The deviation between max-stable-based estimations $\lambda_{mod}$ and empirical estimations $\lambda_{emp}$ are assessed through

i) root mean square error

$$\mathrm{RMSE} = \left\{ \frac{2}{\mathrm{card}(\tau)K(K-1)} \sum_{i=1}^{K-1} \sum_{j=i+1}^{K} \sum_{T\in\tau} \left[\lambda_{mod}(x_i, x_j, z_T) - \lambda_{emp}(x_i, x_j, z_T)\right]^2 \right\}^{1/2}, \quad (2.14)$$

ii) mean absolute error

$$\mathrm{MAE} = \frac{2}{\mathrm{card}(\tau)K(K-1)} \sum_{i=1}^{K-1} \sum_{j=i+1}^{K} \sum_{T\in\tau} \left|\lambda_{mod}(x_i, x_j, z_T) - \lambda_{emp}(x_i, x_j, z_T)\right|, \quad (2.15)$$

iii) root mean square normalized error

$$\mathrm{RMSNE} = \left\{ \frac{2}{\mathrm{card}(\tau)K(K-1)} \sum_{i=1}^{K-1} \sum_{j=i+1}^{K} \sum_{T\in\tau} \left[\frac{\lambda_{mod}(x_i, x_j, z_T) - \lambda_{emp}(x_i, x_j, z_T)}{\lambda_{emp}(x_i, x_j, z_T)}\right]^2 \mathbf{1}_{\lambda_{emp}(x_i,x_j,z_T)\neq 0} \right\}^{1/2}, \quad (2.16)$$

iv) mean absolute normalized error

$$\mathrm{MANE} = \frac{2}{\mathrm{card}(\tau)K(K-1)} \sum_{i=1}^{K-1} \sum_{j=i+1}^{K} \sum_{T\in\tau} \left|\frac{\lambda_{mod}(x_i, x_j, z_T) - \lambda_{emp}(x_i, x_j, z_T)}{\lambda_{emp}(x_i, x_j, z_T)}\right| \mathbf{1}_{\lambda_{emp}(x_i,x_j,z_T)\neq 0}, \quad (2.17)$$

v) and coefficient of determination

$$R^2 = 1 - \frac{\sum_{i=1}^{K-1}\sum_{j=i+1}^{K}\sum_{T\in\tau}\left[\lambda_{mod}(x_i,x_j,z_T) - \lambda_{emp}(x_i,x_j,z_T)\right]^2}{\sum_{i=1}^{K-1}\sum_{j=i+1}^{K}\sum_{T\in\tau}\left[\lambda_{emp}(x_i,x_j,z_T) - \overline{\lambda}_{emp}\right]^2} \tag{2.18}$$

with $K$ the number of stations, $\tau$ the set of the considered return periods, $\overline{\lambda}_{emp}$ the mean of empirical estimations over all $x_i$, $y_j$ and $z_T$, and **1** the indicator function. According to these criteria, the lower the values of RMSE, MAE, RMSNE and MANE, the better the model, and the larger the coefficient of determination $R^2$, the better the model.

#### 2.3.2.3 $N_T$ and FF criteria

The $N_T$ and $FF$ indexes are used in Garavaglia et al. (2011), Renard et al. (2013) and Blanchet et al. (2015) to assess the reliability of univariate distribution estimation. In order to use them for bivariate distributions, we apply them here to $M(i,j) = \min(Z(x_i), Z(x_j))$ which is the minimum at two locations $(x_i, x_j)$ of the max-stable process $Z$. In this case, the $N_T$ and $FF$ criteria assess the reliability of $\hat{F}^{M(i,j)}$, the estimated cumulative distribution function of $M(i,j)$. Specifically, $\hat{F}^{M(i,j)}$ is given by

$$\begin{aligned}
\hat{F}^{M(i,j)}(z) &= \mathbb{P}\left\{Z(x_i) < z \text{ or } Z(x_j) < z\right\} && (2.19)\\
&= \mathbb{P}\left\{Z(x_i) < z\right\} + \mathbb{P}\left\{Z(x_j) < z\right\} - \mathbb{P}\left\{Z(x_i) < z, Z(x_j) < z\right\} \\
&= 2F_{1,1,1}(z) - \hat{F}_{x_i,x_j}(z,z) && (2.20)
\end{aligned}$$

with $F_{1,1,1}(z) = \exp(-1/z)$ the unit Fréchet cumulative distribution function, and $\hat{F}_{x_i,x_j}$ the estimated bivariate cumulative distribution function stemming from the fitted max-stable process for the locations $x_i$ and $x_j$ and defined by (2.5), (2.6) or (2.7), depending on the family of max-stable processes. The expression of the criteria in our bivariate case are detailed in Appendix A.

### 2.3.3 Workflow

#### 2.3.3.1 Transformation to unit Fréchet margins

The GEV distribution is fitted for each station independently by maximum likelihood. Pointwise estimates of parameters are used to transform marginal distributions into unit Fréchet through the transformation (2.3). We consider this unit Fréchet data set only and do not consider the margins in order to keep the same unit Fréchet data set for all the max-stable processes and to focus on the dependence structure only. Thus, we are interested in a process $\{Z(x)\}$ with unit Fréchet margins for which we have observations $\{z_{n,i}\}_{n=1\ldots N, i=1\ldots K}$.

#### 2.3.3.2 Model preselection with CLIC

The Smith, Schlather, Brown-Resnick, geometric Gaussian and extremal-t processes are fitted to the unit Fréchet data set by maximizing the composite log-likelihood (2.8). We use 14 correlation functions for the Schlather, extremal-t and geometric Gaussian processes, and we use the linear and power semivariograms for the Brown-Resnick process (the formulae of the used semivariograms and correlation functions are given in Appendix B).

Anisotropy is directly modeled in the Smith process with a non spherical covariance matrix $\Sigma$ in (2.5). In order to account for anisotropy in the other processes, a spatial transformation is used. In the same way as Blanchet and Davison (2011) and Nicolet et al. (2016), coordinates of $x$ in $\mathbb{R}^3$ are replaced with $x' = Vx$ such as

$$V = \begin{pmatrix} \cos\psi & -\sin\psi & 0 \\ w_1^{-1}\sin\psi & w_1^{-1}\cos\psi & 0 \\ 0 & 0 & w_2 \end{pmatrix} \tag{2.21}$$

with $\psi$ the anisotropy angle, $w_1 > 1$ the anisotropy ratio and $w_2 > 0$ the weight parameter for altitude. Then, CLIC is computed for each estimated model and among each family of max-stable processes, we only keep one model.

#### 2.3.3.3 Cross-validation

After preselection by CLIC of one parameterization for each family, the Smith, Schlather, Brown-Resnick, geometric Gaussian and extremal-t processes are further compared using a leave-two-out cross-validation. For each pair of stations $(x_i, x_j)$ and for several return periods $T$, the distribution of $M(i,j) = \min(Z(x_i), Z(x_j))$ is inferred from the max-stable process estimated by composite likelihood maximization on the remaining 88 stations.

The deviation between max-stable-based estimations $\lambda_{mod}$ and empirical estimations $\lambda_{emp}$ of the probability of joint exceedance are assessed through RMSE, MAE, RMSNE, MANE and coefficient of determination $R^2$ with $T \in \tau = \{2, 3, 5, 7, 10, 15, 20, 25, 33, 50, 100\}$ years, the set of chosen return periods. We consider values of joint exceedance with full dependence hypothesis between two locations

$$\lambda_1(x_i, x_j, z_T) = \mathbb{P}\left\{Z(x_i) > z_T\right\} = \frac{1}{T} \tag{2.22}$$

and with independence hypothesis between two locations

$$\lambda_2(x_i, x_j, z_T) = \mathbb{P}\left\{Z(x_i) > z_T\right\} \mathbb{P}\left\{Z(x_j) > z_T\right\} = \frac{1}{T^2} \tag{2.23}$$

in order to check that max-stable process based estimations outperform them. Next, a finer comparison is done by assessing RMSE, MAE, RMSNE, MANE for each return period separately ($T \in \tau$ = {2}, {3}, {5}, {7}, {10}, {15}, {20}, {25}, {33}, {50} and {100} years).

Also, for each pair of stations $(x_i, x_j)$, we consider $\hat{F}^{M(i,j)}$, the cumulative distribution function of $M(i,j)$, estimated from the model fitted on the remaining 88 stations. The reliability of these estimates are assessed using $N_{10}$, $N_{20}$ and $FF$ criteria. In order to reduce the dependence among the samples of pairs of stations, $N_{10}$, $N_{20}$ and $FF$ criteria are calculated for samples $\mathcal{D}$ of 45 disjoint pairs of stations, that is to say each station appears in exactly one pair. $N_{10}$, $N_{20}$ and $FF$ are assessed for 1000 samples of disjoint pairs of stations and the considered values for model evaluation are the averages of these 1000 values.

#### 2.3.3.4 Sensitivity testing to the number of stations and years

We use a bootstrap method to assess the prediction ability of the max-stable processes when less stations or less observations are available. The five selected max-stable models are fitted on a sample of $n$ stations (and keeping all the 55 years of observations) with $n$ a multiple of 5. For each $n$, 100 samples of $n$ stations are randomly built. Goodness-of-fit for each of these samples is evaluated using the criteria introduced above. On the 100 values, we compute the average and a 95%-confidence interval using empirical quantiles. Then, we adopt a similar procedure by reducing the number $m$ of considered years (and keeping all the 90 stations).

Note that whatever $n$ (respectively, $m$), the reliability criteria are computed using all the stations (resp., years), i.e. both the stations (resp., years) used and not used to estimate the max-stable models. Of course, the lower $n$ (resp., $m$), the lower the number of pairs (resp., years) which are for used in the model estimation. This explains why for this specific sensitivity study an additional cross-validation step was not found necessary.

## 2.4 Results

### 2.4.1 Model preselection with CLIC

In accordance with the results of the CLIC selection, whose details are given in Appendix C, we use the power semivariogram for the Brown-Resnick process and the Gneiting-Matérn function for the extremal-t, geometric Gaussian and Schlather processes. The parameterization of these five retained models is given in Appendix D.

### 2.4.2 Cross-validation

The values of the criteria introduced in 2.3.2.2 and 2.3.2.3 (Table 2.1) show that the Smith and Schlather models are systematically outperformed by the other ones. The Schlather model is the worst according to all criteria. RMSE, MANE, $R^2$, $N_{10}$ and $FF$ confirm the conclusion drawn from CLIC using all data with the extremal-t model slightly better than the Brown-Resnick and geometric Gaussian ones. The geometric Gaussian model shows the best MAE while, according to RMSNE and $N_{20}$ the Brown-Resnick

| Family | RMSE | MAE | RMSNE | MANE | $R^2$ | $N_{10}$ | $N_{20}$ | $FF$ |
|---|---|---|---|---|---|---|---|---|
| E-t | **0.0242** | 0.0159 | 0.559 | **0.403** | **0.918** | **0.200** | 0.195 | **0.193** |
| GG | 0.0243 | **0.0158** | 0.551 | 0.404 | 0.918 | 0.202 | 0.195 | 0.199 |
| B-R | 0.0243 | 0.0158 | **0.550** | 0.404 | 0.918 | 0.201 | **0.195** | 0.199 |
| Sm | 0.0283 | 0.0172 | 0.600 | 0.484 | 0.889 | 0.269 | 0.279 | 0.281 |
| Sc | 0.0308 | 0.0212 | 0.797 | 0.511 | 0.868 | 0.293 | 0.290 | 0.285 |

***Table 2.1:*** *Cross-validation. RMSE, MAE, RMSNE, MANE, $R^2$, $N_{10}$, $N_{20}$ and FF criteria for the extremal-t, geometric Gaussian and Schlather processes with the Gneiting-Matérn correlation function, the Brown-Resnick process with the power semivariogram and the Smith process. Bold values indicate the best value for each criterion (sometimes distinguishable with the $4^{th}$ or $5^{th}$ significant digit only).*

model performs best. However, results remain very close, confirming that the selection between these three models is complicated. In addition, the comparison between Table 2.4 and Table 2.1 show that the results are extremely similar whether using the full data set or in cross-validation.

Figure 2.2 represents the empirical and max-stable-based estimations of the probabilities of joint exceedance for four pairs of stations, lying at different distances and orientations. These pairs of stations are chosen so as to have a good balance between close and distant stations as well as between northeastern and northwestern orientations. Thus we illustrate different strengths of dependence since the stations are more dependent in extremes when they lie in a short distance and when they are oriented toward the northeast (Nicolet et al., 2016). Figure 2.2 shows that regardless of the strength of dependence, the extremal-t, geometric Gaussian and Brown-Resnick models give very similar estimations of the probabilities of joint exceedance, while the Smith model gives the lowest probabilities with very similar values to the independent case. On the contrary, the Schlather model gives higher probabilities of joint exceedance with the closest values to the complete dependent case.

A finer comparison between the models is done in Appendix E by focusing on their performances for different return period separately.

### 2.4.3 Sensitivity to the number of stations and to the number of years

The extremal-t, geometric Gaussian and Brown-Resnick models turn out to be relatively little sensitive to the number of stations when the 55 years of observations are used (Figure 2.3), with similar performances:

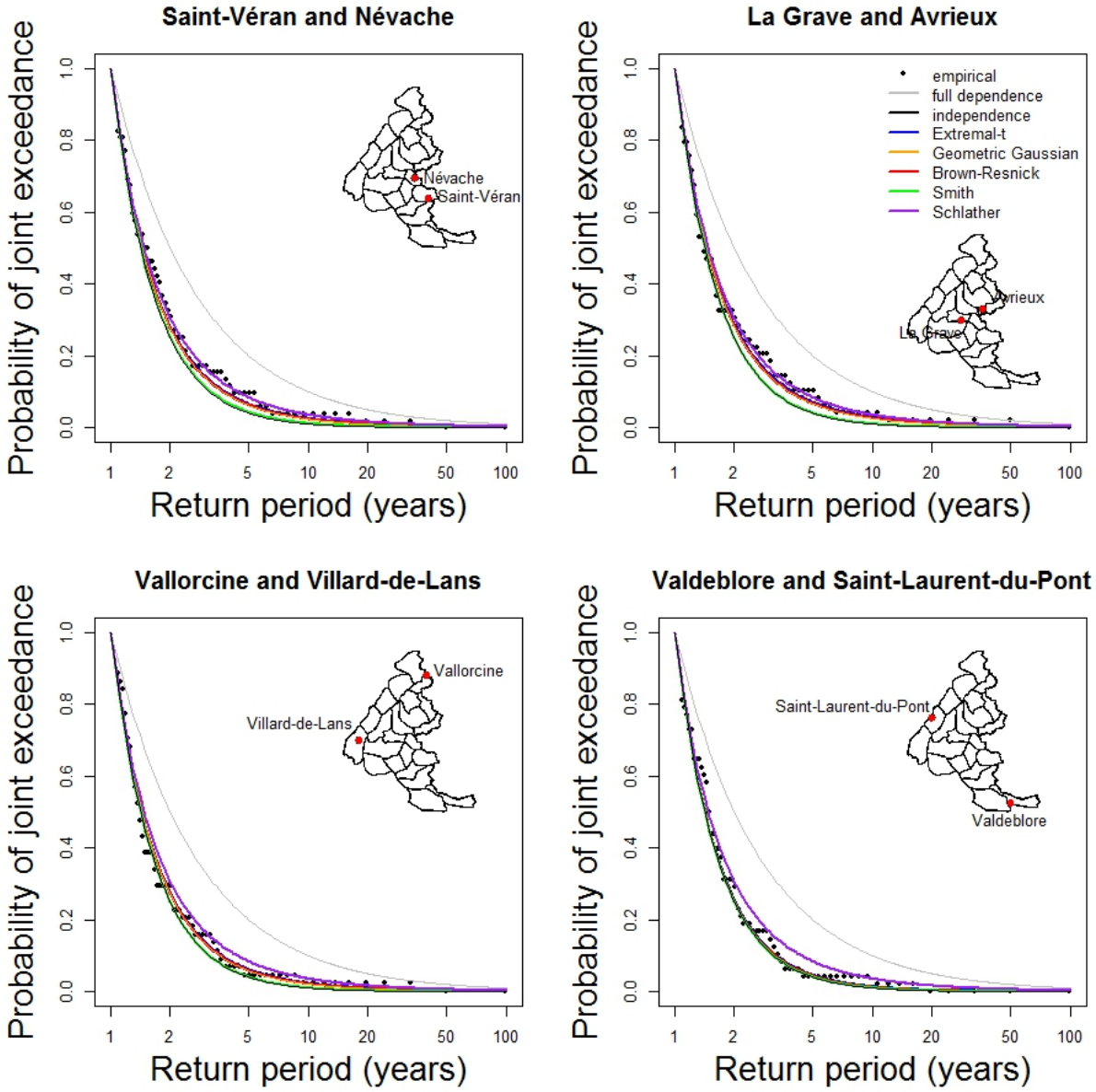


***Figure 2.2:*** *Cross-validation. Joint exceedance probability as function of return period for four pair of stations. Location of each pair of stations is displayed within the map of the 23 massifs of the French Alps.*

- almost no increase of performance when more than 40 stations are used;
- a slight decrease in performance down to 20 stations;
- a more pronounced decrease in performance with less than 20 stations.

Similarly, the three models are little sensitive to the number of observed years when the 90 stations are used (Figure 2.4):

- almost no increase in performance when more than 25 years are observed;
- a slight decrease in performance down to 10 years;
- a more pronounced decrease in performance with less than 10 years.

As expected, the confidence intervals derived from our bootstrap procedure get wider when the number of stations or the number of years decreases. $N_{10}$, $N_{20}$ and $FF$ have the peculiarity that the confidence intervals get wider in both directions (i.e., both smaller and larger errors) due to the additional random selection of 1000 samples $\mathcal{D}$ of 45 pairs of stations (see section 2.3.2.3). All in all, the Brown-Resnick model is slightly less sensitive than the geometric Gaussian and extremal-t models because fewer parameters have to be estimated (however it is more sensitive in the extreme cases of only 5 stations or 5 years of observations).

Under the Smith model, the values of the criteria are quite constant when at least 35 stations or at least 10 years of observations are used (not shown). The Schlather model is almost insensitive to the number of stations and to the number of years (not shown). Indeed, it models the same extremal dependence (which corresponds to the minimal dependence it allows) for almost all the pairs of stations.

## 2.5 Discussion and conclusion

In this paper, we compare five of the most common parametric families of max-stable processes: Smith, Schlather, Brown-Resnick, geometric Gaussian and extremal-t processes, focusing on their predictive ability concerning the spatial dependence structure of extreme values. Each family represents a given way to model extremal dependence in space, and within each of them, several parameterizations exist due to the choice of the correlation function (in the case of the Schlather, geometric Gaussian and extremal-t processes) or of the semivariogram (in the case of the Brown-Resnick process) of the

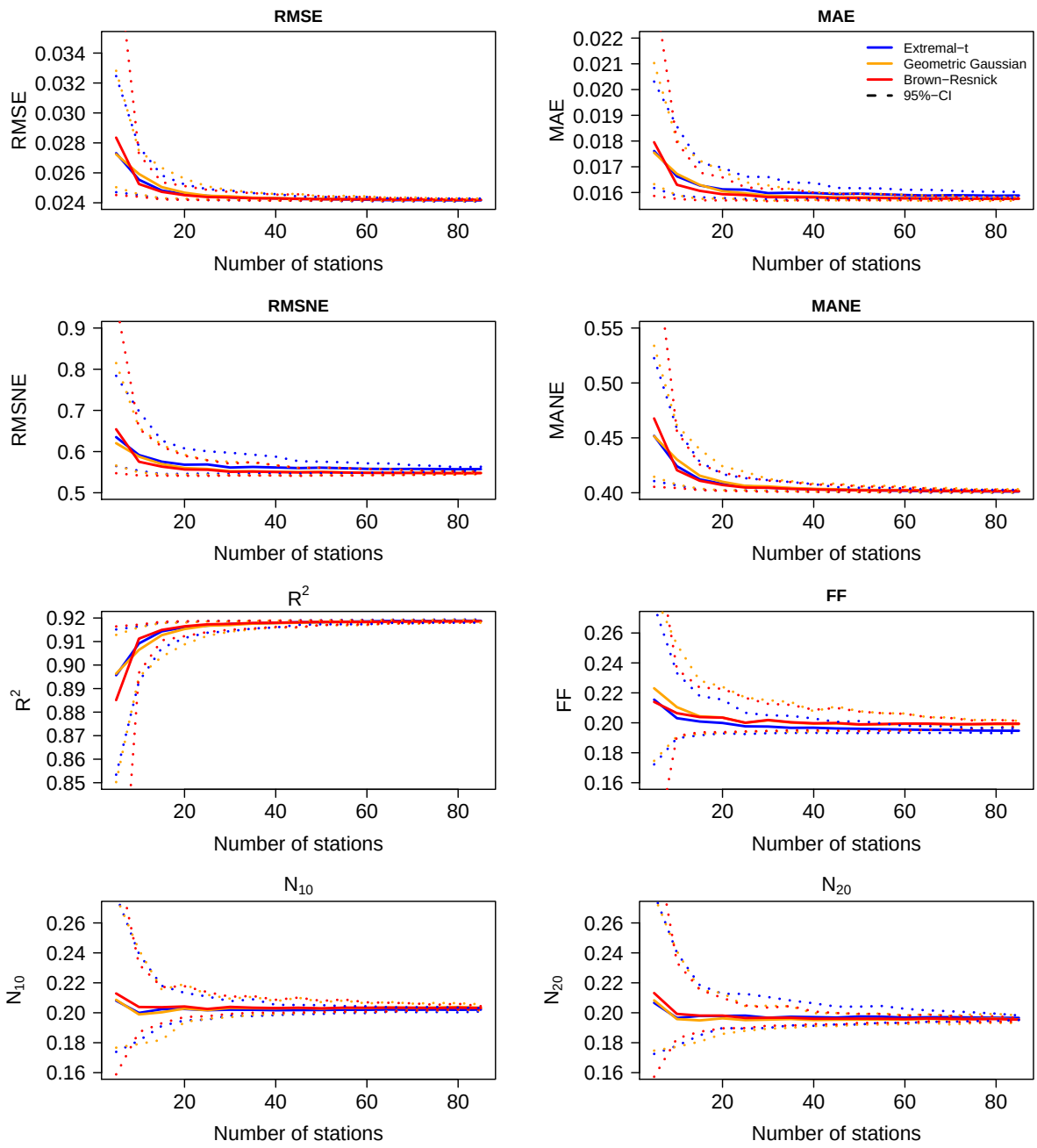


*Figure 2.3:* *RMSE, MAE, $R^2$, RMSNE, MANE, $N_{10}$, $N_{20}$ and FF criteria according to the number of stations, each of them having 55 years of observations. Plain lines represent means. The dotted lines represent the empirical 95%-confidence interval.*

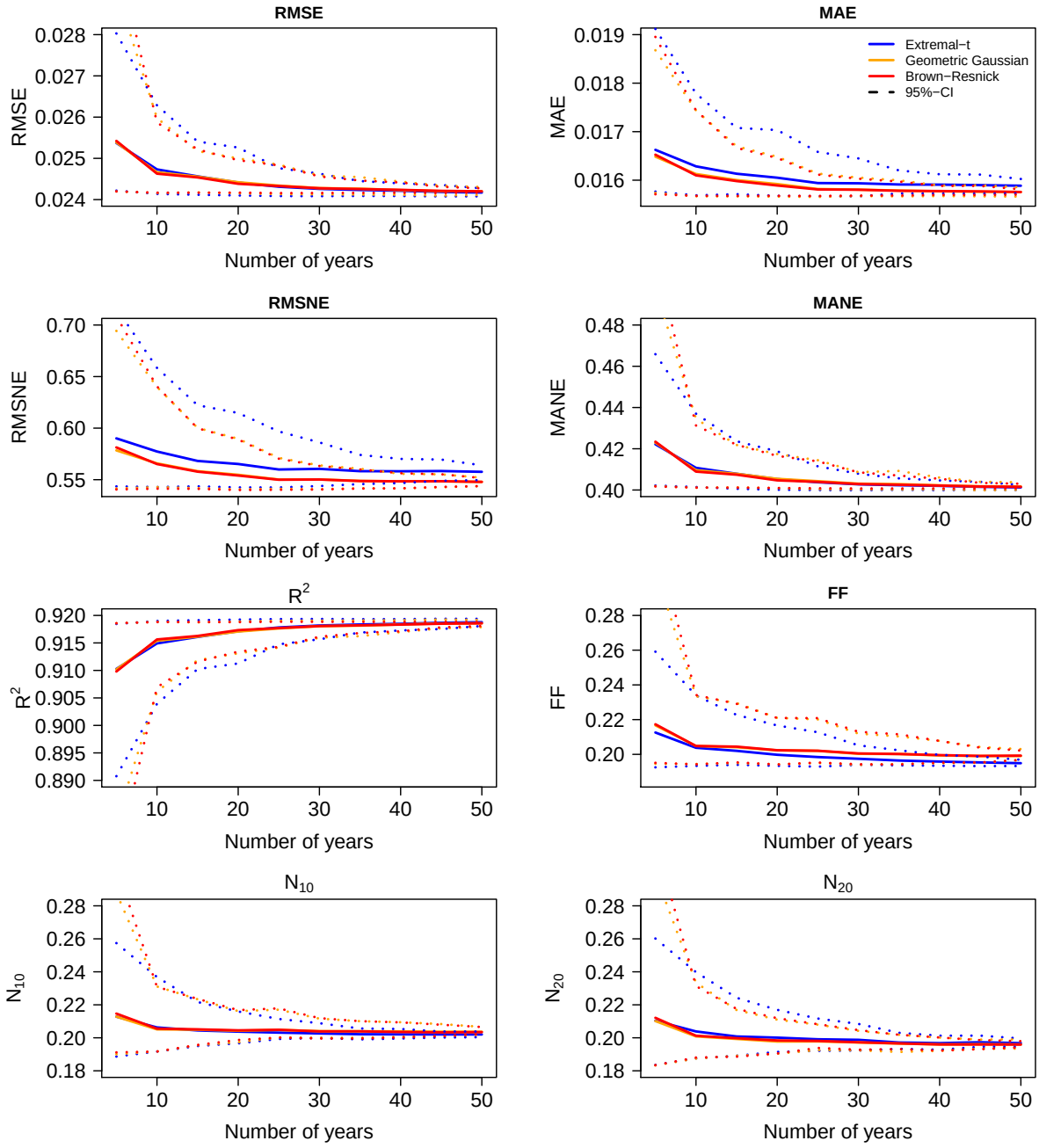


*Figure 2.4:* *RMSE, MAE, $R^2$, RMSNE, MANE, $N_{10}$, $N_{20}$ and FF criteria according to the number of years with 90 stations. Plain lines represent means. The dotted lines represent the empirical 95%-confidence interval.*

underlying spatial process. We use as a case study a large data set of 3-day snowfall annual maxima in the French Alps. First, a preselection driven by comparing the CLIC values is done, using a large set of correlation functions for the Schlather, geometric Gaussian and extremal-t processes. Then, the best parameterization of each family are compared through a leave-two-out cross-validation procedure. Their reliability is assessed focusing on the structure of the spatial dependence by deriving the bivariate distributions from the fitted models. To this aim, a large panel of criteria is introduced to discriminate the models. We compute the RMSE, MAE, RMSNE, MANE and the coefficient of determination for the probabilities of jointly exceeding a given quantile at two locations. In addition $N_T$ and $FF$ criteria, usually used for goodness-of-fit of univariate distributions, are tailored for dealing with bivariate distributions. Finally these criteria are used to investigate the sensitivity of the families of max-stable processes to the number of stations and to the number of years of observations. The cross-validation and the sensitivity investigation needed each one a computational effort of several days.

All in all, we find that the Smith and Schlather models, due to their lack of flexibility, are clearly outperformed by the other tested max-stable models. The Schlather model overestimates the joint exceedance probabilities because very weak dependence is never reached with this process, regardless of the distance apart (Blanchet and Davison, 2011; Davison et al., 2012). This is not appropriate for snowfall (Gaume et al., 2013a,b). The Smith process, which is able to model very low extremal dependence, outperforms the Schlather process, which is consistent with Gaume et al. (2013b). However, in the literature, the Schlather process can be found to be better than the Smith process when the variable of interest is more spatially dependent (Blanchet and Davison, 2011). In our case, the Smith process tends to underestimate the probabilities of joint exceedance and this is why it is less suitable than the extremal-t, geometric Gaussian and Brown-Resnick processes. Thus, none of Schlather or Smith processes is recommended for our data set.

According to CLIC, the extremal-t model is slightly better than the geometric Gaussian and Brown-Resnick models which is also confirmed by RMSE, MANE, $R^2$, $N_{10}$ and $FF$ in cross-validation. Nevertheless, the Brown-Resnick and geometric Gaussian models show better MAE, RMSNE and $N_{20}$. These differences can be explained by the fact that the extremal-t model provides slightly larger probabilities of joint exceedance than the geometric Gaussian and Brown-Resnick models. For instance, the geometric Gaussian and Brown-Resnick models show better MAE with larger $T$ because this criterion penalizes less large errors (here the large underestimations made by these families) than RMSE (Chai and Draxler, 2014). These two models have also better RMSNE and MANE for lower $T$ thanks to the normalization of the errors which penalizes less underestimations

of large quantities than over-estimations of low quantities. On the contrary, the extremal-t model shows better RMSNE and MANE with larger $T$ because these criteria take into account the non zero empirical estimations only, and these estimations are closer to the estimations made by the extremal-t model than those made by the geometric Gaussian and the Brown-Resnick models. However in all cases, the results are very similar for these three models, even when less stations or years are used, or when one focuses on specific return periods.

The low values of RMSE, MAE, RMSNE and MANE prove the quality of the extremal-t, Brown-Resnick and geometric Gaussian models in prediction and make them all suitable for our data. Although the similarity of the results when using the full data set and in cross-validation (Tables 2.4 and 2.1) may suggest that the use of cross-validation is useless, this also shows the robustness of the considered max-stable processes. In addition, the large set of criteria considered proves that well-chosen Brown-Resnick and geometric Gaussian processes are able to capture the structure of dependence of extreme snowfall in the French Alps almost as well as the extremal-t process. So, one could very well use the Brown-Resnick process with a power semivariogram rather than a suitable extremal-t process with the aim to be close to extremal independence for very large distances or to estimate less parameters. Particularly, we find that the Brown-Resnick model is slightly less sensitive to the number of stations or years of observations than the extremal-t and geometric Gaussian models, because less parameters have to be estimated.

Hence, the main practical conclusion of this paper is that the extremal-t, geometric Gaussian and Brown-Resnick processes are almost equally suitable while the Smith and Schlather processes are not flexible enough. It is likely that this result could apply to other data sets or to other families of max-stable processes as flexible as extremal-t, geometric Gaussian and Brown-Resnick processes, and for instance be valid for a wild range of environmental applications. This may be confirmed in the future by replicating the study in other contexts.

From a methodological point of view, in this study, RMSE, MAE, RMSNE, MANE and $R^2$ were computed on probabilities of joint exceedance of return levels. These probabilities of joint exceedance are concrete quantities which are useful for protective measures and make sense for risk management. The set of return periods can be adapted to the considered situation. However, if one prefers not to be dependent on the choice of return periods, it is possible to compute these criteria for the estimated extremal coefficients (Schlather and Tawn, 2003).

More generally, the set of criteria and the leave-two-out cross-validation method introduced in this paper provide a relevant framework for a deep model selection for max-stable processes independently on the data in study. Indeed, these criteria assess the predictive ability of max-stable processes whereas CLIC is a penalized composite likelihood criteria. Also the leave-two-out cross-validation procedure allows assessing the ability of the process to model extremal dependence. Hence, this approach can suitably be used for many other studies dealing with extremes in space.

Specifically, in this work, we considered five families of max-stable processes only: the first max-stable processes to be introduced (Smith and Schlather processes) and three max-stable processes which have previously been found suitable for hydrological applications (Brown-Resnick, geometric Gaussian and extremal-t processes). However, the multi-critera leave-two-out cross-validation procedure we proposed could be straightforwardly applied to other max-stable processes, for instance those mentioned in the introduction (Reich-Shaby, Gaussian-Gaussian, truncated Schlather, Tukey, etc.). Other kinds of spatial models such as asymptotically independent processes (Wadsworth and Tawn, 2012; Davison et al., 2013) could also be considered. This was not done because the asymptotic dependence hypothesis seemed more appropriate in our case. Indeed, asymptotical independence for extreme snowfall would mean that extreme snow events reduce to one infinite snow flake at infinite levels, which is questionable. In addition, from a risk management point of view it is better to overestimate the probabilities of joint exceedance, as in the case of assuming asymptotic dependence when asymptotic independence holds, rather than underestimating them, as in the opposite case. Other studies could be used in the future to compare, within our framework, different classes of asymptotically dependent and independent models.

## Acknowledgments

This work has been supported by a grant from LabEx OSUG@2020 (Investissements d'avenir - ANR10 LABX56). We thank hundreds of snow observers and the Météo-France staff involved in the collection and constitution of the data sets used in this study. We thank Anne-Laure Fougères (Université Lyon 1), Emmanuel Paquet (EDF) and Benjamin Renard (Irstea Lyon) for their advice.

# Appendix A $N_T$ and *FF* criteria

## A.1 $N_T$ and *FF* criteria in the univariate case

The $N_T$ and *FF* criteria are used in Garavaglia et al. (2011); Renard et al. (2013); Blanchet et al. (2015) to assess the reliability of estimation of univariate distributions in several locations.

The $N_T$ index is based on the number of exceedance $N_T^i$ of the estimated $T$-year return level $\hat{q}_T^i$ in location $x_i$

$$N_T^i = \sum_{n=1}^{N(i)} \mathbf{1}_{z_{n,i} > \hat{q}_T^i}. \tag{2.24}$$

with $N(i)$ the number of maxima. If $\hat{q}_T^i$ is a perfect estimation (i.e., $\hat{q}_T^i = q_T^i$), thus $N_T^i$ is a realization from the binomial distribution $\mathcal{B}(N(i), \frac{1}{T})$ (Renard et al., 2013).

The *FF* index measures the goodness-of-fit of the estimation of the cumulative distribution function $\hat{F}^i$ in location $x_i$. We consider

$$FF^i = \hat{F}^i(z_{max,i}) \tag{2.25}$$

with $z_{max,i} = \max_{i=1}^{N(i)} z_{n,i}$. If $\hat{F}^i$ is a perfect estimation (i.e., $\hat{F}^i = F^i$, then $FF^i$ is a realization from a Kumaraswamy distribution $\mathcal{K}(N(i), 1)$ (Renard et al., 2013) whose cumulative distribution function is $F^{\mathcal{K}(N(i),1)}(z) = z^{N(i)}$.

These criteria are tailored to the bivariate case by being applied to $M(i,j) = \min(Z(x_i), Z(x_j))$ the minimum at two locations $(x_i, x_j)$ taken from a sample $\mathcal{D}$ of disjoint pairs of stations.

## A.2 $N_T$ criterion in the bivariate case

For each pair of stations $(i,j)$ of $\mathcal{D}$, we note $n_T^{(i,j)}$ the number of exceedances of the $T$-year return level $m_T^{i,j}$ of $M(i,j)$:

$$n_T^{(i,j)} = \sum_{n=1}^{N(i,j)} \mathbf{1}_{m_{i,j}^n > m_T^{i,j}} \tag{2.26}$$

with $m_{i,j}^n = \min(z_{n,i}, z_{n,j})$ the minimum at locations $(x_i, x_j)$ during the winter $n$, and $N(i,j)$ the number of observations of $M(i,j)$ (i.e., the number of common observations for $z_{n,i}$ and $z_{n,j}$). The $T$-year return level $m_T^{i,j}$ depends on the model through the formula $\hat{F}^{M(i,j)}(m_T^{i,j}) = 1 - 1/T$. If $\hat{F}^{M(i,j)}$ is a perfect estimation, i.e., $\hat{F}^{M(i,j)} = F^{M(i,j)}$, then $n_T^{(i,j)}$ is a realization from the binomial distribution $\mathcal{B}(N(i,j), \frac{1}{T})$ (Renard et al., 2013).

The sample $\{n_T^{(i,j)}\}_{(i,j)\in\mathcal{D}}$ is transformed using the binomial cumulative distribution function in order to have a sample of realizations of uniform $\mathcal{U}([0,1])$ under the hypothesis $\hat{F}^{M(i,j)} = F^{M(i,j)}$. As the binomial distribution is discrete, we use a randomized binomial cumulative distribution function (Renard et al., 2013).

We assess the deviation from the uniform distribution through the area between the empirical histogram (using 10 equal bins between 0 and 1) and the uniform distribution (Blanchet et al., 2015):

$$N_T = \frac{1}{18} \sum_{k=1}^{10} \left| 10 \frac{\#\{n_T^{(i,j)} \in \text{bin}(k), (i,j) \in \mathcal{D}\}}{\#\mathcal{D}} - 1 \right|. \tag{2.27}$$

The division by 18 allows us to keep $N_T$ between 0 and 1 with 0 corresponding to the perfect uniform case when all the bins have the same number of realizations and 1 corresponding to the worst case when all the realizations are in the same bin.

## A.3 *FF* criterion in the bivariate case

For each pair of stations $(i,j)$ in the sample $\mathcal{D}$, we define $ff^{(i,j)}$ by

$$ff^{(i,j)} = \hat{F}^{M(i,j)}(m_{i,j}) \tag{2.28}$$

with $m_{i,j} = \max_{n=1}^{N(i,j)} m_{i,j}^n$. If $\hat{F}^{M(i,j)}$ is a perfect estimation, i.e., $\hat{F}^{M(i,j)} = F^{M(i,j)}$, then $ff^{(i,j)}$ is a realization from a Kumaraswamy distribution $\mathcal{K}(N(i,j), 1)$ (Renard et al., 2013). The sample $\{ff^{(i,j)}\}_{(i,j)\in\mathcal{D}}$ is transformed using the Kumaraswamy empirical cumulative distribution function $F^{\mathcal{K}(N(i,j),1)}(z) = z^{N(i,j)}$ $(0 \leq z \leq 1)$. Thus we have under the hypothesis $\hat{F}^{M(i,j)} = F^{M(i,j)}$ a sample of realizations of uniform $\mathcal{U}([0,1])$. In the same way as in the $N_T$ case, we assess the deviation from the uniform distribution by

$$FF = \frac{1}{18} \sum_{k=1}^{10} \left| 10 \frac{\#\{ff^{(i,j)} \in \text{bin}(k), (i,j) \in \mathcal{D}\}}{\#\mathcal{D}} - 1 \right|. \tag{2.29}$$

# Appendix B Semivariograms and correlation functions used in this work

| Family | Correlation function |
|---|---|
| Circular | $\rho(h) = 1 - \frac{2}{\pi}\left[\tilde{h}\sqrt{1-\tilde{h}^2} + \arcsin\left(\tilde{h}\right)\right]$ |
| Cubic | $\rho(h) = 1 - 7\tilde{h}^2 + \frac{35}{4}\tilde{h}^3 - \frac{7}{2}\tilde{h}^5 + \frac{3}{4}\tilde{h}^7$ |
| Exponential | $\rho(h) = \exp\left\{-\tilde{h}\right\}$ |
| Gaussian | $\rho(h) = \exp\left\{-\tilde{h}^2\right\}$ |
| Gneiting | $\rho(h) = \left[1 + 8s\tilde{h} + 25\left(s\tilde{h}\right)^2 + 32\left(s\tilde{h}\right)^3\right]\left(1 - s\tilde{h}\right)^8$ |
| Spherical | $\rho(h) = 1 - \frac{3}{2}\left(\tilde{h}\right) + \frac{1}{2}\left(\tilde{h}\right)^3$ |
| Wave | $\rho(h) = \sin(\tilde{h})/\tilde{h}$ |
| Bessel | $\rho(h) = \left(\frac{2}{\tilde{h}}\right)^{\kappa}\Gamma\left(\kappa+1\right)J_{\kappa}\left(\tilde{h}\right)$ |
| Cauchy | $\rho(h) = \left[1 + \left(\tilde{h}\right)^2\right]^{-\kappa}$ |
| Gamma | $\rho(h) = 1/\left(1+\tilde{h}\right)^{\kappa}$ |
| Powered exponential | $\rho(h) = \exp\left\{-\left(\tilde{h}\right)^{\kappa}\right\}$ |
| Whittle-Matérn | $\rho(h) = \frac{2^{1-\kappa}}{\Gamma(\kappa))}\left(\tilde{h}\right)^{\kappa}K_{\kappa}\left(\tilde{h}\right)$ |
| Generalized Cauchy | $\rho(h) = \left[1 + \left(\tilde{h}\right)^{\kappa_2}\right]^{-\kappa/\kappa_2}$ |
| Gneiting-Matérn | $\rho(h) = \rho_{\lambda}^{gneiting}(h/\kappa_2)\,\rho_{\lambda,\kappa}^{matern}(h)$ |

***Table 2.2:*** *Correlation functions. We note $\tilde{h} = h/\lambda$ with $\lambda > 0$ the range parameter. The parameter $\kappa > 0$ is the smoothness parameter (for the Bessel family $\kappa \geq \frac{d-2}{2}$ with $d$ the dimension of the space and for the powered exponential family $0 < \kappa \leq 2$). In the expression of the Gneiting correlation function, $s = 0.301187465825$. For the circular, cubic, Gneiting and spherical families $h < \lambda$, and $\rho(h) = 0$ when $h \geq \lambda$. The functions $\Gamma$, $J_\kappa$ and $K_\kappa$ are respectively the Gamma function, the Bessel function of the first kind of order $\kappa$ and the modified Bessel function of order $\kappa$. The correlation functions of the generalized Cauchy and Gneiting-Matérn families own a second smoothness parameter $\kappa_2 > 0$ (for the Generalized Cauchy correlation function $0 < \kappa_2 \leq 2$). In the expression of the Gneiting-Matérn correlation function, $\rho_{\lambda}^{gneiting}$ and $\rho_{\lambda,\kappa}^{matern}$ denote Gneiting and Whittle-Matérn correlation functions respectively, with a range parameter $\lambda$ and a smoothness parameter $\kappa$.*

| Family | Semivariogram |
|---|---|
| Linear | $\gamma(h) = \frac{h}{\lambda}$ |
| Power | $\gamma(h) = \left(\frac{h}{\lambda}\right)^{\kappa}$ |

***Table 2.3:*** *Semivariograms. The parameter $\lambda > 0$ is the range parameter and $\kappa > 0$ is the smoothness parameter.*

# Appendix C Model preselection with CLIC

Results are shown in Figure 2.5. According to CLIC, the best model is the extremal-t process with the Gneiting-Matérn correlation function (rescaled CLIC = 19,442). The extremal-t model with the Gneiting-Matérn, Matérn, powered exponential, exponential, Gamma and generalized Cauchy correlation functions outperforms the best Brown-Resnick (rescaled CLIC = 19,450 with the power semivariogram) and the best geometric Gaussian (rescaled CLIC = 19,452 with the powered exponential correlation function) processes. All extremal-t, geometric Gaussian and Brown-Resnick processes clearly outperform the Smith (rescaled CLIC = 19,537) and all Schlather (rescaled CLIC around 19,556 regardless of the correlation function) processes.

The best correlation functions for the extremal-t process are also the best for the geometric Gaussian process: Gneiting-Matérn, Matérn, powered exponential, generalized Cauchy, Gamma and exponential. Regardless of the correlation function, the extremal-t process outperforms the geometric Gaussian process. For the Schlather process, the values of the rescaled CLIC are almost constant with the 14 correlation functions (from 19,555.68 to 19,556.11).

Hence, we select the power semivariogram for the Brown-Resnick process and the Gneiting-Matérn function for the extremal-t process. As can be seen in Figure 2.5, the Gneiting-Matérn function is also one of the best correlation function for the geometric Gaussian process and there is very little influence of the choice of the correlation function for the Schlather process. In order to keep the same correlation function for the extremal-t, geometric Gaussian and Schlather models, we also select the Gneiting-Matérn function for the geometric Gaussian and Schlather processes.

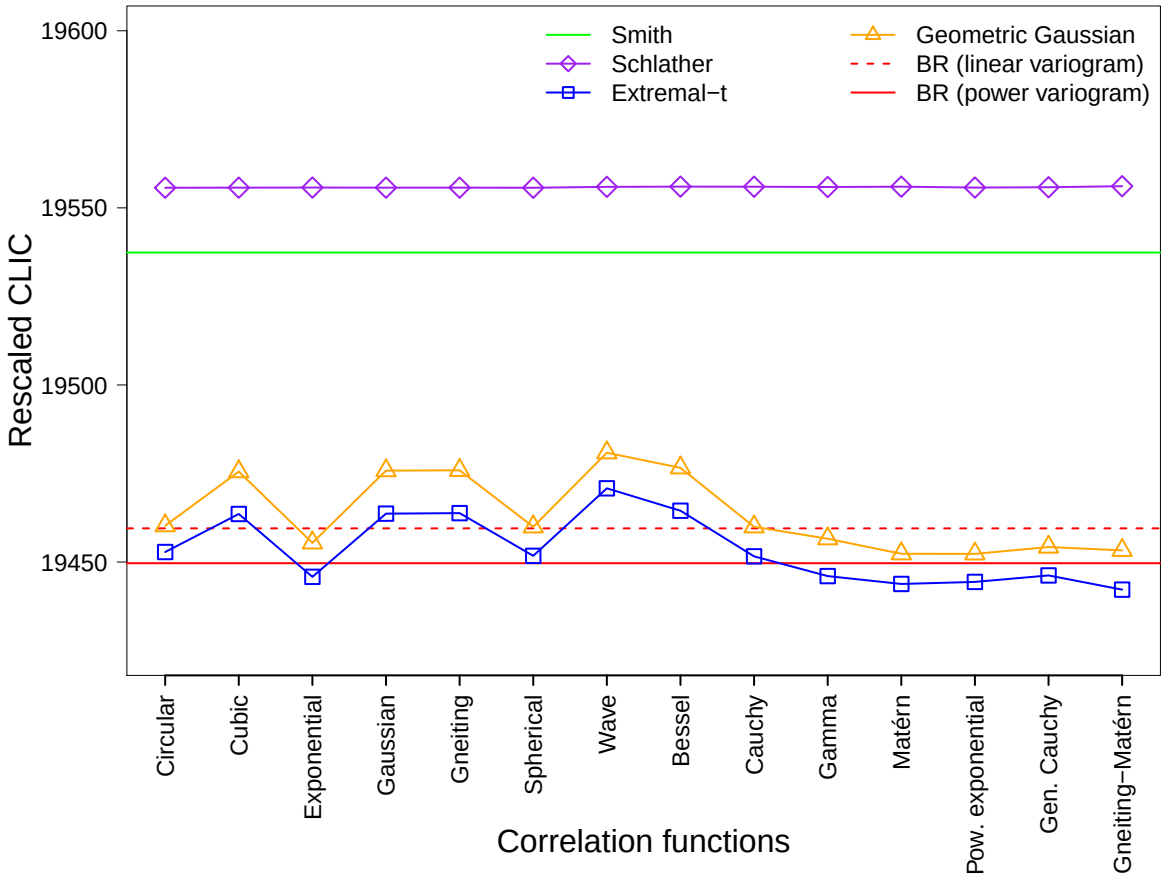


***Figure 2.5:*** *Rescaled CLIC for max-stable processes fitted by composite likelihood. The X-axis represents the correlation functions for the Schlather, geometric Gaussian and extremal-t processes. For the Brown-Resnick process, the dashed line represents the linear variogram and the solid line the power variogram.*

| Family | CLIC | RMSE | MAE | RMSNE | MANE | $R^2$ | $N_{10}$ | $N_{20}$ | $FF$ |
|---|---|---|---|---|---|---|---|---|---|
| E-t | **19,442** | **0.0241** | 0.0158 | 0.556 | **0.400** | **0.919** | 0.203 | 0.196 | **0.194** |
| GG | 19,452 | 0.0242 | 0.0158 | 0.548 | 0.402 | 0.919 | **0.203** | **0.195** | 0.199 |
| B-R | 19,450 | 0.0242 | **0.0158** | **0.548** | 0.401 | 0.919 | 0.203 | 0.196 | 0.200 |
| Sm | 19,537 | 0.0281 | 0.0171 | 0.597 | 0.481 | 0.890 | 0.269 | 0.279 | 0.282 |
| Sc | 19,556 | 0.0308 | 0.0212 | 0.796 | 0.510 | 0.868 | 0.292 | 0.291 | 0.285 |

***Table 2.4:*** *Rescaled CLIC, RMSE, MAE, RMSNE, MANE, $R^2$, $N_{10}$, $N_{20}$ and FF using the full data set for the extremal-t, geometric Gaussian and Schlather processes with the Gneiting-Matérn correlation function, the Brown-Resnick process with the power semivariogram and the Smith process. Bold values indicate the best value for each criterion (sometimes distinguishable with the $4^{th}$ or $5^{th}$ significant digit only).*

Table 2.4 shows the values of the criteria introduced in 2.3.2.2 and 2.3.2.3 using all the data for the extremal-t, geometric Gaussian and Schlather processes with the Gneiting-Matérn correlation function, the Brown-Resnick process with power semivariogram and the Smith process. RMSE, MANE, $R^2$ and $FF$ confirm what CLIC suggests, with a better performance of the extremal-t model. However, the Brown-Resnick model performs best according to MAE and RMSNE and the geometric Gaussian model shows the best $N_{10}$ and $N_{20}$. All in all, the performances of the extremal-t, geometric Gaussian and Brown-Resnick models are very close for all the criteria, and they clearly outperform the Smith and Schlather models (the Schlather model is the worst according to all the criteria).

# Appendix D The parameters of the five retained models for cross-validation

| Family | Number | Anisotropy | Dependence | Sill |
|---|---|---|---|---|
| Smith | 6 | - | $\begin{pmatrix} \Sigma_{1,1} & \Sigma_{1,2} & \Sigma_{1,3} \\ \Sigma_{1,2} & \Sigma_{2,2} & \Sigma_{2,3} \\ \Sigma_{1,3} & \Sigma_{2,3} & \Sigma_{3,3} \end{pmatrix}$ | - |
| Schlather | 6 | $\psi$, $w_1$ and $w_2$ | $\lambda$, $\kappa$ and $\kappa_2$ | - |
| Brown-Resnick | 5 | $\psi$, $w_1$ and $w_2$ | $\lambda$ and $\kappa$ | - |
| Geometric Gaussian | 7 | $\psi$, $w_1$ and $w_2$ | $\lambda$, $\kappa$ and $\kappa_2$ | $\sigma^2$ |
| Extremal-t | 7 | $\psi$, $w_1$ and $w_2$ | $\lambda$, $\kappa$ and $\kappa_2$ | $\nu$ |

***Table 2.5:*** *Parameterization of the five studied models. Anisotropy parameters denote the parameters of the matrix $V$ in (2.21). Dependence parameters are the elements of the symmetric matrix $\Sigma$ used in the calculation of the Mahalanobis distance $a$ in (2.5) in the case of Smith process, the parameters of the Gneiting-Matérn correlation function in the case of Schlather, geometric Gaussian and extremal-t processes, and the parameters of the power semivariogram in the case of Brown-Resnick process.*

# Appendix E Comparison of the models for specific return periods

We compute for each pair of stations the estimated probability of exceeding jointly the return level $z_T$ for $T$ = 2, 3, 5, 7, 10, 15, 20, 25, 33, 50 and 100 years. Figure 2.6 confirms that in mean the Schlather model gives the highest probabilities while the Smith model gives the lowest. The extremal-t model gives slightly higher probabilities of joint exceedance than the Brown-Resnick model which himself gives very slightly higher values than the geometric Gaussian model. Although the number of non-zero empirical estimates decreases with $T$, the average of the empirical estimates are always close to those of the extremal-t, Brown-Resnick and geometric Gaussian estimates. The variability of the estimates provided by the extremal-t, Brown-Resnick and geometric Gaussian models are very similar with a slightly larger interquartile range and a slightly shorter statistical dispersion for the extremal-t model. The estimates of Smith and Schlather models concentrate far from the averages of the empirical estimates and their dispersion is large, which confirms that these models lack flexibility. Error-based criteria computed

specifically for each return period (Figure 2.7) show that the extremal-t, Brown-Resnick and geometric Gaussian models are very similar regardless of $T$. The models providing the lowest probabilities of joint exceedance (first, Smith, second, geometric Gaussian and Brown-Resnick) show better MAE with larger $T$ and better RMSNE and MANE with lower $T$ than those providing the largest probabilities (first, Schlather, second, extremal-t). On the contrary, the models providing the largest probabilities of joint exceedance show better RMSNE and MANE with larger $T$. The decreases in RMSE and MAE with $T$ do not mean an increase in performance. They are due to a decrease in magnitude of the considered probabilities of joint exceedance with $T$. This is not the case of RMSNE and MANE because of the normalization of the errors and to the fact that only the non-zero empirical estimates are taken into account.

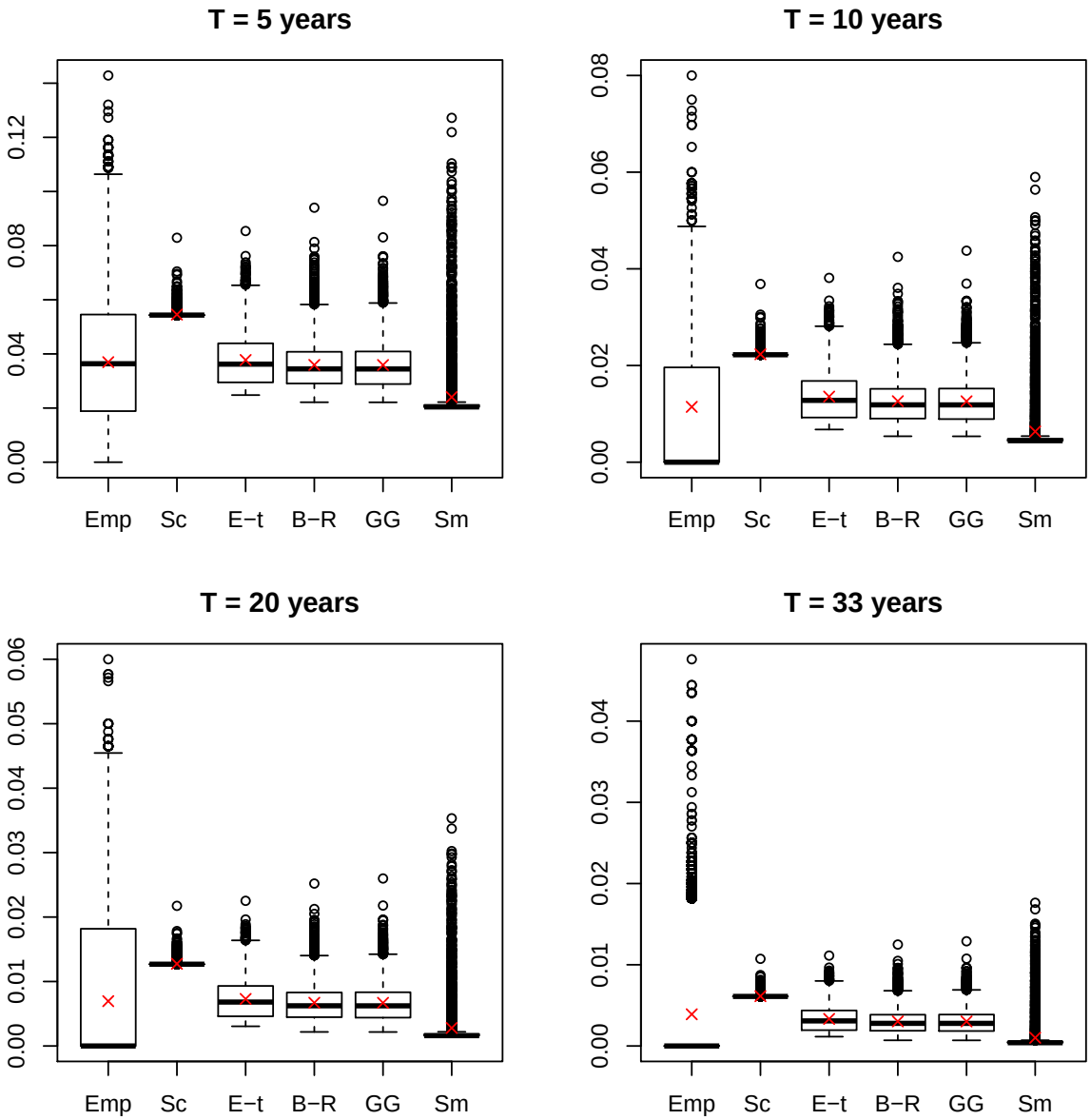


*Figure 2.6:* *Cross-validation. Boxplots of estimates of the probability of exceeding jointly the T-year return level ($T = 5, 10, 20, 33$ years) for all pairs of stations. "Emp", "Sc", "E-t", "B-R", "GG" and "Sm" denote respectively the empirical, Schlather, extremal-t, Brown-Resnick, geometric Gaussian and Smith estimations. The red crosses show the averages.*

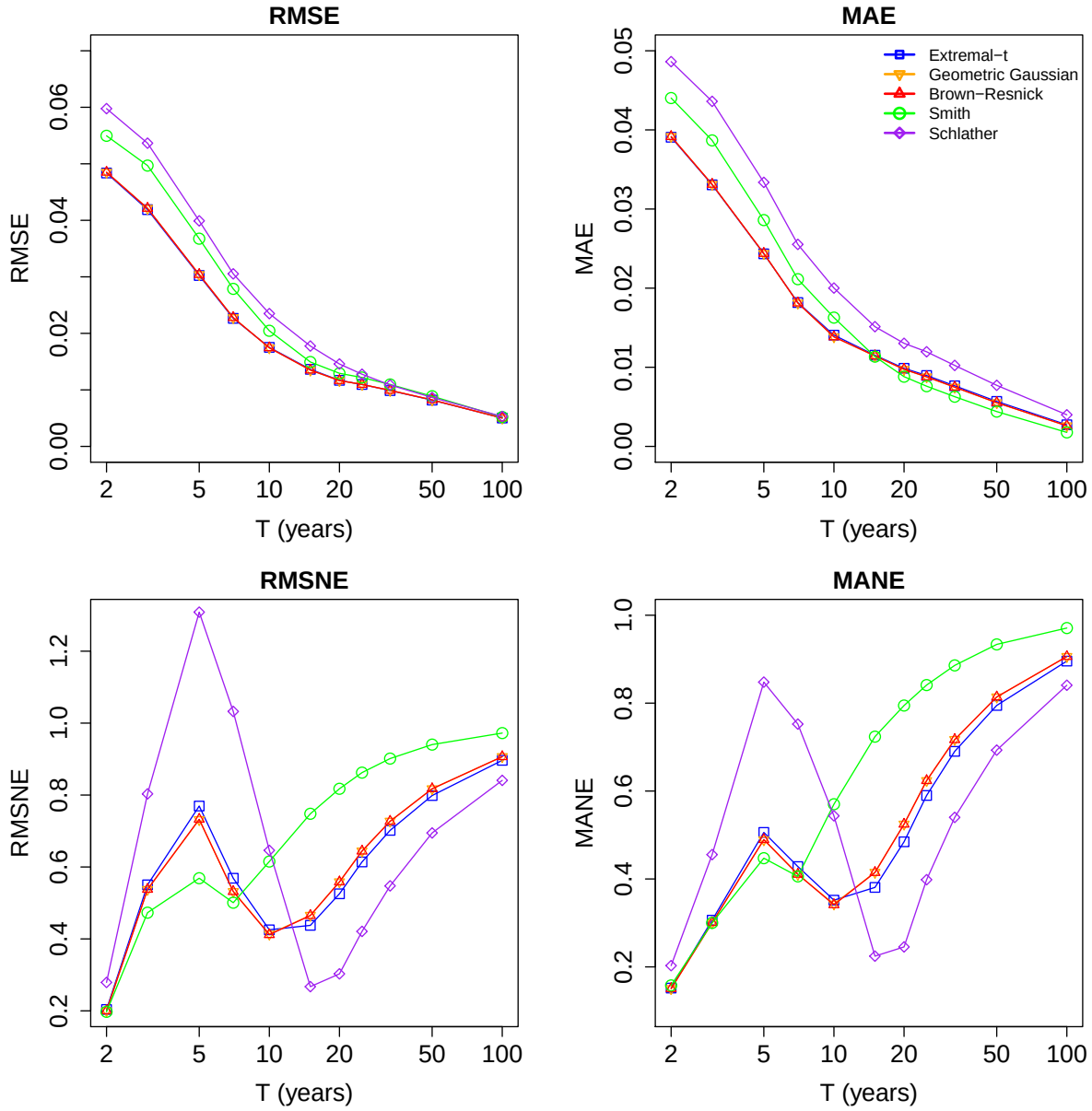


*Figure 2.7:* *Cross-validation. RMSE, MAE, RMSNE and MANE as function of return period. For RMSE and MAE, extremal-t, geometric Gaussian and Brown-Resnick models are almost identical regardless of T (superposed curves) and remain very close for RMSNE and MANE.*

# Chapter 3

# Decreasing spatial dependence in extreme snowfall in the French Alps since 1958 under climate change

The content of this chapter was published in Journal of Geophysical Research: Atmospheres, the citation is
Nicolet, G., Eckert, N., Morin, S., and Blanchet, J. (2016). Decreasing spatial dependence in extreme snowfall in the French Alps since 1958 under climate change. *Journal of Geophysical Research: Atmospheres*, 121(14), 8297-8310.

# Abstract

Whereas changes in magnitude of geophysical extremes under climate change have received significant attention, potential concomitant changes in spatial dependence structures have remained unexplored so far. Here, we provide first evidence of such an effect, highlighting a significant trend in the spatial dependence structure of snowfall extremes in the French Alps at decadal time scale. Specifically, we process a comprehensive data set of winter maximum snowfall from all over the French Alps collected in 90 stations from 1958 to 2012. We estimate extremal dependence over 20-year moving estimation windows taking into account possible anisotropy potentially related to orographic effects and/or patterns in atmospheric flows. For each window, we derive a range representing the distance above which extremes are almost independent. We show that snowfall extremes tended to become less spatially dependent over time, with the dependence range reduced roughly by half during the study period. We demonstrate the connection between this trend and local and synoptic climatic variables associated with the current climate change context. In details, the decreasing pattern in extremal dependence is concomitant with a trend towards less harsh winter conditions. It is attributable at first to the increase in temperature and its major control on the snow/rain partitioning. Yet a magnitude effect, with less dependent extremes due to a decrease in intensity of precipitation, also exists. Finally, we show that our results are largely insensitive to the minimal modeling assumptions necessary to our data-based approach. This robustness makes it potentially suitable for various other studies in the field of geophysical extremes.

## 3.1 Introduction

Extreme snow events are among the most important hazards in mountainous regions. Snowstorms can stop road, railway and air traffic. Extreme snowfalls can cause overloading and collapse of buildings and flooding because of snowmelt. As for other geophysical variables such as rainfall or river discharge for which high percentiles of the distribution are key quantities, extreme value theory (EVT) (Coles, 2001) is a suitable framework to work with. Specifically, it is now well known that block maxima (e.g., annual) should be modeled by the so-called generalized extreme value (GEV) distribution (Blanchet and Lehning, 2010; Sadovskỳ et al., 2012), allowing sound extrapolation beyond the highest observed value.

However, for better mitigating risk and/or improving scientific knowledge about the processes at play, one may be interested not only in pointwise estimates, but also in assessing and using dependence between extremes (extremal dependence) of different measurement stations. For instance, a proper inference of extremal dependence may help in understanding the spatial variation of extremes. This also permits to evaluate joint exceedance probabilities at different positions in space. More recent and refined statistics from the field of multivariate EVT such as extremal dependence measures are useful to this end (Coles et al., 1999; Schlather and Tawn, 2003; Naveau et al., 2009), and some of them have already been used to evaluate dependence in extreme snowfall in Switzerland (Blanchet et al., 2009).

Yet, to fully cope with extremes in space, max-stable processes (de Haan, 1984) (which are the formal extension of multivariate EVT to infinite dimension) are even more suitable. After initial developments [*Smith*, 1990; *Schlather*, 2002], Padoan et al. (2010) showed how different max-stable processes could be fitted to extreme rainfall in the U.S. using composite likelihood maximization techniques. This framework was applied by Blanchet and Davison (2011) to extreme snow depths in Switzerland and by Gaume et al. (2012, 2013b) to extreme snowfall and subsequently to avalanche slab depths in the French Alps. Furthermore, it was used for extreme temperature in Korea (Lee et al., 2013), for extreme wind gusts in the Netherlands (Ribatet, 2013), for extreme wave heights in the North Atlantic Ocean (Raillard et al., 2014) and in the Gulf of Lions (Chailan et al., 2014) and for extreme river discharges in the upper Danube basin (Asadi et al., 2015).

However, all the previous studies assume more or less explicitly temporal stationarity, both in the GEV distributions fitted at any location of observations and, when it is modeled, in the spatial dependence structure of extremes. This is clearly questionable in the current climate change context (Stocker et al., 2013). For instance, due to the

influence of temperature on the rain/snow partitioning of precipitation, snow-related variables are particularly sensitive to the recent warming (Falarz, 2004; Durand et al., 2009a; Valt and Cianfarra, 2010). It is therefore not surprising that potential trends in extreme precipitation assessed within a proper extreme value framework (van den Besselaar et al., 2013; Westra et al., 2013) become all the more clear when one focuses on the sole snow phase. Significant decreasing trends were highlighted in extreme snowfall and snow depths in Switzerland by Marty and Blanchet (2012). In a similar spirit, using time-dependent covariates in marginal GEV distributions and a stationary spatial dependence structure within a max-stable process model, Shang et al. (2011) showed a relation between extreme precipitation in California and El Niño-Southern Oscillation, whereas Westra and Sisson (2011) highlighted the influence of global sea surface temperature and South Oscillation Index on extreme precipitations in Australia.

To the best of our knowledge, only Huser and Davison (2014) tried to cope for possible temporal changes in the spatial dependence structure between extreme precipitation with a time dependent max-stable process. To this end, they developed, in a "model-based" approach, a statistical model which explicitly represents the movement of a heavy rainfall event through time, fed by observations acquired at short time steps. The scope of the current paper is to highlight potential temporal changes at longer time scales (decades) in the spatial dependence structure of snowfall extremes using a "data-based" approach, which means that we try to make as few modeling assumptions as possible in order to give more weight to the data. In addition, we carefully test sensitivity of the few hypotheses we make. By this, we aim at making sure that the revealed change in the extremal spatial dependence structure is with no doubt of geophysical origin rather than a more or less direct consequence of modeling choices.

Specifically, we process a 56 year long data set of winter maximum snowfall from all over the French Alps focusing on the spatial dependence structure only. We estimate extremal dependence over 20-year moving estimation windows and, for each window, we derive a range representing the distance above which extremes are almost independent. We highlight a strong decrease in this range over the study period and we investigate the connection between this trend and local and synoptic climatic variables associated with the current climate change context. Finally, we demonstrate that this decrease does not depend on the choice of the parametric model nor the way the marginal distributions (i.e., the GEV distributions computed for each station) and/or the distance between stations are evaluated.

## 3.2 Data

### 3.2.1 Winter maximum snowfall in the French Alps

Our data set is composed of winter maxima of 3 days cumulated snowfalls with a winter period defined from 15 November to 15 May. We choose a period of 3 days because this is the most usual time scale of winter storms in the studied region and hence is often considered in avalanche forecasting (Bocchiola et al., 2006; Eckert et al., 2010, 2011; Gaume et al., 2012). Daily data are available from 15 November 1958 to 15 May 2013 in the French Alps (Figure 3.1) through observations of precipitation done mostly manually (climatological and dedicated snow observing networks). We use all the observations whose type of precipitation (rain or snow) was registered as snow. If the indication about the phase of precipitation is missing, we retain precipitations measured when minimal daily temperature is lower than 2°. Since several locations of measurement were slightly modified during the study period, we pooled together the stations with less than 100 m difference in elevation and less than 2 km in distance in the 2-D plane. Finally, we retain the 90 stations which have at least 40 winter maximum values (computed from a moving window of 3 days) during the study period (Figure 3.2(a)). Their elevation ranges from 291 m to 2012 m (Figure 3.2(b)). Hence, the station set is a good compromise between spatial and altitudinal coverage and length of records.

### 3.2.2 Local and synoptic variables

In order to better understand the potential changes in extremal dependence in winter maximum snowfall, we introduce several variables that summarize the winter climate of the French Alps over the study period.

The French Alps are divided into 23 massifs (see Figure 3.1), which are generally assumed to be homogeneous in terms of meteorological conditions for a given elevation. In each massif, the daily snow amount and the meteorological conditions are available all over the study period as a function of elevation through reanalyses (Durand et al., 2009a,b). From these reanalyses, the cumulated snowfall, mean snow water equivalent (total mass of snow per unit horizontal surface area), snow precipitation ratio (cumulated snow precipitation divided by total – snow and rain – precipitation), and mean temperature are calculated for two elevation levels (1800 m and 2400 m) for each winter and for each massif. Then, the mean of all the massif values (23 massifs for 1800 m and

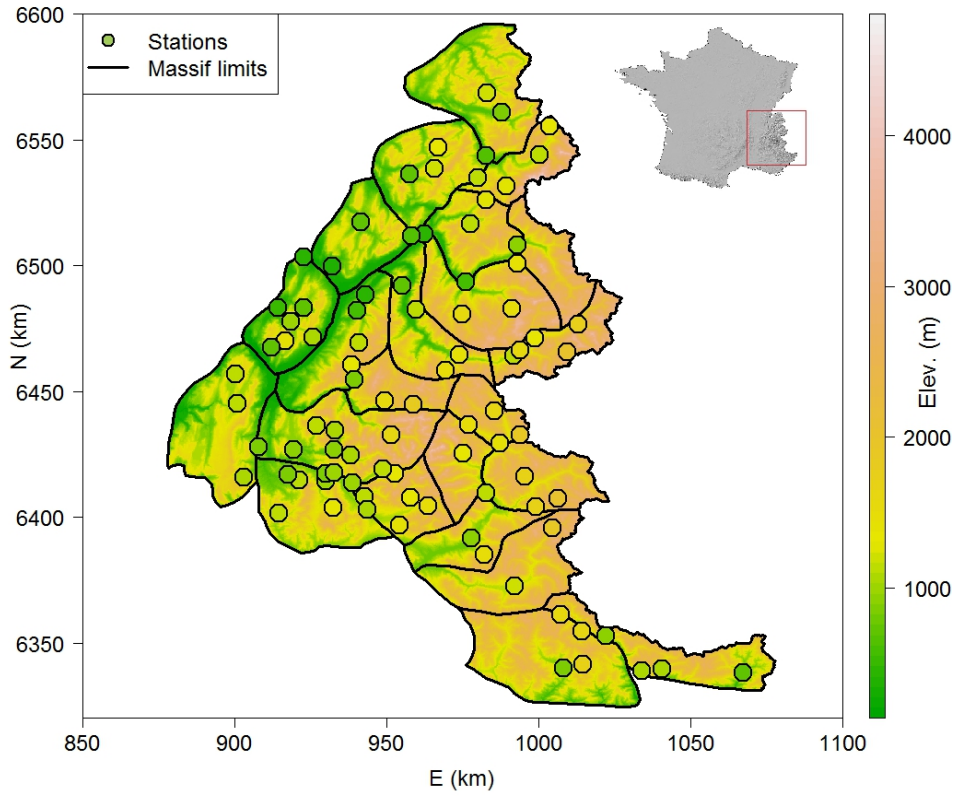


***Figure 3.1:*** *Study area in the southeast of France, where the 23 massifs of the French Alps are located. Lines denote massif limits, and dots denote the positions of the stations. The color code represents elevation.*

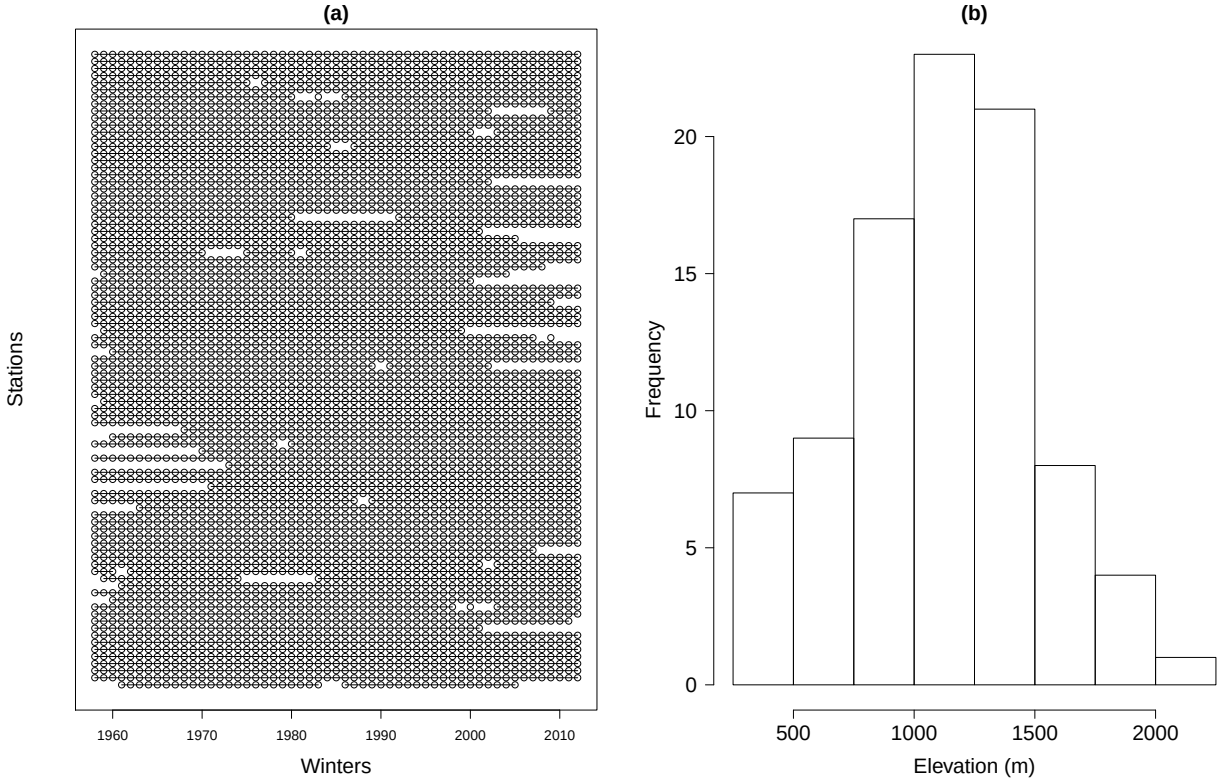


***Figure 3.2:*** *(a) Data availability for each station. Each line represents one station, and each point means that the winter maximum is available for that station. (b) Histogram of station elevation.*

21 massifs for 2400 m because the highest peaks of two massifs are below this elevation) is computed for each winter in order to have, for each variable and each winter, a single value for the entire French Alps notwithstanding the large variability of mean annual conditions (Durand et al., 2009a,b).

The main drivers of winter climate in the French Alps are mostly westerly fluxes coming from the North Atlantic. Thus, we also consider NAO (North Atlantic Oscillation) (Jones et al., 1997; Osborn, 2006) and AMO (Atlantic Multidecadal Oscillation) (Kaplan et al., 1998; Enfield et al., 2001) indices through winter anomalies evaluated from November to April over the study period. NAO and AMO variables summarize the predominant oscillating patterns in the winter climate of the French Alps, in terms of pressure/precipitation and temperature, respectively. Rather than the commonly used detrended version of AMO (Enfield et al., 2001), we use here the nondetrended version which includes the recent climate warming signal in addition to oscillating patterns (Kaplan et al., 1998).

For consistency with the moving time windows approach of section 3.3.5, for each of these variables, 20-year moving averages are derived all over the study period, starting with the 1958-1977 time window and ending with the 1993-2012 time window.

## 3.3 Methods

### 3.3.1 Extreme value statistics in the univariate case and standardization of snowfall maxima

Following EVT, we assume that winter maximum snowfall at a given station is GEV distributed. The cumulative distribution function $F(y;\mu(x),\sigma(x),\xi(x))$ of the GEV distribution is of the form:

$$F(y;\mu(x),\sigma(x),\xi(x)) = \exp\left\{-\left[1+\xi(x)\left(\frac{y-\mu(x)}{\sigma(x)}\right)\right]^{-1/\xi(x)}\right\} \tag{3.1}$$

with $\mu(x)$, $\sigma(x)$ and $\xi(x)$ denoting, respectively, the location, scale, and shape parameters at position $x$, and $y$ is such that $1+\xi(x)\left(\frac{y-\mu(x)}{\sigma(x)}\right) > 0$. The function $F$ is equal to 0 in the case of $\xi(x) > 0$ and $y \leq \mu(x)$, and equal to 1 if $\xi(x) < 0$ and $y \geq \mu(x)$.

A GEV distribution is estimated for each station by likelihood maximization, giving estimates of the GEV parameters $(\mu(x), \sigma(x), \xi(x))$ at each station location $x$. Finally, the pointwise estimates $(\hat{\mu}(x), \hat{\sigma}(x), \hat{\xi}(x))$ are used to transform at each position $x$ the GEV distributed snowfall maxima $\mathrm{SF}(x)$ into a unit Fréchet distributed (i.e., GEV distributed with $\mu(x) = 1$, $\sigma(x) = 1$ and $\xi(x) = 1$) variable $Z(x)$ using the transformation

$$\mathrm{SF}(x) \mapsto Z(x) = \frac{-1}{\log[F\{\mathrm{SF}(x); \hat{\mu}(x), \hat{\sigma}(x), \hat{\xi}(x)\}]}, \tag{3.2}$$

where $\mathrm{SF}(x)$ is the snowfall maxima at location $x$ and $F\{.; \hat{\mu}(x), \hat{\sigma}(x), \hat{\xi}(x)\}$ is the GEV distribution defined in (3.1). By doing this, we obtain a new data set of standardized winter maximum snowfall, $Z(x)$. The extremal dependence in this new data set is addressed in the current study, which is equivalent to but computationally easier than studying the extremal dependence in the original data set $\mathrm{SF}(x)$. Indeed, with the standardized dataset we focus on the spatial dependence structure only and remove the effects of having different distributions for the marginal distributions, for example due to different elevations.

In order to use the same transformation (3.2) for all the 20-year moving windows (see section 3.2.2), we first assume that the marginal distributions do not change with time. This may lead to an artificial temporal trend in the spatial dependence structure since a temporal trend in the marginal distributions may be transferred in the dependence structure. To exclude this possibility, we also assess the temporal evolution of the spatial dependence using a specific transformation (3.2) for each estimation window. To this end, the GEV parameters $\hat{\mu}(x)$, $\hat{\sigma}(x)$, and $\hat{\xi}(x)$ are reevaluated for each window.

### 3.3.2 Extreme value statistics in the spatial case

Let $S$ be a space, e.g., the French Alps. Let $Z(x)$, $x \in S$ be the spatial field of standardized winter maximum snowfall in the French Alps, i.e., with every margin $Z(x)$ unit Fréchet distributed. According to spatial extreme value theory, it is appropriate to model $Z(x)$ as a max-stable process (de Haan, 1984; Davison et al., 2012). Every max-stable process with unit Fréchet margins holds the de Haan's spectral representation (de Haan, 1984):

$$Z(x) = \sup_{i \geq 1} \eta_i W_i(x). \tag{3.3}$$

with $\{\eta_i\}_{i\geq 1}$ the points of a Poisson process on $\mathbb{R}^+$ with intensity $\eta^{-2}d\eta$ and $\{W_i\}_{i\geq 1}$ independent copies of a nonnegative process $W$ with mean 1. Different choices for $W$ lead to different models of max-stable processes (Davison et al., 2012; Cooley et al., 2012). Every multivariate margin is given for any positions $\{x_1, \ldots, x_k\}$ by the formula

$$\mathbb{P}\left(Z(x_1) < z_1, \ldots, Z(x_k) < z_k\right) = \exp\left[-\mathbf{E}\left\{\max_{j=1,\ldots,k} \frac{W(x_j)}{z_j}\right\}\right] \qquad z_j > 0 \quad \forall j. \tag{3.4}$$

### 3.3.3 Extremal coefficient and extremal function

To assess the extremal dependence between two unit Fréchet random variables $Z_1$ and $Z_2$, one can use the extremal coefficient $\theta$ (Schlather and Tawn, 2003; Naveau et al., 2009) defined by

$$\mathbb{P}\left(Z_1 < z, Z_2 < z\right) = \exp\left\{\frac{-\theta}{z}\right\} = P\left\{Z_1 < z\right\}^{\theta}, \qquad z > 0. \tag{3.5}$$

The extremal coefficient ranges between 1 (complete dependence) and 2 (independence). The property

$$\lim_{z\to\infty} \mathbb{P}\left(Z_2 > z | Z_1 > z\right) = 2 - \theta \tag{3.6}$$

holds and means that the probability of observing extreme values of $Z_2$ when $Z_1$ takes extreme values is close to 0 when $\theta$ is near 2 and close to 1 when $\theta$ is near 1.

If $Z_1 = Z(x_1)$ and $Z_2 = Z(x_2)$ with $Z$ a max-stable process defined by (3.3) and $x_1$ and $x_2$ two positions, we have from equations (3.4) and (3.5):

$$\theta(x_1, x_2) = \mathbf{E}\left[\max\left\{W(x_1), W(x_2)\right\}\right]. \tag{3.7}$$

Theorical expressions for $\theta$ in (3.7) are available for all classical max-stable processes (Ribatet, 2013), as functions $\theta(h)$ of the distance $h = |x_2 - x_1|$ between two positions. $\theta(h)$ represents the strength of the dependence as a function of distance and is therefore termed the extremal function.

We tried most of the currently available extremal functions. Among these, the popular Smith (Smith, 1990) and Schlather (Schlather, 2002) extremal functions are by far not flexible enough to be suitable for our case study and were discarded. In this work we consider the main other possible choice, namely, the theoretical extremal functions of the Brown-Resnick max-stable process (Kabluchko et al., 2009) with a power semivariogram along with extremal-t (Opitz, 2013) and geometric Gaussian (Davison et al., 2012) max-stable processes with powered exponential correlation function.

Corresponding Brown-Resnick, geometric Gaussian and extremal-t extremal functions are respectively given by

$$\theta(h) = 2\Phi\left(\frac{\sqrt{2(h/\lambda)^{\kappa}}}{2}\right), \tag{3.8}$$

$$\theta(h) = 2\Phi\left(\frac{\sqrt{2\sigma^2[1-\exp\{-(h/\lambda)^{\kappa}\}]}}{2}\right) \tag{3.9}$$

and

$$\theta(h) = 2T_{\nu+1}\left(\sqrt{\frac{\nu+1}{1-(\exp\{-(h/\lambda)^{\kappa}\})^2}}(1-\exp\{-(h/\lambda)^{\kappa}\})\right) \tag{3.10}$$

with $\Phi$ and $T_{\nu+1}$, respectively, the cumulative distribution functions of the standard normal distribution and Student distribution with $\nu+1$ degrees of freedom, $\lambda > 0$ the scale parameter, and $\kappa > 0$ the smoothness parameter. In order to keep the same degree of freedom for the three models, we fix the sill parameters $\sigma^2 = 7.7$ and $\nu = 5$ of geometric Gaussian and extremal-t extremal functions. These values impose a limit close to 1.95 to $\theta(h)$ when $h$ tends to infinity. By doing this, we assume that extremes are still weakly dependent at two very distant locations which is a realistic hypothesis for snowfall. Therefore, each model of extremal function has two parameters: a range parameter $\lambda$ and a smoothness parameter $\kappa$ to be fitted on the data.

### 3.3.4 Anisotropy and distances

In order to take into account spatial anisotropy in (3.8)–(3.10), we use three appropriate distances.

#### 3.3.4.1 Modified 2-D distance

First, we consider a modified distance in dimension 2 by using a geometric transformation of space; instead of $(x_1, x_2)$, we compute distances using the transformed coordinates $(x'_1, x'_2)$ with

$$\begin{bmatrix} x'_1 \\ x'_2 \end{bmatrix} = \begin{bmatrix} \cos(\alpha) & -\sin(\alpha) \\ r^{-1}\sin(\alpha) & r^{-1}\cos(\alpha) \end{bmatrix} \begin{bmatrix} x_1 \\ x_2 \end{bmatrix} \qquad r > 1 \text{ and } \alpha \in [0, \pi) \tag{3.11}$$

where $r$ and $\alpha$ denote the anisotropy ratio and angle, respectively. The angle $\alpha$ can be interpreted as the direction of strongest extremal dependence for pairs of stations. The parameter $r$ controls the ratio between the direction of strongest dependence and the orthogonal direction. The 2-D Euclidean distance computed after this transformation is referred as the modified 2-D distance.

#### 3.3.4.2 Modified 3-D distance

In (3.11), the elevation of the standardized snowfall maxima is not taken into account. This may lead to some loss of information. Thus, we also considered the 3-D Euclidean distance with the three-dimensional transformed space defined as

$$\begin{bmatrix} x'_1 \\ x'_2 \\ x'_3 \end{bmatrix} = \begin{bmatrix} \cos(\alpha) & -\sin(\alpha) & 0 \\ r^{-1}\sin(\alpha) & r^{-1}\cos(\alpha) & 0 \\ 0 & 0 & w \end{bmatrix} \begin{bmatrix} x_1 \\ x_2 \\ x_3 \end{bmatrix} \qquad r > 1, w > 0 \text{ and } \alpha \in [0, \pi). \tag{3.12}$$

This modified 3-D distance is analogous to the modified 2-D distance but weighting elevation through the parameter $w$. This additional parameter is estimated together with $r$ and $\alpha$.

#### 3.3.4.3 Crossing distance

There exist alternatives to the space transformations (3.11) and (3.12) to take into account spatial anisotropy. Instead of considering closer the pairs of stations located along the direction of strongest extremal dependence $\alpha$ as done in (3.11) and in (3.12), it is also possible to compute the distances by taking into account the geographical aspects of the study area. For instance the "hydrological distance", used for river discharges, associates for each pair of locations the shortest distance in a river network (Asadi et al., 2015). Another distance, referred as the "crossing distance" in Gottardi et al. (2012) and

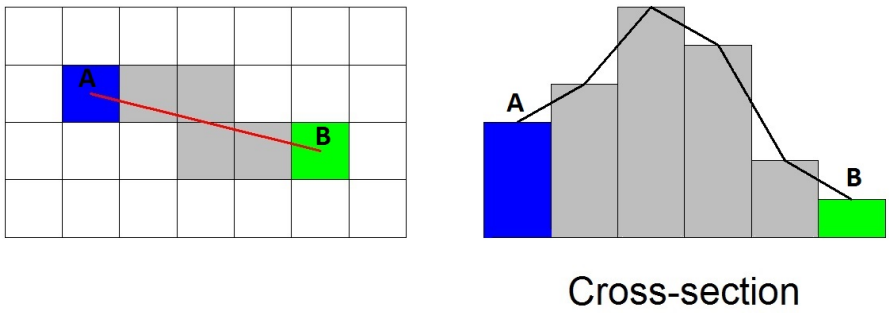


***Figure 3.3:*** *Example of the calculation of the crossing distance between the blue (A) pixel and the green (B) pixel. The pixels crossed by the red line linking the centers of the blue and green pixels are in grey. The crossing distance between the blue pixel and the green pixel is defined by the sum of the lengths of the black segments showed in the cross section.*

more appropriate in our context, is based on the relief variations between each pair of stations. In addition to the modified 2-D distance and to the modified 3-D distance, we also consider this crossing distance. To compute it, the French Alps are divided into pixels of dimension $1 \times 1$ km, and the elevation of each pixel is given by a 1 km digital elevation model. Figure 3.3 shows an example of the calculation of the crossing distance between two pixels. A line linking the centers of these two pixels is drawn (red line in Figure 3.3), and all the pixels crossing this line are considered (in grey in Figure 3.3). The crossing distance is then the sum of the 3-D Euclidean distances between the pixels along this red line (represented by the black segments in the cross section of Figure 3.3). The Euclidean distance is applied using a weight $\Omega$ for elevation: $\sqrt{\sum \Delta x_1^2 + \Delta x_2^2 + (\Omega.\Delta x_3)^2}$. For instance, a weight $\Omega = 20$ is used for precipitation in Gottardi et al. (2008, 2012).

### 3.3.5 Estimation of the extremal dependence over moving time windows

First, we estimate the parameters (e.g., $r$, $\alpha$ , $\lambda$ and $\kappa$ for the modified 2-D distance) by least squares, making use of all the data together over the whole temporal period (1958-2013). Then, we hold fixed the estimations of the anisotropy parameters (e.g., $r$ and $\alpha$ in the 2-D case), while the parameters $\lambda$ and $\kappa$ of the extremal function are reestimated on 20-year moving time windows under this anisotropic transformation.

For each estimation window (from 1958-1977 to 1993-2012) and each pair of stations, the extremal coefficient $\theta$ is estimated as follows:

$$\theta = \frac{1 + 2\nu_F}{1 - 2\nu_F} \tag{3.13}$$

where $\nu_F$ is the F-madogram (Cooley et al., 2006; Naveau et al., 2009) defined by

$$\nu_F = \frac{1}{2}\mathbf{E}\left[|F(Z_1) - F(Z_2)|\right] \tag{3.14}$$

with $F(z) = \exp(-1/z)$ the unit Fréchet cumulative distribution function. These pairwise estimations provide estimations $\hat{\theta}_h$ for all distances $h$ between two stations (grey points in Figure 3.4). Then, the theoretical extremal functions (3.8)–(3.10) are fitted by least squares on the pairwise estimations $\hat{\theta}_h$, leading to $\hat{\beta} = [\hat{\lambda}, \hat{\kappa}]^T$ the vector of parameter estimates, $\Sigma = \begin{bmatrix} \mathrm{var}(\lambda) & \mathrm{cov}(\lambda,\kappa) \\ \mathrm{cov}(\lambda,\kappa) & \mathrm{var}(\kappa) \end{bmatrix}$ the variance-covariance matrix for these estimates, and $\theta(h)$, the estimated extremal function (red curve in Figure 3.4).

### 3.3.6 Range of extremal dependence

We define the range of extremal dependence as the distance $h_0$ such as $\theta(h_0) = 1.9$ (Figure 3.4). The range denotes the distance above which snowfall maxima become weakly dependent in extremes, i.e., close to independence in practice. The stronger the extremal dependence at large distances, the larger the range. Inverting (3.8)–(3.10) gives the following expressions of the range: for the Brown-Resnick extremal function

$$h_0(\beta) = h_0(\lambda,\kappa) = \lambda\left[2\left\{\Phi^{-1}\left(\frac{1.9}{2}\right)\right\}^2\right]^{1/\kappa}, \tag{3.15}$$

for extremal-t extremal function

$$h_0(\beta) = \lambda\left[-\log\left(\frac{1 - \frac{1}{\nu+1}\left\{T_{\nu+1}^{-1}\left(\frac{1.9}{2}\right)\right\}^2}{1 + \frac{1}{\nu+1}\left\{T_{\nu+1}^{-1}\left(\frac{1.9}{2}\right)\right\}^2}\right)\right]^{1/\kappa}, \tag{3.16}$$

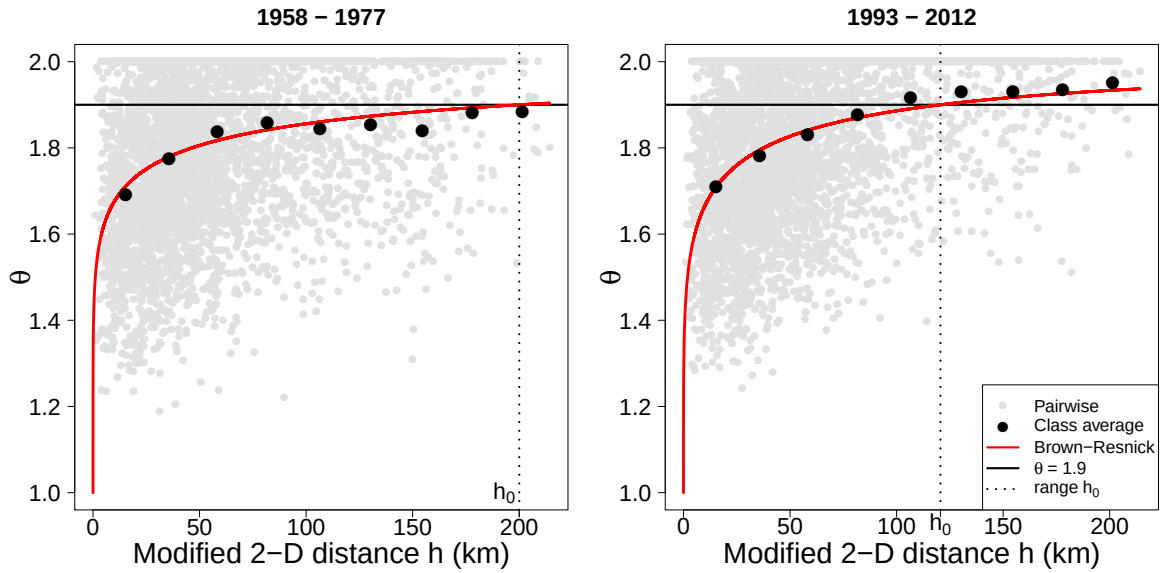


***Figure 3.4:*** *Extremal coefficient function for the first (1958-1977) and the last (1993-2012) estimation windows using the modified 2-D distance: madogram-based pairwise estimations of the extremal coefficient for every pairs of stations (grey dots), by distance class means (black dots), and Brown-Resnick extremal function fitted to all pairwise estimations by least squares (red curve). The range $h_0$ of extremal dependence (equation (3.15)) for the two considered time windows is $h_0 = 200$ km (1958-1977) and $h_0 = 121$ km (1993-2012), respectively.*

and for geometric Gaussian extremal function

$$h_0(\beta) = \lambda \left[ -\log \left( 1 - \frac{2\left\{\Phi^{-1}\left(\frac{1.9}{2}\right)\right\}^2}{\sigma^2} \right) \right]^{1/\kappa}. \tag{3.17}$$

We estimate a 95% confidence interval for each estimation window by the delta method (Cox, 1998), propagating the standard error on $\hat{\beta}$ in equation 3.18. Hence, the 95% confidence interval for $h_0(\beta)$ is given by

$$\left[ h_0(\hat{\beta}) - \frac{\Phi^{-1}(0.975)}{n} \nabla h_0(\hat{\beta})^T \Sigma \nabla h_0(\hat{\beta}), h_0(\hat{\beta}) + \frac{\Phi^{-1}(0.975)}{n} \nabla h_0(\hat{\beta})^T \Sigma \nabla h_0(\hat{\beta}) \right] \tag{3.18}$$

with $\nabla h_0$ the gradient of $h_0$ with respect to $\beta$, $\Sigma$ the variance-covariance matrix for the estimates and $n$ the number of pairwise estimates of the extremal coefficient (number of pairs of stations).

## 3.4 Results and discussion

### 3.4.1 Local and synoptic variables

Figure 3.5 shows the 20-year moving averages of the variables introduced in section 3.2.2. In the considered period, we observe decreases of cumulated snowfall, mean snow water equivalent, and snow precipitation ratio and increases of mean temperature, NAO and AMO. The period of strongest decrease for cumulated snowfall and mean snow water equivalent (at 1800 m and 2400 m) is from 1985 to 1997. For snow precipitation ratio, the period of strongest decrease is from 1981 to 1997 at 1800 m and from 1983 to 1993 at 2400 m. At 2400 m, the snow precipitation ratio is close to 1 during the entire study period, which means that at this elevation most of the precipitation falls as snow. Mean temperature mainly increases from 1978 to 1997 both at 1800 m and 2400 m. NAO index strongly increases from 1978 to 1985, and AMO index increases from 1978 to the end of the period of study. All of these trends come within the scope of the 1980s regime shift (Reid et al., 2015).

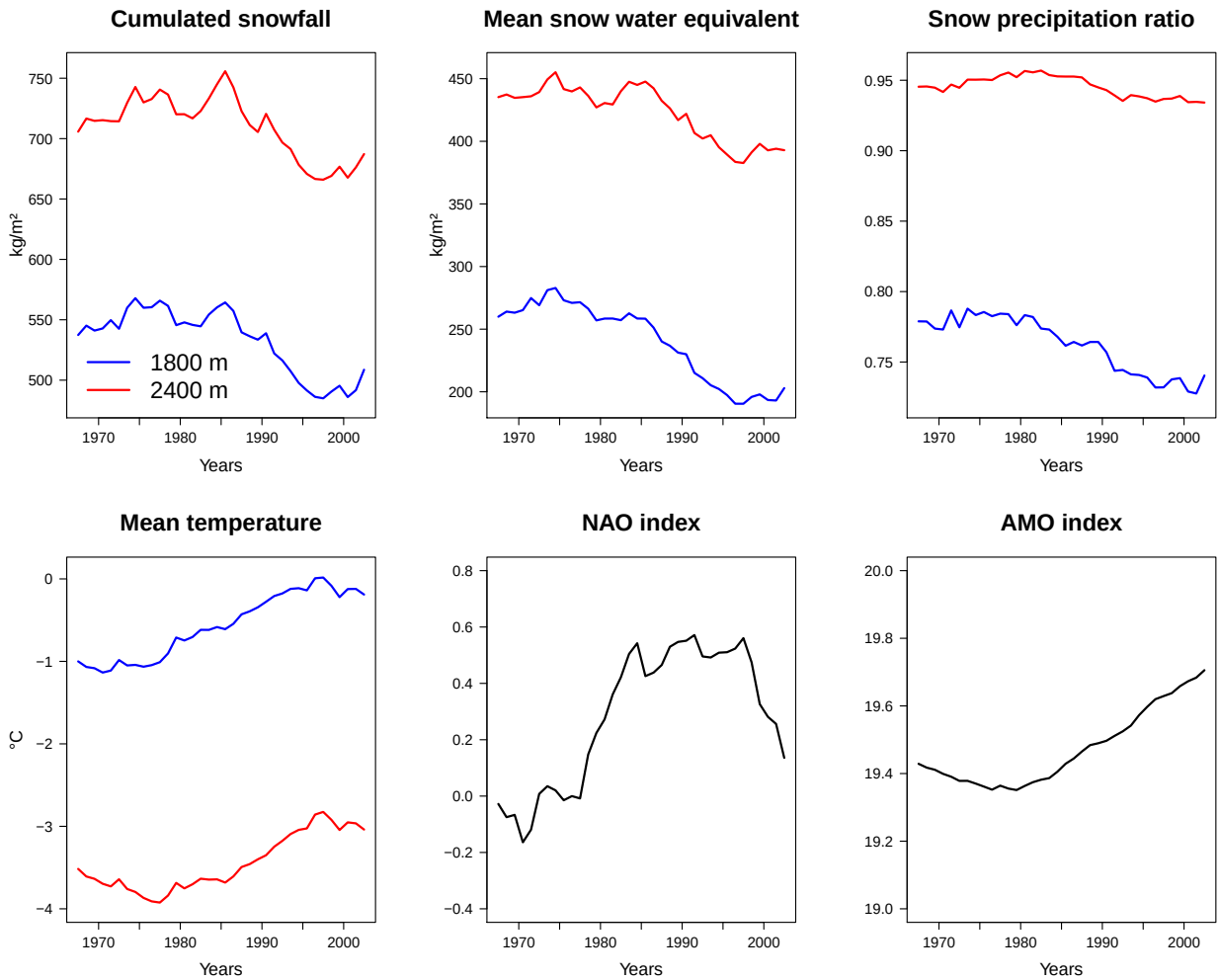


*Figure 3.5:* *20-year moving averages of the considered variables: cumulated snowfall, mean snow water equivalent, snow precipitation ratio, and mean temperature at 1800 m (blue lines) and 2400 m (red lines) elevation levels, NAO and AMO indexes. The X axis represents the center of the 20-year time window.*

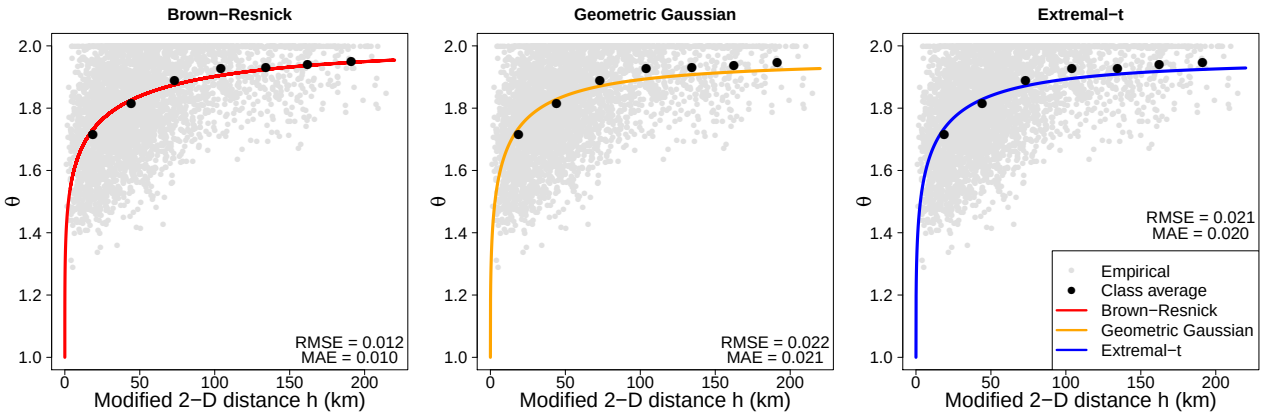


***Figure 3.6:*** *Estimated Brown-Resnick, geometric Gaussian and extremal-t extremal functions in the case of the 2-D modified distance. Here models are fitted on the whole temporal period. RMSE and MAE represent, respectively, root mean square errors and the mean average errors between the fitted extremal functions and the class averages.*

## 3.4.2 Results using the entire study period

### 3.4.2.1 Goodness-of-fit of the models

Figure 3.6 shows the fitted Brown-Resnick, geometric Gaussian and extremal-t extremal functions using the entire study period in the case of the modified 2-D distance. The goodness-of-fit of the models can be assessed comparing the estimated extremal functions to the class averages: a suitable extremal function should be as close as possible to the class averages. We can observe graphically or with the computation of the root mean square errors and the mean average errors that the three extremal functions fit well the class averages. However, the Brown-Resnick extremal function seems to be slightly better, and from now we will mainly consider this extremal function.

### 3.4.2.2 Anisotropy

For the Brown-Resnick extremal function with the modified 2-D distance, we find $\hat{\alpha} = 35.84°$ (with 0° for the east and 90° for the north) and $\hat{r} = 2.78$. This anisotropy corresponds to the orientation of the main mountains and valleys in the French Alps and means that the pairs of stations located along this direction are more dependent at extreme levels. Similar observations were made in Gaume et al. (2013b) for the French Alps with fewer observations (40 stations from 1966 to 2009), in Blanchet and Davison (2011) for the Swiss Alps, and in Padoan et al. (2010) for the Appalachians. This robust pattern may be interpreted as the effect of orography on atmospheric fluxes generating

extreme precipitations. Similar estimations are found using the other extremal functions ($\hat{\alpha} = 36.57°$ and $\hat{r} = 2.78$ with geometric Gaussian extremal function and $\hat{\alpha} = 36.45°$ and $\hat{r} = 2.78$ with extremal-t extremal function) and in the 3-D distance ($\hat{\alpha} = 37.86°$ , $\hat{r} = 2.76$ and $\hat{w} = 42.27$ with Brown-Resnick extremal function). The estimate of the weight parameter $\hat{w} = 42.27$ motivates the use of a weight parameter $\Omega = 40$ for the crossing distance defined in section 3.3.4.3.

### 3.4.3 Results using moving time windows

#### 3.4.3.1 Temporal trend

With the Brown-Resnick extremal function and the 2-D distance, we find a positive temporal trend in the extremal coefficient for distances exceeding 100 modified kilometers (Figure 3.7(a)) and, therefore, a tendency toward less dependence in extremes at large distance in recent years. At short distances (values of the extremal function for small $h$), this decrease in strength of dependence is less visible.

There is a clear negative temporal trend in the range of extremal dependence. The correlation with time is strong (Table 3.1), and a linear fit of the range estimates on the center of the considered estimation window provides a determination coefficient as high as $R^2 = 0.71$ (Figure 3.7(b)). The range of extremal dependence decreased by about 3 km/yr. It reduced by almost half over the 56 year study period, from a maximum of 237 km in 1978 to around 100 km over the most recent time windows. Yet most of the decrease has been concentrated over the 1978-1997 period during which the 1980s regime shift happened (Reid et al., 2015).

The corresponding 95% confidence intervals computed with the delta method (Figure 3.7(b)) show that these variations are significant. The widest confidence interval is in 1978 with a width of 79 km (95% confidence interval [198 km, 277 km]), while the width of the confidence interval is between 15 km and 25 km for the recent period.

#### 3.4.3.2 Correlation with local and synoptic variables

Table 3.1 shows that the range of extremal dependence is strongly positively correlated with the cumulated snowfall, mean snow water equivalent and snow precipitation ratio and is strongly negatively correlated with the mean temperature, AMO and NAO indexes. These correlations are overall slightly higher at 1800 m than at 2400 m, which is consistent with the elevation of the stations of the data set. Yet correlations remain high at 2400 m and correlation with the mean temperature is even slightly higher at 2400 m than at 1800

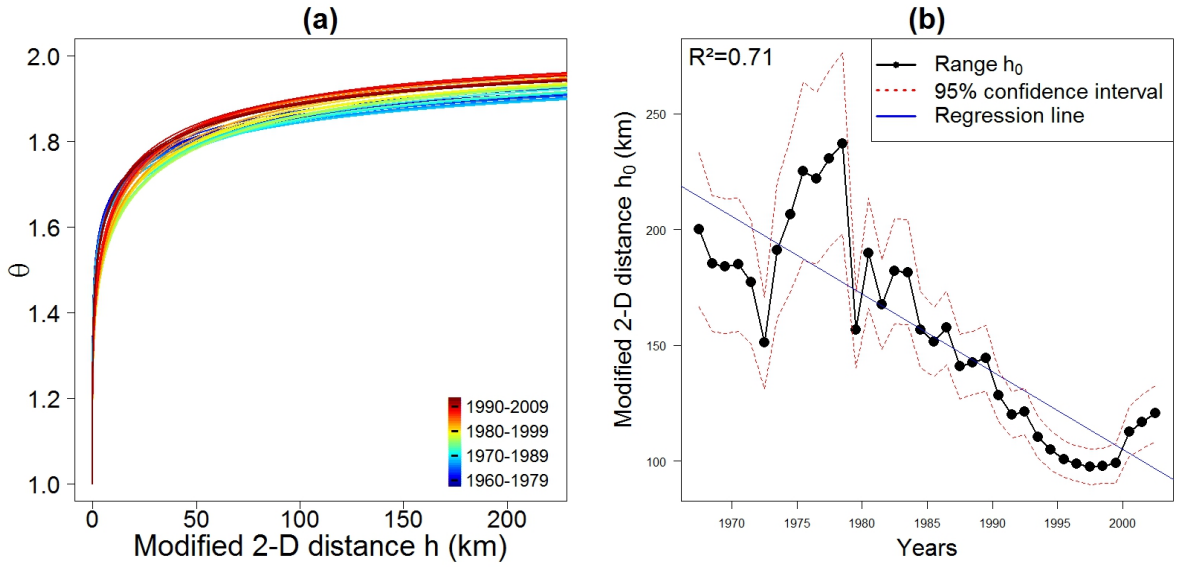


***Figure 3.7:*** *(a) Temporal evolution of the fitted Brown-Resnick extremal functions under the 2-D modified distance, from oldest time windows (blue curves) to the most recent ones (red curves). (b) Temporal evolution of the range of extremal dependence. The range (equation (3.15)) is expressed as a function of the 2-D modified distance (equation (3.11)). It is plotted (black dots) as a function of the center of the considered estimation window. The associated 95% confidence interval is evaluated by the delta method using equation (3.18). The linear fit (straight blue regression line) is made on the winter estimates (black dots).*

***Table 3.1:*** *Correlation table between the range of dependance in extreme snowfall evaluated over 20-year estimation windows and 20-year moving averages of the considered winter climate variables (section 3.2.2)*[a]

| | SF 1800 | SWE 1800 | T 1800 | SPR 1800 | SF 2400 | SWE 2400 | T 2400 | SPR 2400 | AMO | NAO | Time |
|---|---|---|---|---|---|---|---|---|---|---|---|
| Range | 0.86 | 0.90 | -0.90 | 0.91 | 0.78 | 0.84 | -0.92 | 0.76 | -0.86 | -0.68 | -0.84 |
| SF 1800 | - | 0.95 | -0.83 | 0.92 | 0.98 | 0.97 | -0.97 | 0.88 | -0.92 | -0.44 | -0.79 |
| SWE 1800 | - | - | -0.94 | 0.97 | 0.88 | 0.96 | -0.98 | 0.83 | -0.95 | -0.62 | -0.92 |
| T 1800 | - | - | - | -0.93 | -0.72 | -0.86 | 0.90 | -0.65 | 0.86 | 0.83 | 0.96 |
| SPR 1800 | - | - | - | - | 0.82 | 0.91 | -0.96 | 0.84 | -0.95 | -0.60 | -0.91 |
| SF 2400 | - | - | - | - | - | 0.94 | -0.91 | 0.86 | -0.86 | -0.30 | -0.68 |
| SWE 2400 | - | - | - | - | - | - | -0.95 | 0.86 | -0.91 | -0.48 | -0.83 |
| T 2400 | - | - | - | - | - | - | - | -0.88 | 0.96 | 0.56 | 0.86 |
| SPR 2400 | - | - | - | - | - | - | - | - | -0.87 | -0.20 | -0.63 |
| AMO | - | - | - | - | - | - | - | - | - | 0.45 | 0.88 |
| NAO | - | - | - | - | - | - | - | - | - | - | 0.73 |

[a]Cumulated snowfall (SF), mean snow water equivalent (SWE), mean temperature (T) and snow precipitation ratio (SPR), AMO and NAO indexes. Evaluation is made with 36 values for each variable, corresponding to the 36 estimation windows from 1958-1977 to 1993-2012. The 1800 and 2400 indicate the elevation level for SF, SWE, T and SPR. Time denotes the center of each estimation window.

m. Remember that for coherence, these correlations are based on the moving averages of the local and synoptic variables. This makes the correlations stronger than with "raw" annual values but more difficult to interpret in terms of significance level. Yet their high values and physical consistency (see hereafter) is striking.

#### 3.4.3.3 Potential climate control on spatial dependence of extreme snowfall

The negative correlation between the range of extremal dependence and the local and synoptic temperature variables (mean temperature at the French Alps scale and AMO which refers to the temperature of the North Atlantic Ocean sea surface) shows that the dependence in extreme snowfall in the French Alps is weaker when winter temperatures are higher. Somewhat similar results were obtained very recently for extreme storms in Australia, with a reduction of their spatial extent as temperatures increases (Wasko et al., 2016). In our case of extreme snowfall, especially convincing is the concomitance between the strongest decrease in extremal dependence range (see Figure 3.7(b)) and the period of the strongest winter warming (section 3.4.1). Specifically, the concomitant period of strongest decrease of snow precipitation ratio from 1981 to 1997 (section 3.4.1) suggests that the decrease in spatial dependence of snowfall extremes could be due to

a decrease of the snow precipitation ratio caused by the increase of temperature in the context of the 1980s regime shift (Reid et al., 2015). Marty and Blanchet (2012) suggested the same explanation for the negative temporal trends in extreme snowfalls in the Swiss Alps. However, it is important to note that we show here something different, since our results relate to the spatial dependence of extremes, and not to their magnitude. To the best of our knowledge, this has never been shown for any geophysical variable. Hence, the main explanation for the decrease in spatial dependence of extreme snowfall may be that the temperature increase makes these more isolated in space, at least for heavy snowfall events occurring when temperatures are not too low. In such a case, only the highest stations experience snow, while rain falls at low elevations, leading to less spatially coherent patterns in winter maxima.

Yet we cannot exclude a magnitude effect with stronger dependence in extreme snowfall in the French Alps during snowier winters. Indeed, even if the effect of snow/rain partitioning is very low at 2400 m with a snow precipitation ratio close to 1 during the entire study period (section 3.4.1), there is a strong positive correlation between the range and the snow variables (mean snowfall and mean snow water equivalent). This is coherent with the negative correlation with NAO, since a negative NAO anomaly is associated with harsher winter conditions widespread over the western Alps, including colder temperatures but also more intense snowfall (López-Moreno et al., 2011). Consequently, the decrease in intensity of snowfall could be an additional cause of the decrease in dependence of extreme snowfall.

#### 3.4.3.4 Robustness to modeling assumptions

Figure 3.8 shows that a decreasing temporal trend of the range is also found for geometric Gaussian and extremal-t extremal functions (with the 2-D modified distance), showing that this decrease is robust towards the choice of model. Figure 3.9 shows that when transformation into unit Fréchet involves the marginal transformations obtained on each temporal window (instead of the one obtained on the whole study period), then a similar decrease in the range is found. Finally, this decreasing temporal trend of extremal dependence is still observed under both the modified 3-D distance and the crossing distance (Figure 3.10). The decrease is very similar to those either with the 2-D and 3-D modified distances. Nevertheless, the decrease starts slightly later (around 1983) with the crossing distance. Yet in any case we see in Figures 3.8–3.10 that the decrease by half in the range of extremal dependence during the study period is clear, whatever the chosen hypotheses to evaluate it.

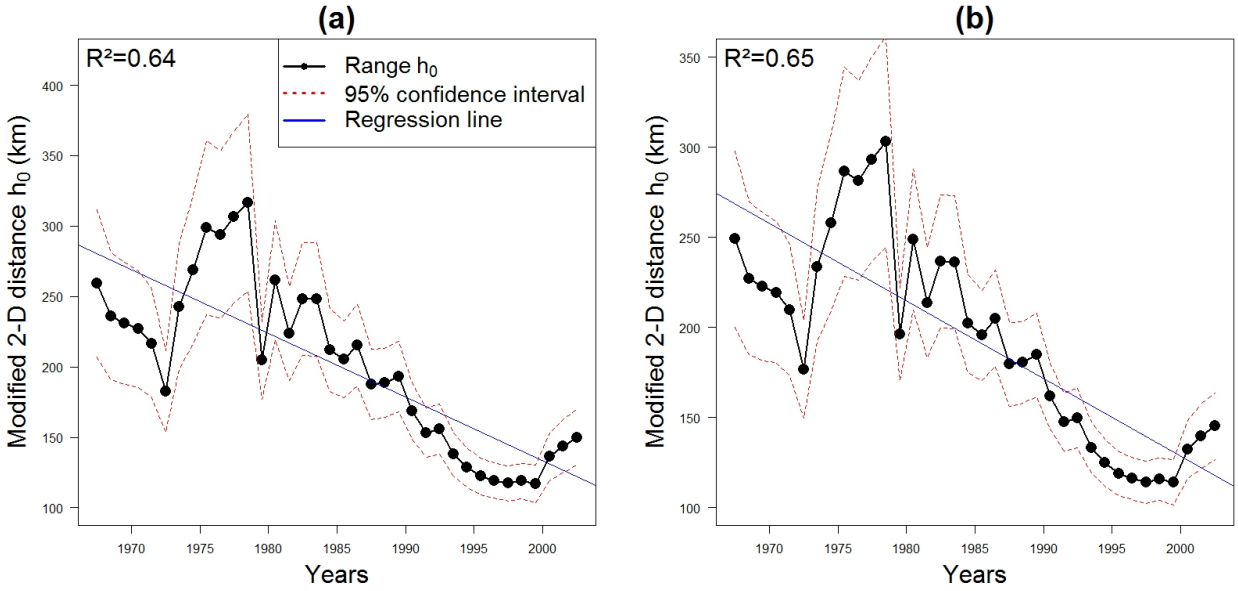


***Figure 3.8:*** *Same as Figure 3.7(b) with (a) geometric Gaussian extremal function and (b) extremal-t extremal function.*

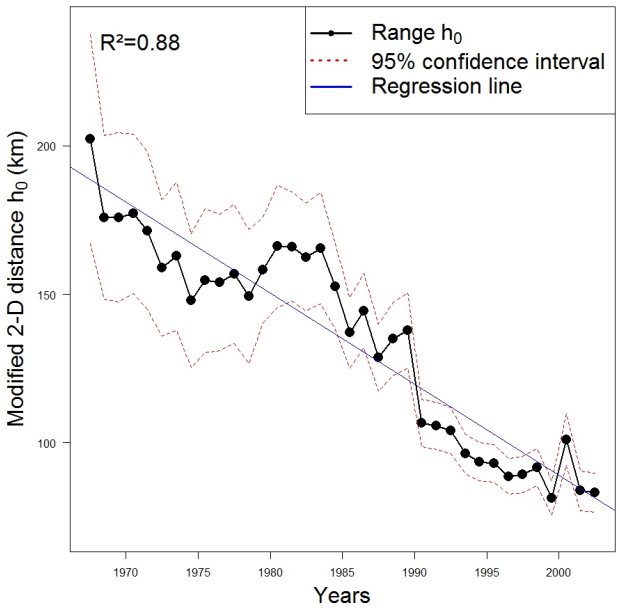


***Figure 3.9:*** *Same as Figure 3.7(b) when the marginal distributions are estimated and transformed into unit Fréchet on each estimation window.*

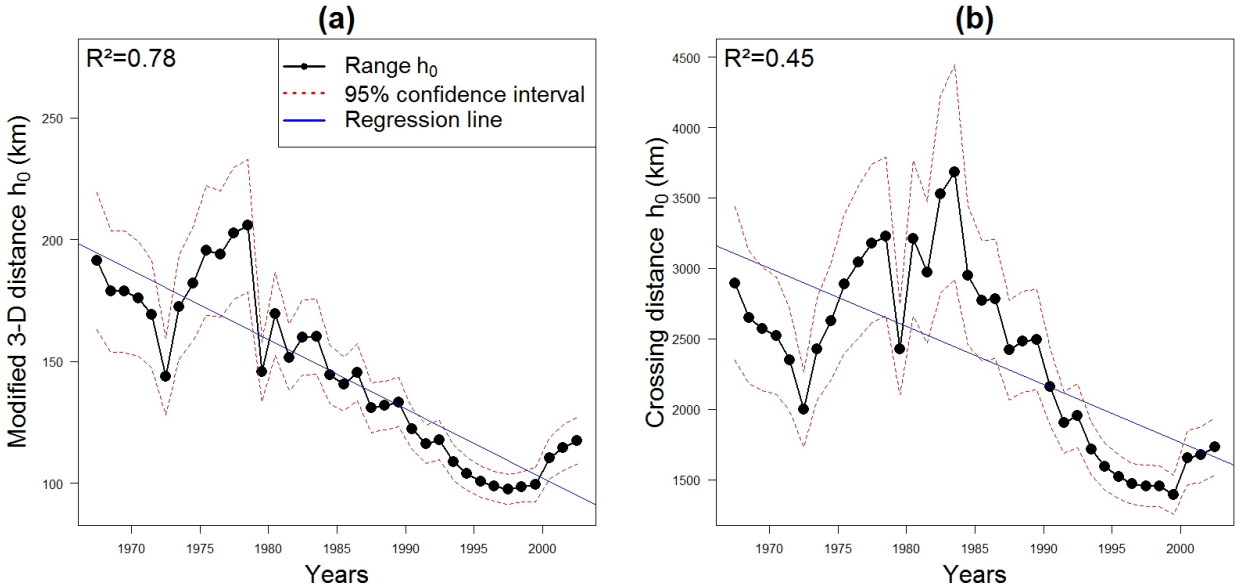


***Figure 3.10:*** *Same as Figure 3.7(b) with (a) modified 3-D distance and (b) crossing distance.*

## 3.5 Conclusion and outlook

In this paper, we show how the spatial dependence structure in extreme snowfall in the French Alps has evolved over the last decades, with a significant negative trend in the strength of extremal dependence for large distances (more than 100 km taking into account anisotropy). Specifically, we highlight a decrease of 3 km/yr of the range of extremal dependence, although this trend seems to slow down over the last years. The division by two of the range over the study period is robust with regard to how the marginal distributions are estimated, to how the way the distance between the stations is defined, and to the choice of the extremal function model, i.e., the few assumptions we had to made to conduct the study.

The decrease in the range is strongly correlated with several climate variables, at both local and synoptic scales. This suggests that climate change can have a significant impact on the spatial dependence structure of extreme snowfall. This is, to the best of our knowledge, the first evidence of such an effect.

The very strong decreasing pattern that we observe is attributable at first to the increase of temperature and to the major control exerted by temperature on the snow/rain partitioning. Yet a magnitude effect, with less dependent extremes due to a decrease in intensity of precipitation, also exists. Our result obtained on snow may therefore be of wider hydrological interest because similar trends could also exist in other variables less influenced by temperature such as rainfall.

From a statistical point of view, we did not try to fit a complete max stable model, and we chose to use a data-oriented approach. Indeed, we used time-dependent windows and took into account anisotropy, so as to highlight potential changes by fitting Brown-Resnick extremal function to pairwise estimations of extremal coefficient. Hence, even if our approach remains simpler than a model-based approach, it involves state-of-the-art tools from multivariate EVT whose inferential power we demonstrate in geophysics. This approach allows us to make minimal modeling assumptions in order to ensure the geophysical origin of the displayed temporal trend rather than a consequence of modeling choices. Our framework could therefore be useful for a variety of other studies addressing geophysical extremes in the context of climate change.

## Acknowledgments

This work has been supported by a grant from LabEx OSUG@2020 (Investissements d'avenir - ANR10 LABX56). We thank hundreds of snow observers and the Météo-France staff involved in the collection and constitution of the data sets used in this study. We thank Anne-Laure Fougères (Université Lyon 1), Philippe Naveau (LSCE), Emmanuel Paquet (EDF), and Benjamin Renard (Irstea Lyon) for their advice. We thank Guillaume Evin (LTHE) and David Penot (EDF) for their help concerning the crossing distance. We thank two anonymous reviewers of a previous version of this manuscript for their useful comments and suggestions. The data for this paper are available upon request from the corresponding author (G. Nicolet, gilles.nicolet@irstea.fr).

# Chapter 4

# Modeling the trend in the spatial dependence of extremes: application to the assessment of climate change impact on snow depth maxima in the French Alps

The content of this chapter is submitted to Water Resources Research. The authors are Gilles Nicolet, Nicolas Eckert, Samuel Morin and Juliette Blanchet.

# Abstract

Max-stable processes are the extension of the univariate extreme value theory to the spatial case and are increasingly used to model climate extremes. In the current context of climate change, several studies have considered max-stable processes with nonstationary marginal distributions. However, this paper is the first attempt of modeling climatic time trends within the spatial dependence structure of extremes. This approach is applied to a data set of snow depth winter maxima in the French Alps (82 stations from 1970 to 2012). Several local and synoptic covariates are used to investigate which ones impact the spatial dependence. We observe a strong decrease in the range of extremal dependence during the 1980s, due to the effect of the increase of temperature on the snow precipitation ratio and to a decrease in the winter cumulated snowfall. Hence, we show that the spatial dependence of extreme snow depths is impacted by climate change in a similar way to that have been observed for extreme snowfall. As a collateral benefit, we show that snow depths are more spatially dependent and a bit less anisotropic. The space-time approach that we introduce may be very useful for assessing evolutions under ongoing climate change in various hydrological or climatic quantities generating risk.

## 4.1 Introduction

Due to their high impacts, natural hazards see a growing interest for risk management. Among them, extreme snow events like snowstorms, extreme snow depths, extreme snowfall and avalanches are particularly crucial in mountainous regions for their potential economic and human damages. In addition, extreme snow depth values are also relevant for water storage, tourism and their impact on ecosystems.

Extreme value theory (Coles, 2001) offers a suitable theoretical framework to extrapolate beyond the highest recorded observation and thus for modeling extreme events. It is mostly used in hydrology (Katz et al., 2002), finance/insurance (Embrechts et al., 2013) and climatology (Naveau et al., 2005). Specifically, univariate extreme value statistics have been applied to three days snowfall in Italian and Swiss Alps (Bocchiola et al., 2006, 2008) and to extreme snowfall and extreme snow depths in Switzerland (Blanchet et al., 2009; Blanchet and Lehning, 2010).

When the variable of interest is spatially dependent in extremes, that is to say when close-enough locations are likely to experience concomitant extremes, it is advantageous to model its spatial dependence structure. Indeed, this allows to estimate joint and conditional probabilities of exceedances, to compute surface integrals, and to infer values at ungauged sites (for instance by conditional simulation). Max-stable processes (de Haan, 1984) are the spatial extension of univariate extreme value theory. They have been applied to extreme snow depths in Switzerland (Blanchet and Davison, 2011), to extreme snowfall and to avalanche slab depths in the French Alps (Gaume et al., 2012, 2013b; Nicolet et al., 2016). Among other results, these studies reveal several characteristics of extreme snow depths and extreme snowfall. For instance, extreme snow depths and extreme snowfall are both anisotropic with more dependence between the pairs of stations angled in the same direction as the main massifs and valleys. A significant difference between the structures of spatial dependence of these two variables is that the spatial dependence between extremes appears stronger for snow depths than for snowfall, due to the cumulative effects involved in the formation of the snow pack. However, this effect has never been highlighted so far for snowfall and snow depth data from the same region.

Most of the studies using max-stable processes assume temporal stationarity both in the distributions of extremes and in the spatial dependence structure of these extremes. In a climate change context (Stocker et al., 2013), this hypothesis is clearly contestable due to the exacerbated response of the cryosphere to warming (Beniston et al., 2017). In the Swiss Alps, decreasing trends have been found for snow depths, duration of continuous

snow cover, number of snowfall days and extreme snowfall (Laternser and Schneebeli, 2003). Mean snow depths and snow cover duration have also negative trends in the French Alps (Durand et al., 2009a). Negative trends of snow duration and snowfall have also been observed in the Italian Alps (Valt and Cianfarra, 2010). Using an extreme value statistics framework but without modeling the structure of spatial dependence, Marty and Blanchet (2012) found negative temporal trends in extreme snow depths and extreme snowfall in Switzerland. In addition to the pointwise magnitude of extreme snowfall, their spatial dependence structure may be also impacted. Thus, Nicolet et al. (2016) recently highlighted a negative temporal trend in the spatial dependence of extreme snowfall in the French Alps.

Some studies model nonstationarity within a spatial model for extremes by using time-dependent covariates for the marginal distributions. By this way, Westra and Sisson (2011) highlighted the influence of global sea surface temperature and South Oscillation Index on extreme precipitations in Australia, whereas Shang et al. (2011) and Zhang et al. (2014) showed a relationship between El Niño Southern Oscillation and extreme precipitation in California and in China, respectively. However these studied all assumed temporal stationarity in the spatial dependence structure of extremes.

Only few studies deal with max-stable process with spatio-temporal dependence structure applied to case studies. Raillard (2011) applied a space-time Smith max-stable process to extreme wave heights with observations recorded at irregular time steps (from few minutes to 3 days). Steinkohl (2013) extended the Brown-Resnick max-stable process to the space-time case using space-time correlation functions and used it for extreme rainfall in Florida using 15-minute incremented observations. Huser and Davison (2014) introduced a space-time troncated Schlather max-stable process and applied it to extreme precipitation in Switzerland with hourly observations. All of these studies consider the short-range temporal dependence of extremes using observations recorded at short time steps. On the other hand, they do not consider possible temporal nonstationarity in the spatial dependence structure at longer (e.g., decadal) time scale.

The issue of nonstationarity in spatial extreme value statistics is crucial. A modeling as adequate as possible is required to provide consistent risk measures for phenomena whose nonstationarity is recognized, such as snow, rain or temperature. Moreover, it is required to realistically anticipate the evolution of risk under climate change. Hence, the objective of this paper is to propose a first ever simple way to account for long range climate nonstationarity in the spatial dependence structure of max-stable processes. The adopted parametric approach can be viewed as a continuation of the data-based work used in Nicolet et al. (2016) with a different data set (snow depths instead of snowfall), but

with the major difference of relying on a explicit model instead of empirical estimates only. We apply this approach for inferring the temporal evolution of the spatial dependence in extreme snow depths under climate change. We process a data set consisting of 82 snow depth winter maxima series in the French Alps. Specifically, we fit different Brown-Resnick processes with temporal trends in the spatial structure of dependence. For each model, the temporal trend is conveyed by different local and synoptic covariates and a rigorous procedure is used to highlight the most relevant ones. This allows us to highlight the climate change impact on the spatial dependence structure of extreme snow depths. As a collateral benefit, these results are compared to those concerning extreme snowfall obtained by Nicolet et al. (2016) over the same area and time-scale.

## 4.2 Data set

### 4.2.1 Snow Depths

Our data set is composed of winter maxima of snow depths with a winter period defined from 15 November to 15 May. These maxima are extracted from 3 databases composed respectively of:

- twice-daily manual measurements (dedicated snow manual observing network) from 1970 to 2013 (17 stations);
- daily automatic measurements (Nivôse stations) from 1980 to 2013 (7 stations);
- weekly manual measurements (dedicated snow manual observing network) from 1983 to 2013 (58 stations).

This provides a data set of 82 stations in the French Alps (Figure 4.1 (a)), from which the annual winter maxima are extracted. Yet, there are many non available observations before 1983 (Figure 4.1 (b)) but the 18 stations with more than 30 winter maxima (in red in Figure 4.1 (a)) are correctly distributed in the study area. In addition, the coverage of station elevation is very appropriate to address mountainous conditions, with many stations above 2000 m (Figure 4.1 (c)).

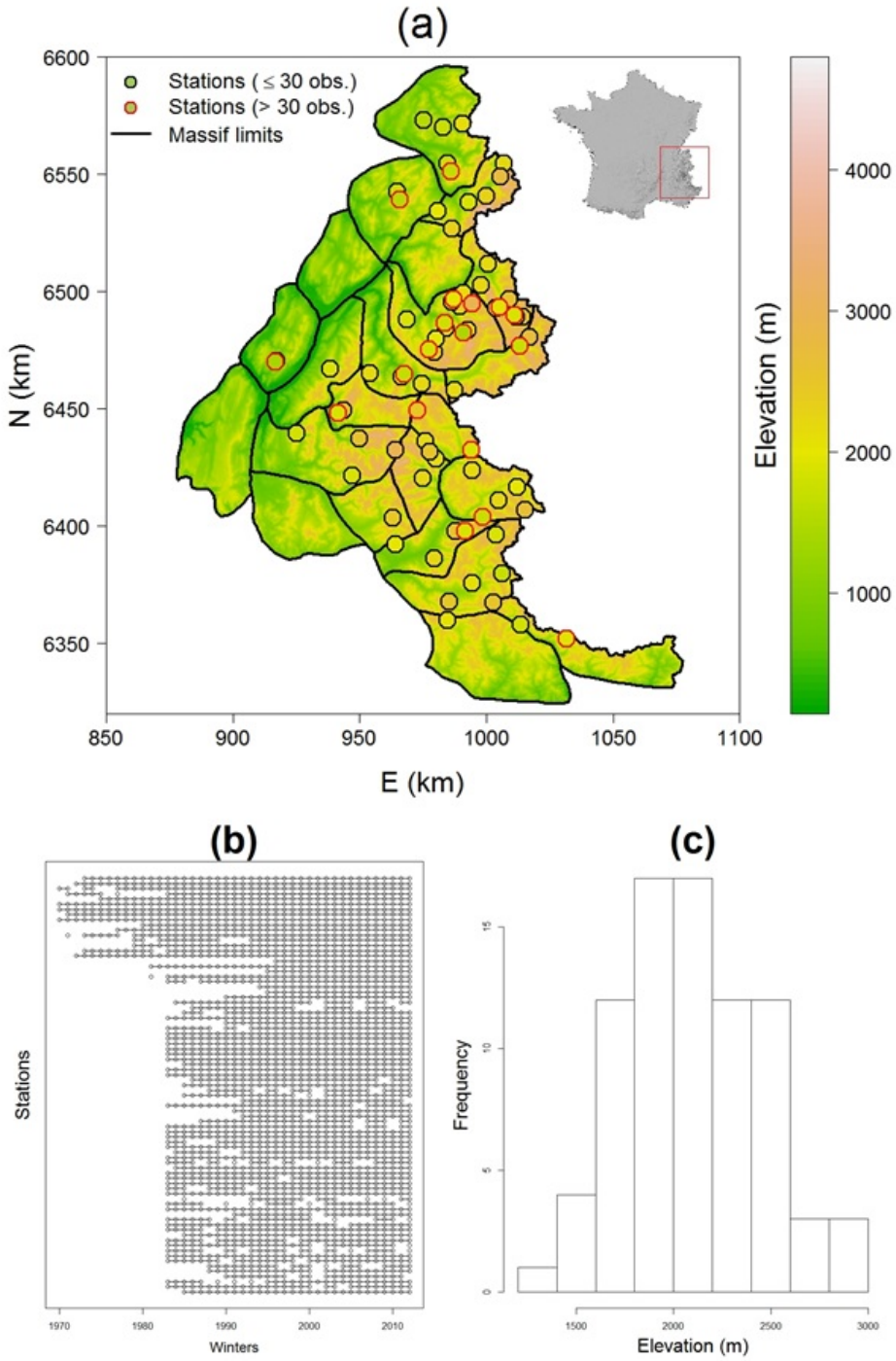


*Figure 4.1:* *Snow depth data set (Section 4.2.1). (a) Study area in the southeast of France, where the 23 massifs of the French Alps are located. Lines denote massif limits, and dots denote the positions of the stations. The stations having more than 30 annual maxima are indicated in red. (b) Data availability for each station. Each line represents one station, and each point means that the winter maxima is available for that station. (c) Histogram of station elevation.*

### 4.2.2 Covariates

In addition to time, we use several covariates that summarize the winter climate of the French Alps over the study period. The French Alps are divided into 23 massifs (see Figure 4.1 (a)), which are generally assumed to be homogeneous in terms of meteorological conditions for a given elevation. In each massif, the meteorological conditions (temperature and precipitation) are available all over the study period as a function of elevation through reanalyses (Durand et al., 2009b) provided by the SAFRAN (Système d'Analyse Fournissant des Renseignements Atmosphérique à la Neige) model (Durand et al., 1993, 1999). From these reanalyses, the cumulated snowfall, snow precipitation ratio (cumulated snow precipitation divided by total –snow and rain– precipitation), and the daily maximum, mean, and minimum temperature are calculated for two elevation levels (1800 m and 2400 m) for each winter and for each massif. Then, the mean of the 23 massif values is computed for each winter in order to have, for each variable and each winter, a single value for the entire French Alps notwithstanding the large variability of mean annual conditions (Durand et al., 2009b).

We also consider NAO (North Atlantic Oscillation Jones et al. (1997); Osborn (2006)) and AMO (Atlantic Multidecadal Oscillation, (Kaplan et al., 1998; Enfield et al., 2001)) indices through winter anomalies evaluated from November to April over the study period. NAO and AMO variables summarize the predominant oscillating patterns in the winter climate of the French Alps, in terms of pressure/precipitation and temperature, respectively. Rather than the more commonly used detrended version of AMO (Enfield et al., 2001), we use here the non-detrended version which includes the recent climate warming signal in addition to oscillating patterns (Kaplan et al., 1998).

We are interested in modeling climate effects in the spatial dependence structure of extreme snow depths. Thus, we need to remove the annual variability in the covariates, which is done by considering time moving averages. We consider 17-year moving averages (Figure 4.2) because the performance of the nonstationary models is slightly better, although very similar, using this value than when considering, e.g., 15 or 19-year moving averages. The value $C_k(n)$ of the covariate $C_k$ for winter $n$ is then the average of the raw values of this covariate from the winter $n-8$ to the winter $n+8$.

In the considered period, we observe decreases of snow precipitation ratio at 1800 m and cumulated snowfall and increases of maximum temperature, mean temperature and AMO. The period of strongest decrease in cumulated snowfall coincide with that of snow precipitation ratio at 1800 m and 2400 m, extending from 1982 to 1995. Temperature and AMO mainly increase during this period. The period of strongest increase is larger

***Table 4.1:*** *Covariates (Section 4.2.2). Correlation table for the 17-year moving averages of covariates*[a]

| | NAO | AMO | $T^{1800}_{min}$ | $T^{1800}_{mean}$ | $T^{1800}_{max}$ | $T^{2400}_{min}$ | $T^{2400}_{mean}$ | $T^{2400}_{max}$ | $SF^{1800}$ | $SF^{2400}$ | $SPR^{1800}$ | $SPR^{2400}$ |
|---|---|---|---|---|---|---|---|---|---|---|---|---|
| Time | 0.01 | **0.97** | -0.32 | **0.84** | **0.94** | 0.46 | 0.80 | **0.89** | **-0.84** | **-0.82** | **-0.85** | -0.69 |
| NAO | **1** | -0.13 | 0.75 | 0.46 | 0.28 | -0.01 | 0.21 | 0.25 | -0.05 | 0.07 | -0.26 | -0.07 |
| AMO | - | **1** | -0.36 | 0.80 | **0.91** | 0.60 | **0.85** | **0.90** | **-0.90** | **-0.89** | **-0.87** | -0.79 |
| $T^{1800}_{min}$ | - | - | **1** | 0.22 | -0.01 | 0.25 | 0.14 | 0.05 | 0.04 | 0.14 | -0.07 | -0.05 |
| $T^{1800}_{moy}$ | - | - | - | **1** | **0.97** | 0.62 | **0.92** | **0.97** | **-0.86** | -0.78 | **-0.94** | -0.78 |
| $T^{1800}_{max}$ | - | - | - | - | **1** | 0.59 | **0.92** | **0.98** | **-0.90** | **-0.84** | **-0.95** | -0.79 |
| $T^{2400}_{min}$ | - | - | - | - | - | **1** | **0.86** | 0.73 | **-0.80** | -0.79 | -0.73 | **-0.87** |
| $T^{2400}_{moy}$ | - | - | - | - | - | - | **1** | **0.98** | **-0.95** | **-0.91** | **-0.96** | **-0.93** |
| $T^{2400}_{max}$ | - | - | - | - | - | - | - | **1** | **-0.94** | **-0.89** | **-0.97** | **-0.88** |
| $SF^{1800}$ | - | - | - | - | - | - | - | - | **1** | **0.99** | **0.94** | **0.90** |
| $SF^{2400}$ | - | - | - | - | - | - | - | - | - | **1** | **0.88** | **0.87** |
| $SPR^{1800}$ | - | - | - | - | - | - | - | - | - | - | **1** | **0.91** |

[a]Time, NAO and AMO indexes, minimum temperature at 1800 m ($T^{1800}_{min}$), mean temperature at 1800 m ($T^{1800}_{mean}$, maximum temperature at 1800 m ($T^{1800}_{max}$), minimum temperature at 2400 m ($T^{2400}_{min}$), mean temperature at 2400 m ($T^{2400}_{mean}$), maximum temperature at 2400 m ($T^{2400}_{max}$), cumulated snowfall at 1800 m ($SF^{1800}$), cumulated snowfall at 2400 m ($SF^{2400}$), snow precipitation ratio at 1800 m ($SPR^{1800}$), snow precipitation ratio at 2400 m ($SPR^{2400}$). Correlations which are larger than 0.8 in absolute value are in bold.

for AMO (from 1978 to 2002) and starts earlier (around 1977) for maximum and mean temperature. NAO increases before 1985 and decreases after 1994. At 2400 m, the snow precipitation ratio is close to 1 during the entire study period, which means that, at this elevation, most of the precipitation falls as snow from 15 November to 15 May regardless of the year.

The correlation table (Table 4.1) shows that many of our covariates are strongly correlated. Although considering moving averages makes these correlations higher than when using "raw" annual values, the strength of these correlations is mainly due to the strong physical connections between these variables. There are 37 pairs showing a correlation lower than 0.8 in absolute value. Only these pairs are considered for the nonstationary models with two covariates, to avoid inference problems related to redundant information.

For computation efficiency, each covariate $C_k$ is zero-centered as follows:

$$C'_k(n) = \frac{C_k(n) - \overline{C_k}}{\text{std}(C_k)} \tag{4.1}$$

with $\overline{C_k}$ and $\text{std}(C_k)$ the mean and the standard deviation of $(C_k(1), ..., C_k(N))$, respectively.

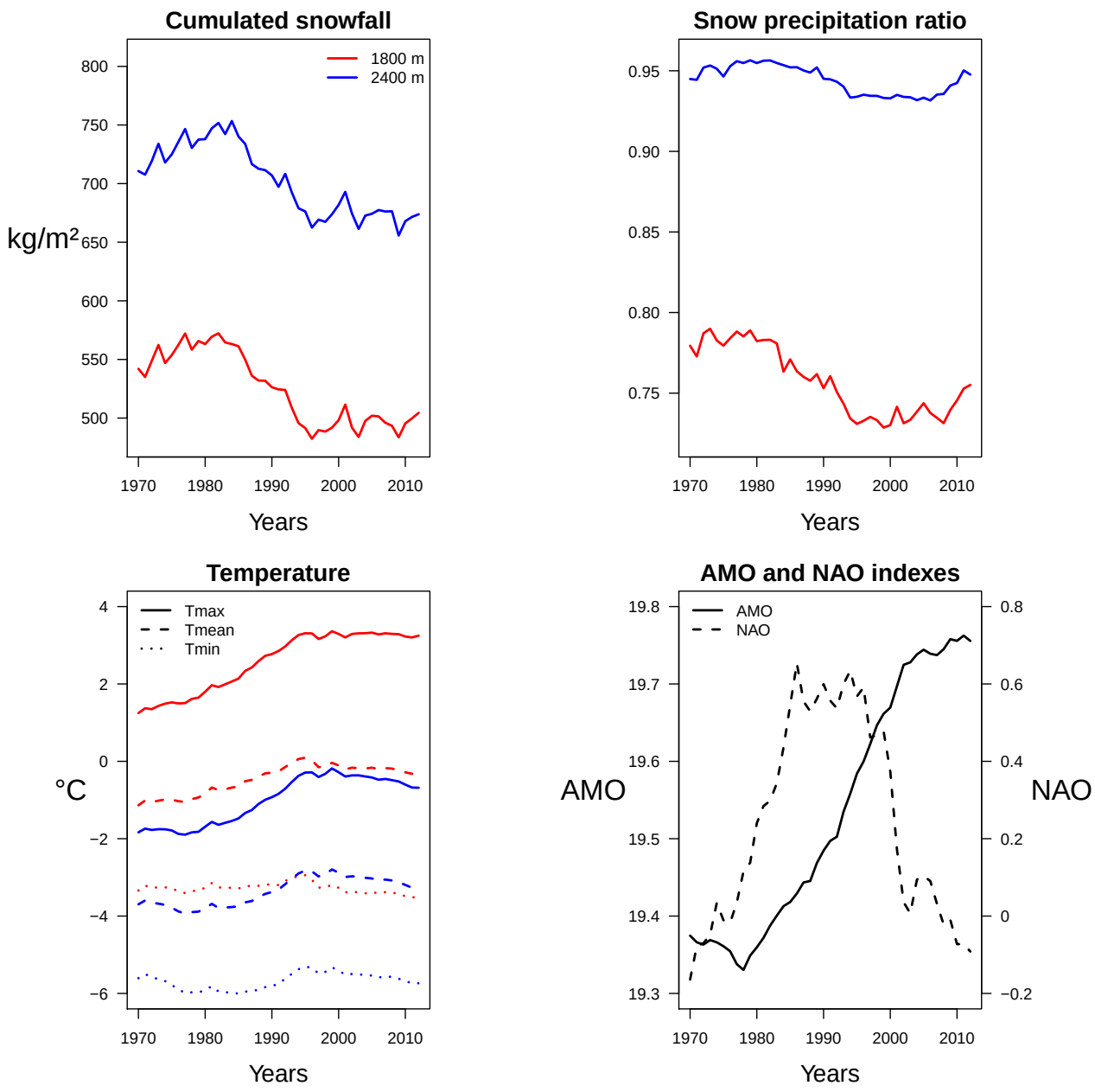


***Figure 4.2:*** *Covariates (Section 4.2.2). The 17-year moving averages of the considered covariates: winter cumulated snowfall, snow precipitation ratio and temperature (daily maximum, mean and minimum) in the French Alps, AMO and NAO. The altitude at which the covariate (except AMO and NAO) is considered is indicated by red (1800 m) or blue (2400 m) lines.*

# 4.3 Method

## 4.3.1 Brown-Resnick Max-Stable Process

### 4.3.1.1 Definition of a Max-Stable Process

Let $\chi$ be the French Alps and $X_i(x)$ the daily snow depths in $x \in \chi$ during the day $i$ of winter ($1 \leq i \leq n_0$ with $n_0$ the number of days in winter). Leadbetter (1983) allows us to consider maxima of daily snow depths despite their temporal dependence, and spatial extreme value theory (Davison et al., 2012; Cooley et al., 2012) insures that the process of winter maximum snow depths

$$\{Z(x)\}_{x\in\chi} = \left\{ \max_{1\leq i\leq n_0} X_i(x) \right\}_{x\in\chi} \tag{4.2}$$

should be modeled as a max-stable process (de Haan, 1984). Every univariate margins $Z(x)$ of a max-stable process $Z$ are GEV($\mu(x)$,$\sigma(x)$,$\xi(x)$) distributed, i.e., with cumulative distribution function

$$F(z;\mu(x),\sigma(x),\xi(x)) = \exp\left\{ -\left[1+\xi(x)\left(\frac{z-\mu(x)}{\sigma(x)}\right)\right]^{-1/\xi(x)} \right\} \tag{4.3}$$

with $\mu(x)$, $\sigma(x)$ and $\xi(x)$ denoting respectively the location, scale and shape parameters at position $x$, and $z$ is such that $1+\xi(x)\left(\frac{z-\mu(x)}{\sigma(x)}\right) > 0$. The function $F$ is equal to 0 in the case of $\xi(x) > 0$ and $z \leq \mu(x) - \frac{\sigma(x)}{\xi(x)}$, and equal to 1 if $\xi(x) < 0$ and $z \geq \mu(x) - \frac{\sigma(x)}{\xi(x)}$. The margins can be transformed into unit Fréchet distribution (i.e., GEV(1,1,1)) through the transformation

$$Z(x) \mapsto \frac{-1}{\log[F\{Z(x);\mu(x),\sigma(x),\xi(x)\}]}. \tag{4.4}$$

### 4.3.1.2 Spectral Representation of de Haan

If all the margins $Z(x)$ of the process $\{Z(x)\}_{x\in\chi}$ are unit Fréchet distributed (i.e. GEV distributed with $\mu(x) = 1$, $\sigma(x) = 1$ and $\xi(x) = 1$), then the process is called simple max-stable process and de Haan (1984) insures that it can be written as

$$Z(x) = \sup_{i\geq 1} \eta_i W_i(x), \qquad x \in \chi \tag{4.5}$$

with $\{\eta_i\}_{i\geq 1}$ the points of a Poisson process on $\mathbb{R}_+$ with intensity $\eta^{-2}d\eta$ and $\{W_i(x)\}_{i\geq 1}$ independent copies of a nonnegative process $\{W(x)\}$ with mean 1. Different choices for $\{W_i(x)\}$ in (4.5) lead to different models of max-stable processes (Davison et al., 2012; Ribatet, 2013). Every multivariate margins are given for any positions $\{x_1, \ldots, x_k\}$ by the formula

$$\mathbb{P}\left(Z(x_1) < z_1, \ldots, Z(x_k) < z_k\right) = \exp\left[-\mathbf{E}\left\{\max_{j=1,\ldots,k} \frac{W(x_j)}{z_j}\right\}\right] \qquad z_j > 0 \quad \forall j. \tag{4.6}$$

#### 4.3.1.3 The Brown-Resnick Process

Kabluchko et al. (2009) generalized a process previously introduced in Brown and Resnick (1977). The Brown-Resnick process arises by taking in (4.5) $W_i(x) = \exp\{Y_i(x) - \gamma(x)\}$, $\{Y_i(x)\}$ independent copies of a Gaussian process with stationary increments and such that $W_i(0) = 0$ almost surely and $\gamma$ its semivariogram. The bivariate distribution of this process for $Z(x_1)$ and $Z(x_2)$ (with $x_1$ and $x_2$ two locations) is

$$\mathbb{P}\left(Z(x_1) < z_1, Z(x_2) < z_2\right) = \exp\left\{-\frac{1}{z_1}\Phi\left(\frac{a}{2} + \frac{1}{a}\log\frac{z_2}{z_1}\right) - \frac{1}{z_2}\Phi\left(\frac{a}{2} + \frac{1}{a}\log\frac{z_1}{z_2}\right)\right\} \tag{4.7}$$

with $\Phi$ the distribution function of the standard normal distribution and $a = \sqrt{2\gamma(h)}$. In this paper, we use a power semivariogram $\gamma(h) = (h/\lambda)^\kappa$ with $\lambda$ and $\kappa$ its scale and shape parameters, respectively.

#### 4.3.1.4 Extremal Coefficient and Brown-Resnick Extremal Function

To assess the extremal dependence between two unit Fréchet random variables $Z_1$ and $Z_2$, one can use the extremal coefficient $\theta$ (Schlather and Tawn, 2003; Naveau et al., 2009) defined by

$$\mathbb{P}\left(Z_1 < z, Z_2 < z\right) = \exp\left\{\frac{-\theta}{z}\right\} = \mathbb{P}\left\{Z_1 < z\right\}^\theta, \qquad z > 0. \tag{4.8}$$

The extremal coefficient ranges between 1 (complete dependence) and 2 (independence). The property

$$\lim_{z\to\infty} \mathbb{P}\left(Z_2 > z | Z_1 > z\right) = 2 - \theta \tag{4.9}$$

holds and means that the probability of observing extreme values of $Z_2$ when $Z_1$ takes extreme values is close to 0 when $\theta$ is near 2 and close to 1 when $\theta$ is near 1.

If $Z_1 = Z(x_1)$ and $Z_2 = Z(x_2)$ with $Z$ a max-stable process defined by (4.5) and $x_1$ and $x_2$ two positions, we have from equations (4.6) and (4.8):

$$\theta(x_1, x_2) = \mathbf{E}\left[\max\left\{W(x_1), W(x_2)\right\}\right]. \tag{4.10}$$

Theorical expressions for $\theta$ in (4.10) are available for all classical max-stable processes (Ribatet, 2013), as functions $\theta(h)$ of the distance $h = |x_2 - x_1|$ between two positions. $\theta(h)$ represents the strength of the dependence as a function of distance, and is therefore termed the extremal function. Specifically, the Brown-Resnick extremal function is given by

$$\theta(h) = 2\Phi\left(\frac{\sqrt{2(h/\lambda)^{\kappa}}}{2}\right). \tag{4.11}$$

#### 4.3.1.5 Range of Extremal Dependence

We define the range of extremal dependence as the distance $h_0$ such as $\theta(h_0) = 1.9$. The range denotes the distance above which snow depth maxima become weakly dependent in extremes, i.e. close to independence in practice. The stronger the extremal dependence at large distances, the larger the range. Inverting (4.8) gives the following expression of the range:

$$h_0(\lambda, \kappa) = \lambda\left[2\left\{\Phi^{-1}\left(\frac{1.9}{2}\right)\right\}^2\right]^{1/\kappa}. \tag{4.12}$$

#### 4.3.1.6 Modeling Anisotropy in the Spatial Dependence Structure

Extremal dependence is generally spatially anisotropic due to the impact of different factors, such as the relief, atmospheric fluxes, etc. Thus, the modeling of extremal dependence between two locations as function of the Euclidean distance only may be too simplistic. In order to account for spatial anisotropy, we use a geometric transformation. The vector of the coordinates $x$ in $\mathbb{R}^3$ is replaced with $x' = Vx$ such as

$$V = \begin{pmatrix} \cos\psi & -\sin\psi & 0 \\ R_1^{-1}\sin\psi & R_1^{-1}\cos\psi & 0 \\ 0 & 0 & R_2 \end{pmatrix} \tag{4.13}$$

with $\psi$ the anisotropy angle, $R_1 > 1$ the anisotropy ratio and $R_2 > 0$ the weight parameter for altitude. The angle $\psi$ is the direction of strongest dependence. The parameter $R_1$ controls the ratio between the direction of strongest dependence and the orthogonal direction in the 2-D plane. The parameter $R_2$ is expected to be widely greater than 1 as a consequence of the strong influence of altitude on snow quantities. The distance computed after this transformation is referred to as the modified 3-D distance.

#### 4.3.1.7 Modeling Trend in the Spatial Dependence Structure

We consider $C'(n) = \{C_k(n)\}_{k\in\{1,\dots,M\}}$ a set of $M$ time-dependent standardized variables ($n$ indicates the winter). To model temporal trends related to changes in climate drivers within the spatial dependence structure, we assume linear models for $\lambda$ and $\kappa$:

$$\begin{cases} \lambda(n) &= \lambda_0 + \Sigma_{m=1}^{M} C'_m(n)\lambda_m \\ \kappa(n) &= \kappa_0 + \Sigma_{m=1}^{M} C'_m(n)\kappa_m. \end{cases} \tag{4.14}$$

### 4.3.2 Inference and Model Selection

#### 4.3.2.1 Inference

Due to computational issues, the full log-likelihood of max-stable processes is usually intractable. To estimate parameters of a Brown-Resnick max-stable process, we can maximize the pairwise composite log-likelihood (Padoan et al., 2010)

$$l(\beta) = \sum_{n=1}^{N} \sum_{i=1}^{K-1} \sum_{j=i+1}^{K} \log f(z_{n,i}, z_{n,j}; C'(n), \beta) \tag{4.15}$$

with $K$ the number of stations, $N$ the number of maxima for each location, $z_{n,i}$ the maxima at location $i$ for winter $n$, $f$ the bivariate distribution of the Brown-Resnick process, and $C'(n) = \{C'_k(n)\}_{k\in\{1,\dots,M\}}$ a set of time-dependent standardized covariates, if any, and $\beta$ the vector of parameters of the bivariate distribution. The vector $\beta$ consists of the $2 \times (M+1)$ parameters for $\lambda(n)$ and $\kappa(n)$, and the 3 parameters $\psi$, $R_1$ and $R_2$ for anisotropy (which are supposed to be time-independent). Thus, a total of $2 \times (M+1) + 3$ parameters have to be estimated (thus 5 in total when no covariates are considered, as in the stationary and moving time window cases of Sections 4.4.2 and 4.4.3).

#### 4.3.2.2 Composite Likelihood Information Criterion

The classical inference criterion to discriminate max-stable models is the CLIC (Composite Likelihood Information Criterion, Padoan et al. (2010))

$$\text{CLIC} = -2\left\{l(\hat{\beta}) - tr(\hat{J}\hat{H}^{-1})\right\} \tag{4.16}$$

with $\hat{\beta}$ the vector which maximizes the composite likelihood $l$ in (4.15), $tr$ denoting the matrix trace, $\hat{H}$ and $\hat{J}$ the Hessian and Jacobian information matrices defined by

$$H = -\sum_{n=1}^{N}\sum_{i=1}^{K-1}\sum_{j=i+1}^{K}\frac{\partial^2 \log f(z_{n,i}, z_{n,j}; C'(n), \hat{\beta})}{\partial\beta\partial\beta^t} \tag{4.17}$$

and

$$J = \sum_{n=1}^{N}\left\{\sum_{i=1}^{K-1}\sum_{j=i+1}^{K}\frac{\partial \log f(z_{n,i}, z_{n,j}; C'(n), \hat{\beta})}{\partial\beta}\right\}\left\{\sum_{i=1}^{K-1}\sum_{j=i+1}^{K}\frac{\partial \log f(z_{n,i}, z_{n,j}; C'(n), \hat{\beta})}{\partial\beta}\right\}'. \tag{4.18}$$

Among a set of competing models, the best one is the one with the lowest CLIC. As in Blanchet and Davison (2011) and in Nicolet et al. (2017a), we rescaled CLIC by dividing by $K-1$.

#### 4.3.2.3 Alternative Model Fitting

A disadvantage in the maximization of the composite log-likelihood $l$ defined in (4.15) is that the winter maxima are taken into account for each winter separately while the covariates are considered through their 17-year moving averages. Thus, annual variability remains in snow depth maxima while it is smoothed in the covariates. To solve this issue, we propose to associate moving window-based and likelihood maximization-based approaches.

Let $w_q$ (from $w_1 = 1962 - 1978$ to $w_N = 2004 - 2020$) the 17-year moving window used in the computation of $C(q)$. We note $l_q$ the composite log-likelihood using the standardized covariates $C'(q)$ computed on $w_q$:

$$l_q(\beta) = \sum_{r\in w_q}\sum_{i=1}^{K-1}\sum_{j=i+1}^{K}\log f(z_{r,i}, z_{r,j}; C'(q), \beta). \tag{4.19}$$

The quantity to maximize is the sum on all $q$ of $l_q(\beta)$:

$$\tilde{l}(\beta) = \sum_{q=1}^{N} l_q(\beta). \tag{4.20}$$

The quantity $\tilde{l}(\beta)$ is referred to as the alternative composite likelihood. The set of parameters to estimate remains identical to that described in Section 4.3.2.1.

## 4.4 Workflow

### 4.4.1 Standardization into Unit Fréchet

In this study, our focus is in the spatial dependence of snow depth maxima and not in the marginal distribution. In other words, we assume that the marginal distributions are known, in which case studying the spatial distribution of maxima is equivalent to studying that of normalized maxima with the same margins. For spatial extremes, it turns out to be convenient to consider normalization to unit Fréchet. So the first step of our analysis is to transform winter maxima at each location into unit Fréchet variables.

A GEV distribution is estimated for each station by likelihood maximization, giving estimates $(\hat{\mu}(x), \hat{\sigma}(x), \hat{\xi}(x))$ of the GEV parameters at each station location $x$. Then, the pointwise estimates are used to transform at each position $x$ the GEV distributed snow depth maxima into a unit Fréchet distributed variable using the transformation (4.4). By doing this, we obtain a data set of unit Fréchet winter maximum snow depths, and from now on, we consider this standardized data set only.

### 4.4.2 Stationary Case

With the later aim of comparing the stationary and nonstationary models, we first fit the Brown-Resnick process to snow depth maxima under the hypothesis of temporal stationarity. Then we compute the extremal function stemming from the fitted process. In parallel, we estimate the pairwise extremal coefficients through the madogram-based estimator (Naveau et al., 2009), and we compute the class averages of these estimation with the aim to check the suitability of the fitted stationary Brown-Resnick process.

In order to be allowed to compare the 3-D modified distances from one model to another, we use the anisotropy parameters $\hat{\psi}$, $\hat{R}_1$ and $\hat{R}_2$ estimated in the stationary case for Sections 4.4.3, 4.4.4 and 4.4.5. Holding these parameters fixed rather than reestimating them in the nonstationary case using each covariate barely affects the results. For instance, the use of nonstationary models by reestimating the anisotropy parameters gives very close values for their estimates ($\hat{\psi}$ contained between 41.9° and 45.8°, $\hat{R}_1$ between 1.67 and 1.87 and, $\hat{R}_2$ between 33.7 and 37.6).

### 4.4.3 Moving Time Window

A preliminary investigation of the temporal evolution of the extremal dependence is done through a data-based approach similar to the one used in Nicolet et al. (2016). In addition to providing results useful to show the consistency of the results obtained by the nonstationary Brown-Resnick processes, this approach allows us to motivate the interest in modeling trends in the parameters of the spatial dependence structure.

We assess the temporal evolution of the extremal dependence by fitting the stationary Brown-Resnick process on a 17-year moving window from 1970-1986 to 2000-2016 (the large number of maxima at the end of the study period allows us to go beyond 2012). We keep the same anisotropy transformation for each estimation window: we apply for all moving window the parameters $\hat{\psi}$, $\hat{R}_1$ and $\hat{R}_2$ estimated in the stationary case using all the data, and we reestimate the parameters $\hat{\lambda}(t)$ and $\hat{\kappa}(t)$ for each estimation window centered on $t$. Then, for each estimation window, we obtain the Brown-Resnick extremal function (4.11) and the range of extremal dependence (4.12).

For each estimation window, we estimate a 95% confidence interval for the range of extremal dependence $h_0(\lambda, \kappa)$ by the delta method (Cox, 1998), propagating the standard error on $\hat{\beta} = (\hat{\lambda}, \hat{\kappa})$ in (4.12). Hence, the 95% confidence interval for $h_0(\beta)$ is given by

$$\left[ h_0(\hat{\beta}) \pm \frac{\Phi^{-1}(0.975)}{\sqrt{n}} \sqrt{\nabla h_0(\hat{\beta})^T \Sigma(\beta) \nabla h_0(\hat{\beta})} \right] \tag{4.21}$$

with $\nabla h_0$ the gradient of $h_0$ with respect to $\beta$, $\Sigma(\beta)$ the variance-covariance matrix of $\beta$ and $n$ the number of pairwise estimates of the extremal coefficient.

### 4.4.4 Nonstationary Case

The Brown-Resnick process is fitted by maximizing the composite likelihood (4.15) using time-dependent covariates $C(n) = \{C_k(n)\}_{k\in\{1,\dots,M\}}$ so as to estimate the functions $\lambda(n) = \lambda_0 + \Sigma_{m=1}^{M} C_m(n)\lambda_m$ and $\kappa(n) = \kappa_0 + \Sigma_{m=1}^{M} C_m(n)\kappa_m$. Again, we held the anisotropy parameters $\hat{\psi}$, $\hat{R}_1$ and $\hat{R}_2$ fixed to the values estimated in the stationary case of Section 4.4.2. Models with one and two covariates are fitted, using the covariates of Table 4.1 but excluding the pairs with a correlation larger than 0.8 in absolute value. The selection is done through CLIC.

### 4.4.5 Alternative Composite Likelihood

Finally, the model selected by CLIC in Section 4.4.4 is fitted by maximizing the alternative composite log-likelihood $\tilde{l}$ defined in (4.20), in order to compare the two approaches and to assess the influence of the annual variability of maxima on the results.

## 4.5 Results

### 4.5.1 Stationary Case

The estimated anisotropy parameters are $\hat{\psi} = 51.52°$, $\hat{R}_1 = 1.79$ and $\hat{R}_2 = 36.66$ and the estimated scale and shape parameters are $\hat{\lambda} = 10.0$ and $\hat{\kappa} = 0.71$, respectively. The extremal function stemming from this estimated process is close to the class averages of the pairwise estimates (Figure 4.3) showing the quality of the estimated Brown-Resnick process. The range of extremal dependence is $\hat{h}_0 = 108$ km.

### 4.5.2 Time Moving Window

Figure 4.4(a) shows the temporal evolution of the extremal function with a 17-year estimation window and holding the anisotropy parameters fixed to the values obtained in Section 4.5.1. We observe a positive temporal trend for the extremal function at large distance, and therefore a negative temporal trend for the extremal dependence. This is confirmed by Figure 4.4(b) which highlights a strong negative temporal trend in the range of extremal dependence. After the first estimates which have to be interpreted carefully due to the low number of observations, we can observe from 1985 to 1992 a division by 2 for the range of extremal dependence (from 200 km to 100 km, which

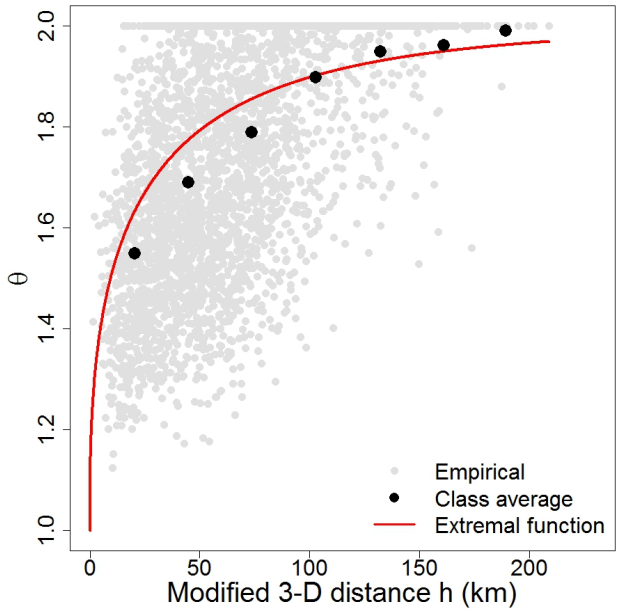


***Figure 4.3:*** *Stationary case (Section 4.5.1). Estimated extremal function under the hypothesis of temporal stationarity (red curve). Grey dots represent the madogram-based pairwise estimations (Naveau et al., 2009) of the extremal coefficient for every pairs of stations and black dots represent the distance class averages.*

corresponds to the range estimated in the stationary case), and after 1992 until the end of the study period a stabilization. Although the first confidence intervals are extremely wide, one can see that this trend is significant because the estimates around the beginning of the decrease (for instance more than 200 km in 1985) are outside the last confidence intervals which extend from about 50 km to 150 km in 1992.

The temporal evolution of the corresponding estimates of $\lambda$ and $\kappa$ with positive trends for both parameters (Figure 4.4 (c–d) confirms the interest in allowing for temporal trends in these parameters.

### 4.5.3 Nonstationary Brown-Resnick Model

According to CLIC, the best model with one covariate uses cumulated snowfall at 1800 m as covariate (Figure 4.5). The second most efficient covariate is snow precipitation ratio at 1800 m and the third one is cumulated snowfall at 2400 m. The four other models outperforming the stationary model use mean temperature and maximum temperature at both considered altitudes. Maximum temperature and cumulated snowfall show better CLIC at 1800 m than at 2400, but the differences are very small.

In order to see if the covariates are positively or negatively correlated to the extremal dependence of extreme snow depths, we assess from the estimated parameters the sign of their contribution on $\theta(100)$, the extremal function measured at the modified 3-D distance 100 km, which is close to the range of extremal dependence estimated in the stationary case. The contribution of a covariate to $\theta(100)$ is referred to as positive (respectively, negative) when $\theta(100)$ increases (respectively, decreases) with respect to an increase in the covariate. Since larger $\theta$ means less dependence at extreme level, a positive contribution to $\theta(100)$ means a negative contribution of the covariate to the extremal dependence at 100 km. This definition is consistent in practice because the function $\theta(100)$ of the covariate is always monotonic in the observed range of this covariate (i.e., between the minimum and the maximum measured values). The covariates showing a positive contribution to $\theta(100)$ are time, NAO, AMO, minimum daily temperature, mean daily temperature and maximum daily temperature (Table 4.2). These covariates have then a negative contribution to the extremal dependence of snow depths. On the contrary, cumulated snowfall and snow precipitation ratio have a positive contribution to the extremal dependence of snow depths.

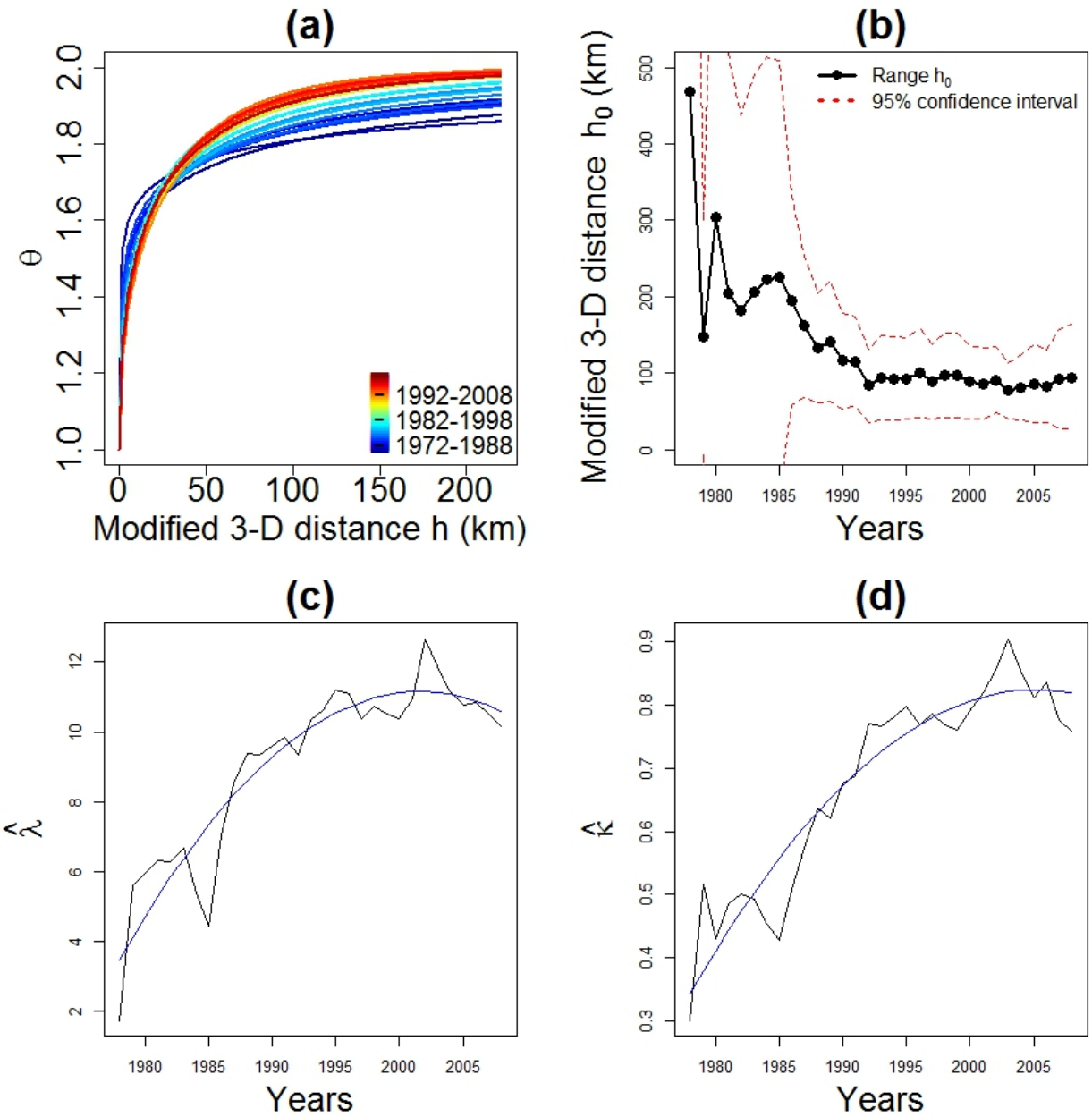


***Figure 4.4:*** *Time moving window (Section 4.5.2). (a) Temporal evolution of the fitted extremal functions, from oldest time windows (blue curves) to the most recent ones (red curves). (b) Temporal evolution of the range of extremal dependence. The range is expressed as a function of the 3-D modified distance. It is plotted (black dots) as a function of the center of the considered estimation window. The associated 95% confidence interval is evaluated by the delta method (Eq. (4.21)). (c–d) Temporal evolution of the estimates of (a) $\lambda$ and (b) $\kappa$. The X axis represents the center of the 17-year time window. The blue curves show for each parameter a second degree polynomial trend fitted by least squares.*

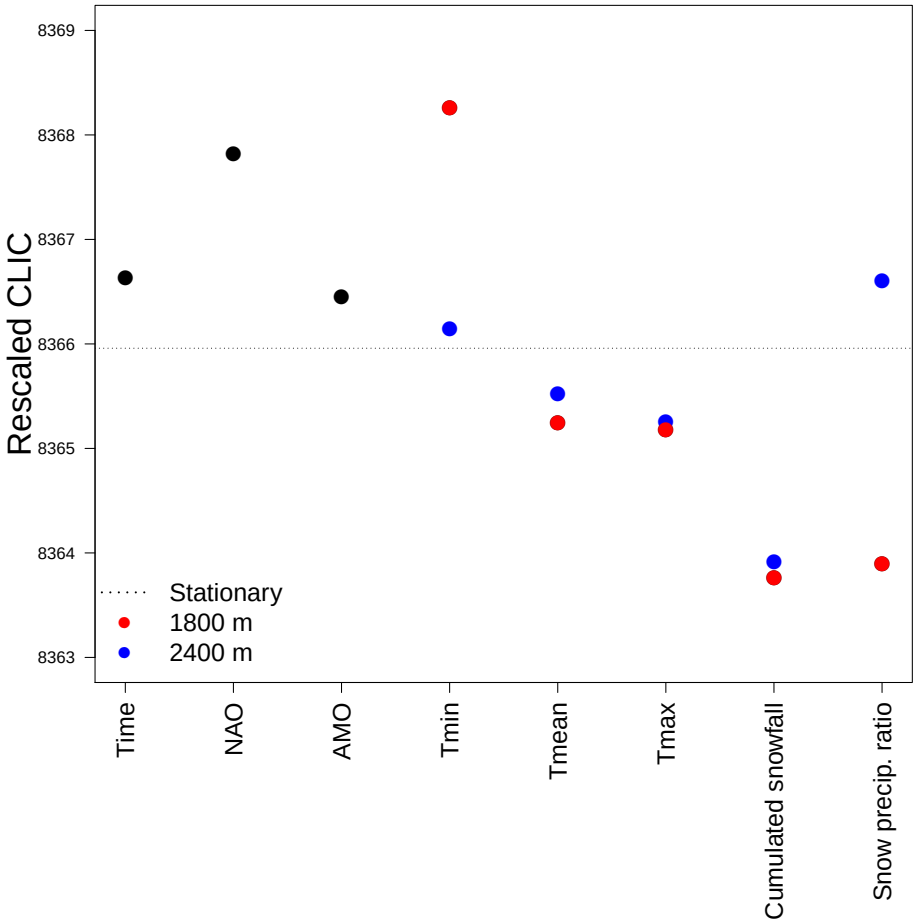


***Figure 4.5:*** *Nonstationary Brown-Resnick model (Section 4.5.3): rescaled CLIC for the models using one covariate. The covariates are time ("Year"), NAO, AMO, minimum temperature, mean temperature, maximum temperature, cumulated snowfall and snow precipitation ratio. The dashed line represents the CLIC for the stationary case. Temperatures, cumulated snowfall and snow precipitation ratio are considered at two elevations: 1800 m (in red) and 2400 m (in blue).*

***Table 4.2:*** *Nonstationary Brown-Resnick model (Section 4.5.3): models with one covariate. Estimated parameters and sign of the contribution to the extremal coefficient $\theta(100)$*[a]

| Covariates | $\hat{\lambda}_0$ | $\hat{\lambda}_1$ | $\hat{\kappa}_0$ | $\hat{\kappa}_1$ | contribution |
|---|---|---|---|---|---|
| Time | 8.6 | 2.8 | 0.63 | 0.19 | positive |
| NAO | 10.0 | -0.3 | 0.69 | 0.03 | positive |
| AMO | 8.6 | 2.8 | 0.63 | 0.19 | positive |
| Tmin (1800) | 9.3 | 1.1 | 0.67 | 0.07 | positive |
| Tmean (1800) | 7.5 | 3.4 | 0.56 | 0.22 | positive |
| Tmax (1800) | 7.7 | 3.7 | 0.57 | 0.23 | positive |
| Cumulated snowfall (1800) | 7.7 | -3.8 | 0.59 | -0.22 | negative |
| Snow precip. ratio (1800) | 8.9 | -1.7 | 0.59 | -0.19 | negative |
| Tmin (2400) | 9.0 | 1.8 | 0.64 | 0.14 | positive |
| Tmean (2400) | 8.5 | 2.3 | 0.60 | 0.17 | positive |
| Tmax (2400) | 8.2 | 2.8 | 0.59 | 0.20 | positive |
| Cumulated snowfall (2400) | 7.4 | -4.3 | 0.58 | -0.24 | negative |
| Snow precip. ratio (2400) | 8.7 | -2.3 | 0.63 | -0.15 | negative |

[a] $\hat{\lambda}_0$, $\hat{\lambda}_1$, $\hat{\kappa}_0$ and $\hat{\kappa}_1$ denote the estimated parameters for each model. The column "contribution" indicates if the extremal coefficient at the distance 100 km (i.e., $\theta(100)$), arbitrarily chosen, increases (positive) or decreases (negative) with respect to an increase in the covariate. Note that a positive contribution to $\theta(100)$ means a decrease in the extremal dependence at the distance 100 km.

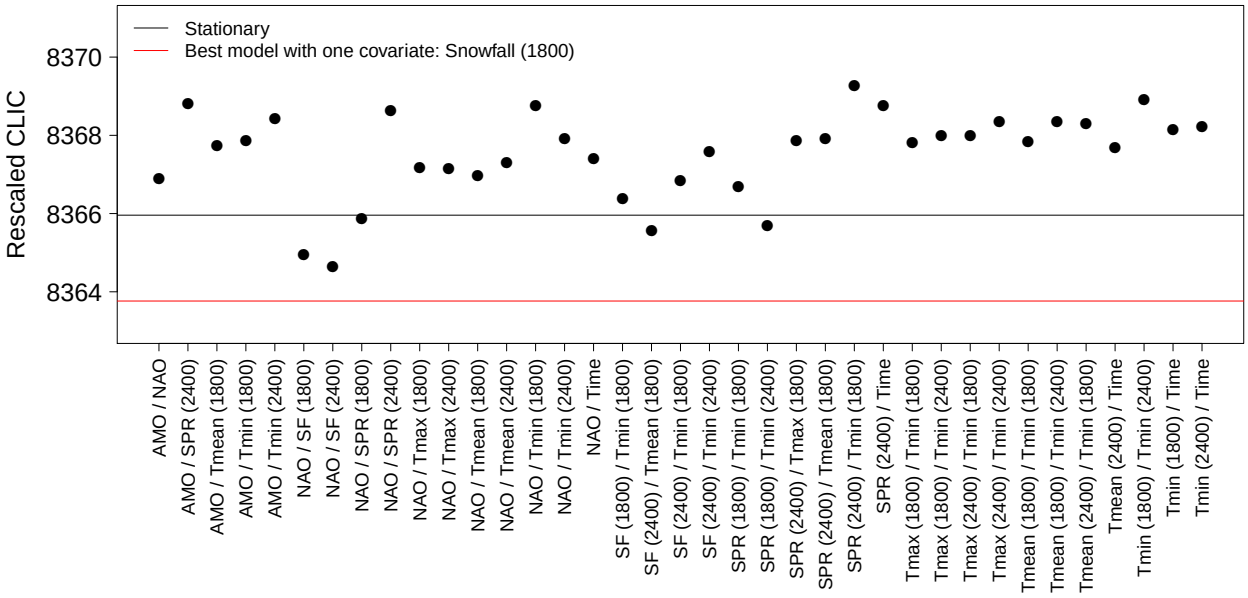


***Figure 4.6:*** *Nonstationary Brown-Resnick model (Section 4.5.3): rescaled CLIC for the models using two covariates. We only consider the pairs of covariates with a correlation lower than 0.8 in absolute value (see Table 4.1). Their are chosen among time (Year), NAO, AMO, and maximum temperature (Tmax), mean temperature (Tmean), minimum temperature (Tmin), cumulated snowfall (SF) and snow precipitation ratio (SPR). Temperatures, cumulated snowfall and snow precipitation ratio are considered at two elevations (1800 m and 2400 m). The dotted line represents the rescaled CLIC of the stationary model while the dashed line represents the rescaled CLIC of the best model with one covariate (i.e., with snowfall at 1800 m).*

None of the models using two covariates show a better rescaled CLIC that the best model with one covariate (Figure 4.6). Only 5 models outperform the stationary model: those using NAO with cumulated snowfall at either 1800 m or 2400 m, cumulated snowfall at 2400 m with mean temperature at 1800 m, snow precipitation ratio at 1800 m with minimum temperature at 2400 m, and NAO with snow precipitation ratio at 1800 m. The model using cumulated snowfall at 1800 m as unique covariate is thus the best one according to CLIC.

With this model, consistently with Section 4.5.2, the extremal coefficient $\theta(h)$ increases with time at large distances, which implies a negative trend in the extremal dependence (Figure 4.7(a)). As in Section 4.5.2, the estimated range of extremal dependence shows a strong decrease during the 1980s and then a stability after 1992 (Figure 4.7(b)). The estimates of the range of extremal dependence is much larger during the first part of

the study period (sometimes larger than 800 km). However, these estimates must be considered with caution due to the lack of observations before 1983. The evolution of the extremal function with respect to the cumulated snowfall (Figure 4.7(c)) confirms that the extremal dependence tends to increase when snowfall increases (i.e., $\theta(100)$ decreases).

### 4.5.4 Alternative Composite Likelihood

The extremal function and the range of extremal dependence stemming from the model fitted by maximizing the alternative composite likelihood $\tilde{l}$ defined in (4.20) and the same covariate show similar temporal evolutions to the case of the classical composite likelihood, even though they are much smoother (Figures 4.8(a,b)). The range of extremal dependence spans a much narrower interval with values not bigger than 260 km (3-D modified distance). The evolution of the extremal function as function of cumulated snowfall shows as before an increase in extremal dependence (i.e., decrease in $\theta(100)$) when snowfall increases but with much less variability over the same range of snowfall events (Figure 4.8(c)).

## 4.6 Discussion

### 4.6.1 Anisotropy in the Spatial Dependence and Comparison with Extreme Snowfall

The results obtained under the stationary hypothesis in Section 4.5.1 can be compared to those provided by the stationary Brown-Resnick model with power semivariogram fitted in Nicolet et al. (2017a). This allows us to compare the extremal dependence of extreme snow depths and extreme snowfall in the French Alps. To the best of our knowledge, this is the first time that the spatial dependence in extremes of these two snow-related variables can be compared over the same region.

For both variables, the estimated anisotropy angle ($\hat{\psi} = 51.52^\circ$ for snow depths and $\hat{\psi} = 37.28^\circ$ for snowfall) corresponds to the orientation of the main massifs and valleys in the French Alps. This pattern has also been observed for extreme snow depths in Switzerland (Blanchet and Davison, 2011) and for extreme precipitation in the Appalachians (Padoan et al., 2010), which confirms its robustness. It may be interpreted as the effect of orography on atmospheric fluxes generating extreme precipitations. One can though note that anisotropy is less marked for extreme snow depths than for extreme

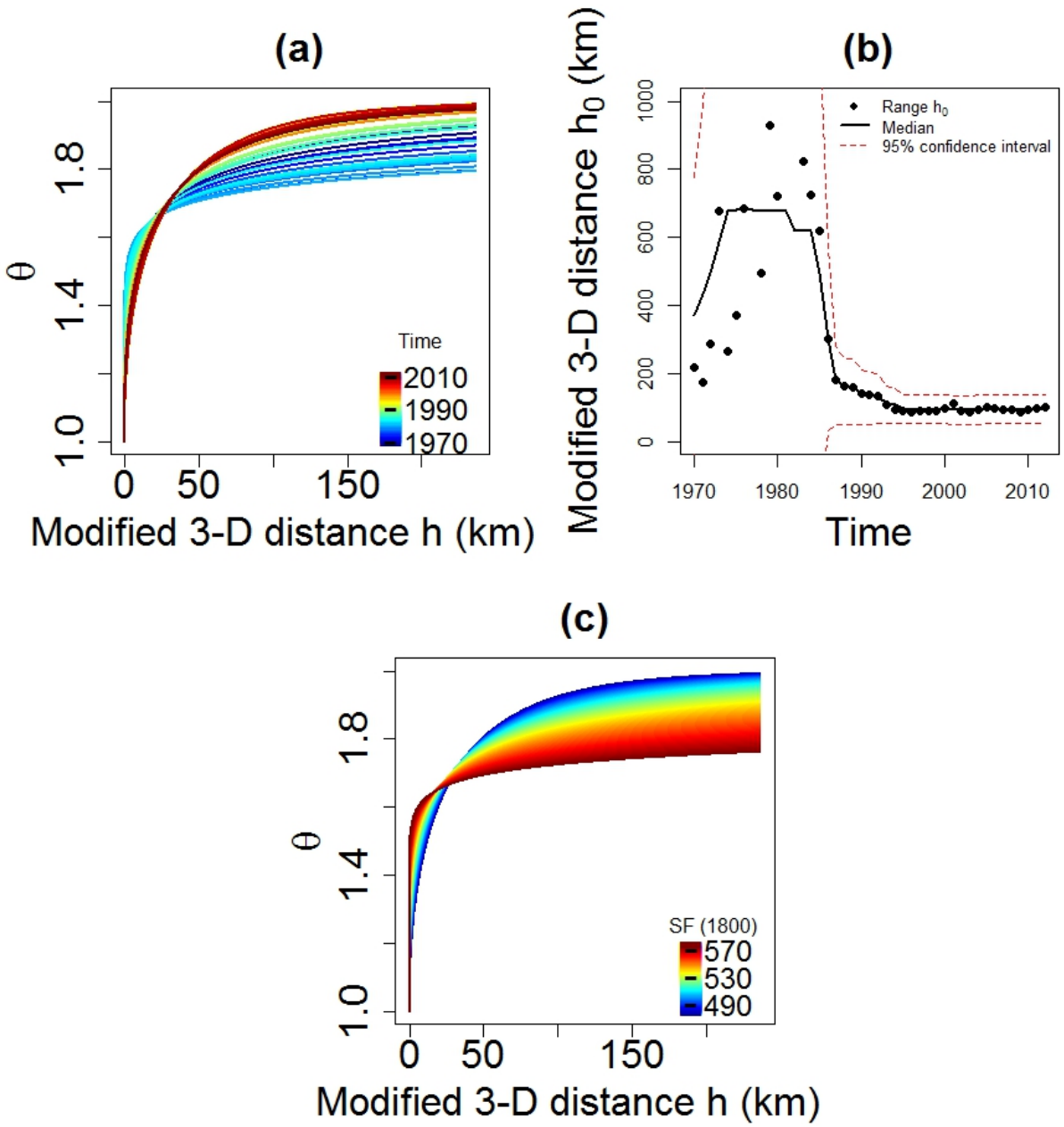


***Figure 4.7:*** *Nonstationary Brown-Resnick model (Section 4.5.3). Model selected by CLIC with cumulated snowfall at 1800 m as covariate. (a) Temporal evolution of the extremal function stemming from the model. (b) Temporal evolution of range of extremal dependence. The solid line represent the median range of extremal dependence computed on a 17-year moving window. The associated 95% confidence interval is evaluated by the delta method. (c) Evolution of the extremal function as function of cumulated snowfall at 1800 (from 480 to 580 kg/m$^2$).*

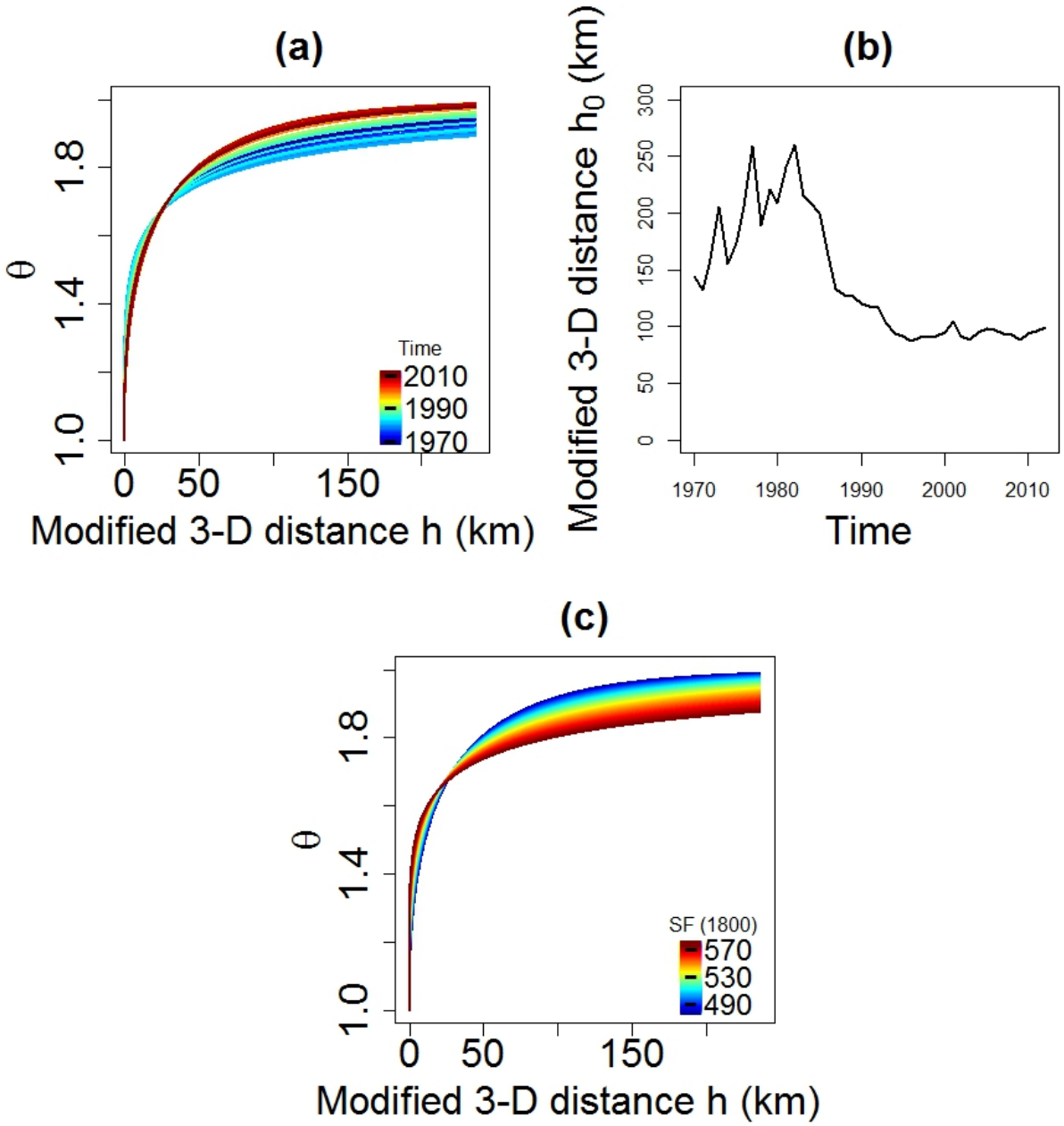


***Figure 4.8:*** *Alternative composite likelihood (Section 4.5.4). Model with cumulated snowfall at 1800 m as covariate but maximizing the alternative composite likelihood $\tilde{l}$. (a) Temporal evolution of the extremal function stemming from the model. (b) Temporal evolution of the range of extremal dependence. (c) Evolution of the extremal function as function of cumulated snowfall at 1800 m (from 480 to 580 kg/m$^2$).*

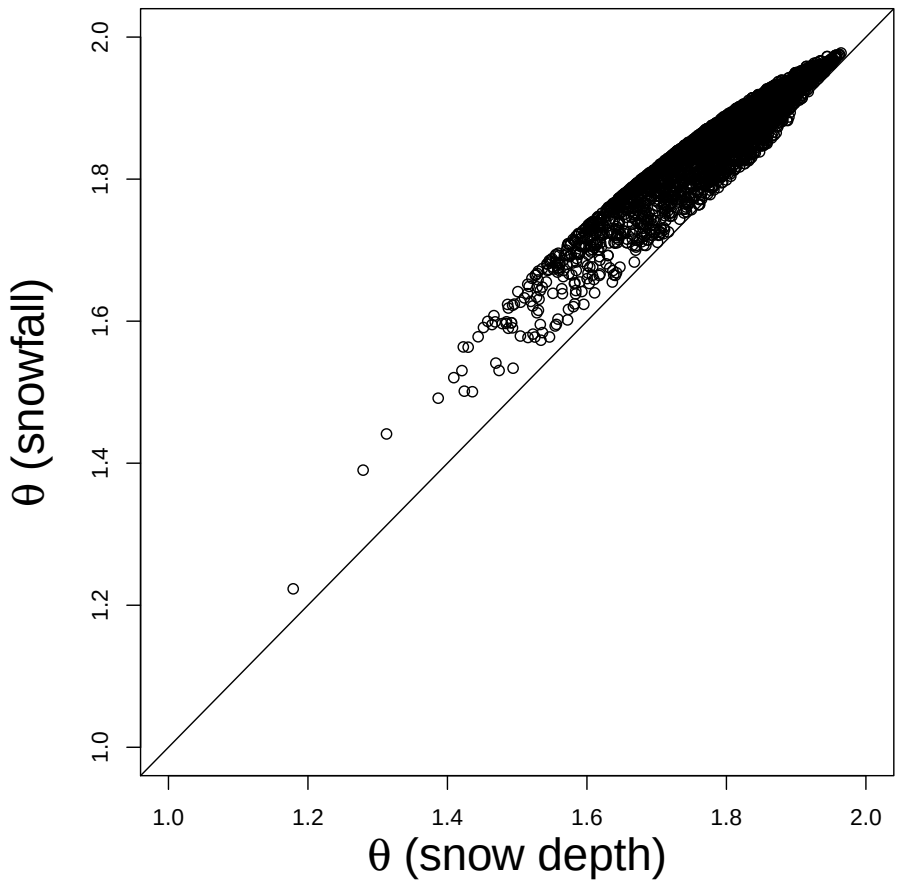


***Figure 4.9:*** *Comparison between snow depth and snowfall model-based estimates of extremal coefficient for all the pairs of stations.*

snowfall (with $\hat{R}_1 = 1.79$ against 3.22 for extreme snowfall) and the effect of altitude is also slightly weaker ($\hat{R}_2 = 36.66$ against 39.95), which may arise from the fact that the effect of interaction between atmospheric flows and orography on snow on the ground is less direct than for precipitation amounts such as snowfall.

The comparison between snow depth and snowfall extremal coefficient for all the pairs of stations highlights that snow depth maxima are more spatially dependent than snowfall maxima for a large majority of pairs of stations (Figure 4.9). As interpreted in Gaume et al. (2013b), this is probably due to cumulative effects involved in the formation of snow cover which make smoother the spatial evolution of extreme snow depths.

### 4.6.2 Temporal Changes

The decreasing trend in the extremal dependence of snow depths in the French Alps is similar to that found in Nicolet et al. (2016) for snowfall in the same area. These two variables show also a strong decrease in the range of extremal dependence concentrated during the 1980s, and then a stability after 1990. This is the first time that such an effect is inferred on extreme snow depths. The consistency with extreme snowfall over the same area pleads for its robustness and its geophysical meaning. This decrease is concomitant with the period of strongest decrease in snowfall and snow precipitation ratio, and with the period of strongest increase in temperature and AMO (Figure 4.2).

One may wonder about a possible influence of the stationarity hypothesis in the marginal distributions on the nonstationarity observed in the spatial dependence structure, with a potential transfer of a temporal trend in the margins to the dependence structure. We checked this by reproducing the procedure of Section 4.4.3 but using the margins estimated on each window (considering for each window only the stations with a least 8 maxima in order to avoid misestimation of GEV parameters). We found very similar results (not shown). Hence, the decreasing trend in the spatial dependence of snow depth maxima is not artificially created by the stationary hypothesis in the margins.

### 4.6.3 Climate Control

The most relevant covariates to model trends in the spatial dependence structure of extreme snow depths are those related to precipitation and temperature: mean temperature, maximum temperature, cumulated snowfall and snow precipitation ratio at 1800 m. However, the use of minimum temperature or snow precipitation ratio at 2400 m leads to models less suitable than the stationary model. The inefficiency of snow precipitation ratio at 2400 m can be explained by the fact that at this altitude level, the snow precipitation ratio is always close to 1 during the entire study period (Figure 4.2) making its explicative power very small.

The covariates time, NAO, AMO and temperature (minimum, mean and maximum) have a negative contribution to the extremal dependence of snow depths in the French Alps while cumulated snowfall and snow precipitation ratio have a positive contribution. All of these signs of contribution are consistent to the correlations computed in Nicolet et al. (2016) concerning extreme snowfall in the French Alps.

Hence, for extreme snowfall (Nicolet et al., 2016), the decreasing temporal trend in the spatial dependence of extreme snow depths seems to be due at first to a decrease of the snow precipitation ratio caused by the increase of temperature over the study period, and particularly in the context of the 1980s climate regime shift (Reid et al., 2015). Specifically, temperature increase makes snowfall more isolated in space. Indeed, when temperature is moderately cold, only the highest stations experience snow while rain falls at low elevations (Nicolet et al., 2016). This leads to less spatially smooth snow depth variations and less coherent patterns for snow depth maxima.

As in the case of snowfall maxima, we cannot exclude a magnitude effect with stronger dependence in extreme snow depths during snowier winters. Indeed, even if snow precipitation ratio at 2400 m is one of the less efficient covariate (due to a very low effect of snow/rain partitioning at this elevation), cumulated snowfall at 2400 m is the second most relevant covariate. Consequently, the decrease in cumulated snowfall observable during the winter season since the 1980s (Figure 4.2) seems an additional cause for the decrease in the spatial dependence of extreme snow depths.

### 4.6.4 Pros and Cons of the Proposed Modeling Approach

Theoretical and applied studies dealing with temporal aspects within the spatial dependence structure of max-stable processes (Davis et al., 2013a,b; Raillard et al., 2014; Huser and Davison, 2014; Embrechts et al., 2016) do it by modeling the short-range temporal dependence of extremes and do not consider a possible long-range temporal evolution of the dependence structure. This paper lays a first stone regarding the modeling of temporal trends at climate time scale in the spatial dependence of extremes, which is an important issue for managing the risks related to spatial extremes and anticipating their evolution under climate change. Even if the approach introduced in this paper is quite simple, with linear trends in the spatial dependence structure of Brown-Resnick process, it obtains results consistent to those which have been obtained by empirical estimation with snowfall maxima in Nicolet et al. (2016). In addition, the robustness of our results is granted by the step-by-step approach we propose: from empirical estimations on moving time windows to a full model taking into account long range patterns in data and covariates coupled with a rigorous model selection procedure.

Hence, the main difference of the model-based approach introduced in this paper with the empirical approach developed in Nicolet et al. (2016) is the explicit incorporation of suitable covariates into the modeling. This is a flexible way to detect time trends because it does not require hypothesis on the nature of the trend (e.g., linear or polynomial of

order 2 (or more)). Furthermore, the use of covariates in the model-based approach has the major advantage of potentially allowing anticipating the evolution of the extremal dependence of snow extremes. Indeed the best fitted model could be easily coupled with the various future climate change scenarios now increasingly available (e.g., Jacob et al. (2014)).

A limitation of the used model is the difficulty to efficiently combine more than one covariate. Indeed, none of the considered models with two covariates shows a better CLIC than the best model with one covariate possibly because the penalization in the CLIC is too strong (one additional covariate means two additional parameters, which is strongly penalized in CLIC). However, we did not considered in this paper the models involving two of the most relevant covariates (cumulated snowfall, mean temperature, maximum temperature, and snow precipitation ratio at 1800 m) together because these covariates are strongly correlated. The best models of this kind show a compensation effect between the two covariates, showing the complication to use them.

Several continuations of this work could be considered. A first one would be to use other selection criteria than the CLIC, for instance the CLBIC (Gao and Song, 2010) or the large set of criteria introduced in Nicolet et al. (2017a). Furthermore, it could be interesting to try nonlinear time trends in the spatial dependence structure with the aim to see if the predictive ability of the model may be improved in this way.

## 4.7 Conclusion and Outlooks

In this paper we introduce a way to account for the temporal nonstationarity in Brown-Resnick max-stable processes, which we apply to study the evolution of the spatial dependence in extreme snow depths in the French Alps since 1970. Several climate covariates are considered to model trends in the spatial structure of dependence and the best model is selected by CLIC. We find a strong negative temporal trend in the spatial dependence of extreme snow depths with a strong decrease in the range of extremal dependence during the 1980s. To account and explain these strong temporal patterns, the most relevant covariates are cumulated snowfall, snow precipitation ratio (considered at elevation impacted enough by snow/rain partitioning) and temperature (maximum and average). Hence, this observed decrease in extremal dependence seems mainly due to the effect of the increase in temperature on the snow precipitation ratio at

low elevation and to a decrease in the winter cumulated snowfall. These results resemble those obtained for extreme snowfall in the same region in previous studies, showing that the spatial dependence of these two snow variables are similarly impacted by climate change.

The space-time approach introduced in this article, which permits to model the spatial dependence of extremes as function of appropriate time-dependent covariates, may be very useful for quantifying spatial extremes and managing the related risk and its evolution under ongoing climate change. It may provide precious insights on their climatic control and open the door to potential prognoses under climate change scenarios. This approach is here applied to extreme snow depths but it may be fruitful for many other geophysical variables.

## Acknowledgments

This work has been supported by a grant from LabEx OSUG@2020 (Investissements d'avenir - ANR10 LABX56). We thank the hundreds of snow observers and the Météo-France staff involved in the collection and constitution of the data sets used in this study.

# Conclusions and perspectives

This thesis followed two main orientations concerning the modeling of the spatial dependence structure of spatial extremes in the field of mountain climate. The first achievement was to introduce a procedure of model selection able to assess the ability of max-stable processes to predict the spatial dependence structure. The second one concerned the investigation and the modeling of temporal nonstationarity in the spatial dependence structure of climate extremes in a context of climate change. These two questions were broached through the examples of extreme snowfall and extreme snow depths in the French Alps.

Two very suitable data sets from Météo France were processed to investigate these two guidelines: a 3-day cumulated snowfall data set (90 stations from 1958 to 2012) and a daily snow depth data set (82 stations from 1970 to 2012). Winter maxima were extracted from these two data sets, and then transformed pointwise into unit Fréchet in order to focus on spatial dependence structure only.

Chapter 1 presented the mathematical tools used in this work. Chapter 2 introduced a leave-two-out cross-validation procedure able to evaluate the predictive ability of max-stable processes to model the dependence structure of spatial extremes. This procedure was applied to compare the Smith, Schlather, Brown-Resnick, geometric Gaussian and extremal-t max-stable processes using the snowfall data set as a case study. Chapter 3 presented a data-based approach to investigate potential temporal changes in the spatial dependence structure of geophysical extremes. This method was used to investigate the temporal evolution of the spatial dependence of extreme snowfall in the French Alps. Chapter 4 introduced a way to account for nonstationarity in the spatial dependence structure of max-stable processes. This approach was adopted to study the temporal evolution of the spatial dependence of extreme snow depths in the French Alps.

# Procedure of model selection for max-stable processes

## A leave-two-out cross-validation and a panel of criteria for evaluating max-stable processes

Chapter 2 introduced a leave-two-out cross-validation procedure for max-stable processes able to evaluate their predictive ability to model the spatial dependence of extremes. For each pair of stations, the bivariate distribution was derived from the model fitted on the remaining stations.

In order to assess the reliability of the models and discriminate them, a large panel of criteria was introduced. Root mean square error (RMSE), mean average error (MAE), root mean square normalized error (RMSNE), mean average normalized error (MANE) and coefficient of determination ($R^2$) were used to measure the deviation between empirical and max-stable-based estimations of the probability of jointly exceeding a given quantile at two locations. $N_T$ and *FF* criteria, usually used for goodness-of-fit of univariate distributions, were tailored for dealing with bivariate distributions by apply them to the minimum at two locations. The $N_T$ criterion is based on the number of exceedances of high quantiles whose distribution should be close to a binomial distribution with a suitable fitting. The *FF* criterion focus on the value taken by the estimated distribution in overall maxima.

Even if we applied this procedure to snowfall maxima, it may be useful in the modeling of other spatial extremes (extreme precipitation, extreme temperature, extreme snow depths, extreme wave heights...). This cross-validation procedure could be used in the case of a selection by Composite Likelihood Information Criterion (CLIC) does not clearly determine the best model. Especially, it may demonstrate that a max-stable model, having some advantages (fewer parameters to estimate, extremal independence for large distances, etc.) over the model with the best CLIC, can be used instead of this model in practice.

## Application of the leave-two-out cross-validation to compare between five max-stable processes on a case study of snowfall maxima in the French Alps

The leave-two-out cross-validation procedure was used to compare five of the most commonly used max-stable processes: Smith, Schlather, Brown-Resnick, geometric Gaussian and extremal-t processes. We considered a large set of correlation functions for the Schlather, geometric Gaussian and extremal-t processes. The 3-day snowfall winter maxima data set was used as a case study.

This cross-validation approach allowed to reconsider the geometric Gaussian and Brown-Resnick processes for which CLIC comparison only would lead to disregard them for the benefit of the extremal-t process. The low values of RMSE, MAE, RMSNE and MANE proved the predictive quality of the these three models in practice. The extremal-t, geometric Gaussian and Brown-Resnick processes were able to represent suitably well

the structure of dependence of the snowfall maxima. This showed that cross-validation may be more relevant than the single use of CLIC for evaluating and selecting max-stable processes. The Smith and Schlather processes, due to their lack of flexibility, were clearly outperformed by the other max-stable processes in competition.

The proposed reliability criteria were also used to investigate the sensitivity of the max-stable processes to the number of stations and to the number of years of observations. Even if the Brown-Resnick process was slightly less sensitive due to less parameters, the performance of the Brown-Resnick, geometric Gaussian and extremal-t processes remained very similar regardless of the number of stations or years.

At this time, the fact that the extremal-t, geometric Gaussian and Brown-Resnick processes are as suitable as each other in practice was also exhibited in our case concerning snowfall maxima in the French Alps. To be generalized, these results have to be confirmed by replicating the study in other contexts (other areas, other variables of interest). Thus, they may be valid for a wide range of environmental applications. Other max-stable processes from the literature (Smith and Stephenson, 2009; Reich and Shaby, 2012; Wadsworth and Tawn, 2012; Davison and Gholamrezaee, 2012; Xu and Genton, 2016; Beranger et al., 2016) may also be taken into consideration in order to see if some of them may outperforming extremal-t, geometric Gaussian and Brown-Resnick processes or at least having similar results .

# Temporal evolution of the spatial dependence of extreme snowfall and extreme snow depths

## A data-based approach to investigate the temporal evolution of the spatial dependence of geophysical extremes

Chapter 3 introduced a data-based approach suitable for highlighting potential temporal changes in the spatial dependence structure of geophysical extremes at decadal time scale. This approach was conducted on the 3-day snowfall data set.

We proposed to assess the temporal evolution of the spatial dependence of extremes by estimating it over 20-year moving estimation windows taking into account possible anisotropy potentially related to orographic effects and/or patterns in atmospheric flows. For each window, extremal dependence was estimated by fitting the Brown-Resnick extremal function to pairwise estimations of extremal coefficient. A range representing the distance above which extremes are almost independent was computed for each window.

This data-based approach allowed us to make minimal modeling assumptions to conduct the study: the temporal stationarity in the marginal distributions, the way to assess the distance between stations, and the choice of the extremal function model. These few modeling assumptions were checked in order to ensure the geophysical origin of the measured temporal changes rather than a consequence of modeling choices.

This data-oriented framework could therefore be useful for a variety of other studies addressing geophysical extremes in the context of climate change. For instance it could be applied to investigate the temporal evolution of the spatial dependence of extreme temperature, extreme precipitation or extreme wave heights.

## Modeling temporal trends in the spatial dependence structure of max-stable processes

Chapter 4 proposed a way to account for temporal nonstationarity in the dependence structure of spatial extremes. This is the first ever modeling of this kind. We used a Brown-Resnick process with temporal trends in the spatial dependence structure able to model the temporal evolution of the spatial dependence of the extremes of the variable of interest. These trends were modeled using time-dependent covariates, allowing to reveal the variables which impact the spatial dependence by comparing the CLIC values of several models.

This approach may be very useful concerning extremes whose spatial dependence structure is not temporally stationary, especially those for which the nonstationarity was highlighted by an data-based investigation similar to the one presented in Chapter 3. Indeed, by modeling the spatial dependence of extremes as function of suitable covariates this approach offers a framework to manage and to anticipate the evolution of related risk under climate change.

## Decreasing spatial dependence in extreme snowfall and extreme snow depths in the French Alps under climate change

The temporal evolution of the spatial dependence of extreme snowfall and extreme snow depths in the French Alps were investigated using two different approaches.

The data-based approach introduced in Chapter 3 was applied to the snowfall maxima data set. Several local and synoptic climatic variables, associated with the current climate change context, were considered. Correlations between these variables and the range of extremal dependence were computed in order to assess their relationship with the temporal evolution of spatial dependence of extreme snowfall in the French Alps.

The model-based method proposed in Chapter 4 was used to study the temporal evolution of the spatial dependence in extreme snow depths in the French Alps. The Brown-Resnick process with nonstationary spatial dependence structure was thus fitted to the snow depth maxima data set. The used covariates were chosen among several climatic variables and the models were selected by CLIC. This permitted to investigate the variables which impact the spatial dependence of extreme snow depths.

By these two different approaches, we found for these two snow variables a strong negative temporal trend in the spatial dependence. These two trends were very similar with a strong decrease in the range of extremal dependence since 1980 and then a stability after 1990. This consistence showed the robustness of these results.

The most relevant covariates to model the spatial dependence of extreme snow depths were snowfall, snow precipitation ratio (considered at elevation impacted enough by snow/rain partitioning) and temperature (daily maxima and averages). The periods of strongest decrease in the range of extremal dependence was concomitant with the periods of strongest decreases in winter cumulated snowfall and in snow/rain ratio, and with the period of strongest increase in temperature. We highlighted that the decreases in spatial dependence concerning these two snow variables were attributable at first to the increase in temperature and its major control on the snow/rain partitioning. A magnitude effect, with less dependent extremes due to a decrease in winter cumulated snowfall was also found.

In addition, these studies gave an opportunity to compare the spatial dependence of these two snow variables in the same region. We confirmed that the spatial dependence of these two snow variables are similarly impacted by orography (due to its influence on atmospheric fluxes generating extreme precipitations) with the direction of strongest dependence between two locations corresponding to the orientation of the main moun-

tains and valleys in the French Alps. However, anisotropy is less marked for extreme snow depths, showing that this effect is less direct for snow on the ground than for snow precipitation. We also found that the spatial dependence of extreme snow depths is stronger, due to cumulative effects involved in the formation of snow cover.

# Perspectives

## Cross-validation procedure with other data sets and/or other models of max-stable processes

It would be interesting to apply the leave-two-out cross-validation procedure in other conditions.

First, this approach may be replicated using other data sets concerning variables which can be modeled by max-stable processes. It could concern other climate variables such as precipitation or temperature, other fields such as hydrology, or even extreme snowfall in another study area than the French Alps. Indeed, the suitability of models of max-stable process depends on the variables of interest. For instance, the Smith process is better than the Schlather process to model extreme snowfall in the French Alps (Gaume et al., 2013b; Nicolet et al., 2017a) whereas it is the opposite when modeling extreme snow depths in Switzerland (Blanchet and Davison, 2011). This is due to the differences between the spatial evolution of these two variables. It would be interesting to check if the Brown-Resnick, geometric Gaussian and extremal-t processes, which have been found as suitable as each other in our case, still provide very close results for other data sets.

This motivates also to consider other models of max-stable process than the five ones in competition in this work (Smith, Schlather, Brown-Resnick, geometric Gaussian and extremal-t). One may wonder if some models, among those at our disposal in the literature (Smith and Stephenson, 2009; Reich and Shaby, 2012; Wadsworth and Tawn, 2012; Davison and Gholamrezaee, 2012; Xu and Genton, 2016; Beranger et al., 2016), are able to outperform the geometric Gaussian, Brown-Resnick and extremal-t processes, or at least to perform as well for our data. Especially, it would be interesting to try the Tukey (Xu and Genton, 2016) and extremal-skew-t (Beranger et al., 2016) processes, which are more flexible than the geometric Gaussian and the extremal-t processes respectively, and the version of extremal-t process with spatially nonstationary dependence structure introduced in Huser and Genton (2016).

The issue of model selection is to become certainly even more difficult due to probable new models of max-stable processes in the future. In order to better discriminate max-stable models when a framework based on goodness-of-fit on bivariate quantities seems to be insufficient, procedures based on the estimation of high-order quantities (e.g., trivariate) may be proposed to discriminate them. However, such procedures would be computationally challenging.

### Use of threshold-based models

In this thesis, we have made the choice to work with winter maxima of snowfall and snow depths. However, it is also possible to deal with threshold exceedances which are classic in the univariate case but less in the spatial case. However, two threshold-based models can be adopted. The first possibility is to use max-stable processes with censored likelihood approach (Thibaud et al., 2013; Huser and Davison, 2014; Raillard et al., 2014). The second one is to use Pareto processes which extend the generalized Pareto distribution (GPD) to the spatial case (Ferreira et al., 2014; Thibaud and Opitz, 2015). These two approaches could be used in our case to enlarge the data sets (i.e., more than one observation per year) and check the robustness of our results. Also, our cross-validation approach could be tailored to this framework. However, the investigation of the temporal evolution of the spatial dependence of extremes at climatic scale would be more tricky because of additional temporal aspects, at shorter time-scale, to consider (for instance temporal dependence).

### Temporal evolution of the extremal dependence of other spatial phenomena

This thesis was a first step in the assessment of temporal changes in extremal dependence of spatial phenomena. To the best of our knowledge, this issue received very little attention, despite its importance in practice. Indeed, due to the current context of climate change, many geophysical extremes are potentially concerned. Thus, it would be very interesting to investigate the temporal evolution of the spatial dependence of other geophysical variables than extreme snowfall and extreme snow depths. For instance, similar approaches to those that we have applied to these two snow-related variables could be applied to extreme temperature or extreme wave height data.

We highlighted two causes in the decreases in spatial dependence of extreme snowfall in the French Alps. The first one was the effect of the increase in temperature on the snow/rain partitioning. The second one was a magnitude effect, with less dependent extremes due to a decrease in winter cumulated snowfall. The investigation of the temporal evolution of the spatial dependence of extreme precipitation in the French Alps could allow to better understand the contribution of each one of these causes. Indeed, it would permit to go further into this question by considering the effects from precipitation only without those concerning snow rain partitioning.

### Marginal distributions and non stationary spatial dependence structure

Temporal nonstationarity is a crucial issue in extreme value analysis because of many extremes potentially impacted by climate change (Cooley, 2009; Katz, 2010). All the risk estimations related to geophysical extremes made under the hypothesis of temporal stationarity are exposed to underestimation. Also, modeling temporal nonstationarity in geophysical extremes is important for better understanding and anticipation of the consequences of climate change. After several studies which have modeled temporal trends in the univariate distribution of extremes, this thesis laid another stone for this issue by modeling temporal nonstationarity within their spatial dependence. However, the estimation of both marginal distributions and spatial dependence structure may be needed for the assessment of risks related to spatial extremes. For instance, they are required to built conditional return level maps (Padoan et al., 2010) and to assess return levels of spatial quantities like minimum, maximum or integral over a specific area (Huser and Genton, 2016). Huser and Genton (2016) showed that modeling spatial nonstationary in the dependence structure may improve the estimation of return levels of spatial quantities when the data are strongly spatially nonstationary. Thus, we may wonder if modeling temporal trends in the spatial dependence structure may ameliorate the estimation of conditional return levels and return levels of spatial quantities when dealing with variables which are temporally nonstationary.

In the case of climate extremes which would have temporal trends both in the univariate distributions and the spatial dependence structure, it would be crucial to investigate the interaction between these two trends and their evolution. This would be all the more important if, instead of considering what happens in a unique location only, the associated risk is related to the occurrence of extremes in several locations or in an area.

Indeed, the effects of these trends could compensate each over and attenuate the related risk. Otherwise, their combination could aggravate the risk, and in this case, a proper modeling of these two trends would be essential to avoid an underestimation of the risk and its increase under climate change.

# Bibliography


Akaike, H. (1974). A new look at the statistical model identification. *Automatic Control, IEEE Transactions on*, 19(6):716–723.

Arlot, S., Celisse, A., et al. (2010). A survey of cross-validation procedures for model selection. *Statistics surveys*, 4:40–79.

Asadi, P., Davison, A. C., and Engelke, S. (2015). Extremes on river networks. *The Annals of Applied Statistics*, 9(4):2023–2050.

Barrett, J. P. (1974). The coefficient of determination–some limitations. *The American Statistician*, 28(1):19–20.

Bechler, A., Bel, L., and Vrac, M. (2015). Conditional simulations of the extremal t process: application to fields of extreme precipitation. *Spatial Statistics*, 12:109–127.

Beirlant, J., Goegebeur, Y., Teugels, J., and Segers, J. (2004). *Statistics of Extremes: Theory and Applications*. Wiley, Chichester.

Beniston, M., Farinotti, D., Stoffel, M., Andreassen, L. M., Coppola, E., Eckert, N., Fantini, A., Giacona, F., Hauck, C., Huss, M., et al. (2017). The European mountain cryosphere: A review of past, current and future issues. *Cryosphere Discuss*, pages 1–60.

Beranger, B., Padoan, S. A., and Sisson, S. A. (2016). Models for extremal dependence derived from skew-symmetric families. *Scandinavian Journal of Statistics*.

Bienvenüe, A. and Robert, C. Y. (2014). Likelihood based inference for high-dimensional extreme value distributions. [Available at http://docs.isfa.fr/labo/2014.6.pdf].

Blanchet, J. and Davison, A. C. (2011). Spatial modeling of extreme snow depth. *The Annals of Applied Statistics*, pages 1699–1725.

Blanchet, J. and Lehning, M. (2010). Mapping snow depth return levels: smooth spatial modeling versus station interpolation. *Hydrology and Earth System Sciences*, 14(12):2527.

Blanchet, J., Marty, C., and Lehning, M. (2009). Extreme value statistics of snowfall in the Swiss Alpine region. *Water Resources Research*, 45(5).

Blanchet, J., Touati, J., Lawrence, D., Garavaglia, F., and Paquet, E. (2015). Evaluation of a compound distribution based on weather pattern subsampling for extreme rainfall in Norway. *Natural Hazards and Earth System Sciences*, 15(12):2653–2667.

Bocchiola, D., Bianchi Janetti, E., Gorni, E., Marty, C., and Sovilla, B. (2008). Regional evaluation of three day snow depth for avalanche hazard mapping in Switzerland. *Natural Hazards and Earth System Sciences*, 8(4):685–705.

Bocchiola, D., Medagliani, M., and Rosso, R. (2006). Regional snow depth frequency curves for avalanche hazard mapping in central Italian Alps. *Cold Regions Science and Technology*, 46(3):204–221.

Brown, B. and Resnick, S. I. (1977). Extreme values of independent stochastic processes. *Journal of Applied Probability*, 14(04):732–739.

Capéraà, P., Fougères, A.-L., and Genest, C. (1997). A nonparametric estimation procedure for bivariate extreme value copulas. *Biometrika*, 84(3):567–577.

Castruccio, S., Huser, R., and Genton, M. G. (2016). High-order composite likelihood inference for max-stable distributions and processes. *Journal of Computational and Graphical Statistics*, 25(4):1212–1229.

Chai, T. and Draxler, R. R. (2014). Root mean square error (RMSE) or mean absolute error (MAE)?–Arguments against avoiding RMSE in the literature. *Geoscientific Model Development*, 7(3):1247–1250.

Chailan, R., Toulemonde, G., Bouchette, F., Laurent, A., Sevault, F., and Michaud, H. (2014). Spatial assessment of extreme significant waves heights in the Gulf of Lions. *Coastal Engineering Proceedings*, 1(34):17.

Coles, S. (2001). *An Introduction to Statistical Modeling of Extreme Values*. Springer, London.

Coles, S., Heffernan, J., and Tawn, J. (1999). Dependence measures for extreme value analyses. *Extremes*, 2(4):339–365.

Cooley, D. (2009). Extreme value analysis and the study of climate change. *Climatic change*, 97(1-2):77–83.

Cooley, D., Cisewski, J., Erhardt, R. J., Jeon, S., Mannshardt, E., Omolo, B. O., and Sun, Y. (2012). A survey of spatial extremes: measuring spatial dependence and modeling spatial effects. *Revstat*, 10(1):135–165.

Cooley, D., Naveau, P., and Poncet, P. (2006). Variograms for spatial max-stable random fields. In Bertail, P., Soulier, P., and Doukhan, P., editors, *Dependence in Probability and Statistics*, volume 187, pages 373–390. Springer, New York.

Cox, C. (1998). Delta method. *Encyclopedia of biostatistics*.

Cressie, N. (1993). *Statistics for Spatial Data*. Wiley, New York.

Davis, R. A., Klüppelberg, C., and Steinkohl, C. (2013a). Max-stable processes for modeling extremes observed in space and time. *J. Kor. Statist. Soc.*, 42(3):399–414.

Davis, R. A., Klüppelberg, C., and Steinkohl, C. (2013b). Statistical inference for max-stable processes in space and time. *Journal of the Royal Statistical Society: Series B (Statistical Methodology)*, 75(5):791–819.

Davison, A. C. and Gholamrezaee, M. M. (2012). Geostatistics of extremes. In *Proceedings of the Royal Society of London A: Mathematical, Physical and Engineering Sciences*, volume 468, pages 581–608. The Royal Society.

Davison, A. C. and Huser, R. (2015). Statistics of extremes. *Annual Review of Statistics and its Application*, 2:203–235.

Davison, A. C., Huser, R., and Thibaud, E. (2013). Geostatistics of dependent and asymptotically independent extremes. *Mathematical Geosciences*, 45(5):511–529.

Davison, A. C., Padoan, S. A., and Ribatet, M. (2012). Statistical modeling of spatial extremes. *Statistical science*, 27(2):161–186.

Davison, A. C. and Smith, R. L. (1990). Models for exceedances over high thresholds. *Journal of the Royal Statistical Society. Series B (Methodological)*, 52(3):393–442.

de Haan, L. (1984). A spectral representation for max-stable processes. *The annals of probability*, 12(4):1194–1204.

de Haan, L. and Ferreira, A. (2006). *Extreme Value Theory: An Introduction*. Springer, New York.

Diggle, P. J. and Ribeiro Jr., P. J. (2007). *Model-based Geostatistics*. Springer, New York.

Durand, Y., Brun, E., Mï¿½rindol, L., Guyomarc'h, G., Lesaffre, B., and Martin, E. (1993). A meteorological estimation of relevant parameters for snow models. *Ann. Glaciol.*, 18:65–71.

Durand, Y., Giraud, G., Brun, E., Mï¿½rindol, L., and Martin, E. (1999). A computer-based system simulating snowpack structures as a tool for regional avalanche forecasting. *J. Glaciol.*, 45(151):469–485.

Durand, Y., Giraud, G., Laternser, M., Etchevers, P., Mérindol, L., and Lesaffre, B. (2009a). Reanalysis of 47 years of climate in the French Alps (1958-2005): Climatology and trends for snow cover. *Journal of applied meteorology and climatology*, 48(12):2487–2512.

Durand, Y., Laternser, M., Giraud, G., Etchevers, P., Lesaffre, B., and Mérindol, L. (2009b). Reanalysis of 44 yr of climate in the French Alps (1958-2002): Methodology, model validation, climatology, and trends for air temperature and precipitation. *Journal of Applied Meteorology and Climatology*, 48(3):429–449.

Easterling, D. R., Evans, J., Groisman, P. Y., Karl, T., et al. (2000). Observed variability and trends in extreme climate events: a brief review. *Bulletin of the American Meteorological Society*, 81(3):417.

Eckert, N., Coleou, C., Castebrunet, H., Deschatres, M., Giraud, G., and Gaume, J. (2010). Cross-comparison of meteorological and avalanche data for characterising avalanche cycles: the example of December 2008 in the eastern part of the French Alps. *Cold Regions Science and Technology*, 64(2):119–136.

Eckert, N., Gaume, J., and Castebrunet, H. (2011). Using spatial and spatial-extreme statistics to characterize snow avalanche cycles. *Procedia Environmental Sciences*, 7:224–229.

Embrechts, P., Klüppelberg, C., and Mikosch, T. (2013). *Modelling extremal events: for insurance and finance*, volume 33. Springer Science & Business Media.

Embrechts, P., Koch, E., and Robert, C. (2016). Space–time max-stable models with spectral separability. *Advances in Applied Probability*, 48(A):77–97.

Enfield, D., Mestas-Nunez, A., and Trimble, P. (2001). The Atlantic multidecadal oscillation and its relation to rainfall and river flows in the continental U.S. *Geophysical Research Letters*, 28(10):2077–2080.

Falarz, M. (2004). Variability and trends in the duration and depth of snow cover in Poland in the 20th century. *International Journal of Climatology*, 24(13):1713–1727.

Ferreira, A., De Haan, L., et al. (2014). The generalized Pareto process; with a view towards application and simulation. *Bernoulli*, 20(4):1717–1737.

Finkenstadt, B. and Rootzén, H. (2003). *Extreme values in finance, telecommunications, and the environment*. CRC Press.

Fisher, R. A. and Tippett, L. H. C. (1928). Limiting forms of the frequency distribution of the largest or smallest member of a sample. *Mathematical Proceedings of the Cambridge Philosophical Society*, 24:180–190.

Gao, X. and Song, P. X.-K. (2010). Composite likelihood Bayesian information criteria for model selection in high-dimensional data. *Journal of the American Statistical Association*, 105(492):1531–1540.

Garavaglia, F., Lang, M., Paquet, E., Gailhard, J., Garçon, R., and Renard, B. (2011). Reliability and robustness of rainfall compound distribution model based on weather pattern sub-sampling. *Hydrology and Earth System Sciences Discussions*, 15:519–532.

Gaume, J., Chambon, G., Eckert, N., and Naaim, M. (2012). Relative influence of mechanical and meteorological factors on avalanche release depth distributions: An application to French Alps. *Geophysical Research Letters*, 39(12).

Gaume, J., Eckert, N., Chambon, G., and Naaim, M. (2013a). Prédétermination des hauteurs de départ d'avalanches : une approche par extrêmes spatiaux. *La Houille Blanche*, 5:30–36. doi:10.1051/lhb/2013040.

Gaume, J., Eckert, N., Chambon, G., Naaim, M., and Bel, L. (2013b). Mapping extreme snowfalls in the French Alps using max-stable processes. *Water Resources Research*, 49(2):1079–1098.

Genton, M. G., Ma, Y., and Sang, H. (2011). On the likelihood function of Gaussian max-stable processes. *Biometrika*, 98(2):481–488.

Gnedenko, B. (1943). Sur la distribution limite du terme maximum d'une série aléatoire. *Annals of mathematics*, pages 423–453.

Gottardi, F., Obled, C., Gailhard, J., and Paquet, E. (2012). Statistical reanalysis of precipitation fields based on ground network data and weather patterns: Application over French mountains. *Journal of Hydrology*, 432:154–167.

Gottardi, F., Obled, C., Paquet, E., and Gailhard, J. (2008). Régionalisation des précipitations sur les massifs montagneux français à l'aide de regressions locales et par type de temps. *Climatologie*, 5.

Gumbel, E. (1958). *Statistics of extremes*. Columbia University Press, New York.

Huser, R. and Davison, A. C. (2013). Composite likelihood estimation for the Brown–Resnick process. *Biometrika*, pages 1–9.

Huser, R. and Davison, A. C. (2014). Space–time modelling of extreme events. *Journal of the Royal Statistical Society: Series B (Statistical Methodology)*, 76(2):439–461.

Huser, R. and Genton, M. G. (2016). Non-stationary dependence structures for spatial extremes. *Journal of Agricultural, Biological, and Environmental Statistics*, 21(3):470–491.

Jacob, D., Petersen, J., Eggert, B., Alias, A., Christensen, O. B., Bouwer, L. M., Braun, A., Colette, A., Déqué, M., Georgievski, G., Georgopoulou, E., Gobiet, A., Menut, L., Nikulin, G., Haensler, A., Hempelmann, N., Jones, C., Keuler, K., Kovats, S., Kröner, N., Kotlarski, S., Kriegsmann, A., Martin, E., van Meijgaard, E., Moseley, C., Pfeifer, S., Preuschmann, S., Radermacher, C., Radtke, K., Rechid, D., Rounsevell, M., Samuelsson, P., Somot, S., Soussana, J.-F., Teichmann, C., Valentini, R., Vautard, R., Weber, B., and Yiou, P. (2014). EURO-CORDEX: new high-resolution climate change projections for European impact research. *Regional Environmental Change*, 14(2):563–578.

Jones, P. D., Jonsson, T., and Wheeler, D. (1997). Extension to the North Atlantic Oscillation using early instrumental pressure observations from Gibraltar and South-West Iceland. *International Journal of climatology*, 17(13):1433–1450.

Kabluchko, Z., Schlather, M., and de Haan, L. (2009). Stationary max-stable fields associated to negative definite functions. *The Annals of Probability*, 37(5):2042–2065.

Kaplan, A., Cane, M., Kushnir, Y., Clement, A., Blumenthal, M., and Rajagopalan, B. (1998). Analyses of global sea surface temperature 1856-1991. *Journal of Geophysical Research: Oceans*, 103(18):567–18.

Kass, R. E. and Raftery, A. E. (1995). Bayes factors. *Journal of the american statistical association*, 90(430):773–795.

Katz, R. W. (2010). Statistics of extremes in climate change. *Climatic Change*, 100(1):71–76.

Katz, R. W., Parlange, M. B., and Naveau, P. (2002). Statistics of extremes in hydrology. *Advances in water resources*, 25(8):1287–1304.

Keller, F., Goyette, S., and Beniston, M. (2005). Sensitivity analysis of snow cover to climate change scenarios and their impact on plant habitats in alpine terrain. *Climatic Change*, 72(3):299–319.

Klein Tank, A. and Können, G. (2003). Trends in indices of daily temperature and precipitation extremes in Europe, 1946-99. *Journal of Climate*, 16(22):3665–3680.

Laternser, M. and Schneebeli, M. (2003). Long-term snow climate trends of the Swiss Alps (1931–99). *international Journal of climatology*, 23(7):733–750.

Leadbetter, M. (1983). Extremes and local dependence in stationary sequences. *Probability Theory and Related Fields*, 65:291–306.

Lee, Y., Yoon, S., Murshed, M. S., Kim, M.-K., Cho, C., Baek, H.-J., and Park, J.-S. (2013). Spatial modeling of the highest daily maximum temperature in Korea via max-stable processes. *Advances in Atmospheric Sciences*, 30(6):1608–1620.

López-Moreno, J. I., Vicente-Serrano, S. M., Morán-Tejeda, E., Lorenzo-Lacruz, J., Kenawy, A., and Beniston, M. (2011). Effects of the North Atlantic Oscillation (NAO) on combined temperature and precipitation winter modes in the Mediterranean mountains: Observed relationships and projections for the 21st century. *Global and Planetary Change*, 77(1):62–76.

Marty, C. and Blanchet, J. (2012). Long-term changes in annual maximum snow depth and snowfall in Switzerland based on extreme value statistics. *Climatic Change*, 111(3-4):705–721.

Naveau, P., Guillou, A., Cooley, D., and Diebolt, J. (2009). Modelling pairwise dependence of maxima in space. *Biometrika*, 96(1):1–17.

Naveau, P., Nogaj, M., Ammann, C., Yiou, P., Cooley, D., and Jomelli, V. (2005). Statistical methods for the analysis of climate extremes. *Comptes Rendus Geoscience*, 337(10):1013–1022.

Nicolet, G., Eckert, N., Morin, S., and Blanchet, J. (2016). Decreasing spatial dependence in extreme snowfall in the French Alps since 1958 under climate change. *Journal of Geophysical Research: Atmospheres*, 121(14):8297–8310.

Nicolet, G., Eckert, N., Morin, S., and Blanchet, J. (2017a). A multi-criteria leave-two-out cross-validation procedure for max-stable process selection. submitted for publication.

Nicolet, G., Eckert, N., Morin, S., and Blanchet, J. (2017b). Modeling the trend in the spatial dependence of extremes: application to climate change on snow depth maxima in the French Alps. submitted for publication.

Opitz, T. (2013). Extremal t processes: Elliptical domain of attraction and a spectral representation. *Journal of Multivariate Analysis*, 122:409–413.

Osborn, T. J. (2006). Recent variations in the winter North Atlantic Oscillation. *Weather*, 61(12):353–355.

Padoan, S. A., Ribatet, M., and Sisson, S. A. (2010). Likelihood-based inference for max-stable processes. *Journal of the American Statistical Association*, 105(489)(489):263–277.

Pickands, J. (1975). Statistical inference using extreme order statistics. *the Annals of Statistics*, pages 119–131.

Pujol, N., Neppel, L., and Sabatier, R. (2007). Regional tests for trend detection in maximum precipitation series in the French Mediterranean region. *Hydrological Sciences Journal*, 52(5):956–973.

Raillard, N. (2011). *Modélisation du comportement extrême de processus spatio-temporels. Applications en océanographie et météorologie.* PhD thesis, Université Rennes 1.

Raillard, N., Ailliot, P., and Yao, J. (2014). Modeling extreme values of processes observed at irregular time steps: Application to significant wave height. *The Annals of Applied Statistics*, 8(1):622–647.

Reich, B. J. and Shaby, B. A. (2012). A hierarchical max-stable spatial model for extreme precipitation. *The annals of applied statistics*, 6(4):1430.

Reid, P. C., Hari, R. E., Beaugrand, G., Livingstone, D. M., Marty, C., Straile, D., Barichivich, J., Goberville, E., Adrian, R., Aono, Y., et al. (2015). Global impacts of the 1980s regime shift. *Global change biology*.

Reiss, R.-D. and Thomas, M. (2007). *Statistical analysis of extreme values*. Springer.

Renard, B., Kochanek, K., Lang, M., Garavaglia, F., Paquet, E., Neppel, L., Najib, K., Carreau, J., Arnaud, P., Aubert, Y., et al. (2013). Data-based comparison of frequency analysis methods: A general framework. *Water Resources Research*, 49(2):825–843.

Ribatet, M. (2013). Spatial extremes: Max-stable processes at work. *Journal de la Société Française de Statistique*, 154(2):156–177.

Ribatet, M. and Sedki, M. (2012). Extreme value copulas and max-stable processes. *Journal de la Société Française de Statistique*, 153(3):138–150.

Sadovskỳ, Z., Faško, P., Mikulová, K., and Pecho, J. (2012). Exceptional snowfalls and the assessment of accidental snow loads for structural design. *Cold Regions Science and Technology*, 72:17–22.

Schlather, M. (2002). Models for stationary max-stable random fields. *Extremes*, 5(1):33–44.

Schlather, M. and Tawn, J. A. (2003). A dependence measure for multivariate and spatial extreme values: Properties and inference. *Biometrika*, 90(1):139–156.

Schneebeli, M. and Laternser, M. (2004). A probabilistic model to evaluate the optimal density of stations measuring snowfall. *Journal of Applied Meteorology*, 43(5):711–719.

Schwarz, G. et al. (1978). Estimating the dimension of a model. *The annals of statistics*, 6(2):461–464.

Shang, H., Yan, J., and Zhang, X. (2011). El Niño–Southern Oscillation influence on winter maximum daily precipitation in California in a spatial model. *Water Resources Research*, 47(11).

Smith, E. L. and Stephenson, A. G. (2009). An extended gaussian max-stable process model for spatial extremes. *Journal of Statistical Planning and Inference*, 139(4):1266–1275.

Smith, R. L. (1990). Max-stable processes and spatial extremes. [Available at http://www.stat.unc.edu/postscript/rs/spatex.pdf].

Srivastava, A. K., Srivastava, V. K., and Ullah, A. (1995). The coefficient of determination and its adjusted version in linear regression models. *Econometric reviews*, 14(2):229–240.

Steinkohl, C. K. (2013). *Statistical Modelling of Extremes in Space and Time using Max-Stable Processes*. PhD thesis, Technische Universität München.

Stocker, T. F., Qin, D., Plattner, G. K., Tignor, M., Allen, S. K., Boschung, J., Nauels, A., Xia, Y., Bex, B., and Midgley, B. M. (2013). IPCC, 2013: climate change 2013: the physical science basis. Contribution of working group I to the fifth assessment report of the intergovernmental panel on climate change.

Thibaud, E., Aalto, J., Cooley, D. S., Davison, A. C., and Heikkinen, J. (2017). Bayesian inference for the brown–resnick process, with an application to extreme low temperatures. *The Annals of Applied Statistics*, 10(4):2303–2324.

Thibaud, E., Mutzner, R., and Davison, A. (2013). Threshold modeling of extreme spatial rainfall. *Water resources research*, 49(8):4633–4644.

Thibaud, E. and Opitz, T. (2015). Efficient inference and simulation for elliptical pareto processes. *Biometrika*, 102(4):855–870.

Valt, M. and Cianfarra, P. (2010). Recent snow cover variability in the Italian Alps. *Cold Regions Science and Technology*, 64(2):146–157.

van den Besselaar, E. J. M., Klein Tank, A. M. G., and Buishand, T. A. (2013). Trends in European precipitation extremes over 1951-2010. *International Journal of Climatology*, 33(12):2682–2689.

Vuong, Q. H. (1989). Likelihood ratio tests for model selection and non-nested hypotheses. *Econometrica: Journal of the Econometric Society*, pages 307–333.

Wadsworth, J. L. and Tawn, J. A. (2012). Dependence modelling for spatial extremes. *Biometrika*, 99(2):253–272.

Wasko, C., Sharma, A., and Westra, S. (2016). Reduced spatial extent of extreme storms at higher temperatures. *Geophysical Research Letters*, 43(8):4026–4032.

Westra, S., Alexander, L. V., and Zwiers, F. W. (2013). Global increasing trends in annual maximum daily precipitation. *Journal of Climate*, 26(11):3904–3918.

Westra, S. and Sisson, S. A. (2011). Detection of non-stationarity in precipitation extremes using a max-stable process model. *Journal of Hydrology*, 406(1-2):119–128.

Wipf, S., Stoeckli, V., and Bebi, P. (2009). Winter climate change in alpine tundra: plant responses to changes in snow depth and snowmelt timing. *Climatic change*, 94(1-2):105–121.

Xu, G. and Genton, M. G. (2016). Tukey max-stable processes for spatial extremes. *Spatial Statistics*.

Zhang, D., Wells, M. T., and Peng, L. (2008). Nonparametric estimation of the dependence function for a multivariate extreme value distribution. *Journal of Multivariate Analysis*, 99(4):577–588.

Zhang, Q., Xiao, M., Singh, V. P., and Chen, Y. D. (2014). Max-stable based evaluation of impacts of climate indices on extreme precipitation processes across the Poyang Lake basin, China. *Global and Planetary Change*, 122:271–281.

# Appendix I. List of the stations of the snowfall data set

| Name | E (km) | N (km) | Alt (m) |
|---|---|---|---|
| Albertville | 962 | 6513 | 333 |
| Allemond | 939 | 6460 | 1270 |
| Allevard | 940 | 6482 | 495 |
| Ancelle | 954 | 6397 | 1345 |
| Arvieux | 996 | 6416 | 1683 |
| Aussois | 994 | 6466 | 1478 |
| Autrans | 900 | 6457 | 1090 |
| Avrieux | 992 | 6464 | 1102 |
| Barcelonnette | 992 | 6373 | 1155 |
| Beaufort | 978 | 6516 | 1030 |
| Bessans | 1013 | 6477 | 1713 |
| Besse | 949 | 6446 | 1525 |
| Bourg-Saint-Maurice | 993 | 6508 | 865 |
| Briançon | 987 | 6429 | 1326 |
| Ceillac | 999 | 6404 | 1664 |
| Challes-les-Eaux | 932 | 6500 | 291 |
| Chamonix-Mont-Blanc | 1000 | 6544 | 1043 |
| Champcella | 983 | 6410 | 1100 |
| Champoléon | 958 | 6408 | 1275 |
| Chantelouve | 933 | 6434 | 1000 |
| Chichilianne | 903 | 6416 | 1010 |
| Col de Porte | 917 | 6470 | 1325 |
| Corps | 933 | 6418 | 935 |
| Embrun | 978 | 6391 | 872 |
| Entraigues | 933 | 6427 | 809 |
| Epine | 923 | 6504 | 311 |
| Guillaumes | 1008 | 6340 | 792 |
| Hauteluce | 983 | 6526 | 1215 |
| Isola | 1022 | 6353 | 870 |
| La Chapelle | 953 | 6417 | 1270 |
| La Clusaz | 966 | 6538 | 1164 |
| La Ferrière | 941 | 6469 | 1081 |
| La Grave | 959 | 6445 | 1785 |
| La Motte-en-Champsaur | 943 | 6408 | 1099 |
| La Mure | 920 | 6427 | 875 |
| La Rochette | 943 | 6488 | 350 |
| Lanslebourg | 1009 | 6466 | 2000 |
| Lavaldens | 927 | 6436 | 1070 |
| Le Grand-Bornand | 967 | 6547 | 1281 |
| Le Monêtier | 977 | 6437 | 1456 |
| Les Contamines | 989 | 6531 | 1180 |
| Les Gets | 983 | 6569 | 1172 |
| Les Orres | 982 | 6385 | 1445 |
| Lescheraines | 942 | 6517 | 590 |
| Lus-la-Croix-Haute | 915 | 6401 | 1059 |

***Table 3:*** *List of the stations of the snowfall data set (part 1)*

| Name | E (km) | N (km) | Alt (m) |
|---|---|---|---|
| Megève | 980 | 6535 | 1086 |
| Mens | 918 | 6417 | 780 |
| Monestier-de-Clermont | 908 | 6428 | 800 |
| Montgellafrey | 960 | 6483 | 1050 |
| Montgenèvre | 994 | 6433 | 1850 |
| Moûtiers | 976 | 6493 | 480 |
| Névache | 986 | 6442 | 1603 |
| Orcières | 964 | 6405 | 1435 |
| Peisey-Nancroix | 993 | 6501 | 1350 |
| Pellafol | 930 | 6414 | 940 |
| Pellafol | 930 | 6417 | 800 |
| Pelvoux | 975 | 6425 | 1267 |
| Péone | 1015 | 6341 | 1661 |
| Pralognan-la-Vanoise | 991 | 6483 | 1419 |
| Proveysieux | 912 | 6468 | 600 |
| Sallanches | 983 | 6543 | 541 |
| Samoëns | 988 | 6561 | 749 |
| St-Alban-des-Hurtières | 955 | 6492 | 614 |
| St-Baudille-et-Pipet | 921 | 6415 | 1040 |
| St-Bonnet-en-Champsaur | 944 | 6403 | 1012 |
| St-Christophe-en-Oisans | 951 | 6433 | 1570 |
| St-Dalmas-le-Selvage | 1007 | 6361 | 1500 |
| St-Etienne-en-Dévoluy | 933 | 6404 | 1308 |
| St-Etienne-de-Tinée | 1014 | 6355 | 1607 |
| St-Firmin | 939 | 6414 | 950 |
| St-Hilaire | 926 | 6471 | 960 |
| St-Laurent-du-Pont | 914 | 6483 | 389 |
| St-Martin-Vésubie | 1041 | 6339 | 1018 |
| St-Martin-de-Belleville | 975 | 6481 | 1500 |
| St-Michel-de-Maurienne | 974 | 6465 | 1360 |
| St-Paul | 1005 | 6396 | 1905 |
| St-Pierre-de-Chartreuse | 919 | 6478 | 945 |
| St-Pierre-d'Entremont | 923 | 6483 | 644 |
| St-Véran | 1006 | 6408 | 2012 |
| Tende | 1067 | 6338 | 645 |
| Termignon | 999 | 6471 | 1284 |
| Thônes | 958 | 6536 | 629 |
| Valdeblore | 1034 | 6339 | 1009 |
| Valjouffrey | 938 | 6425 | 980 |
| Valloire | 969 | 6458 | 1451 |
| Vallorcine | 1004 | 6555 | 1300 |
| Vaujany | 939 | 6455 | 772 |
| Verrens-Arvey | 958 | 6512 | 530 |
| Villar-Loubière | 949 | 6419 | 1069 |
| Villard-de-Lans | 901 | 6445 | 1030 |

***Table 4:*** *List of the stations of the snowfall data set (part 2)*

# Appendix II. List of the stations of the snow depth data set

| Name | E (km) | N (km) | Alt (m) |
|---|---|---|---|
| Bessans | 1013 | 6477 | 1707 |
| Ceillac NIVO | 999 | 6404 | 1700 |
| Col de Porte | 917 | 6470 | 1325 |
| Courchevel | 984 | 6487 | 1775 |
| Flaine | 986 | 6551 | 1640 |
| Isola | 1032 | 6352 | 1915 |
| L'Alpe d'Huez (SATA) | 941 | 6448 | 1860 |
| La Clusaz | 966 | 6539 | 1500 |
| La Plagne | 987 | 6497 | 1970 |
| Les Karellis | 968 | 6465 | 1610 |
| Les Menuires | 977 | 6475 | 1800 |
| Montgenèvre | 994 | 6433 | 1860 |
| Pralognan | 991 | 6482 | 1416 |
| Puy St-Vincent | 975 | 6421 | 1600 |
| Tignes | 1005 | 6493 | 2080 |
| Val d'Isère Joseray | 1011 | 6490 | 1850 |
| Vars | 992 | 6398 | 1855 |
| Bellecote | 994 | 6495 | 3000 |
| Bonneval sur Arc | 1017 | 6480 | 2720 |
| Col Agnel | 1015 | 6407 | 2630 |
| Le Chevril | 1009 | 6497 | 2560 |
| Les Ecrins | 964 | 6432 | 2978 |
| Les Rochilles | 973 | 6449 | 2450 |
| Restefond | 1003 | 6367 | 2550 |
| Abriès | 1012 | 6417 | 2000 |
| Auris en Oisans | 947 | 6422 | 1860 |
| Auron | 1014 | 6358 | 1790 |
| Avoriaz | 991 | 6571 | 2100 |
| Bellevaux | 975 | 6573 | 1520 |
| Ceillac | 999 | 6404 | 2300 |
| Cervières | 995 | 6424 | 2160 |
| Col de Porte | 917 | 6471 | 1325 |
| Courchevel | 984 | 6484 | 2100 |
| Flaine | 986 | 6551 | 2250 |
| L'Alpe d'Huez (SATA) | 941 | 6448 | 2000 |
| L'Alpe d'Huez 2350 | 944 | 6449 | 2450 |
| L'Alpe du Grand Serre | 925 | 6440 | 1800 |
| La Clusaz | 966 | 6539 | 2450 |
| La Foux d'Allos | 985 | 6360 | 2050 |
| La Plagne | 987 | 6496 | 2160 |
| La Plagne Bellecote | 994 | 6496 | 2970 |

***Table 5:*** *List of the stations of the snow depth data set (part 1)*

| Name | E (km) | N (km) | Alt (m) |
|---|---|---|---|
| La Plagne Champagny | 990 | 6494 | 2300 |
| La Plagne Montchavin | 991 | 6499 | 2100 |
| La Rosiere | 1001 | 6512 | 2200 |
| Larche | 1006 | 6380 | 1700 |
| Le Corbier | 954 | 6465 | 2200 |
| Le Grand Bornand | 965 | 6542 | 1700 |
| Le Molard | 1014 | 6489 | 2560 |
| Le Monêtier | 976 | 6436 | 2200 |
| Le Sauze | 994 | 6376 | 2070 |
| Le Tour | 1007 | 6554 | 2190 |
| Les 2 Alpes (Toura NE) | 950 | 6437 | 2600 |
| Les Arcs | 998 | 6503 | 2250 |
| Les Arcs 1600 | 998 | 6503 | 2070 |
| Les Carroz d'Arâches | 985 | 6554 | 1770 |
| Les Contamines Montjoie | 987 | 6527 | 2270 |
| Les Gets | 983 | 6570 | 1720 |
| Les Karellis | 967 | 6464 | 1950 |
| Les Menuires | 980 | 6474 | 2380 |
| Les Orres | 980 | 6386 | 2220 |
| Lognan | 1006 | 6549 | 2780 |
| Maljasset | 1004 | 6396 | 1900 |
| Megève | 981 | 6534 | 2000 |
| Meribel Mottaret | 980 | 6480 | 2000 |
| Molines | 1005 | 6411 | 2250 |
| Orcières PNE | 963 | 6403 | 2450 |
| Plan de l'Aiguille | 1000 | 6541 | 2300 |
| Pra Loup | 985 | 6368 | 2450 |
| Pralognan | 993 | 6484 | 1950 |
| Prapoutel | 938 | 6467 | 1900 |
| Prarion | 993 | 6538 | 1850 |
| Puy St-Vincent | 975 | 6421 | 2250 |
| Réallon | 964 | 6392 | 2010 |
| Risoul | 988 | 6398 | 2550 |
| Serre Chevalier | 980 | 6429 | 2100 |
| Tignes | 1004 | 6493 | 2400 |
| Val d'Isère Joseray | 1012 | 6489 | 2530 |
| Val Fréjus | 987 | 6458 | 2200 |
| Valmeinier | 975 | 6461 | 2200 |
| Valmorel | 969 | 6488 | 1850 |
| Vars | 992 | 6398 | 2270 |
| Villeneuve la Salle | 978 | 6432 | 2500 |

***Table 6:*** *List of the stations of the snow depth data set (part 2)*

**Abstract**
Risk management in mountainous regions requires a precise assessment of snow extremes. We adopt the framework of max-stable processes, which connect extreme value statistics and geostatistics, to investigate the spatial dependence of winter maxima of 3-day snowfall and snow depths in the French Alps. Two important issues are broached: model selection and temporal non-stationarity. First, we introduce a cross-validation procedure which is used to assess the predictive ability of several max-stable processes to capture the spatial dependence structure of snowfall maxima. Then, we highlight a decrease in spatial dependence of extreme snowfall during the last decades. Lastly, we show a way to model temporal trends in a spatial dependence of extremes through the example of snow depth maxima. For both extreme snowfall and extreme snow depths, we find that the spatial dependence is strongly impacted by climate change, at first by the effect of the increase in temperature on the snow rain partitioning, also by the decrease in winter cumulated snowfall.

**Keywords**: snowfall, snow depths, spatial extremes, max-stable processes, climate change, French Alps

**Résumé**
La gestion des risques dans les régions montagneuses nécessite une caractérisation des extrêmes neigeux. Nous utilisons le cadre des processus max-stables, qui relient statistique des valeurs extrêmes et géostatistique, pour étudier la dépendance spatiale des maxima hivernaux de cumuls de chutes de neige sur 3 jours et de hauteurs de neige dans les Alpes françaises. Deux questions sont abordées : la sélection de modèle et la non-stationnarité temporelle. Nous commençons par introduire une procédure de validation-croisée que nous utilisons pour évaluer les capacités de plusieurs processus max-stables à capturer la structure de dépendance spatiale des maxima de chutes de neige. Ensuite, nous mettons en évidence une baisse de la dépendance spatiale des chutes de neige extrêmes durant ces dernières décennies. Enfin, nous montrons comment modéliser des tendances temporelles dans une structure de dépendance spatiale des extrêmes à travers l'exemple des maxima de hauteurs de neige. Pour les extrêmes de chutes comme de hauteurs de neige, la dépendance spatiale est fortement impactée par le changement climatique, premièrement par l'effet de la hausse de la température sur la phase (neige ou pluie) de la précipitation, et ensuite par la baisse du cumul hivernal des chutes de neige.

**Mots clés**: chutes de neige, hauteurs de neige, extrêmes spatiaux, processus max-stables, changement climatique, Alpes françaises.